Under Lake Infrastructure for thermal capture and Storage of Solar Energy (ULISSE)

Exploratory study of the SOUR Call 1-2021 Project ULISSE

Appendix of the Final report (extended English version)

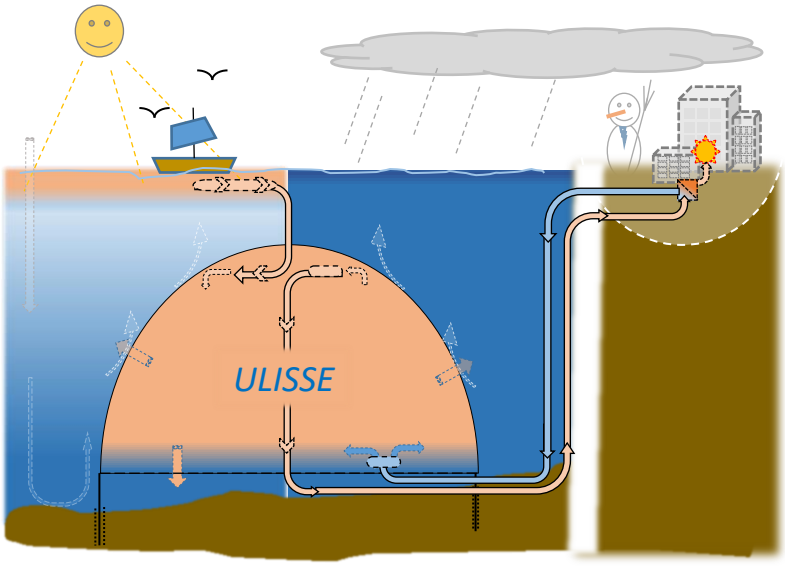

Under Lake Infrastructure for thermal capture and Storage of Solar Energy

Source: © CvS énergies sàrl

William van Sprolant, CvS énergies sàrl
Boulevard Helvétique 36, 1207 Geneva, Switzerland

Host institute

hepia
Haute école du paysage, d'ingénierie et d'architecture de Genève
Hes·so GENÈVE
Haute Ecole Spécialisée de Suisse occidentale

Date: 25.01.2024

Location: Bern

Project start – end: 01.09.2021 – 31.05.2023

Subsidy recipient:
Institution HEPIA
Rue de la Prairie 4, CH-1202 Genève
www.hesge.ch/hepia

Author:
William van Sprolant, CvS Énergies sàrl, cvs-energies@mecacerf.ch

Collaborations/Contributions: HEPIA (Alphabetical order):
Alain Dubois, Reto Camponovo, Daniel Bello Mendes, Jean-François Rubin, Peter Gallinelli, Jeremy Olivier, Roland Rozsnyo Gilles Trisconne, Zsolt Vecsernyes https://www.hesge.ch/hepia/annuaire

The author bears the entire responsibility for the content of this report and for the conclusions drawn therefrom.

Foreword

The present report concerns the exploratory study of the system/project ULISSE (***Under Lake Infrastructure for capture and Storage of Solar Energy***). The study was funded by the Swiss Federal Office of Energy (SFOE) in response to the "SOUR Call 1-2021" (*SWEET Out the box Rethinking*) as part of Switzerland's Energy Transition 2050.

As an innovative and unconventional project (Outside-the-box), the present study explores several complementary and new concepts in their realizations, which requires substantial explanations and the development of the merits of the project, however "*without exhausting the subject"*.

As *Appendix* of the Final report, the extended original French written report, from which the present English version is translated by DeepL, explains the corresponding language of some figures, abbreviations and symbols. The Final report and Appendix are published on the ARAMIS database of research, innovation and evaluation projects financed or executed by the Confederation (https://www.aramis.admin.ch/).

sweet swiss energy research for the energy transition

Summary

Faced with climate change, the *Swiss Energy Strategy* 2050 (SES-2050) is aiming for *"double neutrality*" *nuclear & carbon* (2035-2050) and forecasts a structural deficit in the winter semester of 9 TWh of electric energy (equivalent to the national hydroelectric storage capacity). This is the result of the planned withdrawal of nuclear power in 2035 and the increase in demand for electricity, for electric mobility, heat pumps for air conditioning, room heating and domestic hot water, as well as for the decarbonisation of industry. The major challenge for the SES-2050 is therefore to have enough "doubly *neutral*" electricity available in winter.

This study explores the potential of the novel ULISSE system (*Under Lake Infrastructure for capture and Storage of Solar Energy*), as well as the possibility to be combined with the CORSAIRE "*free heating"* process (without heat pumps). ULISSE aims to improve the efficiency of the Thermal Lacustrine Networks (TLNs), to be potentially installed in the 15 major Swiss lakes, while providing advantageously deep oxygenation of said lakes, induced by external thermal convection of the ULISSE reservoirs. CORSAIRE free heating aims to reduce the negative energy impact on buildings caused by the winter drop in temperature of the public Drinking Water Network (DWN).

The ULISSE system concept consists of large seasonal heat storage reservoirs anchored to the lake bed (typical unit capacity: 2 million m^3 & 125 TJ). In summer, they are filled with temperate water, either from the upper layer of the lake heated by the sun, or from industrial and air-conditioning waste heat. The ULISSE reservoirs would constitute a source of winter heat from the lake water at around 20°C, instead of the usual 5-6°C. This can double the efficiency of the heat pumps and halves their electricity consumption, reducing the volume of water by a factor of 5 and the electrical energy required to pump and circulate the water in the TLNs by 95%.

The study provides an initial energetic potential and feasibility analysis of a possible structure (envelope, anchoring) for the ULISSE reservoir, a sketch of its thermal loading/discharging system and some hints regarding its potential interactions with the lake ambient (thermal, hydrodynamic, environmental). More specifically, a cross-study (with converging results) of the efficiency of the seasonal thermal storage of the ULISSE reservoir was also carried out, using three complementary approaches: the construction of a theoretical model, a mock-up with a fundamental analysis of the Temporal Scaling Factor, and a numerical simulation (COMSOL).

As a major example, the study analyses the overall energy performance of the ULISSE - CORSAIRE system applied to the GeniLac TLN and the DWN in Geneva, and compares it with the system for capturing and storing seasonal "terrestrial" solar heat (collector field + covered basin), then extrapolates it to the national scale.

As a result, and conclusion from the project, around 300 ULISSE reservoirs spread invisibly across the 15 major Swiss lakes and combined with CORSAIRE *free heating* (including outside the lake regions) could have the potential to supply almost 60 PJ or 30% of the 200 PJ of national energy-heat requirements for ambient heating and domestic hot water. For an overall investment estimated to around CHF 3 to 4 billion (ULISSE reservoirs, CORSAIRE heat exchangers, pipelines), this would save 3 TWh of gross electricity in the winter semester 2050, i.e., 1/3 of the 9 TWh winter electricity deficit and equivalent to twice the winter production of Switzerland's largest hydroelectric complex, Grande Dixence (2 x 1.5 TWh).

Finally, the study proposes a pilot ULISSE Reservoir, connected to the TLNs on the EPFL-UNIL campuses, with observations by the LéXPLORE floating laboratory as well as a pilot CORSAIRE in the Cité du Lignon (6,500 inhabitants and shops) and supplied with thermal waste from the Aïre wastewater treatment plant in Geneva.

Keywords: thermal lacustrine network, free cooling, free heating, seasonal sub-lacustrine heat storage, winter de-icing, temperature correction of drinking water network, heat pump, GeniLac, Geneva.

Résumé

Face aux changements climatiques la Stratégie Énergétique Suisse 2050 (SES-2050) vise la « double neutralité » nucléaire & carbone (2035-2050) et prévoit un déficit structurel en semestre hiver de 9 TWh d'électricité (équivalent à la capacité nationale d'accumulation hydroélectrique). Il résulte du retrait planifié de l'électricité nucléaire en 2035 et de l'augmentation de la demande d'électricité, pour la mobilité électrique, les pompes à chaleur (HP) pour la climatisation, le chauffage du bâti et l'eau chaude sanitaire, ainsi que pour la décarbonation de l'industrie. L'enjeu majeur de la SES-2050 est donc de disposer de suffisamment d'électricité « doublement neutre » en hiver.

La présente étude explore le potentiel du système inédit ULISSE (Under Lake Infrastructure for capture and Storage of Solar Energy) associé à la possibilité de combiner le procédé CORSAIRE « free heating » (sans HP). ULISSE vise à améliorer l'efficacité des Réseaux Thermo Lacustres (RTLs), potentiellement implantés dans les 15 grands lacs suisses, tout en induisant avantageusement l'oxygénation profonde desdits lacs par la convection thermique externe des réservoirs ULISSE. Le CORSAIRE free heating quant à lui vise à réduire l'impact énergétique négatif sur le parc immobilier induit par la chute hivernale de la température du Réseau public d'Eau Potable (REP).

Le système ULISSE est constitué de grands réservoirs de stockage saisonnier de chaleur ancrés sur les fonds lacustres (capacité unitaire : 2 millions m3 & 125 TJ). Ils sont chargés en été d'eau tempérée, soit issue de la couche supérieure du lac chauffée par le soleil, soit par des rejets de chaleur industrielle et de climatisation. Les réservoirs ULISSE sont une source lacustre de chaleur hivernale d'eau à environ 20°C, au lieu d'ordinaire à 5-6°C. Ceci peut doubler l'efficacité des HP et diminuer de moitié leur consommation électrique, réduire d'un facteur 5 le volume d'eau et de 95 % l'énergie électrique de pompage et de circulation de l'eau dans le RTL.

L'étude réalise une première analyse du potentiel énergétique et d'une possible structure (enveloppe, ancrage) du réservoir ULISSE, l'esquisse de son système de chargement/déchargement thermique ainsi que ses potentielles interactions lacustres (thermiques, hydrodynamiques, environnementaux). Plus spécifiquement est aussi réalisé une étude croisée (aux résultats convergents) de l'efficacité du stockage thermique saisonnier du réservoir ULISSE, ceci par trois approches complémentaires : l'élaboration d'un modèle théorique, une maquette avec analyse fondamentale du facteur d'échelle temporelle ainsi qu'une simulation numérique (COMSOL).

À titre d'exemple majeur, l'étude analyse les performances énergétiques globales du système ULISSE - CORSAIRE appliqué au RTL GeniLac et au REP à Genève, les comparent au système de capture et de stockage saisonnier de chaleur solaire « terrestre » (champ de capteurs + basin couvert), puis l'extrapole à l'échelle nationale.

En résulta et conclusion du projet, environ 300 Réservoirs ULISSE répartis de façon invisible dans les 15 grands lacs suisses et en association avec le free heating CORSAIRE (y compris hors des régions lacustres) pourraient potentiellement fournir près de 60 PJ soit 30 % des 200 PJ des besoins nationaux d'énergie-chaleur pour le chauffage ambiant et l'eau chaude sanitaire. Pour un investissement global estimé à environ 3 à 4 milliards de CHF (réservoirs ULISSE, échangeurs de chaleur CORSAIRE, conduites), ceci permettrait d'économiser 3 TWh d'électricité brut en semestre d'hiver 2050 soit le 1/3 des 9 TWh de déficit hivernal d'électricité et équivalent au double de la production hivernale du plus grand complexe hydroélectrique suisse de la Grande Dixence (2 x 1,5 TWh).

Finalement, l'étude propose la réalisation d'un Réservoir ULISSE pilote. Celui-ci serait relié aux RTLs des campus EPFL-UNIL, avec observations par le laboratoire flottant LéXPLORE ainsi qu'un pilote CORSAIRE sur la Cité du Lignon (6'500 habitants et commerces) et alimentée avec les rejets thermiques de la Station d'épuration des eaux usées d'Aïre à Genève.

Mots-clefs : réseau thermo lacustre, free cooling, free heating, stockage saisonnier de chaleur sous-lacustre, déglaçage hivernal, correction température du réseau d'eau potable, pompe à chaleur, GeniLac, Genève.

Zusammenfassung

Angesichts des Klimawandels strebt die Schweizer Energie Strategie 2050 (SES-2050) eine "doppelte Neutralität" in Nuklear & Kohlenstoff (2035-2050) an und prognostiziert im Wintersemester ein strukturelles Defizit von 9 TWh Strom (entspricht der nationalen Speicherkapazität von Wasserkraft). Das Defizit resultiert aus dem geplanten Atomausstieg im Jahr 2035 und dem steigenden Strombedarf für Elektromobilität, Wärmepumpen (WP) für Klimatisierung, Gebäudeheizung und Warmwasserbereitung sowie für die Dekarbonisierung der Industrie. Die grosse Herausforderung für die SES-2050 besteht daher darin, im Winter genügend „doppelt neutralen“ Strom zur Verfügung zu haben.

Diese Studie untersucht das Potential des neuartigen ULISSE-Systems (*Under Lake Infrastructure for capture and Storage of Solar Energy*) sowie die Möglichkeit zur Kombination mit dem CORSAIRE " freie Heizung " (Prozess ohne WP). Ziel von ULISSE ist es, die Effizienz der Thermische Seenetzwerke (TSNs) zu verbessern, die möglicherweise in den 15 grossen Schweizer Seen installiert werden sollen, und gleichzeitig eine vorteilhafte Tiefensauerstoffanreicherung dieser Seen zu gewährleisten, die durch externe thermische Konvektion der ULISSE-Reservoirs induziert wird. CORSAIRE freie Heizung zielt darauf ab, die negativen Energieauswirkungen auf den Immobilienbestand zu reduzieren, die durch den winterlichen Temperaturabfall der Trinkwassernetze (TWN) verursacht werden.

Das ULISSE-System besteht aus grossen saisonalen Wärmespeicherreservoirs, die am Seeboden verankert sind (Einheitskapazität: 2 Millionen m^3 und 125 TJ). Im Sommer werden sie mit temperiertem Wasser gefüllt, entweder aus der von der Sonne erwärmten oberen Schicht des Sees oder aus Industrie- und Klimaanlagenabwärme. Die ULISSE-Reservoirs würden im Winter eine Wärmequelle aus dem Seewasser mit etwa 20 °C statt der üblichen 5-6 °C darstellen. Dadurch kann die Effizienz der Wärmepumpen verdoppelt und ihr Stromverbrauch halbiert werden, wodurch die Wassermenge um den Faktor 5 und die elektrische Energie, die zum Pumpen und Umwälzen des Wassers in den TSNs erforderlich ist, um 95 % reduziert werden.

Die Studie liefert eine erste energetische Potenzial- und Machbarkeitsanalyse einer möglichen Struktur (Hülle, Verankerung) für das ULISSE-Reservoir, eine Skizze seines thermischen Lade-/Entladesystems und einige Hinweise zu seinen möglichen Wechselwirkungen mit der Seeumgebung (thermisch, hydrodynamisch, umweltbedingt). Genauer gesagt wurde auch eine Kreuzstudie (mit konvergierenden Ergebnissen) der Effizienz der saisonalen Wärmespeicherung des ULISSE-Reservoirs durchgeführt, wobei drei komplementäre Ansätze zum Einsatz kamen: die Konstruktion eines theoretischen Modells, ein Modell mit einer grundlegenden Analyse von der zeitliche Skalierungsfaktor und eine numerische Simulation (COMSOL).

Als Beispiel, die Studie analysiert die Energieleistung des ULISSE-CORSAIRE-Systems, welches auf das TSN GeniLac und das TWN in Genf angewendet wird, und vergleicht sie mit dem saisonalen "terrestrischen" Solarwärmeerfassungs- und -Speicher System (Kollektorfeld + überdachtes Becken). Anschliessend wird es auf die nationale Ebene hochgerechnet.

Als Ergebnis und Fazit des Projekts könnten rund 300 ULISSE-Reservoirs, die unsichtbar über die 15 grossen Schweizer Seen verteilt sind, in Kombination mit der freien Heizung von CORSAIRE (auch ausserhalb der Seeregionen) das Potential haben, fast 60 PJ oder 30 % der 200 PJ des nationalen Energie-Wärme-Bedarfs für Raumheizung und Warmwasser bereitstellen. Bei einer geschätzten Gesamtinvestition von rund 3 bis 4 Milliarden Franken (ULISSE-Speicher, CORSAIRE-Wärmetauscher, Rohrleitung) würde dies im Winterhalbjahr 2050 3 TWh Bruttostrom einsparen, also 1/3 des Winterstromdefizits von 9 TWh. Das entspricht der doppelten Winterproduktion des grössten Wasserkraftwerks der Schweiz, Grande Dixence (2 x 1,5 TWh).

Schliesslich schlägt die Studie die Schaffung eines Pilot-ULISSE-Reservoirs vor, das mit den TSNs auf den EPFL-UNIL-Campussen verbunden ist, mit Beobachtungen durch das schwimmende LéXPLORE-Labor sowie eines Pilot-CORSAIRE der Cité du Lignon (6.500 Einwohner und Geschäfte), der mit thermischen Abfällen aus der Kläranlage Aïre in Genf versorgt.

Schlüsselwörter: Seewärmenetz, freie Kühlung, freie Heizung, saisonale Wärmespeicherung unterhalb des Sees, Winter Temperaturkorrektur des Trinkwassernetzes, Wärmepumpe, GeniLac.

Riassunto

Di fronte ai cambiamenti climatici, la Strategia Energetica Svizzera 2050 (SES-2050) punta alla "doppia neutralità" Nucleare & Carbone" (2035-2050) e prevede un deficit strutturale nel semestre invernale di 9 TWh di elettricità (equivalente di cahpità al fabbisogno nazionale accumulo idroelettrico). Deriva dal previsto ritiro dell'energia elettrica dal nucleare nel 2035 e dall'aumento della domanda di energia elettrica per la mobilità elettrica, le Pompe Di Calore (PDC) per la climatizzazione e il riscaldamento degli edifici, nonché per la decarbonizzazione dell'industria. La sfida principale del SES-2050 è quindi quella di avere abbastanza elettricità "doppiamente neutrale" in inverno.

Questo studio esplora il sistema originale ULISSE (*Under Lake Infrastructure for capture and Storage of Solar Energy*) associato al CORSAIRE "*free heating*" (senza PDC). ULISSE mira a migliorare l'efficienza delle Reti Termo-Lacustri (RTL) potenzialmente impiantato dei 15 grandi laghi svizzeri, e proteggendo al tempo stesso questi laghi dal riscaldamento globale, in particolare attraverso l'ossigenazione profonda (Hypolimnion) indotta dalla convezione esterna dei serbatoi sublacustri dell'ULISSE. Il CORSAIRE *free heating* mira a ridurre l'impatto energetico negativo sul patrimonio immobiliare indotto dal abbassamento invernale della temperatura della Reti pubbliche di Acqua Potabile (RAP).

Il sistema ULISSE è costituito da grandi serbatoi di accumulo termico stagionale, ancorati ai fondali lacustri (cahpità unitaria: 2 milioni di m^3 e 125 TJ). D'estate si caricano con acqua temperata, o dallo strato superiore del lago (Epilimnion) riscaldata dal sole, o dal calore di scarto industriale e di climatizzazione. I Bacini di ULISSE sono una fonte lacustre di caldo invernale intorno ai 20°C, superiore all'ordinario a 5-6°C. This increases the efficiency of heat pumps and reduces their electricity consumption, cutting water volume by a factor of 5 and reducing electricity consumption for pumping and circulating water in the Reti Thermo Lacustre (RTL) by 95%.

Lo studio prevede un primo sviluppo ed analisi di una possibile struttura (involucro, ancoraggio) del bacino di tipo ULISSE, lo schema del suo sistema di carico/scarico termico nonché le sue potenziali interazioni lacustri (termiche, idrodinamiche, ambientali), senza tuttavia "esaurire i soggetti". Più nel dettaglio, viene effettuato anche uno studio trasversale (con risultati convergenti) dell'efficienza dell'accumulo termico stagionale del giacimento ULISSE, utilizzando 3 approcci complementari : modello teorico, modello con analisi fondamentale del fattore di scala temporale nonché uno studio numerico simulazione (COMSOL).

Lo studio analizza le prestazioni energetiche del sistema ULISSE - CORSAIRE applicato al RTL Genilac e al RAP di Ginevra, confrontarli con il sistema stagionale di cattura e accumulo del calore solare "terrestre" (campo collettori + bacino coperto), poi lo estrapola alla scala nazionale.

Di conseguenza, circa 300 serbatoi ULISSE distribuiti invisibilmente nei 15 grandi laghi svizzeri e in associazione al riscaldamento gratuito CORSAIRE (senza pompa di calore e anche al di fuori delle regioni lacustri), potrebbero fornire quasi 60 PJ ovvero il 30% dei 200 PJ del fabbisogno nazionale di calore energia per il riscaldamento degli ambienti e l'acqua calda sanitaria. For a total investment of around 3-4 billion franchi (ULISSE hot water tanks, CORSAIRE heat recovery systems, piping), this would allow 3 TWh of northern electricity to be recovered in the winter half of 2050, ovvero 1/3 del deficit di elettricità invernale di 9 TWh, pari al doppio della produzione invernale del più grande complesso idroelettrico svizzero di Grande Dixence. (2 x 1.5 TWh).

Infine, lo studio propone di creare un bacino pilota e dimostrativo ULISSE (P+D), collegato agli RTL dei campus EPFL-UNIL, con osservazioni da parte del laboratorio galleggiante LéXPLORE, e di un CORSAIRE pilota in la Cité du Lignon (6.500 abitanti e negozi) e alimentato con i rifiuti termici dell'impianto di depurazione dell'Aïre a Ginevra.

Parole chiave: rete termale lacustre, free cooling, free heating, accumulo di calore sublacustre stagionale, correzione della temperatura invernale della rete di acqua potabile, pompa di calore, GeniLac, Ginevra.

Acknowledgements

First of all, I would like to extend my warmest thanks to Olivier Epelly, former Director of the Geneva Cantonal Energy Office and a former colleague, for having so kindly informed me of the Federal Office of Energy's "*Out the box Rethinking"* call for projects; without him, I would simply have ignored *the call*, and the ULISSE project would not have been subsidised out of 77 proposals**.**

I would also like to thank Reto Camponovo and Gilles Trisconne, who made it possible for HEPIA to be the indispensable 'host institute' for the project, not forgetting the invaluable and enlightened advice of the LECEA laboratory, including that of Peter Gallinelli and his colleagues. Many thanks to the professors, Alain Dubois, Jean-François Rubin, Jeremy Olivier, Roland Rozsnyo and Zsolt Vecernyes, for their fruitful exchanges on topics such as numerical simulation, sub-lacustrine currents and the reaction of fishermen. And thanks also to Daniel Bello Mendes for his master's work on the numerical simulation of the experimental model of the ULISSE reservoir.

I would like to thank Gilles Ottaviani (Project Manager, Thermal Engineering, Services Industriels de Genève) and Marcel Rüegg (Director, Academic and Institutional Relations, SIG), who gave me access to essential data from the GeniLac project (*Flagship of* the Thermal Lake Networks in Switzerland) and provided me with an example of how to apply the ULISSE system. Thanks also to Stanislas de Froment of FOAMGLAS Switzerland (cellular glass insulation) and Mario Sappupo of Georg Fischer Pipe Systems (Switzerland) AG.

"The Solution of the Pollution is NOT the Dilution"

Lucien Borel, Professor of Thermodynamics at EPFL from 1954 to 2007

Table of contents

1 Introduction: Challenge/deficit of the Swiss Energy Transition 2050

In the face of climate change, Switzerland has drawn up its Energy Strategy, which aims to be "carbon neutral" by 2050 and "nuclear neutral" by 2035 **[1]**. Given the urgency and the current situation with regard to these objectives, its *Energy Transition* needs to be stepped up. While this involves replacing fossil fuels, which emit greenhouse gases (GHGs), with 584 PJ of GHG-free renewable energies, it also has to deal with a **structural Winter deficit of 9 TWh electricity, its main "intermediate energy vector"**.

The Swiss Energy Strategy 2050 is based largely on the energy renovation of buildings, with the almost widespread use of heat pumps (HP) for heating and air conditioning, requiring 1/3 electrical energy, plus the electrification of mobility, industry (decarbonisation) and the end of nuclear power (2035); all **under the threat of Switzerland's exclusion from the EU's *Clean Energy Package* [1.1],** which would restrict winter electricity imports and could destabilise the Swiss grid.

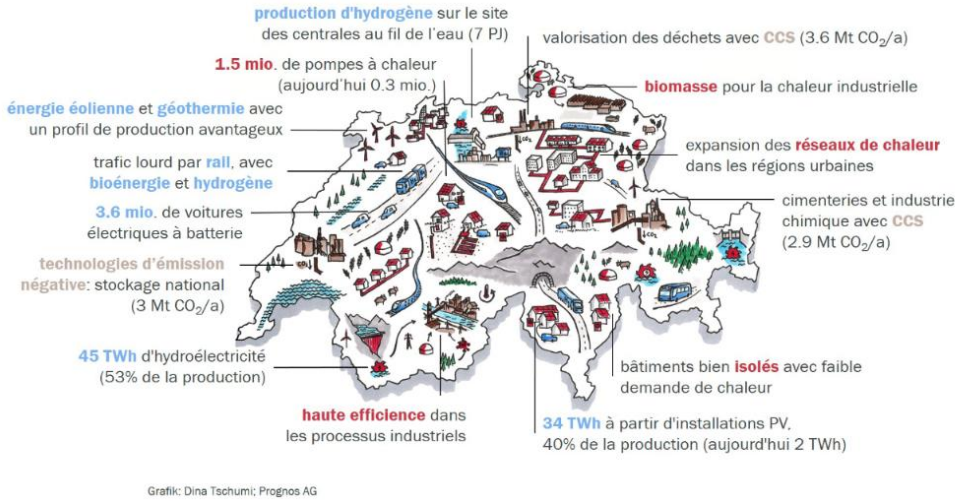

Figure 1.1: Swiss Federal Office of Energy SFOE, Energy Outlook 2050+ Summary Report, November 2020

1.1 Impact of climate change on the energy needs of buildings

The *ClimaBau - BFE 2017 study* ***[3]*** shows that between the "1980-2009" and "2045-2074" periods, the temperature of the Swiss Plateau will rise by an average of 2˚C and (given the current state of energy efficiency) the surface heating requirements (per m^2) of residential buildings will "passively" reduce by 20 to 30% (Fig. 1.2) (excluding domestic hot water, DHW). On the other hand, cooling requirements (air conditioning) will increase exponentially (+48% D-J cold in 2050) to reach half of heating requirements.

Notwithstanding this, the imperative "active" reduction in GHG emissions will certainly involve reducing air conditioning, but above all improving heating efficiency, to achieve an energy reduction in buildings of 40 to 60% by 2050.

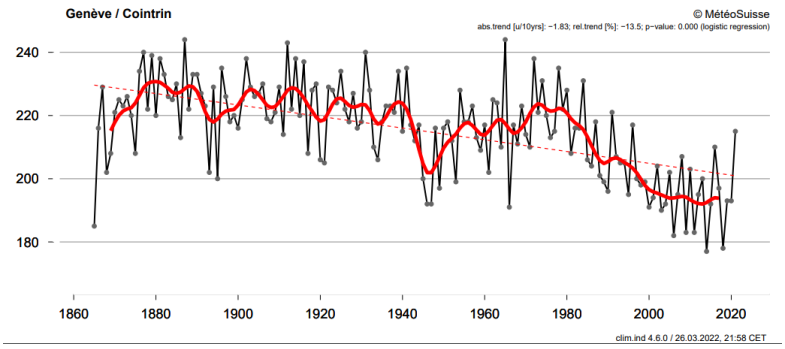

Figure 1.2: Change in the annual number of heating days (NJC_{12}) at Geneva Cointrin from 1866 to 2021: -1.83 D/decade, -13.5%. (Source: MeteoSwiss).

1.2 Energy renovation of buildings (≈ 1/2 of total energy requirements)

Final energy is around 750 PJ/year in 2020 and should fall to around 520 PJ/year in 2050 (according to the Zero-base scenario, fig. 1.3). Overall, it has two equal uses: equivalent "motor" needs (various processes, mobility, transport) and equivalent heat needs (processes, RH & DHW). The main way to improve the energy efficiency of buildings is to improve insulation (which benefits heating and cooling) and to make massive use of Heat Pumps (HP) to provide around **200 PJ/year in 2050** (Fig. 1.3) of final heat for Room Heating (RH) and Domestic Hot Water (DHW) production [**1.2**].

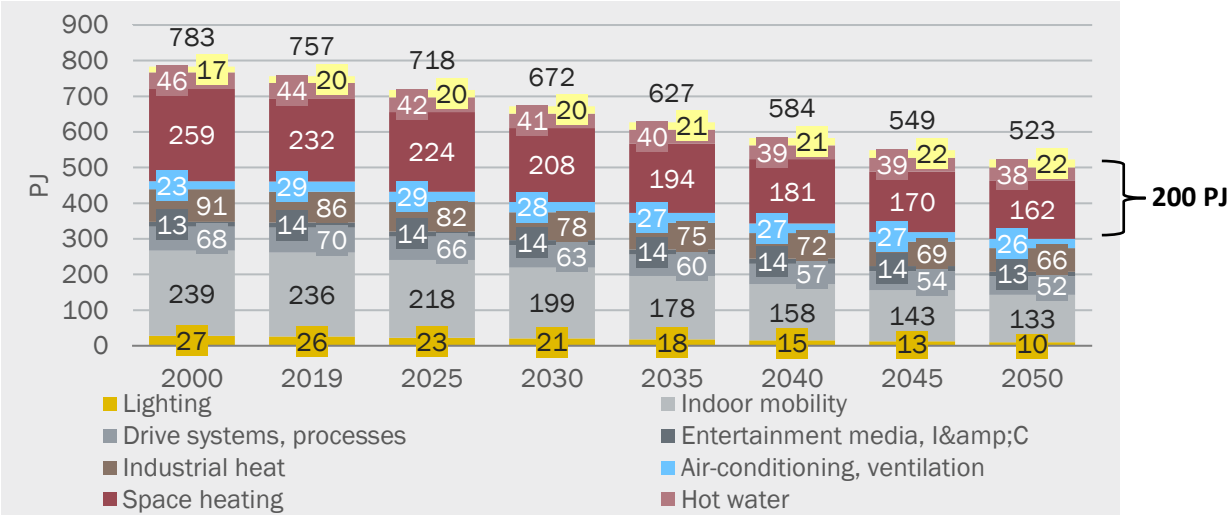

Figure 1.3: Change in final energy consumption by application (domestic consumption excluding consumption by international air traffic, ZERO baseline scenario, in PJ). ***Room Heating and DHW will account for 200 PJ in 2050*** *Source: Prognose AG / TEP Energy GmbH / INFRAS AG 2020* [**1.2**].

Powering these heat pumps will require at least 19 TWh/year (COP = 3). To this will be added 17 TWh/year for electric mobility and 20 TWh/year to replace nuclear power in 2035 (1/3 of national production). In 2050, 39 TWh of renewable electricity will have to be produced in addition to the 45 TWh of hydroelectricity, for an annual consumption of 76 TWh "net" (without pumped storage, Zero-base scenario) [**1.2**].

In order to control electricity consumption, summer air conditioning can first of all make preventive use of passive solar protection, natural night-time ventilation and then free cooling (without a heat pump), as well as "sliding set point" regulation according to the outside temperature, which is more difficult to apply (acceptable) for heating.

1.3 An underestimated key factor:

1.3.1 Annual temperature evolution in the public Drinking Water Network (DWN)

In the current state of the building stock, the production of Domestic Hot Water (DHW) accounts for 1/4 to 1/3, or almost 30%, of the Heat Demand Index (HDI), which is the annual room heating + DHW requirement per m^2 of Energy Reference Area (ERA). In Geneva, HDIs of 600-800 MJ/m^2year are still common, but from 1st September 2022, buildings with HDIs above 450 MJ/m^2year will be required to undergo energy-efficiency upgrades.

In detail, the need for heat for DHW evolves inversely with the (seasonal) temperature of the public Drinking Water Network (DWN). On the Swiss Plateau, the latter evolves sinusoidally with an amplitude of around 10˚C (minimum at 5-6˚C in winter) [**54**]. This winter drop in DWN temperature naturally leads to **a relative doubling (on average vs. summer) of the winter heat requirement for DHW, and even of the electricity consumption of washing machines and dishwashers** (Figure 1.4 below).

In a *High Energy Quality* (HEQ) building, DHW can account for almost half of the HDI and, like washing machines and dishwashers, which use 70-80% of the electricity to heat water, can be significantly affected by seasonal changes in the temperature of the public drinking water network (DWN)!

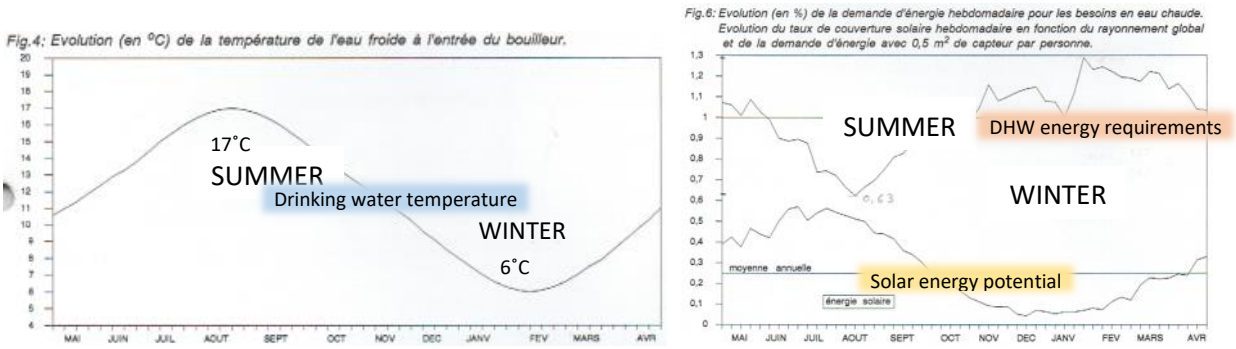

Figure 1.4: Seasonal evolution of the cold-water temperature at the building entrance (Fig. left) and of the energy requirement (Fig. right), for domestic hot water (DHW), measured on several rental buildings (1000 dwellings), for the evaluation of solar installations for DHW preheating. Ville de Genève / Service de l'Energie, June 1990. **[43, 46]**

1.3.2 The changing mix of room heating and domestic hot water

With Global Warming (less cold winters) and the future energy renovation of buildings (reducing specific energy needs), heating needs for room heating (RH) will "doubly" tend to decrease significantly.

On the other hand, those for DHW production will be reduced to a lesser extent, since they are more dependent on user habits (although these may also change). What's more, the strategy for reducing electricity consumption will also involve abandoning electric ambient heating and electric water heating (through the Joule effect) as well as supplying household appliances (washing machines and dishwashers) inevitably with "thermodynamic" DHW production (using a heat pump) and, of course, by solar thermal energy.

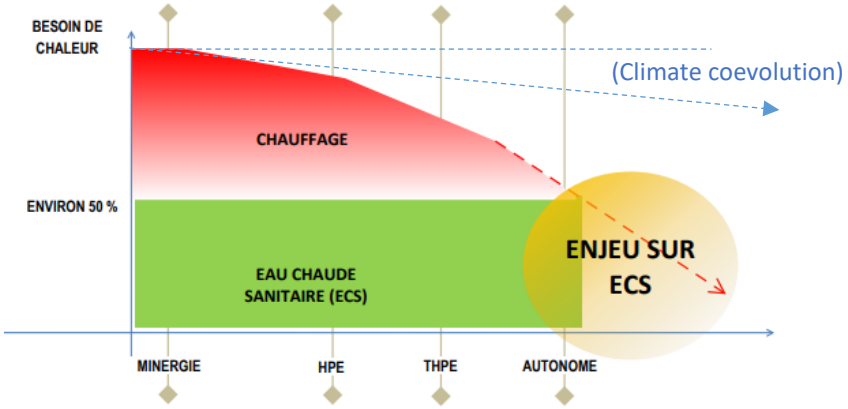

Figure 1.5: Change in the ratio (MixH/W) of heat required for room Heating and domestic hot Water (ECS), as a function of the energy efficiency of buildings (intrinsic performance). Source: Riedweg et Gendre SA

There is therefore a huge challenge or impact on the way domestic hot water (DHW) is produced!

1.4 Renewable energy resources intermittency and storage problems

Local and indigenous renewable energy resources (of solar or primary origin) are mainly biomass, wind, solar-thermal/PV, hydraulic and aerothermal or atmospheric. The latter (atmospheric temperature) is particularly important for air conditioning and heating needs. Because of their production variability, each of these resources has its own specificity, an important one of which is its short- and long-term storage potential to be available on demand.

Electrical energy is the "intermediate vector" (transmission chain), which is of course the preferred energy source, but has limited storage capacity (on a large scale and for a long time, like hydraulic energy). In addition to its storage capacity, hydrogen is also an intermediate energy carrier subject to the efficiency losses of the (long) chain of multiple bidirectional energy transformations (*primary-final-use*)!

In addition to the potential of solar thermal energy storage on surface (basin, reservoir) and bore-loop shallow storage, deep geothermal energy is also a "renewable" source of energy (on a human scale) and, a priori, without *greenhouse gas* (GHG). Geothermal energy deserves to be developed, but requires major forward-looking investments (with risks) and technical precautions to be taken (seismic, aquifer and groundwater pollution, etc.).

1.5 Development of photovoltaic solar energy and wind power

The Swiss Energy Strategy 2050 makes particular provision for the development of photovoltaics (PV), with a specific annual production of 34 TWh, which will require the installation of around 150 km^2 of PV panels (31 GWp), equivalent to 1/4 of the surface area of Lake Geneva, at a cost of CHF 41 billion (*source: AWS scenario (Anreiz WinterStrom): BFE-D-CE6 13401/311*).

Around 1/3 of solar production (PV and thermal) takes place during the winter semester (PV ≈ 11 TWh). The winter stratus over the Swiss Plateau is only partly the cause, even though this Plateau is where most of the roofs available for PV are located and in the immediate vicinity of its final/useful urban use.

Some people therefore estimate a theoretical potential in the Alpine valleys and mountain areas of 30 km^2 of PV installations (the surface area of Lake Brienz), around twice the surface area already installed in Switzerland and 4438 wind turbines ≈ x 100 of the current number, i.e., 4 TWh in 2050, 2/3 of which in winter; this ignores the economic constraint (*source: EPFL-CRYOS/WSL*).

As a result, with the massive development of photovoltaics (PV), the summer surplus (to the additional needs of air conditioning) and the lack of sufficient seasonal intermediate storage, risks leading to the paradoxical and absurd recourse to "*solar peak-sheaving*" to avoid overloading the electricity grid!

Despite the expected increase in the overall need for air conditioning in summer, the demand for electricity in winter will remain proportionally higher (ambient heating, DHW). It will be further exacerbated (in terms of price) by lower availability of photovoltaic (and solar-thermal) energy, as well as by the additional non-renewable (GHG penalty) and temporarily limited share of imported primary energy or electricity.

Switzerland's neighbours are also in the process of "decarbonising", with a similar strategy and a structural (and natural) deficit of winter electricity, so they will have less to sell in this area...

1.6 Switzerland will be short of 9 TWh of electricity in the winter semester 2050

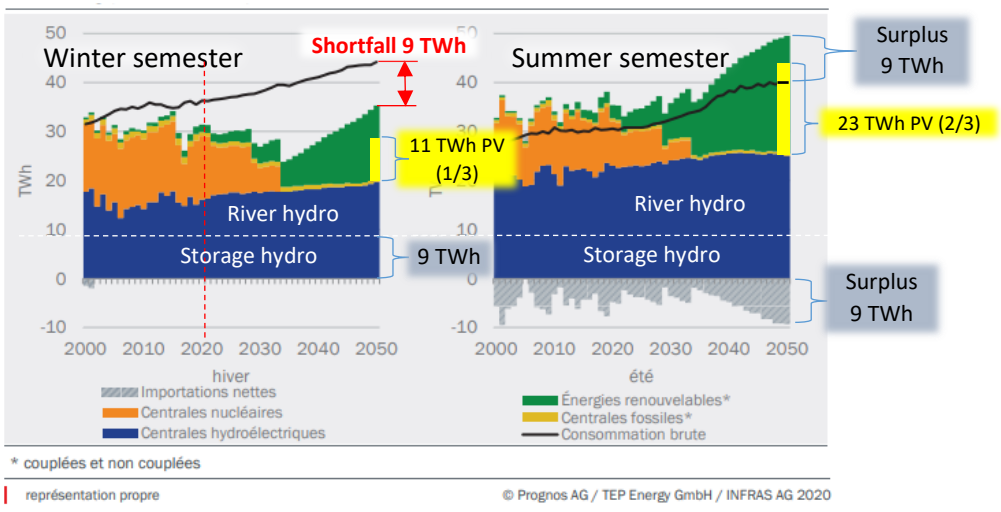

Figure 1.6: Development of gross electricity production during the winter and summer months in the ZERO-baseline scenario, "balanced annual balance" strategic variant in 2050, in TWh (source: SFOE EP2020+)

Out of a winter electricity consumption of 45 TWh in 2050, there will be a deficit of 9 TWh (Fig. 1.6). This corresponds to the total current capacity of Swiss hydroelectric storage dams, with a double annual filling rate, since in 2020 storage power stations produced, in equal parts, 9 TWh in summer and 9 TWh in winter (after deducting storage pumping) [**15**].

1.7 Potential for hydroelectric development

Switzerland has 200 large storage facilities and 222 reservoirs under the supervision of the SFOE.

The total volume of water stored in the dams is 4 billion m^3, for a surface area of 456 km^2 (eq. 4.5% of the volume and 80% of the surface area of Lake Geneva). Simply extrapolating the 6 million m^3 of unreinforced concrete of the Grande Dixence gravity dam, the construction of the dams would have required 50 million m^3 of concrete and/or backfill; not counting the ancillary structures (e.g., digging the feeder tunnels) and the hydroelectric power stations to provide the 9 TWh of electricity in winter.

The potential for developing hydroelectricity would still be between 1 and 3 TWh (SFOE 2012b), or at best 1.5 TWh in the winter semester. This is of the order of the capacity of the Grande Dixence hydroelectric Complex (GDC), which produces 0.5 TWh in summer and 1.5 TWh in winter, or 20% of Switzerland's storage electricity.

To make up the winter shortfall of 9 TWh, the equivalent of 6 GDCs would be needed (6 x 1.5 TWh in winter), each comprising in addition to 3 dams (Ferpècle, Z'Mutt and Grande Dixence), 100 km of adduction tunnels and conduits, the 3 hydroelectric power plants (total installed capacity: 2 TW), transformer stations, and so on. [**16.1**].

Figure 1.7: Grand Dixence gravity dam, 6 million m^3 of unreinforced concrete (source: https://www.swissdams.ch)

At what cost and with how many potential objections and legal arbitration procedures against a backdrop of protected areas? According to a study by the Association of Swiss Electricity Companies (AES/VSE) [**16**], the investment cost of new storage power plants is CHF 4,750/KW, i.e., CHF 9.5 billion for a single unit with a production capacity equivalent to that of the GDC, whereas 6 would be needed for the winter semester!

1.7.1 Impact of Global Warming on hydroelectricity production

As the climate warms up, a number of mountain lakes will be formed (with a total surface area of 50 to 60 km^2 by the end of the 21^e century (source: *Forschungybericht NFP 61, vdf Hochschulverlag AG, 2013*). The expected change in the hydraulic inflow to dams (partly due to the **retreat and disappearance of the glaciers that feed them**) will mean that the increase in storage capacity (including projects to raise the height of existing and new dams) will have to be compensated for by electrical energy to fill them. This will result in an overall drop in "net" hydroelectric productivity (after deducting pumped storage energy: 4.5 TWh, or 11% of "gross" hydroelectric production of 40.6 TWh in 2020). This is still equal to half the current capacity of Swiss dams (*Source: SFOE 2021*).

1.7.2 Maintaining nuclear power would only exacerbate the water stress on rivers caused by global warming.

For technical and economic reasons, a nuclear power plant generally operates as a "ribbon" throughout the year, which means that it also operates during the summer months, apart from planned maintenance shutdowns [**18, 19**]. **The Swiss nuclear power plant at Leibstadt** (1220 MW, 9 TWh/year) is cooled by a semi-closed-circuit "wet" cooling tower. **During the summer months alone, it discharges the equivalent of 2/3 of its "primary" energy (nuclear fuel)** in the **form of vapor using around 14 million m³ of water extracted from the Rhine (0.75 to 1 m³/s).** The Gösgen nuclear power plant (fig. 1.9) is not to be outdone, with almost 10 million m³ of water evaporated from the Aare River over the same period.

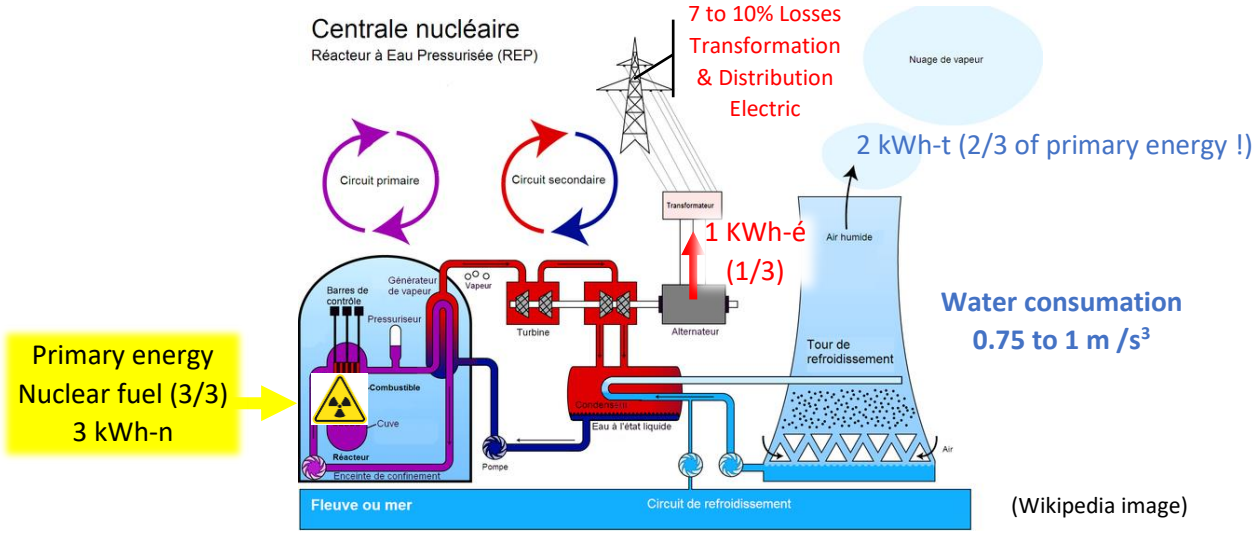

(Wikipedia image)

Figure 1.8: Schematic diagram of a boiling water nuclear power plant/reactor (BWR) and cooled by a cooling tower fed by a river or the sea (semi-closed circuit)

As the summer drought increases, and is exacerbated by more recurrent heatwaves, the increased need for water for other uses (prioritisation), including agriculture, will (already has) become critical. As a result, **thermoelectric power stations (nuclear as well as fossil-fired, coal, fuel oil or gas) that cannot operate without cooling water** (by using their thermal waste in cogeneration) will be forced to shut down or drastically reduce their production in the summer half-year, and will therefore no longer be economically "competitive" and a fortiori less present or available in the winter semester.

Apart from other considerations (financial, security, foreign fuel, nuclear and chemical waste, decommissioning or bacteriological such as **legionella in cooling tower basins** [**19.2**]), France and Germany, our main importers of winter electricity, face the same water problems [**19, 19.1**] and the same climate commitment as Switzerland...

(Wikipedia image)

Figure 1.9: *Gösgen pressurised water nuclear power plant (BWR) on the Aare River (900 MW-é) with its water-vapor plume* ***(0.75 m³/s: 10 million m³ of water taken from the Aare River during the summer semester)***

1.8 Lake hydrothermal resources

1.8.1 Thermal potential (1/3 of national "Cooling" & "Heating" needs)

Switzerland has 171 towns and urban municipalities and almost as many (175) lakes, 15 of which are over 10 km^2 and total 1233 km^2 of surface area with depths often exceeding 60 m. A quarter of Switzerland's population (≈ 9 million inhabitants) is located in the direct vicinity of these 15 large lakes and could potentially be connected to a *low-temperature Thermal Lacustrine Network (TLN)* system *for "cooling" and "heating" needs.*

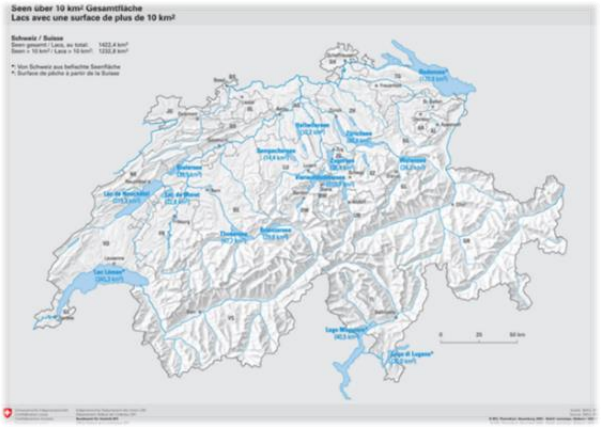

Fig. 1.10: The 15 major Swiss lakes over 10 km²

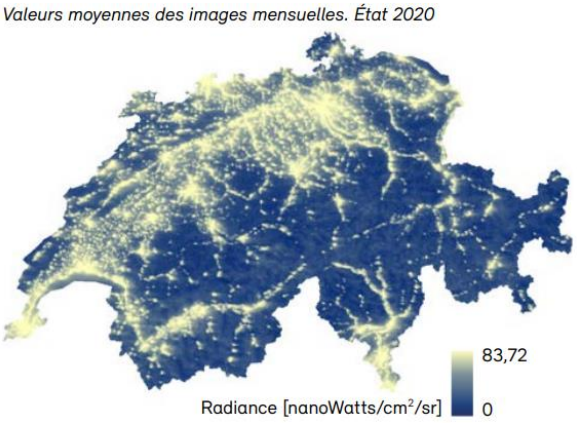

Fig. 1.11: Satellite image of light emissions (2020)

It comes as no surprise to see from the image of light emissions (Fig. 1.11 above) that the majority of the Swiss population lives, works and consumes energy on the Plateau, where the large lakes are also located (Fig. 1.10). *Source: Landscape change © FOEN/WSL 2022*.

According to a study by Eawag and EPFL [**27**], the total demand for final heat around lakes is estimated at 25 PJ of cooling and 135 PJ of heat, i.e., almost 1/3 of current national requirements (70 PJ of cooling & 360 PJ of heat in 2020). Demand around rivers is 37 PJ of cooling and 205 PJ of heat, with some municipalities being assigned to both a lake and a river. The hydrothermal potential of lakes (large circles in figures 1.12 below) identified by Eawag, the Swiss Federal Institute of Technology's water research institute, is several times greater than local demand for cooling and heating. It can be close to the national needs mentioned above. https://thermdis.eawag.ch/fr

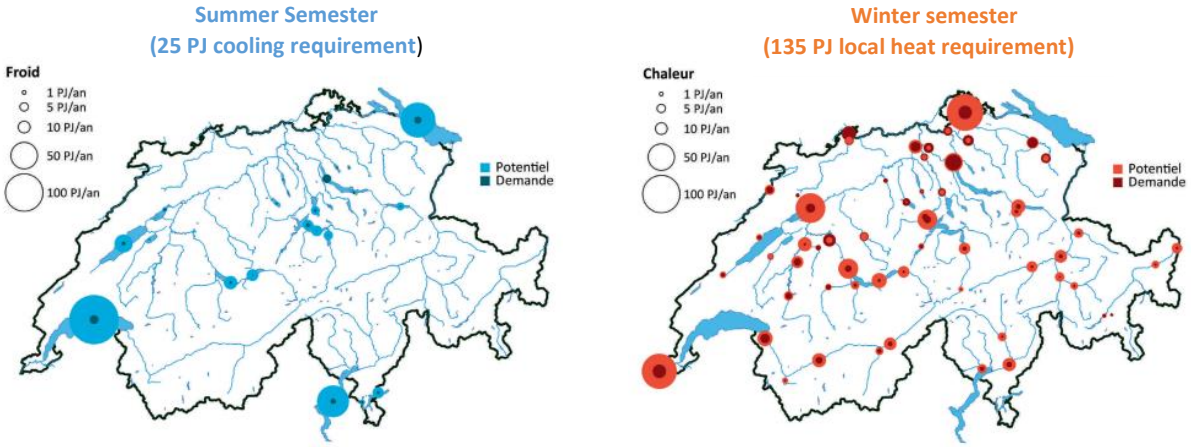

Figure 1.12: Thermal potential & demand of Swiss lakes for heat extraction (winter) and cooling (summer) Source: Thermal use of surface waters A. Gaudard; M. Schmid, Eawag; A. Wüest, Eawag and EPFL, AQUA & GAS N° 6

Since 2021, based on Eawag data, the geo-information service of the Swiss Federal Office of Energy (SFOE) has created a new interactive map showing the heating and cooling potential of Swiss lakes and rivers. https://opendata.swiss/fr/dataset/potenzial-der-seen-und-flusse-fur-warmeentzug-und-warmeeinleitung [**27.1**]

1.8.2 Development of thermal networks

Switzerland's 2050 energy strategy calls for the massive development of district heating and cooling networks. They are designed to supply the corresponding needs, on a large scale and economically, using renewable energy sources and/or waste heat. This is provided that the spatial density of heat demand is sufficient **[12, 13]**. To this end, a charter has been signed by towns, municipalities, cantons and the Confederation with the aim of accelerating the development of thermal networks [**14**].

Residential or administrative buildings are the most suitable for a thermal network, especially at low temperatures that are conducive to the production and distribution of heat energy. An area with a heat density equal to or greater than 700 MWh/y per hectare is considered suitable. These are, of course, the medium and large urban agglomerations, which are clearly visible on the map of Switzerland below.

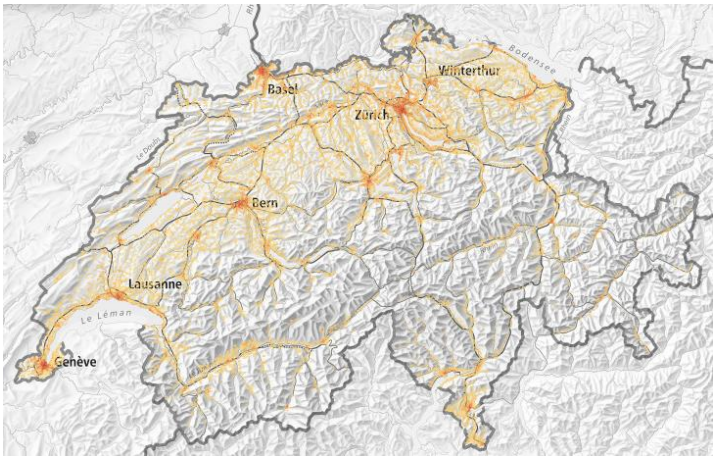

Figure 1.13: Location of heat demand in Switzerland represented as heat density per hectare and highlighted using a colour palette (source: SFOE, Building and Housing Statistics -StatBL- 2014) https://opendata.swiss/fr/dataset/thermische-netze-nachfrage-wohn-und-dienstleistungsgebaude

The potential of district heating and cooling systems (thermal networks) varies from a technical, ecological and economic point of view. The 2014 white paper "*District heating in Switzerland*" shows that the thermal potential far exceeds the heat requirement **[13].**

Source de chaleur	Potentiel thermique technique	Attribution géographique*	Part possible de la chaleur à distance future
Rejets de chaleur de la valorisation des déchets	5,7 TWh/a	3,6 TWh/a	21%
Rejets de chaleur industriels	3,6 TWh/a	Non attribué	Non attribué
Rejets de chaleur des stations d'épuration des eaux usées	7,7 TWh/a	1,9 TWh/a	11%
Utilisation de la chaleur de l'eau souterraine	12,2 TWh/a	1,9 TWh/a	11%
Lacs	97 TWh/a	5,1 TWh/a	29%
Cours d'eau	21,3 TWh/a	1,8 TWh/a	10%
Bois	20,5 TWh/a	1,7 TWh/a	10%
Géothermie	70 TWh/a	1,3 TWh/a	8%
Total	**238 TWh/a**	**17,3 TWh/a**	**100%**

* Des zones présentant un besoin de chaleur élevé au niveau local (densité de raccordement suffisante) ont été attribuées au potentiel technique

CORSAIRE!

ULISSE!

Table 1.14: Technical potential of district heating networks according to the White Paper

It can be seen (**for ULISSE**) that **lakes represent 39% of the total technical potential (29% of the possible share of District Heating, future DH)** but not necessarily ecological and/or economic. The same applies to low-temperature waste heat from Wastewater Treatment Plants (WTPs), which represents 3.2% of the total potential and 11% of the share of district heating that could potentially be exploited via CORSAIRE free heating.

1.8.3 Thermal Lacustrine Networks

Illustrated in Figure 1.15 below, the cooling and heating of buildings near lakes requires Thermal Lacustrine Networks (TLNs) to capture the "heat-carrying" water, transport and distribute it to the urban areas served and finally return it to the lakes in a closed loop.

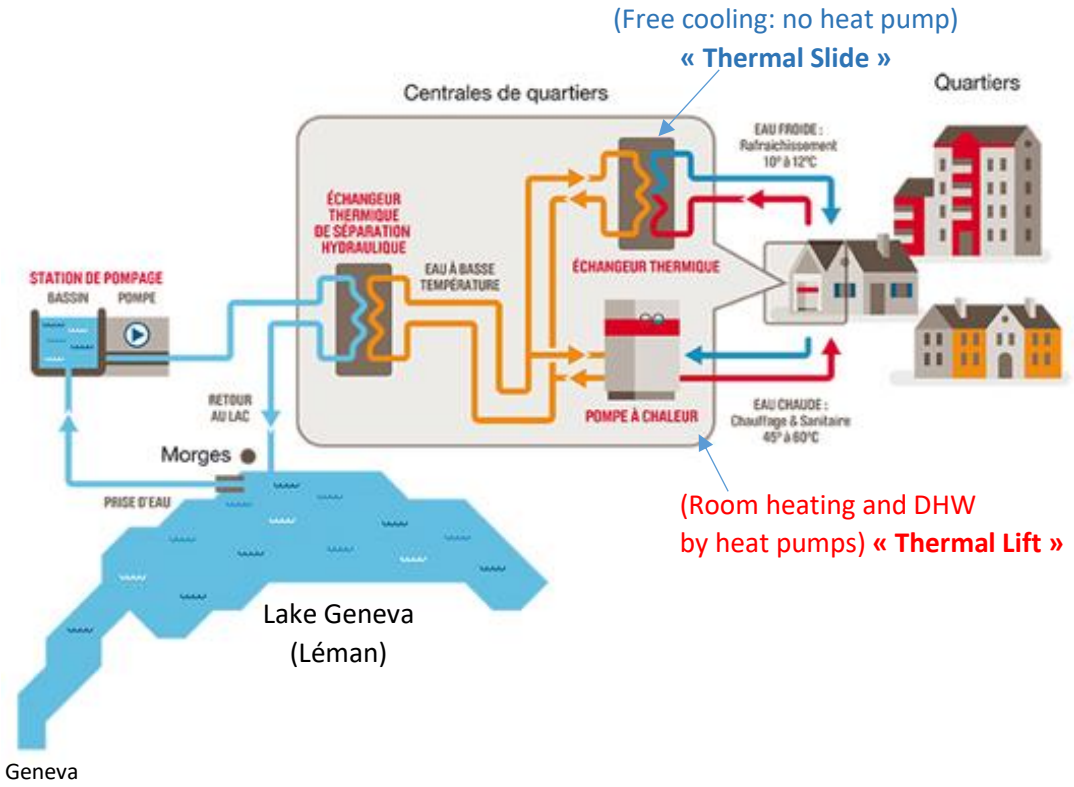

Figure 1.15: Example of a Thermal Lacustrine Network (TLN) with MorgesLac in the town of Morges (VD)

1.8.3.a Seasonal energy performance

TLNs such as those on Lake Geneva (*GLN-GeniLac* in Geneva, *MorgesLac*, EPFL-UNIL, etc.) are very efficient for free cooling in summer (without heat pumps), using cold water (5-7°C) pumped from the bottom of the lake (*Hypolimnion* zone) and acting as a real "***thermal slide***". Its electrical Coefficient of Performance (COP) can reach 18 (GeniLac SIG forecast), i.e., 5.5% of electricity is required to introduce into Lake Geneva the heat energy extracted from the buildings in summer (compared with a COP ≤ 3 for a conventional air conditioner).

On the other hand, winter heating of buildings is 4 to 5 times less efficient than *free cooling in* summer. This is because of the inevitable use of heat pumps to extract heat from the lake and raise its temperature, like a "**thermal lift**", to the level required for Room Heating and DHW production. The winter temperature at which the water is collected from the lakes has a direct impact on the heat pumps' Coefficient of Performance (COP), but also on the exploitable temperature difference (ΔT) between the outward and return flows of the lake water (which is lower than in summer), which also means that the water has to be pumped and circulated in the TLNs. All in all, this contributes to increasing the winter electricity consumption of the TLNs [**7-11, 58, 59**].

In winter, the temperature of the lakes is minimal and almost uniform throughout their depth. What's more, at the bottom they are virtually stable throughout the year. The characteristic thermal cycle begins with an isothermal state in winter, followed by complete or partial mixing towards the end of winter, then stratification from May to October, culminating in summer. This seasonal evolution of temperature is well illustrated by the example of the 4 lakes in figures 1.16 below, where it can be seen that regardless of their size, in summer all the lakes have a thermal difference (ΔT) of around 15K between the top (Epilimnion) and the bottom (Hypolimnion) [**27.1**]. To complete the picture, their volumes and the *Heat Injection Potential and Heat Extraction Potential* for cooling and heating respectively (HIP & HEP in TWh/year) according to Eawag are also given.

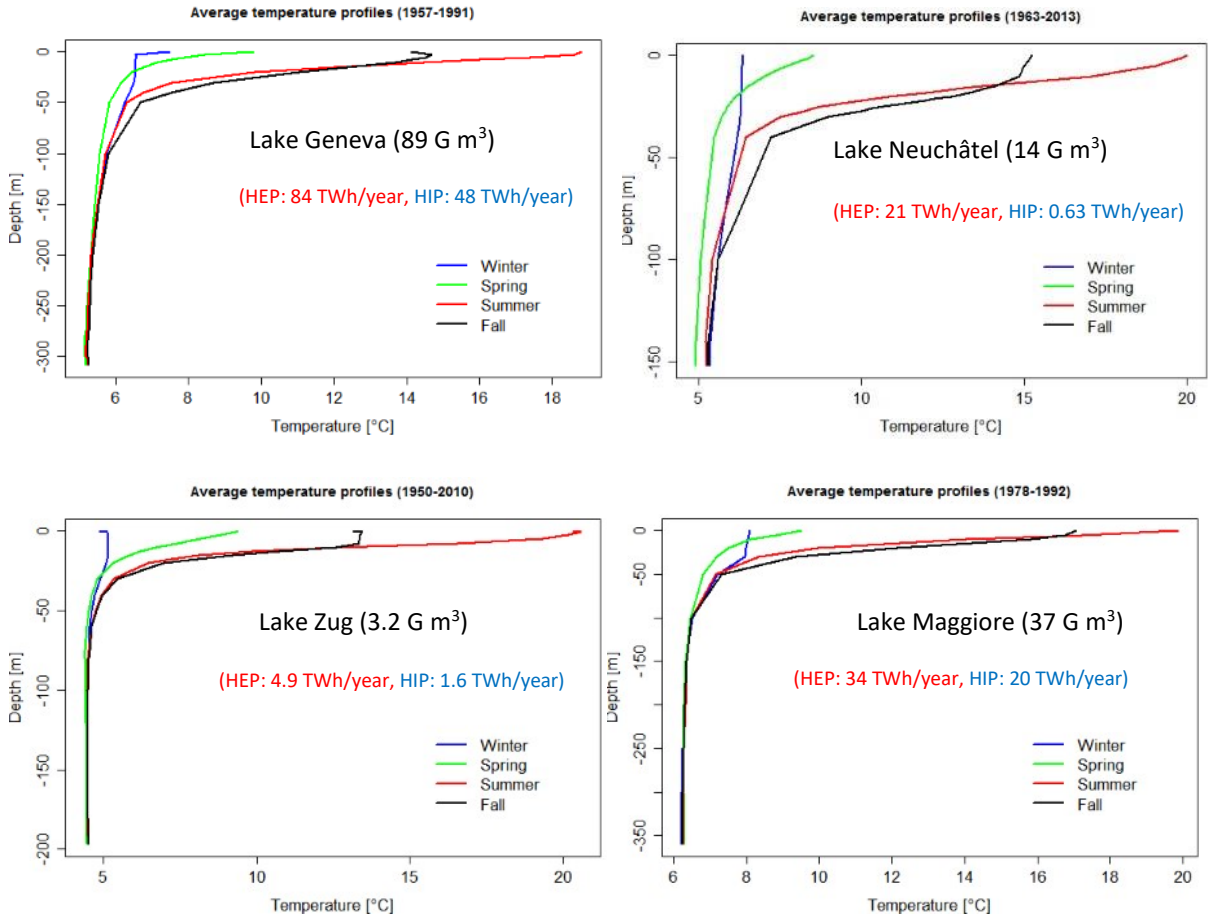

Fig. 1.16: Seasonal temperature trends in 4 lakes as a function of depth (SFOE, Eawag) [**27.1**].

1.8.3.b Environmental limits of thermal exploitation of lakes

As a result of Global Warming, the average surface temperature of our lakes has risen by around two degrees over the last 40 years. As a result of the colder winters, **the warmer surface waters reduce the depth of the annual water mix and therefore the oxygenation vital to aquatic life [27].**

Although the thermal potential of lakes is several times greater than local needs (Table.1.12), in order not to further impact the aquatic ecosystem, thermal use of lakes is limited and regulated (*Federal Water Protection Ordinance, OEaux*), mainly in terms of the depth and temperature of water intake and release.

The maximum change in temperature (ΔT) for heat injection and extraction is 0.5 and 1˚C respectively when the water is returned to the lake [OEaux]. It is intended to avoid increasing the "*Thermocline*" (thermal transition zone) by heating the surface layers (*Epilimnion* zone) in summer (Air Conditioning) or cooling the deep layers (*Hypolimnion*) in autumn and winter (for Ambient Heating and Domestic Hot Water production needs), which can ultimately delay/prevent the said mixing at depth, favourable to reoxygenation and the circulation of nutrients, leading to asphyxiation and eutrophication of the lakes [**27, 31].**

One of the challenges of Switzerland's 2050 Energy Strategy, based above all on an environmental imperative, is therefore to develop the thermal-lake potential for our "cold" and "heat" needs, while PROTECTING our lakes against the harmful effects of Global Warming[1] [**35**]**!**

[1] **https://www.nationalgeographic.fr/environnement/2021/07/le-changement-climatique-asphyxie-les-lacs**

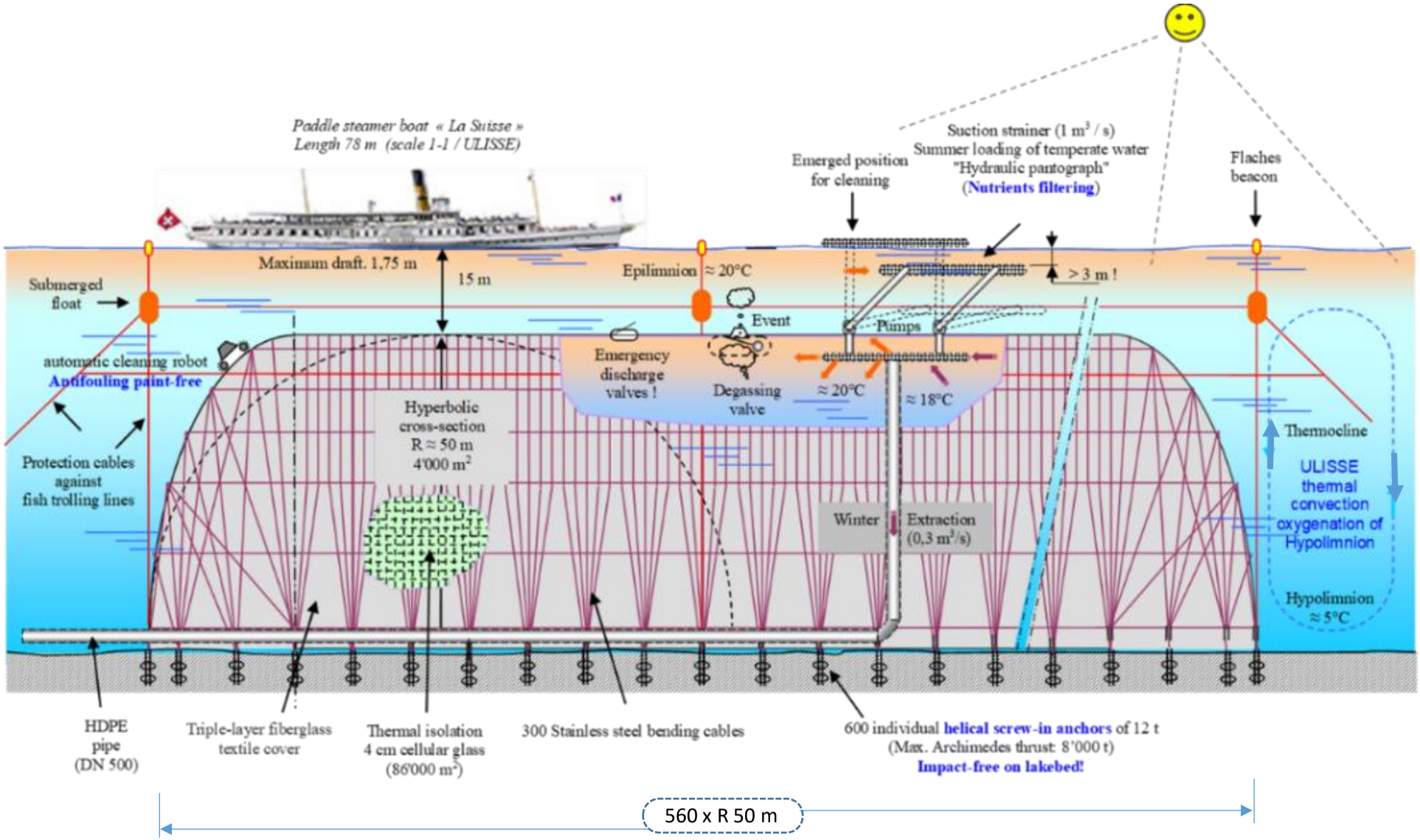

Fig. 2.0: Longitudinal truncated diagram of a typical ULISSE tank of 2 M m³ (CGN ship to scale) The arrangement of the bending and anchoring cables can be significantly different.

2 Summary of the ULISSE combined with CORSAIRE free heating

The exploratory study of the ULISSE-CORSAIRE system is preceded here by the Synthesis and Origin of the overall project, before moving on to the study of its energy impact applied as an example to the GeniLac TLN.

Booster for thermal lacustrine networks

To overcome the limitations of Thermal Lacustrine Networks (TLNs), the ULISSE system proposes firstly to supply a source of winter lake heat at around 20°C, instead of the usual 5-6°C **[54]**. On the one hand, this will double the efficiency of the Heat Pumps (HPs), halving their electricity consumption, and on the other hand, with the increase (x5) in the extractable energy density of the water (J/m^3), it will reduce the flow of circulating water in the TLNs by a factor of 5, which will reduce pressure losses by 96% (1-1/5^2) and therefore also the electrical energy absorbed by the hydraulic pumps.

This ULISSE heat source consists of large tunnel-like Reservoirs (length 560 m x 50 m hyperbolic transverse radius), anchored to the lake bed, with a unit storage volume of 2 million m^3 and a thermal capacity of 125 TJ each. In summer, these ULISSE Reservoirs are charged with tempered water, either from the upper layer of the lake (*Epilimnion*) heated by the sun, or from industrial and air-conditioning waste heat. The charging pumps are powered by photovoltaic electricity, which absorbs summer production peaks from photovoltaic (PV) installations and avoids the need for *peak-shaving* **[17.2]**.

Free Heating CORSAIRE of the public Drinking Water Network

The second way of using the tempered water supplied by the ULISSE Reservoirs or other thermal waste is to correct (by 5 to 10˚C) the winter drop in temperature in the public Drinking Water Networks (DWN) using the CORSAIRE *free heating* process (without a heat pump). All DWNs are potentially concerned by "free heating", which can supply 30% of the heat for domestic hot water (DHW), reduce the electricity consumption of washing machines/dryers connected to the DHW and increase the electrical efficiency of the TLNs **[42 to 52]**.

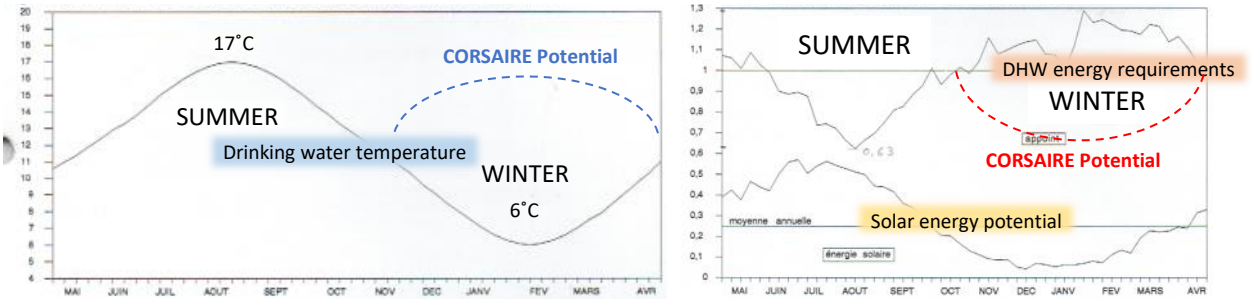

Figure 2.1: Potential and impact of correcting the DWN's winter temperature drop via CORSAIRE free heating.

National potential

The ULISSE concept/project, with around 300 Reservoirs distributed invisibly across the 15 major Swiss lakes and in association with the CORSAIRE *free heating system* (including outside the lake regions), could supply almost 60 PJ or 30% of the 200 PJ of national energy-heat requirements for room heating and domestic hot water. This would save 3 TWh of gross electricity in the winter semester (1/3 of the 9 TWh winter electricity deficit or the equivalent of twice the winter semester production of the Grande Dixence hydroelectric complex: 1.5 TWh).

Environmental impacts (Lake protection against Global Warming)

External convection currents, induced by heat loss through the biocompatible envelope (textile-and cellular-glass) of ULISSE Reservoirs, can improve the circulation of nutrients and oxygenation of the lake bed, protecting the aquatic ecosystem against eutrophication and Global Warming. The presence of reservoirs can create ecological niches that are protected from fishing, thereby encouraging the development of aquatic fauna. Selective capture (filtration of phytoplankton) would make it possible to regulate blooms (toxic algal blooms) if necessary, and to recover greenhouse gases and CH_4 (energy use). Containing the heat captured in the reservoirs would lower the lake's surface temperature, reduce water loss through evaporation and further increase the oxygen dissolved in the water **[20 - 34]**.

2.1 Origin of the ULISSE and CORSAIRE project - *and state of the art*

• **Following the 1992 Rio Conference (UNCED)**, on October 20, 1992, the author proposed to local authorities the **VERTCAD project of "*Exegetical Valorisation of Thermal Waste for District Heating*"**, involving sources from CERN and industrial installations in the Canton of Geneva and neighbouring France. **Compared to traditional thermal networks with superheated water (130˚C), it is an avant-garde concept of a medium to low temperature thermal network** and on the regional scale of "*Grand Genève*" or the *Agglomeration Franco-Valdo-Genevoise*. However, with the exception of the Director General of CERN at the time, the Nobel Prize winner Carlo Rubbia, this project was received "freshly", notably on the grounds that it would be necessary to "open" 1 street out of 2 in Geneva to connect the buildings to this low temperature District Heating network (Fig. 2.2) …

Un ingénieur veut chauffer Genève avec de l'énergie gaspillée

William van Sprolant affirme pouvoir le faire en utilisant notamment les rejets thermiques du Cern et des Cheneviers

27 TRIBUNE DE GENEVE LUNDI 30 NOVEMBRE 1992

GENEVE

Un ingénieur belge veut chauffer Genève «à distance» en récupérant les formidables quantités de chaleur «perdues» du Cern et de l'usine d'incinération des Cheneviers. Un projet mammouth qui inclut la transformation des usines hydroélectriques de Verbois et de Génissiat (près de Bellegarde) pour qu'elles tournent à plein régime, même en hiver lorsque le débit du Rhône est faible. Chasse au gaspi ou simple folie d'un inventeur? Un peu des deux. Le Cern se dit «intéressé» mais doute de la faisabilité du projet de William van Sprolant, ingénieur ETS qui, bien que travaillant au Cern, a réalisé son étude sur une base strictement personnelle.

Les aimants géants des accélérateurs de particules dégagent une importante chaleur dont une bonne partie s'évanouit dans la nature. Le constat n'est pas nouveau. En 1988, on a cultivé des tomates dans des serres spéciales chauffées grâce aux rejets du Cern. Mais les fruits et légumes revenaient trop chers et l'expérience fut abandonnée. Le Cern continue d'éliminer à perte des millions de tonnes d'eau de 35 à 85 degrés dont la puissance thermique est évaluée à 225 Mégawatts (MW). A titre de comparaison la centrale thermique du Lignon qui chauffe 2380 appartements dispose d'une puissance de 130 MW, mais avec l'avantage de fournir de l'eau à 130 degrés.

Partant de ce constat, William van Sprolant a imaginé un projet infiniment plus audacieux: un gigantesque système de chauffage à distance pour l'équivalent de 300 000 habitants (bureaux, halles, habitations...) de la région genevoise, Palexpo et aéroport compris. Objectif: économiser quelque 100 000 tonnes d'équivalent pétrole par année et se chauffer plus «propre». Les brûleurs à mazout collectifs passeraient progressivement à la casse au profit d'un réseau de plusieurs centaines de kilomètres de tuyauterie qui irrigueraient les quartiers d'une eau chaude en bonne partie recyclée.

W. van Sprolant. Service

Voici les principes du projet:

● En été le Cern pale l'énergie environ trois fois moins cher qu'en hiver. Raison pour laquelle il est à l'arrêt pendant deux mois et demi de grand froid. Il fonctionnerait donc enfin en hiver, période où sa chaleur excédentaire est utile et commercialisable.

● Les usines hydro-électriques de Verbois et Génissiat qui fonctionnent au ralenti en raison du faible débit du Rhône en hiver seront couplées à des centrales gaz-vapeur. Elles pourront alors pourvoir à l'importante consommation des accélérateurs du Cern. W. van Sprolant a déposé un brevet pour ce «couplage» original entre les deux types de centrales.

● L'usine d'incinération des Cheneviers, pièce maîtresse du projet, serait également branchée sur le réseau de chauffage.

● Un ancien accélérateur (ISR) du Cern serait utilisé comme réservoir d'eau chaude pour faire face aux fluctuations de consommation.

● L'eau chaude provenant de ces diverses sources serait distribuée par deux canaux principaux. 1. Une croix de tuyauterie Cern-Annemasse-Versoix-Saint-Julien. 2. Des conduites disposées dans l'accélérateur du LEP «irrigueraient» des localités situées dans l'Ain.

● L'ingénieur estime, calculs à l'appui et pertes déduites, que ce système fournirait 2400 Giga-Watts/heure dont un quart environ proviendrait du Cern, moins de la moitié (1000 GWH) des Cheneviers et le reste de Génissiat et Verbois.

Pierre Ruetschi □

Contestations autour du projet

Au tarif moyen de 60 francs le MWH défini par les Services industriels, les divers exploitants du réseau pourraient facturer un total de 146,45 millions de francs. Cela sera-t-il suffisant pour amortir l'investissement? Van Sprolant y croit, mais sans avoir chiffré le prix de son dessein. Hans Hoffmann, directeur technique du Cern, est plus que sceptique: «Le projet présente des difficultés techniques, mais celles-ci sont toujours surmontables. On peut fabriquer une maison totalement autarcique sur le plan de l'énergie. Reste à savoir à quel prix. Nous sommes prêts à étudier le projet avec son auteur, mais il faut garder les pieds sur terre.»

Du côté des Services industriels de Genève (SIG), Gabriel Blondin n'est pas moins dubitatif, vu les bouleversements considérables que suppose le projet: «Il présente des incohérences techniques. A commencer par l'utilisation d'eau chauffée à des températures trop basses. Le système de chauffage à distance qui date de 1966 et alimente aujourd'hui 2380 appartements dans le secteur du Lignon montre qu'il faut 130 degrés.» Le fait qu'il faudrait éventrer une rue sur deux pour poser la tuyauterie ne fait que renforcer ses doutes. Reste qu'à une moindre échelle, les SIG sont favorables à une extension du chauffage à distance à Genève. Le projet des Cheneviers longuement élaboré et qui prévoit d'alimenter quelque 20 000 habitants grâce aux ordures brûlées est actuellement entre les mains du Conseil d'Etat. Inutile de dire qu'il a quelques longueurs d'avance sur celui de van Sprolant. Ce dernier reconnaît que son travail, résumé dans un document de 180 pages, est loin d'être achevé: «J'ai voulu lancer le débat. Mon espoir est que l'on me donne les moyens de réaliser une étude de faisabilité complète du projet.»

P. R. □

UN CHAUFFAGE À L'ÉCHELLE DE LA RÉGION

Fig. 2.2: Proposal for the Franco-Geneva cross-border project VERTCAD (Exegetical Valorization of waste heat for Low Temperature District Heating Network), article by Pierre Ruetschi, Tribune de Genève, November 30, 1992.

•To circumvent the above objections, the subject of the author's EPFL master's thesis (1995) was the use of waste heat from CERN (700 GWh thermal or 2.5 PJ) in the **winter correction of the temperature (ΔT: 5 to 10°C) of the (existing) Drinking Water Network in the canton of Geneva (*CORSAIRE free heating*), without any new district heating network [43].** Without seasonal heat storage, the waste heat would have to be mostly produced and availably during the winter semester, and therefore implies the restrictive summer displacement of the annual *shutdown of* CERN's accelerators and experiments.

• As an alternative of this latest restriction, the author then proposed a complementary ***Seasonal Lacustrine Heat Storage* (SLHS)** to recover the warm cooling water from CERN during the summer semester and use it during the heating season (when CERN is normally in *shutdown*). A precursor of the ULISSE project, the author presented (summarily) this extended concept (Fig. 2.3 below) at the 10^{em} *General Conference of the European Physical Society* (EPS 10 *Trends in Physics*) in Sevilla, Spain, September 1996. **[44]**

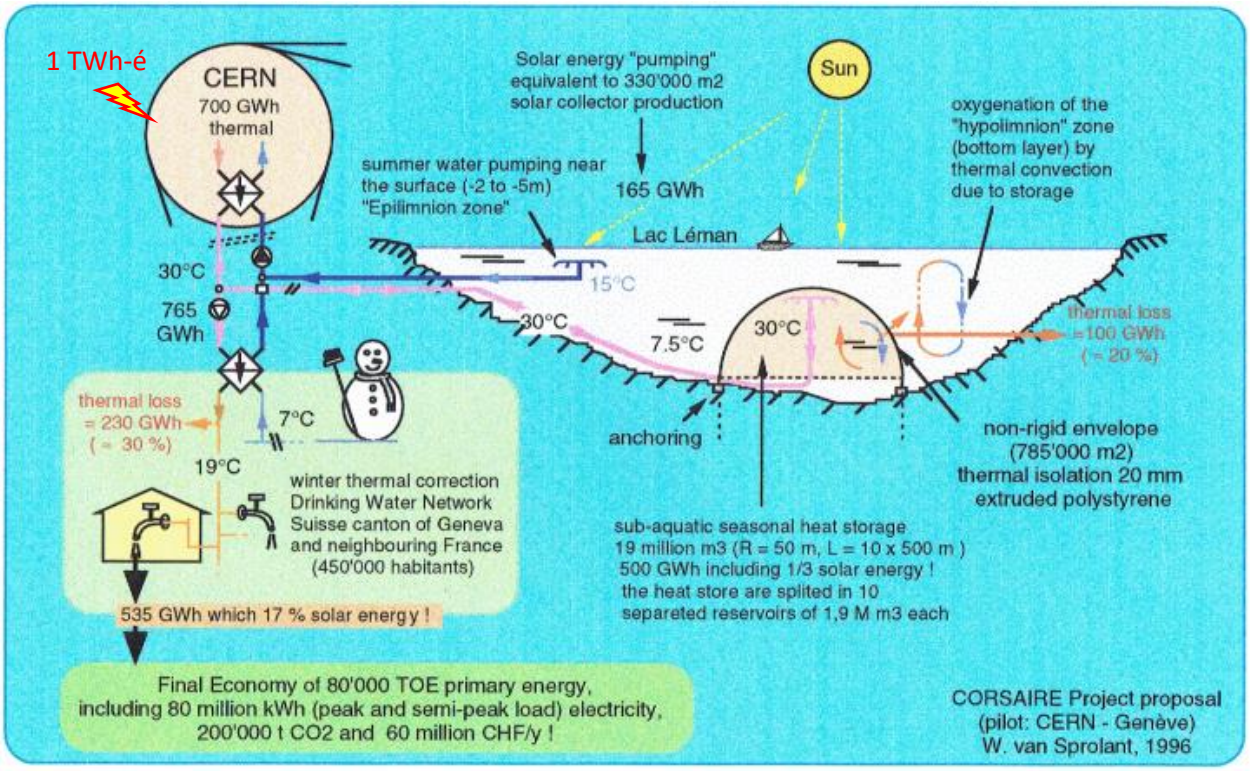

Figure 2.3: Addition of the SLHS to the study of the recovery of CERN's thermal waste (EPFL master's thesis 1995)
Contribution on the EPS 10 Trends in Physics, 10th General conference of the European Physical Society, Sevilla 1996

The basic study in question (EPFL master's work 1995) of the CORSAIRE concept/project, of "free heating" (without a heat pump) of the Public Drinking Water Network (REP), shows an energy saving potential which can reach 10% of the IDC of residential buildings on the scale of an entire city, given the current state of their renovation and without any additional intervention or equipment on the buildings [65]!

• At the instigation of the *Office Cantonal de l'ENergie* (OCEN), **the CORSAIRE project was included in the Canton of Geneva's Energy Master Plan (2001-2005)**, and in November 2005, under the supervision of the project's initial author and financed by the OCEN, part -1 of the multidisciplinary impact study began on a pilot residential building made available by the City of Geneva **[46]**. Alas, 3 months after it began, the study was abruptly halted, due to an unforeseen budget cut by the OCEN! Since then, the project has never been reconsidered, despite Geneva's ambitious energy objective (a *2000 W nuclear-free society by 2050*)!

• Meanwhile, **since 2006, the CORSAIRE principle has been used (in summer) in the Canadian city of Toronto** (3 million inhabitants, 1/3 the size of Switzerland) with its "*Deep* Lake *Water Cooling*" (DLWC). With a cooling capacity of 360 MW, the thermal energy extracted from the air conditioning is injected into Toronto's public drinking water network via a battery of heat exchangers (fig. 2.4), in the same way as the CORSAIRE free heating process but in summer! **[51, 52, 53]**

Toronto's DLWC on Lake Ontario has one of the world's largest thermo-lacustrine air-conditioning systems. Similar to the TLN GeniLac network in Geneva, thanks to free cooling it saves 90 GWh of electricity and 1 million m^3 of water a year, compared with compression and wastewater refrigeration machines (electricity savings ≈ 80%, source Enwave). **[51, 52, 53]**

However, in seasonal contrast to CORSAIRE free heating in the winter semester, the heat from the DLWC system's is used to "deglaze" ($\Delta T \approx 8$ K) 1/4 of the City of Toronto's drinking water network in summer, witch finally avoids dumping the waste heat from the air conditioning into Lake Ontario.

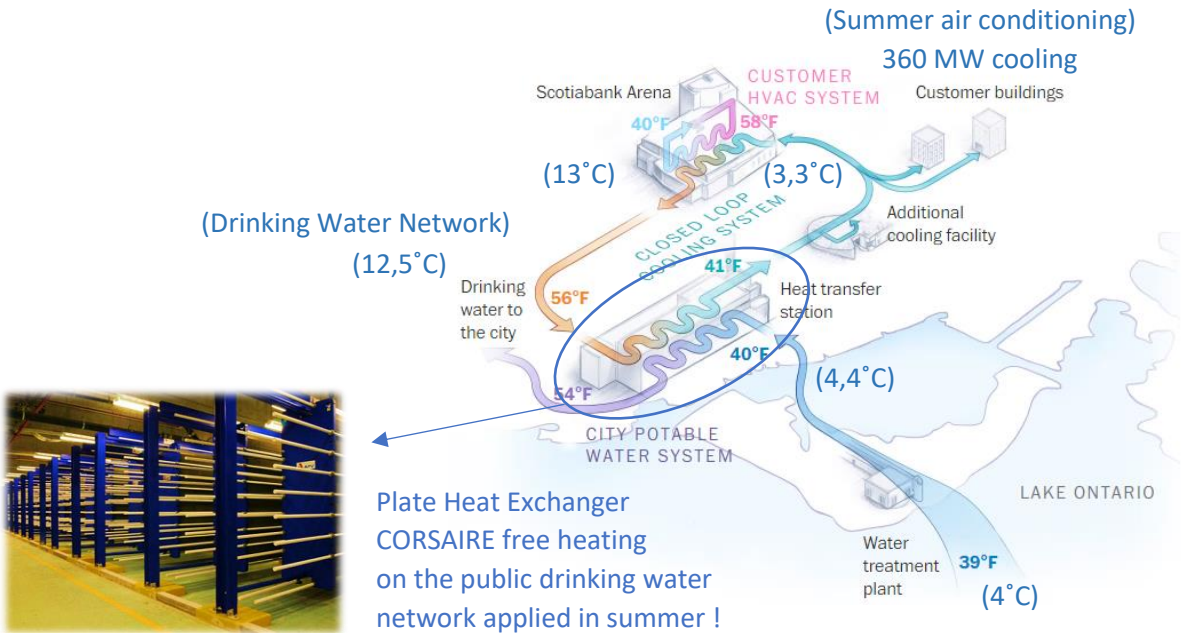

Figure 2.4: Schematic diagram of the lake cooling system in Toronto (2006),
with thermal energy injected into the public drinking water network via a heat exchanger (source: Enwave)

• **Finally, in 2021, the author proposed the ULISSE project** in response to the SFOE's SOUR 1-2021 call for projects and received initial financial support from the SFOE for this exploratory study of the ULISSE project.

2.2 Precursor to a floating lake thermal reservoir

In 1980 the Swedish designer P. Margen suggested a hot water tank (90˚C) floating on the surface of a lake or the sea (figure 2.5 below). This tank consists of a thermally insulated rigid caisson, open at the base and fitted with floating pontoons, all securely lashed with cables to anchor blocks. The caisson emerges variably above the surface of the body of water depending on the quantity and temperature of the water in the caisson (0.5 m at 90˚C). **[36, 37]**

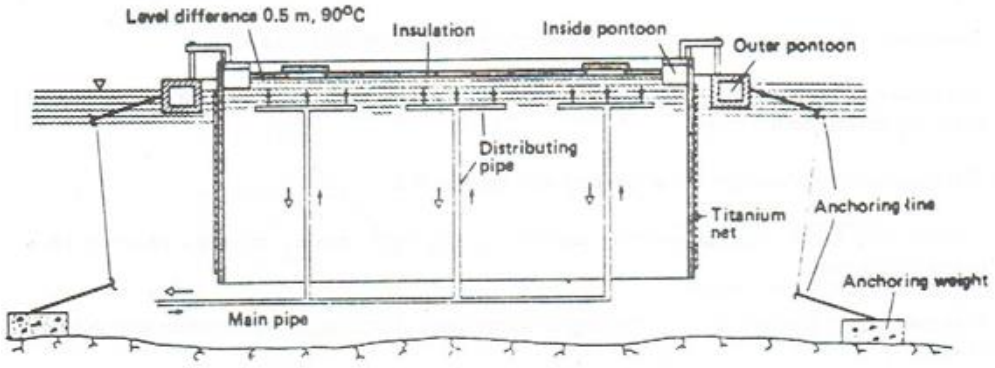

Figure 2.5: Swedish designer P. Margen's proposal for a floating hot water tank (1980),
*Source: SIA OFEN 1987, Guide to Seasonal Heat Storage, J-C. Hadorn **[37]***

Potential sites should be very limited. Not only would local residents not appreciate the visual impact on the landscape, but **this device emerging from the water like an iceberg in a variable manner would constitute an unacceptably high hazard to shipping**. More, this floating structure would be subject to wave action, which could destabilise and tear it apart in the event of strong winds or storms (waves in Lake Geneva can reach 2 m).

The installation of such a structure, which would be difficult to install in shallow waters, would be unavoidably confined to the coastal or littoral zone (*lake shore*), where a large part of the flora (seagrass beds) and fauna of the lake are located. The latter would be in direct potential contact with scalding water, which could also be expelled from the caisson by the eddies and movements generated by strong winds...

2.3 Organisation of the ULISSE exploratory study (SOUR)

As a reminder, the 3 main objectives of the ULISSE concept associated with CORSAIRE are:

1) Improve the electrical efficiency of TLN networks potentially located in the 15 large Swiss lakes,
2) To protect the lakes concerned against Global Warming using ULISSE Reservoirs,
3) Reduce the negative energy impact of the winter temperature drop in the public DWN (CORSAIRE).

As part of the SFOE's SOUR programme, the exploratory study of the ULISSE project carried out at HEPIA includes the following points:

- Analysis of the situation and the challenge of the Swiss Energy Strategy 2050,
- Proposal and summary of the ULISSE system associated with the CORSAIRE free heating system, background (origin) and state of the art,
- Structural study, material composition and operation of the ULISSE Reservoir,
- Carrying out resistance tests on cellular glass (FOAMGLAS) under hydrostatic pressure,
- Energy analysis of the ULISSE - CORSAIRE combined system on the GeniLac TLN and Geneva's DWN,
- Extrapolation of GeniLac results to the national level,
- Technical and economic comparison with alternative thermal networks, fed by solar thermal collectors and an earth basin for seasonal heat storage,
- Exploring the potential environmental impacts of lakes hosting ULISSE Reservoirs.

More specifically, establishing the seasonal storage efficiency of the ULISSE Reservoir involves the following points:

- Analysis of the heat transfer coefficient of the ULISSE Reservoir shell,
- Creation of an experimental Mock-up to reproduce the various operating phases,
- Establishment of *the Temporal Scale Factor (TSF)* between the real full-scale Reservoir and the reduced-scale Mock-up.

In addition, heat losses are calculated using 3 complementary approaches:

- 1. calculations based on a simplified theoretical model of the Mock-up and the full-scale Reservoir,
- 2 Calculations based on data acquired by the Mock-up Experiment,
- 3. numerical simulation (COMSOL Multiphysics) of the Mock-up and the real full-scale Reservoir.

Finally, the study proposes a sequel (Next Step) with two Pilots and Demonstrations of the ULISSE and CORSAIRE systems.

3 The Geneva Thermal Lacustrine Networks GLN and GeniLac

The "Genève-Lac-Nation" (GLN) system is a low-temperature Thermal Lacustrine Network (TLN) using water from Lake Geneva and 100% renewable electricity. It mainly provides cooling (80% = 20 GWh/y) and heating (20% = 5 GWh/y) for international organisations, schools and collective housing in Geneva. Following its success, Service Industrielles de Genève (SIG) is currently building a "x 10" extension (GeniLac) to the city centre and airport area (fig. 3.1).

The water is drawn from the Lake Geneva at a depth of 45 metres, at a temperature of around 7°C in summer and 5°C in winter. It is then conveyed to a lake pumping station (LPS "Vengeron"), passes through a heat exchanger (only for the airport sector in a semi-closed loop), and is then transported through underground and lake pipes to the connected buildings. The water containing the heat extracted from the buildings is then returned to the lake and the Rhône downstream at a temperature of around 12°C. This free-cooling system (without heat pumps), with a Coefficient of system Performance (COPsys) of 18 (advertised by SIG), reduces the summer electricity consumption by 70 GWh, or 80% compared with conventional air-conditioning systems (reversed heat pumps) operating with an average COP of 2.8.

The GeniLac TLN network will also enable the connected buildings to be heated using Heat Pumps (HP) instead of existing fossil-fuel boilers. By 2035, GeniLac will reduce CO_2 emissions in Geneva by 70,000 tonnes a year. [**7, 8, 9, 10, 11**]

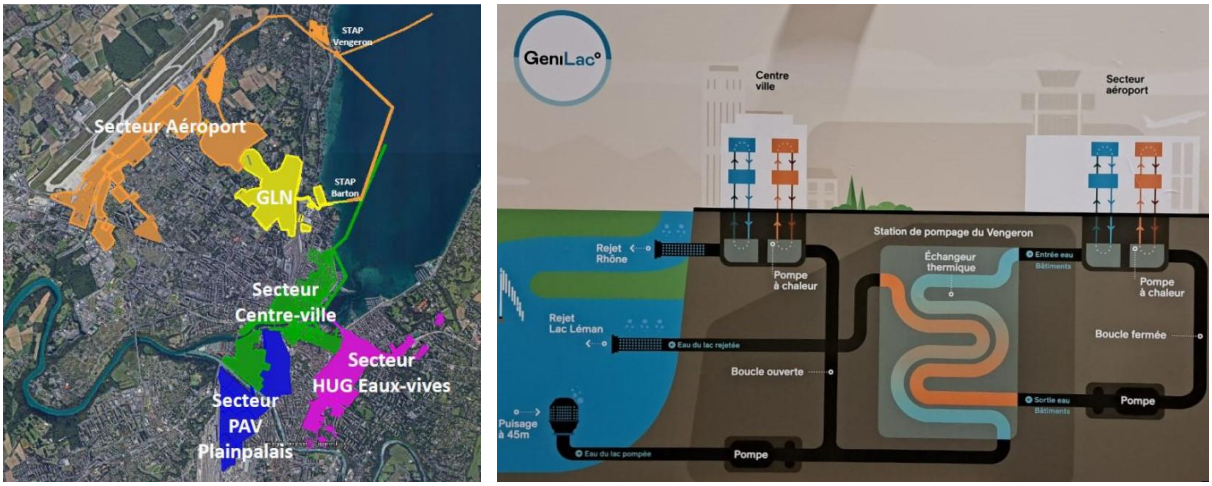

Figure 3.1: Schematic diagram of the GeniLac cooling and district heating system with Lake Geneva (Source: SIG)

3.1 Impacts of lake water temperature

As described above, summer cooling of the buildings using *free cooling* (without a heat pump) is very effective, with water at around 7-8°C pumped from the bottom of the lake (hypolimnion zone) and returned to the lake at around 12-13°C. The temperature differential between pumping and return ΔT is around 5 K or even more, depending on the epilimnion zone and the dispersion of the discharge. The ratio (COP) between the cold energy supplied and the electricity used to pump the lake water is announced at 18!

On the other hand, in general, extracting heat from the lake for winter heating is more complex and less efficient, mainly due to the reduction in the temperature difference available from the lake (ΔT ≈ 3 K), which is then reduced by half to a third compared with summer, as well as the impact on the efficiency of the heat pumps.

3.1.2 Hydraulic impact (volume of lake water)

For winter thermal power to be extracted from the lake, the smaller temperature difference between winter and summer (ΔT: 3K vs. 5K) implies an inversely proportional increase in the volume of water pumped and circulated. This results in pressure losses that are proportional (squared) to the flow rate and a corresponding increase in the energy absorbed by the hydraulic pumps. Their annual electricity consumption represents 1/4 of the total, including that of the heat pumps. Added to this is a proportion of gravitational energy linked to the difference in level between the lake and the network which is not fully recovered by turbine the water as it returns to the lake.

This explains, for the most part, the efficiency and predominance of summer cooling over winter heating via a conventional Lake Thermal Network. The typological ratio of connected buildings (ratio of cooling to heating) for GLN, for example, is 4, while that of its extension, GeniLac, is 0.9, i.e., practically in balance with heating or in equal parts.

3.1.3 Thermodynamic impact (COP of heat pumps)

On the other hand, the low ΔT in winter has a negative impact on the performance of *heat* pumps for heating and can even lead to the risk of frost. Represented by the diagram in figure 3.2 below, the Coefficient of Performance (COP) of a heat pump is the ratio between the "useful" heat energy supplied |Q| (heating Qc or cooling Qf) and the electrical energy absorbed W (Work) by the heat pump compressor and/or circulation pump, to transfer the heat energy between the said "cold source" and the said "hot source".

$$\mathbf{COP = |Q| / W} \qquad (1)$$

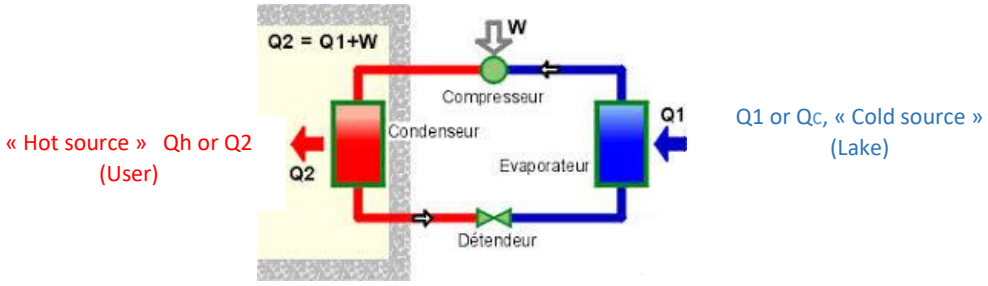

Figure 3.2: Thermodynamic schematic diagram of a heat pump in "heating" mode (Wikipedia image)

In the case of a conventional refrigeration or air-conditioning machine (with a thermodynamic fluid compression/expansion cycle), the Evaporator is inside the room (User) and the Condenser outside, in this case on the Lake side. For heating, it's the other way round.

According to the 1ère (conservation) and 2eme (reversibility) laws of thermodynamics, we can define that:

(Q2) or Qh = Qc + W => W = Qh - Qc (2)

Theoretical heating COP-h = Qh / Wh => Qh / (Qh - Qc) => Th / (Th - Tc) (3)

Theoretical cooling COP-c = Qc / Wf => Qc / (Qh - Qc) => Tc/ (Th - Tc) (4)

COP-heating = COP-cooling + 1 (5)

Th (>) Tc are the absolute temperatures (K) of the corresponding sources.
The theoretical heating COP-h, [Th / (Th - Tc)], is also known as the thermodynamic *Carnot Factor* (CAF).

However, the real COP is lower than the theoretical and is the product of the unavoidable thermodynamic Carnot factor and the technical efficiency η_{hp} of the heat pump:

Real COP = Theoretical COP * η_{hp} or CAF* η_{hp} (6)

The technical efficiency η_{hp}, which is of the order of 40 to 60%, depends on the design features of the heat pump, including:

- the surface area and transfer coefficient of the heat exchangers, which influence the temperature drops (pinches) between the water in the inlet circuit (evaporator) and outlet circuit (condenser) and those of the heat pump's internal thermodynamic fluid, which ultimately has a direct influence on the CAF,
- and the efficiency of the compressor and its electric drive motor.

As soon as the energy from the network external to the heat pump (pumps, parasitic heat exchange from the network, etc.) is included, it is no longer just the COP of the heat pump (COPhp) but that of the entire system (COPsys).

The COP is therefore directly influenced by the temperature of the said *cold source*, in this case for GeniLac that of the water from Lake Geneva taken at a depth of 45 m (hypolimnion zone), with a relatively stable temperature throughout the year (5 to 8°C, with an average of 6.5°C). However, the temperature at the water intake can be

subject to sudden variations. This phenomenon has been observed (Fig. 3.3) by the SIG on the GLN network (water capture at -35 m) during the unexpected overturning (stirring) of Petit-Lac Léman in mid-season on days of heavy rainfall, when the temperature at the water intake suddenly drops from a minimum of 5°C to a maximum of 17°C.

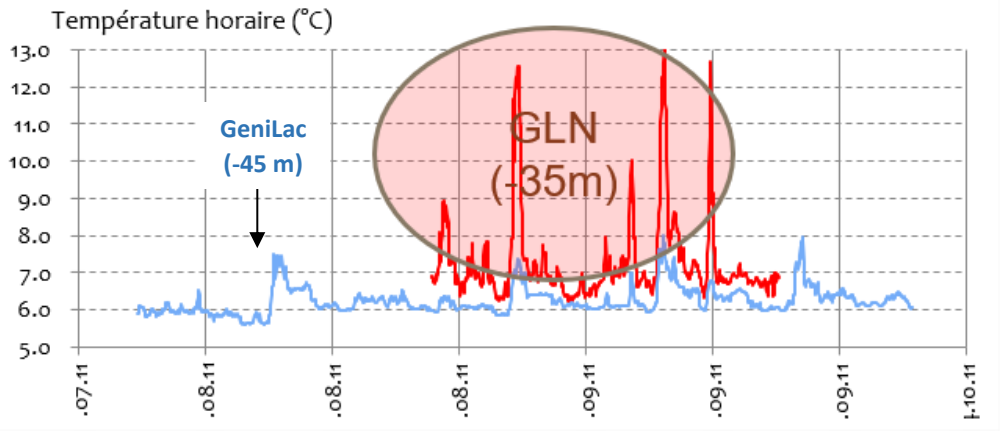

Figure 3.3: Fluctuations in temperature at the water intake as a function of depth in the Petit-Lac Léman (GIS)

According to the SIG data[2] for the GeniLac system (table 3.4 below), the COPhp of a heat pump (with the Building Sub-Station pumps), increases by 23% when the lake water is at 15°C instead of 3°C. The heat pumps' electricity consumption then decreases by the same proportion (23%) for a 12°C increase in temperature at the lake water intake (Δ ≈ 2%/°C). The heat pump is of the water/water type, TRANE RTSF 110 [**63**].

Average temperature of the cold source: **6.5 °C** @ - 45 m

Données de la PAC								
Nom et type de PAC								
Données de puissance de la PAC		**Pompes:**	Consenseur	inclus dans le COP		Evaporateur	inclus dans le COP	
				Données introduites en ordre croissant selon la température de la source				
Chauffage	T Dep	Température de la source de chaleur:	°C	3	5	8	12	15
	°C	Puissance therm.	kW	352.65	375.4	410.3	459.6	498.96
T Dep 35 °C	35	COP	-	4.614	4.801	5.076	5.432	5.689
ECS eau chaude sanitaire	T Dep	Température de la source de chaleur:	°C	3	5	8	12	15
	°C	Puissance therm.	kW	313	330.72	357.8	397.04	428.8
T Dep 65 °C	65	COP	-	2.561	2.659	2.808	3.013	3.172

Table 3.4: Performance of heat pumps with circulation pumps (COPsys) in the building substation, depending on the temperature of the lake cold source and the use (Room Heating & DHW)

In Table 3.4 above, we can clearly see the difference in "COPhp" depending on the temperature of the cold source (lake) and that of the use (Room Heating or DHW). Again, due to the *Carnot Factor* (CAF), the COPhp is almost double for Room Heating (start at 35˚C => COP = 4.93), compared to DHW (start at 65˚C => COP = 2.73).

The Room Heating (RH) vs. DHW ratio influences the performance of the GeniLac network (COPhp-mix, from 2.73 to 4.93). This is illustrated in Table 3.5 below and calculated on the basis of the data in Table 3.4 above, for different RH and DHW mixes. For the current state of renovation of the building stock, with a typical 70/30% mix between RH and DHW, we would obtain an average winter COPhp-mix for heat pumps of 3.97:

$$\text{Average COPhp-mix} = 1/((0.7/\text{COP-rh}) + (0.3/\text{COP-dhw})) = 3.97 \quad [-] \qquad (7)$$

The COPhp of the RH/DHW mix (Tab 3.5, lines 9 to 17) is calculated using the Carnot Factor (CAF, lines 21-22) and the respective Technical Efficiency (Rt, lines 26-27) taken from the COPhp at 100% space Heating (line 6) and 100% DHW (line 7). For the COPsys (of the overall system with the GeniLac network), the technical efficiency must also include the energy absorbed by the GeniLac main network circulation pump.

[2] https://www.cuepe.ch/html/enseigne/pdf/semin-19-20-5.pdf The challenges and development of low-temperature heating networks in Geneva, Fabrice Malla, Services Industriels de Genève.

Average temperature of cold source
6.5 ˚C @ - 45 m

	A	B	C	D	E	F	G	H
1		Temp. source froide (Tf)			(Moyenne hivernale)		GeniLac seul	
2		°C	3	5	6,5	8	12	15
3	COPAC mix	°K	276	278	279,5	281	285	288
4	Chauffage / ECS	Tc source	COPAC GeniLac seul (données soures SIG)					
5	Ch.% / ECS %	chaude (K)	(données)	(données)	(calcul)	(données)	(données)	(données)
6	100 % Chauffage	308	4,61	4,80	4,93	5,08	5,43	5,69
7	100 % ECS	338	2,56	2,66	2,73	2,81	3,01	3,17
8	Mix Ch / ECS	(calcul)	(calcul)	(calcul)	(calcul)	(calcul)	(calcul)	(calcul)
9	77 % / 23 %	315	3,90	4,05	4,16	4,28	4,59	4,81
10	70 % / 30 %	317	3,72	3,87	3,97	4,09	4,38	4,60
11	63 % / 37 %	319	3,56	3,70	3,80	3,91	4,19	4,40
12	60 % / 40 %	320	3,49	3,63	3,73	3,84	4,11	4,32
13	55 % / 45 %	322	3,39	3,52	3,62	3,72	3,99	4,19
14	50 % / 50 %	323	3,29	3,42	3,52	3,62	3,88	4,07
15	40 % / 60 %	326	3,12	3,24	3,32	3,42	3,67	3,85
16	30 % / 70 %	329	2,96	3,07	3,15	3,24	3,48	3,66
17	20 % / 80 %	332	2,81	2,92	3,00	3,08	3,31	3,48
18								
19	COPAC mix	Tc source	Calcul Facteur de Carnot (FAC) des PAC GeniLac = Tc / (Tc-Tf)					
20	Chauffage / ECS	chaude (°K)						
21	100 % Chauffage	308	9,63	10,27	10,81	11,41	13,39	15,40
22	100 % ECS	338	5,45	5,63	5,78	5,93	6,38	6,76
23								
24	COPAC mix	Tc source	Calcul Rendement technique (Rt) des PAC GeniLac = COP / FAC					
25	Chauffage / ECS	chaude (°K)						
26	100 % Chauffage	308	0,48	0,47	0,46	0,44	0,41	0,37
27	100 % ECS	338	0,47	0,47	0,47	0,47	0,47	0,47

Table 3.5: Performance of the heat pumps, with upstream and downstream pumps, of the GeniLac system (COPsys?) as a function of the temperature of the lake cold source and the RH / DHW mix (calculations)

Changes in the climate and in the energy efficiency of buildings (ECEEB-2050) will gradually bring the MixH/W, of the Room Heating vs Domestic Hot Water, closer to balance in 2050 (55/45, line 12, Table 3.5) and will eventually be reinforced by the supply of DHW to household appliances. It will also have the effect of lowering the future winter performance of Thermal Lacustrine Networks (TLN) such as GeniLac. **So, there's a huge issue at stake here in terms of the impact of domestic hot water production!**

3.2 Energy balance for the GeniLac system alone (without ULISSE or CORSAIRE)

The hydraulic and thermodynamic impact of seasonal changes in the temperature of the lake water intake are reflected in the overall energy balance and in GeniLac's latest energy forecasts[3] . According to SIG data, the free-cooling cold (Qc) and heat (Qh) supplies and associated annual energy consumption for GeniLac are as follows:

Summer semester cooling by free-cooling (Qc):	**245**	**[GWh-thermal]**	**(8)**
Heating + DHW winter semester (Qc ≈ 1 PJ):	**277**	**[GWh- thermal]**	**(9)**
Annual Electricity for pumping lake water (Epwan):	23	[GWh-electrical]	(10)
Winter semester Electricity for heat pumps (EPhp):	69	[GWh- electrical]	(11)
Backup (?) Natural gas heating (Qgas):	27	[GWh-thermal]	(12)

The nominal regimes for the temperature of the water extracted from and returned to the lake, for Summer (Cooling) and Winter (Heating), are approximately as follows, with a corresponding round-rip temperature difference (ΔT):

Summer (air conditioning): 13/18 ˚C (nominal); 7/12˚C (average extraction/restitution lake); $\Delta T_S = 5$ K (13)
Winter (Heating): 5/2 ˚C (nominal); 6.5/3.5˚C (average extraction/restitution lake); $\Delta T_W = 3$ K (14)

[3] 1) De GLN à GeniLac, 10 ans d'apprentissage dans la valorisation thermique des eaux du Léman, ARPEA 27/9/2019, Sophie Durandeux, SIG. 2) The Genilac programme, Energy forecasts, April 2022, Gilles Ottaviani, SIG.

3.2.1 Introductory remarks and considerations

- Normally, heating requirements are not strictly limited to the winter semester (WS). During the summer semester (SS), domestic hot water (DHW) is also produced using the heat pumps, which are partly supplied by lake water.
- Typically, in the shoulder seasons (autumn/spring), cooling and heating requirements can sometimes be balanced with the hydrothermal network in GeniLac's airport sector, which operates in a semi-closed loop (energy-free loop, limited exchanges with the lake).
- However, for the purposes of this comparative report, it is assumed that cooling and heating are provided only in the summer and winter semester respectively, each continuously for 4380 hours.
- Given the small temperature differences between the network and the ground (ΔTr-t < 10 K), heat exchanges are considered negligible (for GeniLac alone) and with ULISSE by a minimum of targeted insulation of the network.
- The Nominal Lake Flow (**or DNL: Débit Nominal Lacustre**) of the Vengeron pumping station is 10 m^3/s.
- The additional fuel (27 GWh gas), representing 10% of the heating requirements (Q), is considered to be for backup supply. It is therefore not included in the network's balance sheet.

3.2.2 What about integrating "gas back-up"?

The additional supply of energy-heat from natural gas (fossil gas) should only be **used as a backup for the GeniLac network**, but not to cover peak heat demand.

The Nominal Lake Flow (DLN: 10 m^3/s) of the Vengeron Pumping Station (STAP) and the water circulation in the GeniLac network (without the help of ULISSE) can theoretically extract nearly 550 GWh heat (QLN^-) from the lake over the duration of the Winter Semester (Hiver) or district heating (tm_H: 4,380 h). This is three times the average lake extraction capacity (QL^-: 177 GWh, eq.36), with a rated power (PLN^-) of 125 MW-t (eq.37.bis) and twice the average daily useful power supplied by the heat pumps (PU^+) of 57 MW-thermal (eq.44).

$$QLN^- = DLN * c * \Delta T_H * tm_H = \quad 548{,}7 \quad [GWh] \quad (15)$$

$$PLN^- = DLN * c * \Delta T_H = QLN^- / tm_H = \quad 125{,}3 \quad [MW\text{-}t] \quad (37.bis)$$

However, compared with the average winter requirement for energy and useful heating capacity (QU+: 250 GWh & PU+: 57 MW-t), the thermal requirement varies daily depending on the atmospheric temperature (impacting ambient heating) and the temperature of the drinking water network (impacting the energy requirement for DHW).

Its two temperature parameters logically follow (*in phase opposition*) the natural solar contribution, which varies *sinusoidally and* seasonally, with an *amplitude* (nominal value) and an annual *periodicity.* The average or "rms" value equals 1/√2 of the amplitude or nominal value of the said sinusoidal variation. Over the Winter semester period, the nominal or peak demand for Useful heat power (PUp^+) is therefore √2 or 1.414 times the "effective" or medium demand (PUm^+):

$$PUp^+ = \sqrt{2} * PUm^+ = 1.414 * 57\ MW\text{-}t = \quad 81 \quad [MW\text{-}t] \quad (16)$$

The 27 GWh of gas back-up can either be injected from the said network, or be supplied in parallel via the existing gas network in the substations of the buildings where the heating and DHW heat pumps are also installed. In both cases, the primary energy from the gas has to be converted into useful thermal energy (QU+) using a combustion boiler or a Heat and Power Cogeneration unit (HPC).

A large energy plant (boiler or HPC) for injection into the GeniLac network would benefit from an economy of scale (in terms of investment and operation/maintenance), compared with a multitude of small boilers spread across the substations of the buildings connected to GeniLac. Except that a single power station is subject to failure to the detriment of the entire GeniLac network, or vice versa. What's more, the latter (SIG) has a **contractual obligation to supply captive customers** (requiring redundancy and backup).

A HPC plant is only economically viable after 3,000 hours of operation, i.e., at constant optimum operating conditions. However, because it starts up so quickly, it can also be used as an emergency generator.

By way of example, the combustion/conversion of the 27 GWh of energy-heat by a HPC unit (centralised or not) would produce 40% electricity (10.8 GWh), 50% useful heat (13.5 GWh) and 10% losses. Direct injection of the 27 GWh or 6.16 MW thermal of gas back-up into the water network upstream of the heat pump evaporator would generate a gain of 0.45˚C (ΔTgas), bringing the cold source to 7˚C or 280 K:

$$\Delta Tgas = Pgas / (DLm_H * c) = 6.16\ MW\text{-}t / (3.3\ m^3\ s^{-1} * 4.18\ MJ\ m^{-3}\ K^{-1}) = \quad 0.45 \quad [K] \quad (17)$$

In Table 3.5 (column F), the COP-mix 70/30 (line 10) then rises from 4.27 (E-10) to 4.34 (F-10) and the total electrical energy absorbed by the heat pumps (Ehp+) is then almost 64 GWh:

$$Ehp+ = QU+ / COPhp\text{-}mix\ 70/30 = (250 + 27)\ GWh / 4.34 = \quad 63.8 \quad [GWh] \quad (18)$$

This would mean 4.8 GWh of additional electricity absorbed by the heat pumps, compared with 59 GWh (11.bis) for GeniLac alone (without gas back-up or ULISSE). The specific gas COP would then be 5.6.

$$Cop\text{-}gas = 27\ GWh / (63.8 - 59\ GWh) = \quad 5.6 \quad [-] \quad (19)$$

Conclusion: the 59 GWh of base load power for heat pumps is a priori of renewable origin (GHG-free). It would therefore be counter-productive (in terms of greenhouse gases) to partially substitute them with the 27 GWh of gas produced by HPC cogeneration units (a source of greenhouse gases).

3.2.3 Initial energy and water flows for GeniLac in the *Current Climatic and Energy Efficiency Building Condition* (ECEEB-A)

With a summer free-cooling COPsys (without heat pump) of 18 (COPsysE**)**, the summer share of hydraulic pump energy (EPH_E), to supply cooling (Qc) of 245 GWh, is the ratio Q /COP_{EE} **(index "E" for Eté)**:

$$EPH_E = Qc / COPsysE = 245 / 18 = \quad 13.6 \quad [GWh] \quad (20)$$

As a first approximation, we can therefore estimate the **electrical energy** (EPH) **required for hydraulic pumping** and circulation of lake water in the GeniLac network for winter heating **(index "H" for Hiver)**:

$$EPH_H = Epan - EPH_E = 23\ GWh - 13.6\ GWh = \quad 9.4 \quad [GWh] \quad (21)$$

After deducting the gas back-up (Qg) of 27 GWh, exclusively in winter (index "H" for Hiver), the minimum heat supplied by the heat pumps (Qhp) is as follows:

$$Qhp = Q_H - Qg = 277\ GWh - 27\ GWh = \quad 250 \quad [GWh] \quad (22)$$

To supply the 250 GWh of heat (Qhp), the total winter system electrical energy ($Esys_H$) is the sum of the electrical energy from the heat pumps (Ehp) and the winter pumping electrical energy (EPH_H, rounded to 10 GWh):

$$Esys_H = Ehp + EPH_H = 69\ GWh + 10\ GWh = \quad 79 \quad [GWh] \quad (23)$$

According to the heat pump performance relationships (eq.1 to 6), without the winter hydraulic pumping energy (EPH_H), the COPhp is the quotient of the energy-heat (eq.22) supplied by the heat pumps (Qhp) and the electricity absorbed (Ehp):

$$COPhp = Qhp / Ehp = \quad 250\ GWh / 69\ GWh\text{-}e = \quad 3.62 \quad [-] \quad (24)$$

$$\text{with pumping energy, the } COPsysE = Qhp / (Ehp + EPH_H) = \quad 3.2 \quad [-] \quad (25)$$

3.2.4 Comments: COPhp or COPsys

According to Table 3.5, a COPsys with pumps of 3.2 would correspond to a Room Heating vs. DHW ratio close to 30/70%, which seems surprising at first sight (disproportion of DHW?).

The COP in Table 3.5 does not include the energy of the circulation pumps in GeniLac's main circuit (COPsys). On the other hand, GeniLac's latest forecast data for the electricity consumption of the heat pumps (69 GWh) may (mistakenly) include the winter share of energy used to pump and circulate lake water ($EPH_H \approx 10$ GWh).

In this case, the heat pumps' electricity consumption is closer to 63 GWh (11.bis), with a COPhp = 3.97 for a MixH/W (Mix Room Heat vs. DHW): 70/30. However, this only affects winter operation.

With this assumption, the calculation (11.bis) for total winter electrical energy ($Esys_H$) and COPhp become:

$Esys_H$ = Ehp + EPH_H = 63 GWh + 10 GWh = 73 [GWh] (26)

COPhp = Qhp / Ehp = 250 GWh / 63 GWh = 3.97 [-] (27)

A COPhp of 3.97 corresponds to the COPsys 70/30 mix of 3.43 calculated in Table 3.5, deduced from Table 3.4 and which is close to the current state of Geneva's building stock (70/30 Heating/DHW mix).

Similarly, with pump energy the COPsys = Qhp / (Ehp + EPH_H) = 3.43 [-] (28)

According to Table 3.5, this corresponds to a Heating/DHW mix close to 45/55, which is also more realistic, in any case considering the potential development of energy efficiency in buildings, with an increasing or even dominant share for DHW (ECEEB).

The winter electricity for heating of 73 GWh ($Esys_H$, eq.26) should be put into perspective with the 14 GWh of summer electricity from the free-cooling hydraulic pumps (EPH_E, eq.20). In addition, the $Esys_H$ is almost identical to the 70 GWh of electricity saved by free-cooling, except that they are not at the same rate (winter/summer)!

3.2.5 Initial water volume, flow rate and power in summer (free cooling) at ECEEB-A

The removal of 245 GWh of heat from summer cooling (Q_E) from the buildings, together with the electrical energy from hydraulic pumping (EPH_E: 14 GWh, physically dissipated as 14 GWh heat), represents **259 GWh of energy-heat to be injected into the lake (QL^+)**:

$QL^+ = Q_E + Ep_E$ = 245 GWh + 14 GWh = 259 [GWh] (29) ***=> TAB. 5.12: D-28***

With a ΔT_E = 5 K (13), this represents a summer volume of lake water pumped (V_E) of almost 45 M m^3:

$V_E = QL^+ / (c * \Delta T_E)$ = 259 GWh / (1.16 kWh m^{-3} K^{-1} * 5 K) = 45 10^6 [m^3] (30) ***=> TAB. 5.12: D-26***

c: heat density of water 1.16 kWh m^{-3} K^{-1}

With a Nominal Lake Flow of 10 m^3 /s (DLN) and a ΔT_E of 5 K (eq.13), between the supply pipe and the return pipe to the lake, the Nominal Thermal Power introduced into the lake (PLN^+) is as follows:

PLN^+ = DLN * c * ΔT_E = 10 m $s^{3\,-1}$ * 4.18 MJ m^{-3} K^{-1} * 5 K = 209 [MW] (31) ***=> TAB. 5.12: D-29***

c: heat density of water 4.18 MJ m^{-3} K^{-1}

This corresponds to a "nominal" time (t_{NE}) of 1,236 hours equivalent to full summer power:

$t_{NE} = V_E$ / DLN = 44.7 10^6 m^3 / 10 m^3 s^{-1} = 1240 [h] (32) ***=> TAB. 5.12: D-7***

However, assuming that the free-cooling period runs continuously throughout the summer half-year, i.e., for 4,380 hours (t_{mE}), the average thermal power introduced into the lake (PLM^+) is the quotient of the energy-heat introduced (QL^+) and the average time of summer operation (t_{mE}):

$PLM^+ = QL^+ / t_{mE}$ = 259 GWh / 4'380 h = 59 [MW] (33) ***=> TAB. 5.12: D-31***

average pumping power (PPM_E) = EPH_E / t_{mE} = 3 [MW] (34) ***=> TAB. 5.12: D-34***

and the average summer flow (DLM_E) = V_E / t_{mE} = 2.83 [m^3/s] (35) ***=> TAB. 5.12: D-25***

3.2.6 Water volume, flow rate and power in winter (Heating + DHW) at ECEEB-A

For room Heating and DHW, the heat extracted from the lake (QL^-) of 177 GWh (eq.36) corresponds to the 250 GWh (eq.22) of heat supplied by the heat pumps (Qhp, QU^+, eq.1) at the level of the heat pump condensers, less the 73 GWh (eq.26) of electrical energy ($Esys_H$), which is the sum of 10 GWh (eq.21) from hydraulic pumps (EPH_H) and 63 GWh (11.bis) from heat pumps, all converted as heat (PLM^+):

QL^- = Qhp - $Esys_H$ = 250 GWh - 73 GWh = 177 [GWh] (36) *=> TAB.5.12: E-28*

With the ΔT_H limited to 3 K (14), we deduce the winter pumped volume (V_H):

$V_H = QL^- / (c * \Delta T_H)$ = 177 GWh / (1.16 kWh m^{-3} K^{-1} * 3 K) = 51 10^6 [m^3] (29) *=> TAB. 5.12: E-26*

With a nominal lake water flow rate of 10 m^3/s (DLN) and a ΔT_H of 3 K (14), between the supply pipe and the return pipe to the lake, we deduce the nominal thermal power extracted from the lake (PLN): -

PLN^- = DLN* c * ΔT_H = 10 m^3 s^{-1} * 4.18 MJ m^{-3} K^{-1} * 3 K = 125 [MW] (37) ***=> TAB. 5.12: E-29***

This corresponds to a nominal time (t_{NH}) of 1,445 hours equivalent to full winter power:

t_{NH} = Vp_H / DLN = 51 10^6 m^3 / 10 m^3 s^{-1} = 1,445 [h] (38) ***=> TAB. 5.12: E-7***

As in the case of air conditioning, the heating period is continuous throughout the winter half-year, i.e., over 4,380 hours (t_{mH}). The thermal power extracted from the lake on average (PLM^-) is therefore the quotient of the heat extracted (QL_H) and the average winter operating time (t_{mH}):

PLM^- = QL_H / t_{mH} = 177 GWh / 4,380 h = 40 [MW] (39) ***=> TAB. 5.12: E-31***

The electrical power absorbed by the heat pump compressors (Php^+) is the quotient of the electrical energy absorbed (Ehp^+) and the average winter operating time (t_{mH}):

Php^+ = Ehp^+ / t_{mH} = 63 GWh / 4,380 h = 14 [MW] (40) ***=> TAB. 5.12: E-37***

The electrical power absorbed by winter pumping (PPM_H^+) is the quotient of the electrical energy absorbed (Ep_H^+) and the average winter operating time (t_{mH}):

PPM_H^+ = Ep_H^+ / t_H = 10 GWh / 4,380 h = 2.28 [MW] (41) ***=> TAB. 5.12: E-34***

Average winter lake flow (DLM_H): V_H / t_{mH} = 3.23 [m^3/s] (42) ***=> TAB. 5.12: E-25***

For verification, on the basis of the average flow rate (DLM_H) of 3.3 m^3/s (eq.42), the winter heating capacity extracted from the lake (PLM^-) is found (eq.39 = eq.32):

PLM^- = DLM_H * c *ΔT_H = 3.12 m^3 s^{-1} * 4.18 MJ m^{-3} K^{-1} * 3 K = 41.3 [MW] (43) **=> TAB. 5.12: E-31**

Finally, the average useful thermal power (PU^+, Pm, eq.44) supplied by the heat pumps (excluding gas back-up in winter) is the quotient of the heat energy supplied (QU^+, Qhp eq.22) and the average winter operating time (t_{mH}):

Pm or PU^+ = QU^+ / t_{mH} = 250 GWh / 4,380 h = 57 [MW] (44) ***=> TAB. 5.12: E-17***

It is also the sum of the average thermal power extracted from the lake (PLM^-, eq.43) with the electrical power of the hydraulic pumps located in the STAP du Vengeron (PPH^+, eq.41) and that of the heat pumps (Php^+, eq.40):

Pm or PU^+ = PLM^- + PPM^+ + Php^+ = 40 + 2.3 + 14 = 57 [MW] (44.bis) **=> TAB. 5.12: E-17**

Figure 3.6 below shows all the flows related to the average lake water pumping rate (DLM_H: 3.3m^3/s) for the supply by the heat pumps of the heat energy needed for ambient heating and DHW in the winter semester (250

GWh, excluding gas back-up). The heat pumps are installed in the substations located in the buildings, with the heat exchangers separating the heat pump circuit from the Thermal Lacustrine Network (GeniLac). All the values are shown in **Table 5.12.**

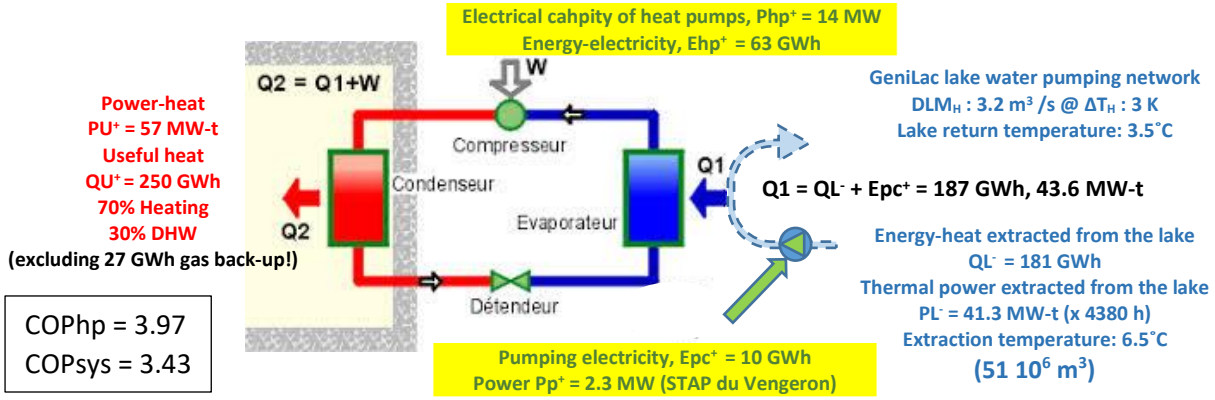

*Figure 3.6: Diagram of winter water and energy flows for GeniLac heat pumps (ECEEB-A, **TAB. 5.12, D-E**)*

3.2.7 Consequences of the Climate and Energy Efficiency Status of Buildings in 2050

Based on the *ClimaBau - BFE 2017* study **[3],** it has been considered that Global Warming between now and 2050 will increase the need for cooling (Air Conditioning) by 20% and conversely will reduce Room Heating (RH) by 20%. In addition, improving the energy efficiency of buildings will reduce RH by a further 20%.

It is proposed here (recommendation) and hypothesized for 2050 **the widespread connection of washing machines and dishwashers to domestic hot water (DHW), using heat pumps**, which will increase demand by a further 20%. This is on the grounds that it would be paradoxical to continue heating the water in these household appliances by the "joule effect" (direct degradation of electricity into heat).

The concomitant change in the *energy efficiency of buildings* (CEEB-2050) in residential buildings will therefore reduce (in equal parts) the Heating Demand Index specifically for room Heating (HDI-H), expressed in MJ/m^2 ERS (Energy Reference Surface), by around 40%.

With a 40% reduction in HDI-H, the "MixH/W" falls from 70/30% (as it stands today) to 55/45% in 2050. As a result, the spatial energy density (J/m^2) of TLN networks (such as GeniLac) will fall by just 22%, due to the concomitant 20% increase in DHW demand.

To maintain the overall supply of useful heat (Qu$^+$: 250 GWh for GeniLac), TLN networks will have to expand spatially to cover a larger urban area or a greater number of building connections and users (≈ 30%).

Without the network extension and taking into account the evolution of the ECEEB-2050, the flow rate (DPH) and hydraulic pumping energy (EPH) will initially decrease by 23 and 40% respectively (DPH or PLM: 3.23 => 2.46 m^3/s, **TAB. 5.12: E-25 => G-25**, EPH: 10 => 6 GWh**, TAB. 5.12: E-35 => G-35**).

With the extension of the network, hydraulic pressure losses will increase in proportion to the length of the said extension and will result in an increase in electrical energy for circulation pumps (EPH) to the current forecast level of 10 GWh for GeniLac alone (without ULISSE) in 2050 (**=> TAB. 5.12: I-35)**.

The energy-heat (Q1) at the evaporator should then be 181 GWh (**I-27**), with a corresponding flow rate relatively close to that of the current or initial GeniLac:

DLM = (Q1-EPH) / c* ΔT_H = (181 - 10 GWh) / 1.16 kWh m^{-3} K^{-1} * 3 K = 3.12 [m^3/s] (45) **=> TAB. 5.12: I-25**

At the same time, and still based on the current climate, the COPhp mix 70/30 = 3.97 (Tab.4.1, E-10 or **TAB. 5.12: E-18**), will fall in 2050 to a COPhp mix 55/45% = 3.62 (Tab.4.1, E-12 or **TAB. 5.12: G-18**). Without grid extension, the electrical energy from heat pumps will initially fall from 63 GWh (**TAB. 5.12: E-36)** to 54 GWh (**TAB. 5.12: G-36),** then rise again with extension to almost 69 GWh (**TAB. 5.12: I-36)**.

Illustrated and summarised in Figure 3.7 below, compared with the current situation (ECEEB-A), for GeniLac in 2050, total electricity consumption (Esys), including that of hydraulic pumps (EPH) and heat pumps (Ehp), will rise from 73 to 79 GWh (Esys: **TAB. 5.12: E-38 => I-38)**, and the winter COPsys will then fall from 3.43 to 3.18 (**TAB. 5.12: E-19 => I-19)**.

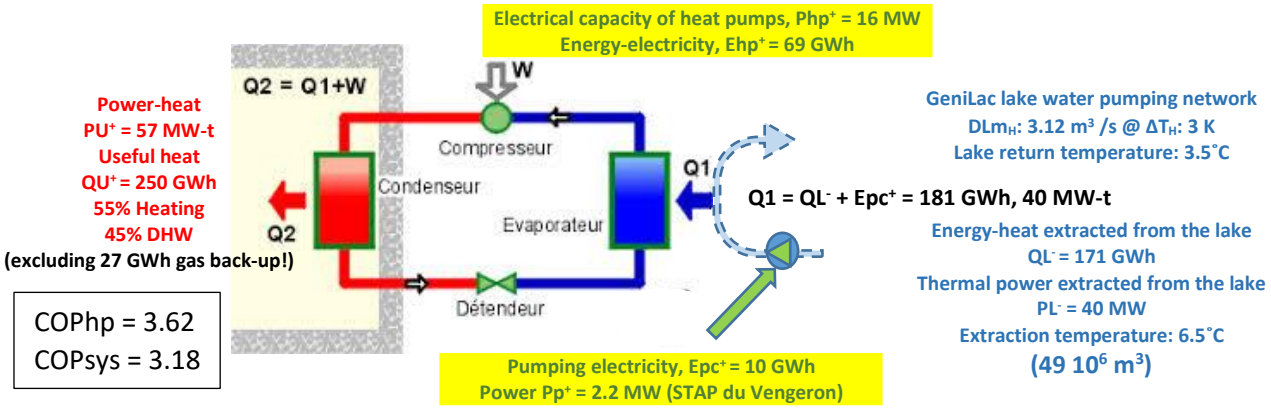

*Figure 3.7: Diagram of winter water and energy flows for GeniLac heat pumps with 1st Network extension (ECEEB-2050, **Tab.5.12, column I**)*

For the summer free cooling service, in ECEEB-2050 with an initial TLN network extension, the following consequences will apply:

- cooling demand (Qc) by TLN rises from 245 to 376 GWh (+53%) => **TAB. 5.12: D-10 => H-10,**
- volume of lake water pumped and returned (VL) rises from 44 to 71 M m^3 (+58%) => **TAB. 5.12: D-26 => H-26,**
- electricity for hydraulic pumps (EPH) rises from 14 to 33 GWh (+135%) => **TAB. 5.12: D-35 => H-35,**
- coefficient of performance of the energy system (COPsys) falls from 18 to 11 (-39%) **=> TAB. 5.12: D-19 => H-19.**

As the energy challenge is less acute in summer (enough PV electricity and less heat demand by heat pumps), in contrast to the structural deficit of electrical energy in winter, the study will focus more on the operation of the TLN network in the winter semester.

4 Integration of ULISSE into the GeniLac Thermal Lake Network

Thanks to ULISSE, by using lake water collection during the winter months at an average temperature of 19°C instead of 6.5°C (GeniLac alone), i.e., an average gain of 12.5°C in the cold source (Tc), the energy balance is improved: 1) in terms of the heat pumps and 2) in terms of the hydraulic pumps.

4.1 Impact on the current climate and energy efficiency of buildings (ECEEB-A)

Extrapolating (Table 4.1 below) the initial data from GeniLac (Table 3.4), with a cold source (Tc) at 19°C (ULISSE) compared with 6.5°C (GeniLac alone), we can see on lines 6 and 7 that the COPhp for room heating at 35°C (308 K) rises from 4.93 to 8.42 (+ 70.68%) and for DHW production at 65°C (338 K) from 2.73 to 3.47 (+ 26.87%).

In reality, for reasons of efficiency, the production of hot water for room Heating and DHW is carried out by different heat pumps.

			Temperature of GeniLac catchment alone 6.5°C (winter average)						ULISSE 18 - 20°C			
	A	B	C	D	E	F	G	H	I	J	K	L
1		Temp. source froide (Tf)		(Moyenne hivernale)			GeniLac seul		Température Tf avec ULISSE			Gain COPAC
2		°C	3	5	6,5	8	12	15	18	19	20	ULISSE /
3	COPAC mix	°K	276	278	279,5	281	285	288	291	292	293	GeniLac seul
4	Chauffage / ECS	Tc source	COPAC GeniLac seul (données soures SIG)						Calcul COPAC avec ULISSE			(Tf 19°C/6,5°C)
5	Ch.% / ECS %	chaude (K)	(données)	(données)	(calcul)	(données)	(données)	(données)	(COPAC = FAC * Rt)			(%)
6	100 % Chauffage	308	4,61	4,80	4,93	5,08	5,43	5,69	7,92	8,42	8,98	70,68
7	100 % ECS	338	2,56	2,66	2,73	2,81	3,01	3,17	3,39	3,47	3,54	26,87
8	Mix Ch / ECS	(calcul)	(calcul)	(calcul)	(calcul)	(calcul)	(calcul)	(calcul)	(calcul)	(Moyenne)	(calcul)	
9	77 % / 23 %	315	3,90	4,05	4,16	4,28	4,59	4,81	6,06	6,33	6,64	52,26
10	70 % / 30 %	317	3,72	3,87	3,97	4,09	4,38	4,60	5,66	5,89	6,15	48,33
11	63 % / 37 %	319	3,56	3,70	3,80	3,91	4,19	4,40	5,30	5,51	5,73	44,92
12	60 % / 40 %	320	3,49	3,63	3,73	3,84	4,11	4,32	5,16	5,36	5,56	43,59
13	55 % / 45 %	322	3,39	3,52	3,62	3,72	3,99	4,19	4,95	5,12	5,31	41,53
14	50 % / 50 %	323	3,29	3,42	3,52	3,62	3,88	4,07	4,75	4,91	5,08	39,64
15	40 % / 60 %	326	3,12	3,24	3,32	3,42	3,67	3,85	4,40	4,53	4,67	36,30
16	30 % / 70 %	329	2,96	3,07	3,15	3,24	3,48	3,66	4,09	4,21	4,33	33,44
17	20 % / 80 %	332	2,81	2,92	3,00	3,08	3,31	3,48	3,83	3,93	4,03	30,67

Table 4.1: Extrapolation of the performance of GeniLac's water-to-water heat pumps (COPhp) with ULISSE depending on the temperature of the lake cold source up to 20°C with ULISSE

Starting from the calculation for the COPhp of GeniLac alone of 3.97 (eq.27), we observe (Table 4.1, line 10) that it corresponds to a 70/30 room Heating/DHW Mix, in the *Climatic and Energy Efficiency Condition of the Building - Current* (ECEEB-A). With ULISSE, providing a cooling source averaging 19°C, the COPhp rises to 5.69, a gain of 48.33% compared with GeniLac alone.

To supply the same quantity of useful heat (QU^+, without the gas backup) of 250 GWh (eq.22) but with a COPhp-mix 70/30 of 5.69 the electrical energy absorbed by the Hp (Ehp^+) is then:

$Ehp^+ = QU^+ / COPhp\text{-}mix$ = 250 GWh / 5.69 = 42 [GWh] (46) **=> TAB. 5.12: J-36**

The electrical energy of the heat pumps (Ehp^+), with ULISSE (42 GWh) compared with GeniLac alone (63 GWh, TAB. 5.12: E-36) is therefore reduced by 21 GWh, i.e., a reduction of 1/3!

The electrical power absorbed by the heat pump compressors (Php^+) is the quotient of the electrical energy absorbed (Ehp^+) and the average winter operating time (t_H):

$Php^+ = Ehp^+ / t_H$ = 42 GWh / 4380 h = 10 [MW] (47) **=> TAB. 5.12: D-37**

The reduction in electricity used by the heat pumps increases the heat energy to be supplied to the heat pump evaporator (Q1), which is the difference between the useful heat energy (QU^+ = 250 GWh) and the electrical energy (Ehp^+) absorbed by the heat pumps:

$Q1 = QU^+ - Ehp^+$ = 250 GWh - 42 GWh = 208 [GWh] (48) **=> TAB. 5.12: D-27**

It is supplied by water from ULISSE Reservoirs at a higher temperature than GeniLac alone.

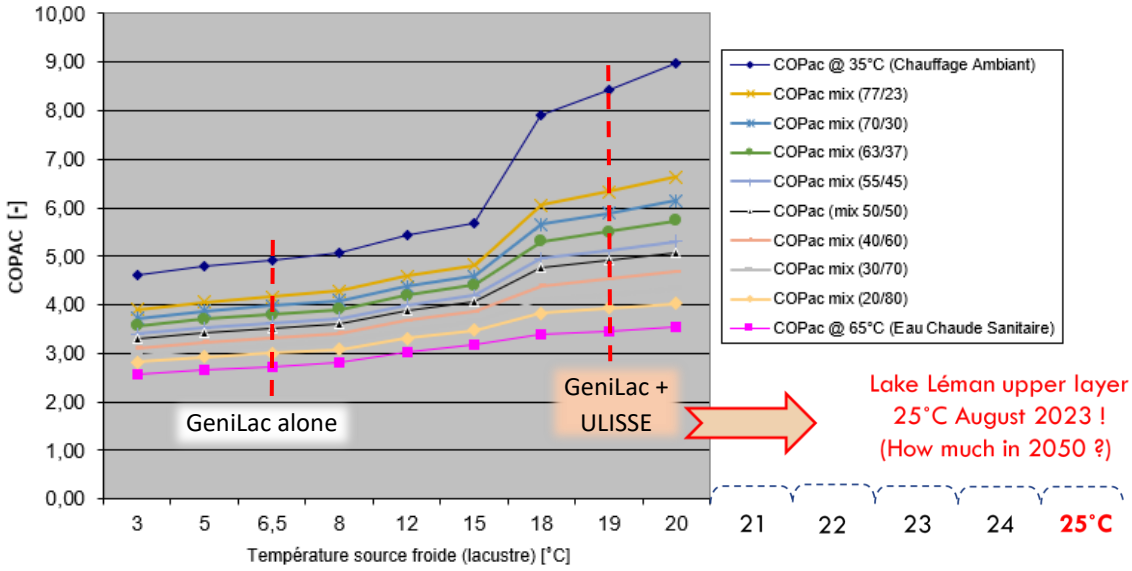

Fig. 4.2: Heat pump performance (COPhp) as a function of the temperature of the heat source (lake) and the Mix room Heating/DHW.

4.2 Hydraulic impact at ECEEB-A

With water returned to the lake at an unchanged temperature of 3.5°C, the difference with that of winter extraction (ΔT_H) of 3 K (14) for GeniLac alone (6.5°C - 3.5°C), rises to 15.5 K with ULISSE (19°C - 3.5°C). This corresponds to an inverse factor or ratio of the respective ΔT_H $F_{\Delta TH}$ of 5.2:

$$Fr = \Delta T_{ULISSE} / \Delta T_{GeniLac} = 15.5K / 3K = 5.2 \quad [-] \quad (49)$$

As a first approximation, for the same amount of heat extracted from the lake (QL^-) or the same amount of heat to be transmitted to the heat pump evaporator (Q1), the winter volume (V_H) and flow rate (DLM_H) of water required are reduced by the same factor (Fr) of 5.2, i.e., reductions of 81%.

Moreover, pressure losses in any hydraulic network are proportional to the square of the flow rate (DL). The hydraulic power (Phyd) and energy (Ehyd) of pumping and circulating water in the GeniLac network are therefore also reduced proportionally to the square of the same factor (Fr^2), equal to 27.4, i.e., a reduction of 96% (1-1/Fr^2):

$$Fr^2 = 5.2^2 = 27.04 \quad [-] \quad (50)$$

However, the heat at the heat pump evaporator (Q1) with ULISSE (214 GWh (Q1, eq.48) and that to be extracted from the lake are not the same as with GeniLac alone (191 GWh = QL^- + Epc^+). This is because, given the lower electrical energy absorbed by the heat pumps, more energy needs to be extracted from the lake.

The supply with ULISSE at the evaporator of the (214 GWh (Q1, **TAB. 5.12, J-27**), with the ΔT_H of 15.5 K, we deduce the volume of winter water (V_H) more precisely required:

$$V_H = QL^- / (c * \Delta T_H) = 208 \text{ GWh} / (1.16 \text{ kWh m}^{-3} \text{ K}^{-1} * 15.5 \text{ K}) = 11.5\ 10^6 \text{ [m}^3\text{]} \quad (51) \Rightarrow \textbf{TAB. 5.12, J-26}$$

The volume of water used by GeniLac with ULISSE, compared with GeniLac alone, is reduced by 77%.

The average duration of winter operation (t_{mH}) is used to calculate the average winter lake discharge (DLm_H):

$$DLM_H = V_H / t_{mH} = 11.5\ 10^6 \text{ m}^3 / 4{,}380 \text{ h} = 0.73 \quad [\text{m}^3/\text{s}] \quad (52) \Rightarrow \textbf{TAB. 5.12, J-25}$$

From the volume (V_H) or flow rate (DLM_H), the mean time (t_{mH}) and the ΔT_H of 15.5 K, we can determine the energy-heat extracted from the lake via the ULISSE reservoirs (QL^-):

$$QL^- = V_H * c * \Delta T = 11.5\ 10^6 \text{ m}^3 * 1.16 \text{ kWh m}^{-3} \text{ K}^{-1} * 15.5 \text{ K} = 207 \quad [\text{GWh}] \quad (53) \Rightarrow \textbf{TAB. 5.12, D-28}$$

The Reduction Factor (Fr) for Volume (V_H) and Water Flow (DLM_H) with ULISSE is 4.4 instead of 5.2.

The water pumping power and energy are reduced by 95% by the Fr factor^2 = 19.4 $(4.4)^2$, instead of 26.7, giving PPH: 0.12 MW and EPH: 0.52 GWh-e respectively. (54) => **TAB. 5.12, J-34 and J-35.**

In the *Climate-Energy Efficiency Building Condition - Actual* (ECEEB-A), the energy and electrical power of GeniLac with ULISSE, compared with the initial GeniLac, are reduced by 48%.

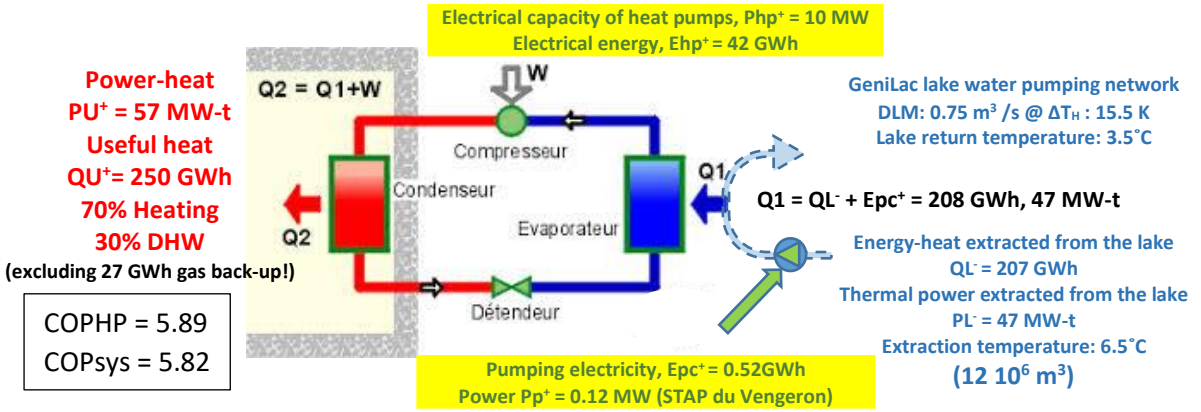

*Figure 4.3: Winter water and energy flows for the initial GeniLac + ULISSE heat pumps (ECEEB-A, **Tab.5.12, column J**)*

4.3 Consequences of extending the GeniLac network with ULISSE to ECEEB-2050

Independently of ULISSE "on its own" (without CORSAIRE), *the Climate-Energy Efficiency of Buildings* (ECEEB-2050) will also reduce the spatial energy density (J/m^2) of TLN networks (such as GeniLac) by 40% and restrict their proportionate extension in order to cover a larger urban area for the same service.

However, unlike GeniLac alone, with ULISSE the flow rate (DLM_H: 0.73 m^3/s, eq.52) and the hydraulic energy circulating in the network (EPH: 0.52 GWh, eq.54) are initially reduced by 95%, so a subsequent increase in the network extension of around 30% remains negligible (1.28 x 0.52 = 0.7 GWh).

At the same time, still compared to the initial or current situation (ECEEB-A), the COPhp mix 70/30 = 5.89 (Tab.4.1, J-10), is likely to change in 2050 to a COPhp mix 55/45 = 5.12 (Tab.4.1, J-12). Electrical energy from heat pumps (Ehp) will also increase from 42 to almost 49 GWh (**TAB. 5.12, J-36 => L-36)**. The heat (Q1) at the evaporator should fall to 201 GWh (**Tab. 5.12, J-27 => L-27)** with a corresponding flow rate (DLM):

$DLM = (Q1\text{-}Epc^{+}) / c^{*} \Delta T_H = (201 - 0.7\ GWh) / 1.16\ kWh\ m^{-3}\ K^{-1} * 15.5\ K \approx 0.71\ [m^3/s]$ (55) => **TAB. 22, L-24**

Summarised in Figure 4.4 below, in ECEEB-2050, with the first extension of the GeniLac network, the electrical energy from the heat pumps will be 49 GWh, with a COPhp of 5.12 and, slightly lower, a COPsys of 5.07.

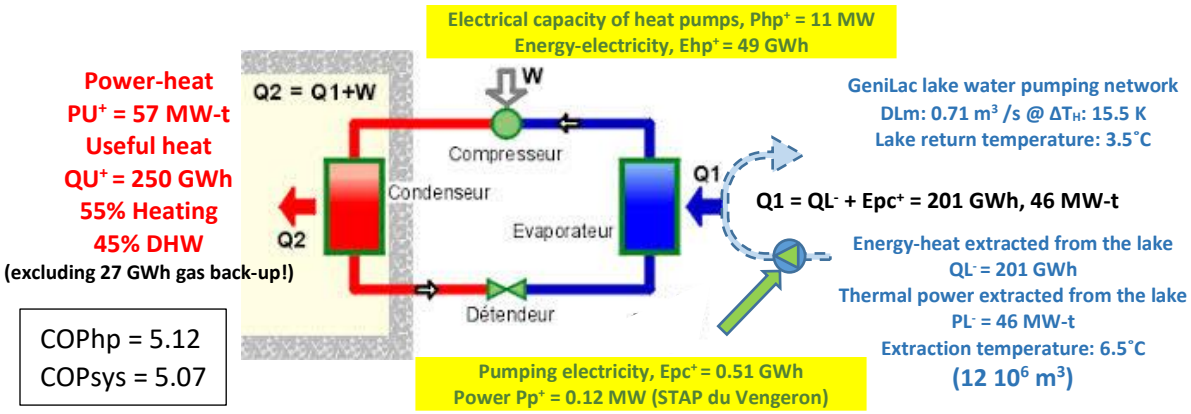

*Fig. 4.4: Winter water and energy flows for heat pumps in 1st GeniLac + ULISSE extension (ECEEB-2050, **Tab.5.12, colon. L**)*

5 Association of CORSAIRE *free heating* with ULISSE at TLN GeniLac

5.1 Operating principle

Like summer "*free cooling*", CORSAIRE winter "*free heating*" *does* not use a heat pump. Winter de-icing of the *Drinking Water Network (DWN)* is mainly carried out using a stainless-steel or titanium plate Heat Exchanger (HE) (fig. 5.1). The drinking water is de-iced by counter-current exchange with the heat flow from the primary water circuit (thermal source) [**43-47**].

In this case, the primary heat source is the ULISSE reservoirs. It can also come from other sources, such as water leaving a wastewater treatment plant (STEP **d'Aïre**), which still contains a thermal potential before final discharge, or any other source of low-temperature thermal waste **[4].**

The exchanger is located at the outlet of the Drinking Water pumping *and distribution Station* (DWS **"l'Arquebuse"**) in the Geneva DWN network, so that the drinking water is always at excess pressure to that of the primary water in order to avoid contamination in the event of a leak in the heat exchanger. The pressure at the Potable *Water Tower* (PWT) has the same hydrostatic protection effect when the DWS is shut down.

A variant of the CORSAIRE process is to use directly the water from the ULISSE Reservoirs to supply the **Prieuré** Drinking Water Treatment plant (DWT). This *direct - free heating* (DFH) eliminates the need of the heat exchanger (HE). This is a logical option, given that many "lakeside towns" already get their drinking water from this source. About 200 M m^3/year (20%) of Switzerland's drinking water comes from lakes via 30 drinking water treatment plants (DWT).

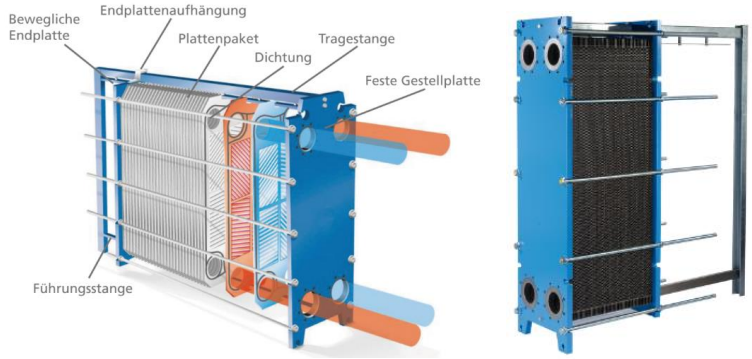

Figure 5.1: Plate heat exchanger (PHE) for the CORSAIRE Indirect Free Heating (IFH) process (source: WT Heat Exchange Technologies AG)

5.2 Heat loss in the public DWN and sanitary quality of de-iced water in winter

As the public DWN is not thermally insulated, other than by the subsoil in which it is housed, it is subject to sinusoidal seasonal variations in ground temperature at the depth of its burial. This is induced by the thermal conductivity of the soil, the atmospheric temperature and the propagation of solar flux. The amplitude of the variation in the thermal wave decreases with the depth of burial. To stay above the freezing point of water, the DWN is generally located at a depth of around one metre on the Swiss Plateau.

The amplitude of the seasonal variation in drinking water temperature is around 10 K, peaking at 16˚C in summer and falling to 6˚C in winter **[54].** This results in a variation, both in the volume of DHW (from simple to double) and in the energy per m^3, this is to the detriment of the winter semester as for room Heating (see Fig. 1.3 of introduction § 1.3). While this has an impact on the thermal energy used for drinking water, it also influences changes in its sanitary quality.

While bacteriological activity generally tends to increase with temperature, within certain limits, the kinetics and efficiency of the processes (physical, chemical and biological) used to make water drinkable are also positively influenced by the temperature of temperate water rather than icy water in winter; this is particularly true with the use of oxidising disinfectants (chlorine, CLO_2) at the end of treatment in the DWT plant [**42, 49, 50**].

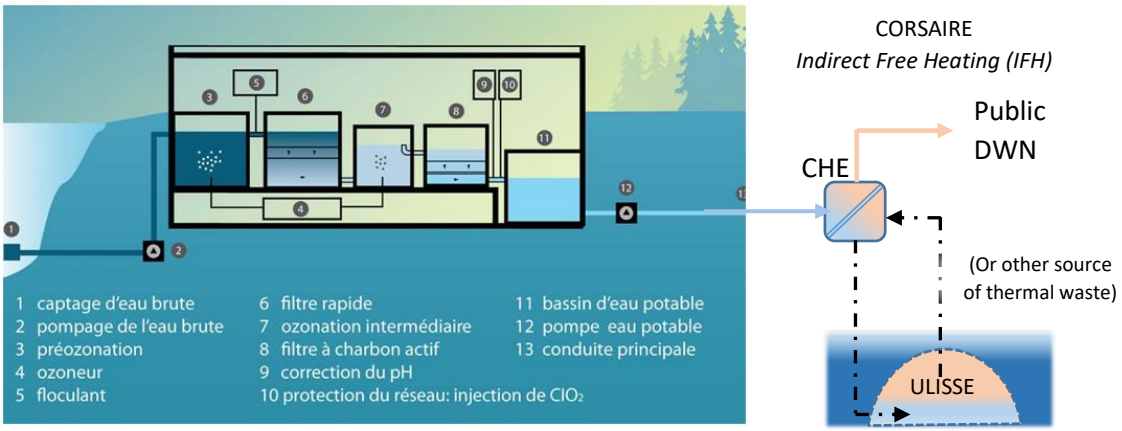

Figure 5.2: Lake water potabilization station (source: SSIGE) linked to ULISSE & CORSAIRE (IFH)

In addition, the rapid passage of drinking water (several m^3/s) through the CORSAIRE Heat Exchanger (CHE), produces a sudden thermal shock (ΔT/s). This is likely to generate a bactericidal effect, firstly by a sudden reduction in the number of bacteria and then by a delay in the growth of the number of Bacteria Colony Forming Units (CFU) **[43].**

The standard (ISO 8199) for water potability is < 300 CFU/ml (Petri dish) **[5]**. In addition, the World Health Organisation (WHO) recommends a target temperature of 8 to 15˚C, with a maximum permitted of 25˚C for mains drinking water supplies.

Microbiological degradation of drinking water in networks can be encouraged in summer by gradual heating under the bitumen of sun-heated roads and/or by insufficient flow, or even prolonged stagnation at the end of the network. Prophylactic or curative strategies are normally implemented for this (targeted or continuous purging, fountains, shock re-chlorination at the end of a network at risk, etc.) **[4, 42, 49, 50].**

On the other hand, in winter, drinking water de-iced by the CORSAIRE process and which is delayed in being distributed (outside the density of the town centre), would naturally see its temperature fall back to that of a "refrigerator" (conducive to the preservation of foodstuffs, such as drinking water). The typical summer problem of the thermal degradation of drinking water in the network cannot therefore be transposed to the winter impact of the CORSAIRE process. The winter temperature correction does not exceed that of the summer.

The CORSAIRE process would therefore be applicable below the WHO limit, in urban areas of sufficient density where the distribution of drinking water is rapid (a few hours) from its "production" (DWT) plant and obviously where its original winter temperature is low (minimum climatic condition).

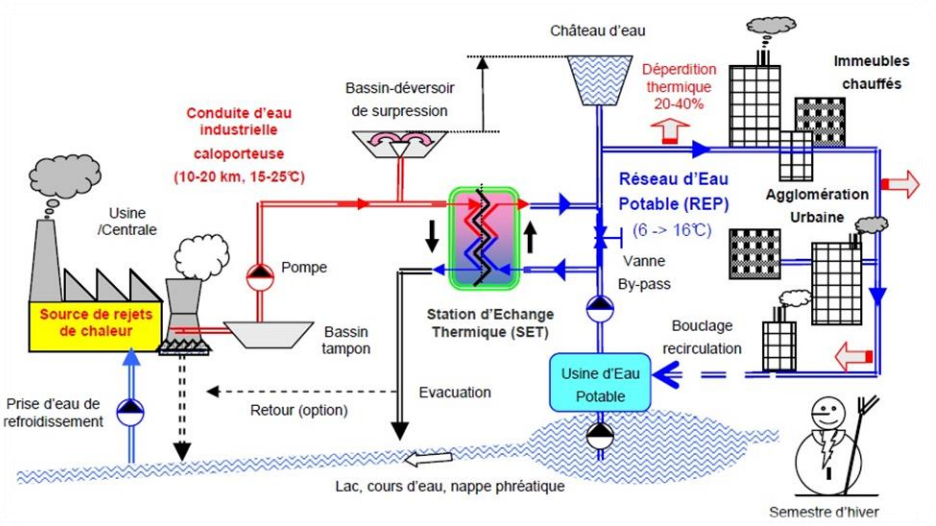

Figure 5.3: Principle of the CORSAIRE free heating process with an industrial waste heat source (SET= heat exchanger)

5.3 Use of drinking water and energy interaction with buildings

Swiss water distributors supply 1 billion cubic metres of drinking water every year, with around 12% network losses (source: SSIGE). Physiologically, a person needs around 2 litres of water a day (for drinking or eating), whereas in Switzerland we consume 140 litres for all purposes combined. How many glasses of fresh water are drunk instantly from the tap?

During the winter months, most drinking water is used indoors and undergoes thermal processes in heated buildings. This is done by DHW mixed with Cold Drinking Water (CDW), heated water by electricity in washing machines, dishwashers, coffee machines, kitchens, cleaning and unintentionally in the entire uninsulated DHW network and in toilet tanks (impacting room heating).

The stagnation of cold water in toilet cisterns and bowls is a "parasitic" and unexpected (neglected) source of heat loss during the heating semester in buildings. Each flush of a toilet can remove up to 0.7 MJ (0.2 kWh) of heat energy (13 litres of water @ 13K ΔT).

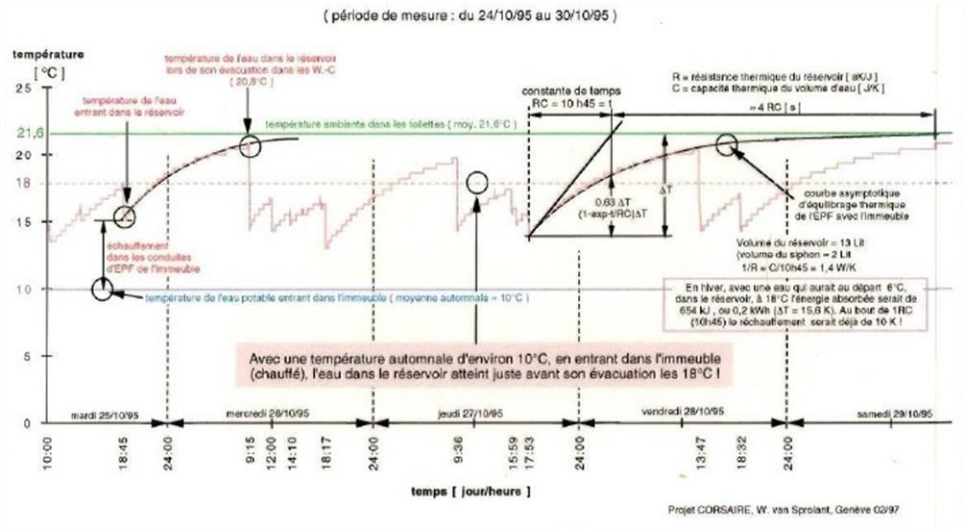

Fig. 5.4: Asymptotic evolution of the temperature of cold water in toilets (WC) in Geneva (average increase of 8˚C already at the beginning of the heating semester). ***Toilets (WC) = 1/3 of household drinking water consumption!***

However, the final impact of the toilet will depend on the residence time of the water in the tank and the toilet bowl, its thermal insulation and the ventilation of the premises (timed, double flow recovery, etc.).

5.3.1 Seasonal trends in demand for domestic hot water (DHW)

The Heat Demand Index (HDI) represents the annual heat requirement for room Heating (Qh) and domestic hot water production (Qww for warm water) divided by the heated floor area of the building or Energy Reference Surface (ERS) and is expressed in MJ/m^2 y. This depends on the category of building.

Catégorie d'ouvrage	Besoin de chaleur pour l'eau chaude sanitaire Q_{ww}
Habitat collectif	75
Habitat individuel	50
Administration	25
Écoles	25
Commerces	25
Restauration	200
Lieux de rassemblement	50
Hôpitaux	100
Industrie	25
Dépôts	5
Installations sportives	300
Piscines couvertes	300

Table 5.5: Qww (warm wasser), heat requirement (MJ/m^2 ERS) for domestic hot water (annex A standard SIA 380/1)

By way of example, taken from the UNIG Zgraggen 2010 thesis [**64**], in the case of the Giacometti central building in the Pommier housing complex in Geneva, for a Minergie standard building the share of energy for DHW is 45% of the HDI, and can reach almost 50% or even more for higher standards (HPE, § 3, Fig. 3.6). The thermal balance of the Giacometti building from 1er June 2006 to 31 May 2007 is characterised by a particularly mild winter in 2006/2007 and foreshadows climate change (CEEB-2050).

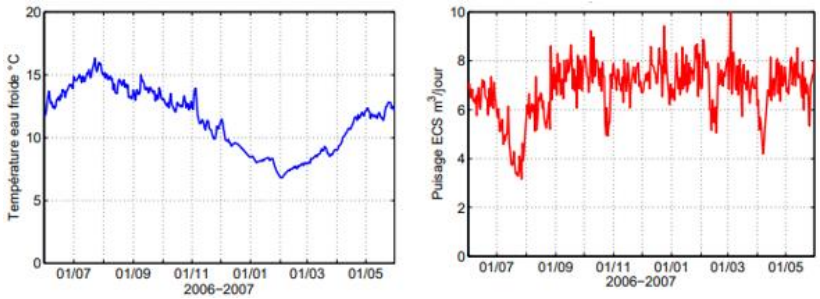

Fig. 5.6: Seasonal variation in cold water temperature in the Pommier boiler room and daily DHW volume.

On the other hand, due to the variation in the temperature of the cold water, the heat requirement for DHW varies seasonally, peaking at twice as much in winter as in summer, as does the Mix with room heating.

Mois 2006/07	Q Ecs MJ	Q Ch MJ
juin	25556	3514
juillet	16941	0
août	24301	2223
septembre	27695	744
octobre	29636	11927
novembre	30880	56343
décembre	34725	98090
janvier	35656	89638
février	31146	70166
mars	34455	65188
avril	27011	13169
mai	29645	8450
Total MJ/m²	75.5	91.1

au Pommier (*Zgraggen, 2010*)

	chauffage	ECS	total	hrs
janvier	18%	10%	16%	340
février	16%	9%	14%	320
mars	16%	10%	15%	200
avril	5%	8%	6%	120
mai	5%	9%	6%	120
juin	1%	7%	3%	60
juillet	0%	5%	2%	60
août	2%	7%	3%	60
sept.	1%	8%	3%	60
oct.	4%	9%	5%	120
nov.	12%	9%	11%	200
déc.	20%	10%	17%	340
				2000

Fluctuation
Sine wave

Table 5.7: MixH/W between energy for room heating and DHW in Minergie building (Zgraggen 2010) [**64**]

At the outlet of the storage boiler, the DHW at 55°C is hardly ever used directly, but is mixed with the Cold Drinking Water (CDW). Via the loop and the recirculation pump, it is distributed to the homes at an average temperature of around 45°C (Td). Heat dissipation in the mixed DHW circulation loop can be around 5°C and is relatively constant throughout the year (relatively stable temperature in the service ducts where the pipes run). In the dwellings, the DHW is then mixed again with cold water at a use temperature (Tu) of around 35-40°C throughout the year.

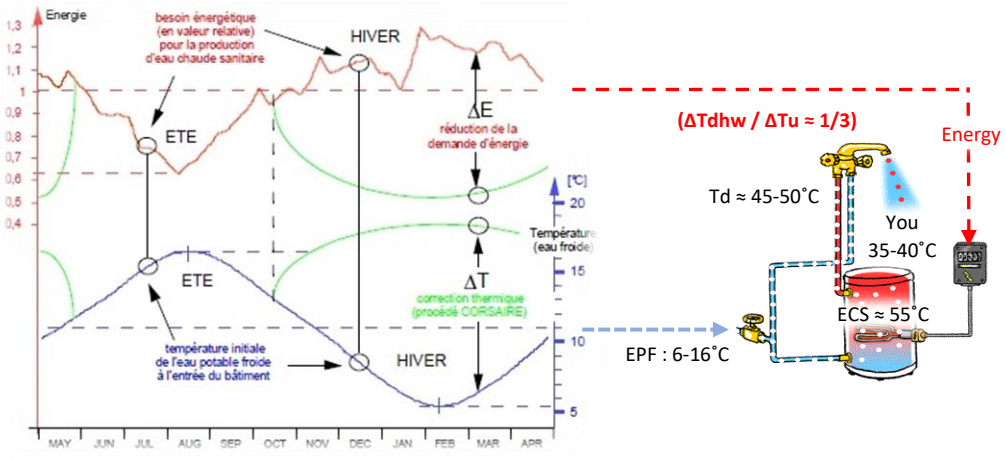

Figure 5.8: Seasonal trends in the public DWN temperature and heat demand for DHW and potential CORSAIRE impact

Illustrated in Figure 5.8 above, during the winter semester, CORSAIRE free heating can substitute the equivalent of approximately 1/3 of the heat requirement **(ΔTdhw / ΔTu ≈ 1/3)** for the production of Domestic Hot Water (DHW) as well as for the supply of washing machines and dishwashers (CEEB-2050).

Eventually, the heating requirements (Qh) of buildings will decrease, due to the reduction in their heat loss (Minergie, HQE, etc.) and the reduction in the number of heating degree-days and heating days, induced by climate change (-1.8 D/decade, § 1 Fig. 1.2, source Météo Suisse). The relative share of energy for DHW (Qww) will therefore increase in the future, and hence the importance of the impact of CORSAIRE's contribution to curbing it throughout the public DWN network and beyond the perimeter of the TLN network **[42].**

5.4 Contribution of ULISSE with CORSAIRE free heating to the TLN network

Unlike the GeniLac TLN (30-45 km), the DWN of Geneva is much larger (> 1,200 km, 160,000 m^3/d). Heat loss from the (uninsulated) DWN is consequently greater, losing around 1/3 of its temperature during distribution. At the entrance to the buildings, however, this results in a gain from 5 to 10°C on the initial temperature in the winter semester.

Compared with the situation of 1st Extension of the TLN GeniLac + ULISSE network in ECEEB-2050 (fig. 3.7), the CORSAIRE process can supply 35 GWh via the DWN in winter, i.e., 30% of the 115 GWh for DHW. The GeniLac TLN network can therefore reduce its share of DHW production, which raises the Room Heating/DHW mix from 55/45% to 63/37%, with a COPhp mix 63/37% = 5.51 (**TAB. 5.12, O-18**) and a COPsys = 5.46 (**TAB. 5.12, O-19**).

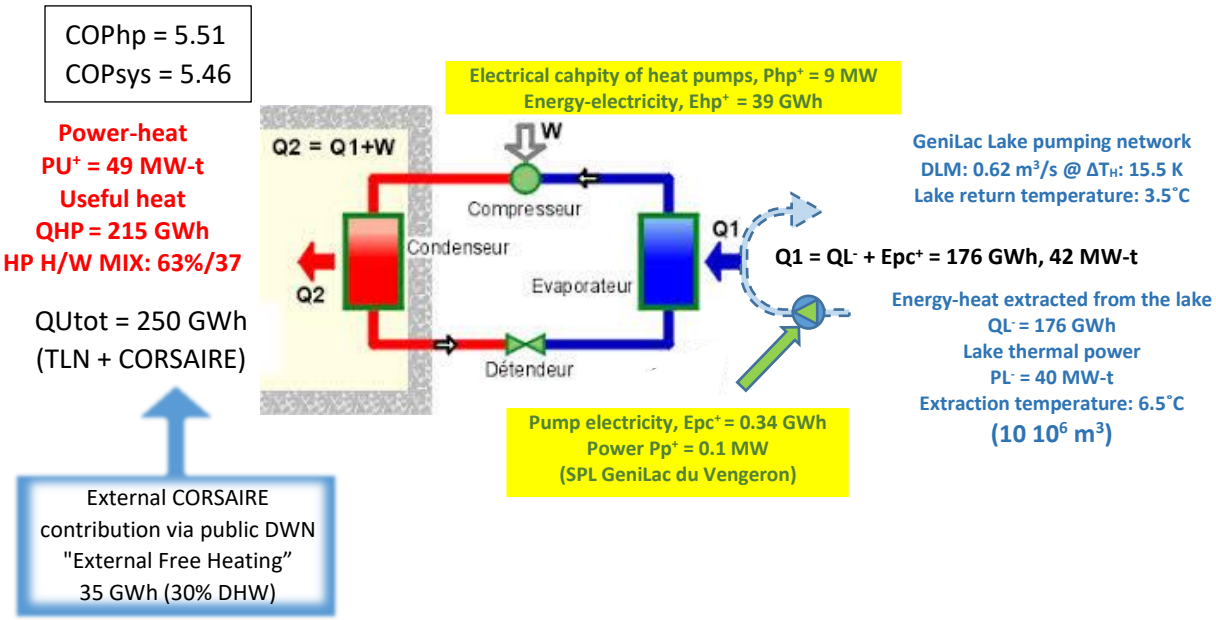

*Figure 5.9: Winter water and energy flows for heat pumps in GeniLac + ULISSE + CORSAIRE first External DWN extension (ECEEB-2050, **Tab. 5.12, column O**)*

5.4.1 Variant integrating free heating in the building

A variant of the CORSAIRE free heating process involves placing the heat exchanger inside the Building Sub-Station (BSS). This has no impact on the performance of the heat pumps, so the COPhp remains at 5.51.

The only difference in this case is that the urban DWN network is not used. The thermal input for free heating (Qfh, Qcor) is provided by the GeniLac TLN itself, which increases the volume of lake water circulated by 20%, from around 10 to 12 M m^3. Given that the hydraulic pumping energy (EPH) represents less than 1% of that of the heat pumps (Ehp), the increase in hydraulic energy remains negligible. As a result, the COPsys of the TLN increases from 5.46 to 6.32 **(Tab. 5.12, P-19)**!

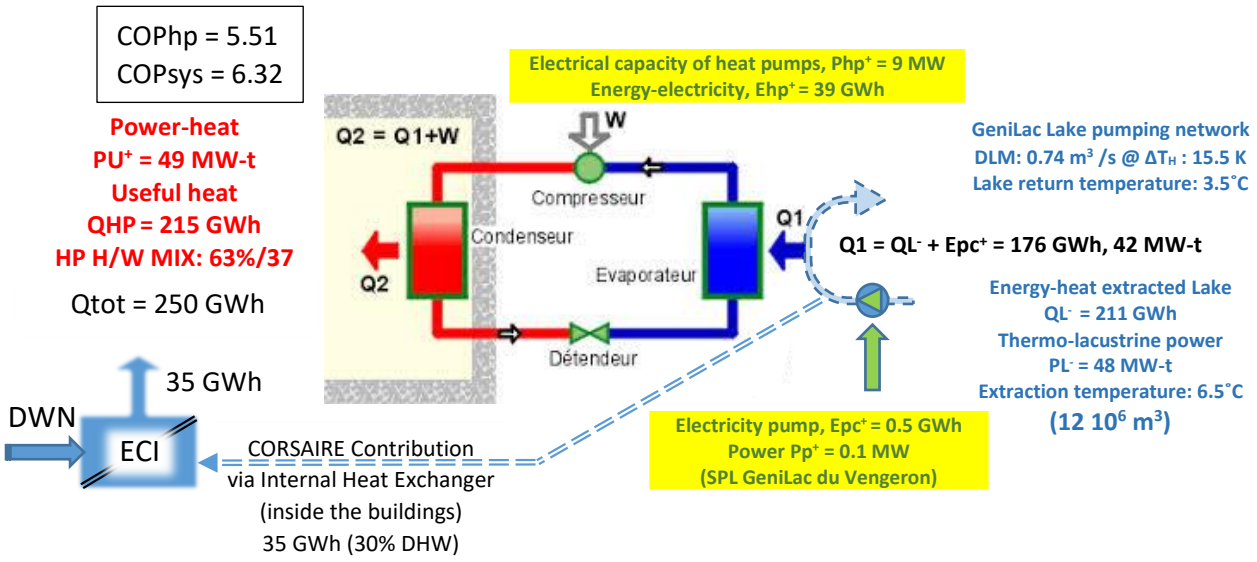

*Figure 5.10: Winter water and energy flows for heat pumps in 1st GeniLac + ULISSE + CORSAIRE extension (Internal) (ECEEB-2050, **Tab. 5.12, column P**)*

This variant (internal free heating inside the buildings) is considered here because free heating by the public DWN is not necessarily implemented and the DWN applies to the entire urban agglomeration, well beyond the capacity of the GeniLac TLN network. For example, the DWN in the canton of Geneva covers more than 1,200 km, i.e., 40 times more than the GeniLac network (30 km). It also has a daytime flow rate of around 2 to 3 m^3/s.

The External contribution of CORSAIRE, via the public DWN (Fig. 5.11), involves practically no additional electrical energy, other than that linked to pressure drops in the CORSAIRE Heat Exchanger (CHE). This is because the drinking water is transported and distributed to all the buildings in the town anyway.

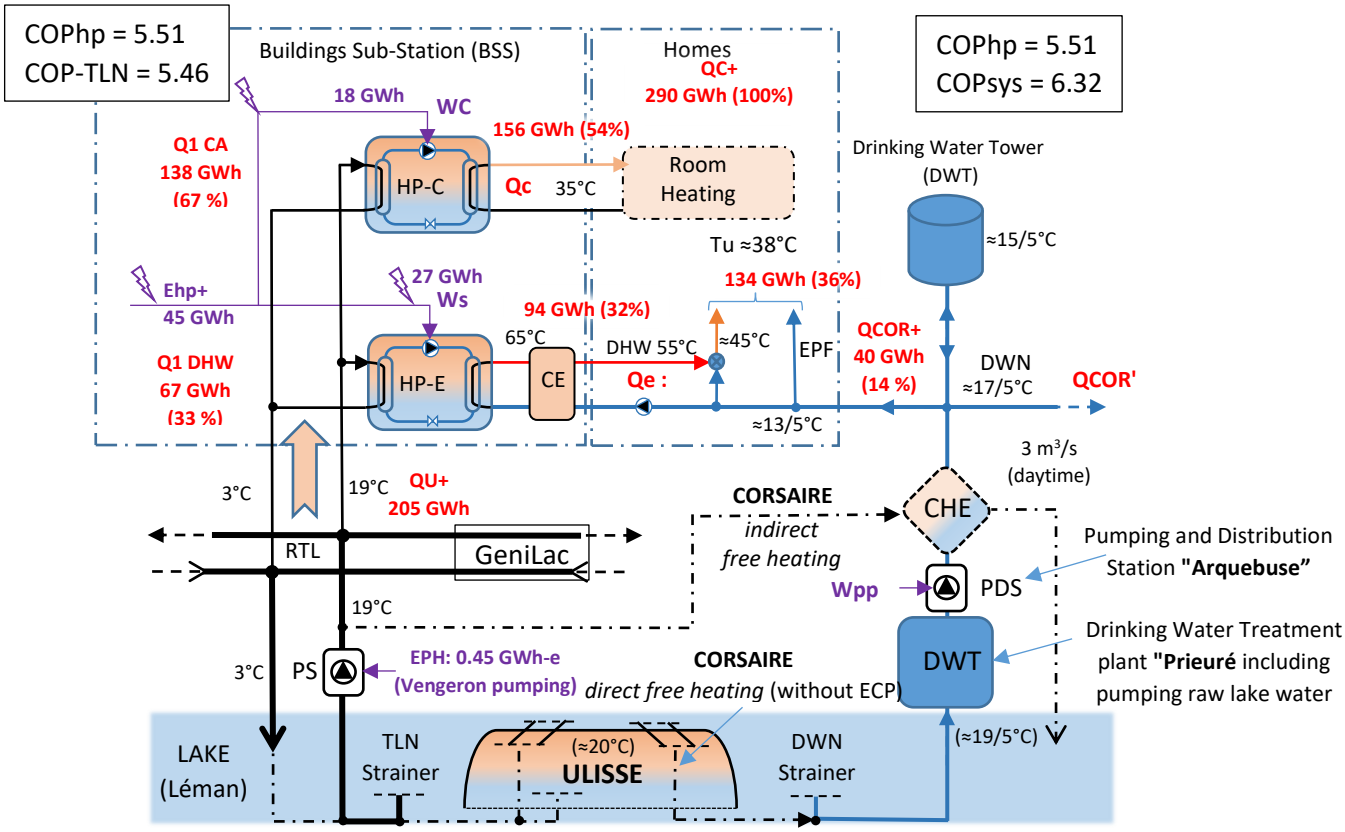

Figure 5.11: Combination of the GeniLac TLN network in the winter semester with ULISSE & CORSAIRE (ECEEB-2050)

5.5 Summary and preliminary conclusions for the TLN GeniLac

This energy impact analysis of the integration of ULISSE and CORSAIRE on the GeniLac TLN used as an example, compared the current state of the system in question with that in 2050. It has taken into account the consequences of Global Warming and planned improvements in the energy efficiency of buildings (*État Climato Efficience Énergétique du Bâti*, ECEEB).

Beforehand, it was considered that Global Warming (+ 2˚C in 50 years), by 2050 will increase the need for cooling (air conditioning) by 20% and "passively" reduce room heating (RH) by 20%. In addition, improving the energy efficiency of buildings will "actively" reduce RH by a further 20%. Finally, in 2050, **all washing machines and dishwashers will be connected to the domestic hot water (DHW) system, increasing demand by 20%, while the CORSAIRE process will provide 30% of the DHW (ECEEB-2050).**

Based on these variable parameters (ECEEB), the following elements in particular are identified and calculated:

- temperature of the lake cold source (Summer & Winter),
- volume, lake flow in hydraulic circulation in the TLN and associated electrical energy (EPH),
- lake heat (QL) converted into useful energy (Qc/h) and electricity absorbed by the heat pumps (Ehp), located in the substations of buildings connected to the DWN,
- performance of the heat pumps (COPhp: Qc/Ehp) and the DWN system incorporating hydraulic energy (COPsys)
- Coefficient of performance from the building's point of view (COPbat) including the contribution of ULISSE and Urban CORSAIRE (External to DWN).

All these data and the calculated values are shown in the table in **Table 5.12** below and the differentiated graphs (tables and figures: 3.4/5/6; 4.1/2/3/4; 5/9/10/11).

	A	B	C	D	E	F	G	H	I	J	K	L	M	N	O	P	Q	R
1				GeniLac	Actuel (A	GeniLac	2050 (B.)	GeniLac 2050 (E.)		Actuel	2050	2050	**GeniLac+ULISSE+CORSAIRE**				**2em Extension**	
2	**GeniLac + ULISSE + CORSAIRE**			(-100%)	(-100%)	(+20%)	(-40%)	Extension Réseau		ULISSE.	ULISSE.	ULISSE	Actuel	2050	2050	2050	2050	2050
3							(+20%)	(E.) ≈ 1,28 x (B.)		(A.+U.)	(B.+ U.)	(E.+ U.)	(A.+U.+C)	(B.+U.+C)	(E.+U.+C)	COR.IN	Ext.COR	Ext.COR.
4	Dénomination	bréviatio	Unités	Froid	Chaud	Froid	Chaud	Froid	Chaud	Chaud	Chaud	Chaud	Chaud	Chaud	Chaud	Chaud	Chaud	Froid
5	Longueur Réseau Thermo Lacu	LRTL	km	30	30	30	30	38	38	30	30	38	30	30	38	38	45	45
6	Nombre Raccordements Bâtis	NRB	-	300	300	300	300	384	384	300	300	384	300	300	384	384	446	446
7	Temps réduit au régime Nomina	t	h	1240	1413	1236	1413	1236	1413	1445	1445	1445	1445	1445	1445	1445	1445	1445
8	Temps régime continu semestr	t	h	4 380	4 380	4 380	4 380	4 380	4 380	4 380	4 380	4 380	4 380	4 380	4 380	4 380	4 380	4380
9	**Utilisateur Froid & Chaud**	**UF / UC**	**GWh-t**	**245**	**250**	**294**	**195**	**376**	**250**	**250**	**195**	**250**	**250**	**195**	**250**	**250**	**290**	**437**
10	RTL-froid / -chaleur Utilisateur	**QF / Qc**	**GWh-t**	**245**	**250**	**294**	**195**	**376**	**250**	**250**	**195**	**250**	**228**	**168**	**215**	**250**	**250**	**437**
11	RTL-PAC-Mix Chauffage / ECS	Mix C/E	≈ % / ≈ %	-	70. / 30.	-	55. / 45.	-	55. / 45.	70. / 30.	55. / 45.	55. / 45.	77. / 23.	63. / 37.	63. / 37.	63. / 37.	63. / 37.	-
12	RTL-PAC Chauffage Ambiant	QCA	GWh-t		175		105		135	175	105	135	175	105	135	135	156	
13	RTL-PAC Eau Chaude Sanitaire	QECS	GWh-t	récup.(*)	75	récup.(*)	90	récup.(*)	115	75	90	115	53	63	81	81	94	récup.(*)
14	Apport CORSAIRE ECS (30 %)	QCOR	GWh-t										23	27	35	35	40	
15	Puissance Nominale RTL Utilis	Pn	MW-t	198	198	196	185	251	204	691	686	697	684	679	687		694	188
16	Puissance Pointe RTL Utilist.	Pp	MW-t	78	80	94	62	120	80	80	62	80	73	54	69		80	140
17	Puissance Moyenne RTL Utilis	Pm	MW-t	56	57	67	45	86	57	57	45	57	52	38	49		57	100
18	Coefficient Performance PAC	COPac	-	0	**3,97**	0	**3,62**	0	**3,62**	**5,89**	**5,12**	**5,12**	**6,33**	**5,51**	**5,51**	**5,51**	**5,51**	0
19	Coefficient Système (RTL)	COPsys	-	**18**	**3,43**	**15**	**3,26**	**11**	**3,18**	**5,82**	**5,08**	**5,07**	**6,25**	**5,47**	**5,46**	**6,32**	**5,46**	**9**
20	Coefficient Perform. Bâtiment	COPbât	-	-	-	-	-	-	-	-	-	-	**6,87**	**6,35**	**6,34**	**6,32**	**6,33**	-
21	Dif. Temp. lac free cooling	**ΔT-f**	**°K**	**5**	-	**5**	-	**5**	-	-	-	-	-	-	-	-	-	**5**
22	Dif. Temp. lac Hiver (chauffage)	**ΔT-c**	**°K**	-	**3**	-	**3**	-	**3**	**15,5**	**15,5**	**15,5**	**15,5**	**15,5**	**15,5**	**15,5**	**15,5**	-
23	Débit Lacustre Nominal	DLN	m³/s	10	10	10	10	10	10	10	10	10	10	10	10	10	10	10
24	Débit Lacustre de Pointe	DLP	m³/s	3,96	4,52	4,81	3,45	6,15	4,37	1,02	0,77	0,99	0,94	0,68	0,87	1,04	1,01	7,41
25	Débit Lacustre Moyen	DLM	m³/s	2,83	3,23	3,43	2,46	4,39	3,12	0,73	0,55	0,71	0,67	0,48	0,62	0,74	0,72	5,30
26	Volume Lacustre	VL	M m³	45	51	54	39	71	49	12	9	11	11	8	9,8	11,7	11	84
27	Energie-Chaleur Evaporateur	QI-tot	GWh-t	0	187	0	141	0	181	208	157	201	192	138	176	176	205	0
28	Energie-Chaleur Lacustre	QL	GWh-t	259	177	314	135	401,90	171	207	157	201	191	137	176	211	204	484
29	Puissance Lacustre Nominale	PLN	MW-t	209	125	209	125	209	125	648	648	648	648	648	648	648	648	209
30	Puissance Lacustre Pointe	PLP	MW-t	83	57	100	43	128,46	55	66	50	64	61	44	56	67	65	155
31	Puissance Lacustre moyen	PLM	MW-t	59	40	72	31	92	39	47	36	46	44	31	40	48	47	111
32	Puissance Pompe Nominale	PPN	MW-é	10,96	7,08	13,29	5,53	17,01	7,02	1,63	1,29	1,63	1,49	0,96	1,26	1,50	1,44	20,50
33	Puissance Pompe Pointe	PPP	MW-é	4,35	3,20	6,39	1,91	8,18	3,07	0,17	0,10	0,16	0,14	0,07	0,11	0,16	0,15	15,20
34	Puissance Pompe Moyenne	PPM	MW-é	3,11	2,28	4,56	1,36	7,48	2,19	0,12	0,07	0,12	0,10	0,05	0,08	0,11	0,10	10,86
35	Energie Pompe Hydraulique	EPH	GWh-é	14	10	20	6	33	10	0,52	0,31	0,51	0,44	0,20	0,34	0,49	0,45	48
36	Energie électrique PAC	EPac	GWh-é	0	63	0	54	0	69	42	38	49	36	30	39	39	45	0
37	Puissance Electrique Moyen. P	PEMpac	MW-é	0	14	0	12	0	16	10	9	11	8	7	9	9	10	0
38	Energie électrique Système	**Esys**	**GWh-é**	**14**	**73**	**20**	**60**	**33**	**79**	**43**	**38**	**49**	**36**	**31**	**39**	**40**	**46**	**48**

***Table 5.12**: Summary of the impact of changes in the Climate Condition and Energy Efficiency of Buildings (ECEEB) for the TLN GeniLac alone and with ULISSE and CORSAIRE*

The joint changes to the ECEEB modify the Heat Demand Index (HDI) in MJ/m² ERS (Energy Reference Surface) specific to Summer Cooling (HDI-C) and Winter Heating (HDI-H ↘).

For DWNs, the supply of Heating energy decreases for each building connection (HDI ↘) and is offset by first Extension (+28%) of the TLN network (Tab. 5.12, column I); this is to restore the network's initial capacity (Qh, line 10, 250 GWh).

As a result, the total cold supply (Qc, H-10) of the TLN network increases by 53% due to the combined effect of global warming (HDI-C) and the first Extension of the network (+28% Number of NRB Building Connections, rising from 300 to 384, I-6).

Independently of the TLN network extension, the ULISSE and CORSAIRE systems do not affect the *free cooling* supply. However, ULISSE's storage capacity means that the volume of water and waste heat from air conditioning can be recovered and contained. This will reduce the negative impact on the lake and possibly increase the capacity of the thermo-lacustrine air conditioning system to an acceptable level.

ULISSE has an impact on the summer electricity balance only at the level of the hydraulic pumps for thermal loading of the ULISSE Reservoirs and possibly the heat pumps for increasing the temperature in the case of loading the said Reservoirs instead of a "diluting" discharge directly into the lake or downstream watercourse.

Compared with GeniLac alone in 2050 (**Tab. 5.12, column G**) and despite the first network Extension, **the winter contribution of ULISSE** (cold lake source at 18-20°C instead of 6.5°C) for room heating (RH) and DHW, reduces the flow rate by 70% (L-25) and the volume of lake water (L-26) and the energy of the hydraulic pumps by 95% (EPH, L- 35). ULISSE also increases the efficiency of the heat pumps by 41%, the COPhp (I-18: **3.62** => **5.12**: L- 18) and the COPsys (I-19: **3.18** => **5.07**: L-19) by 59%.

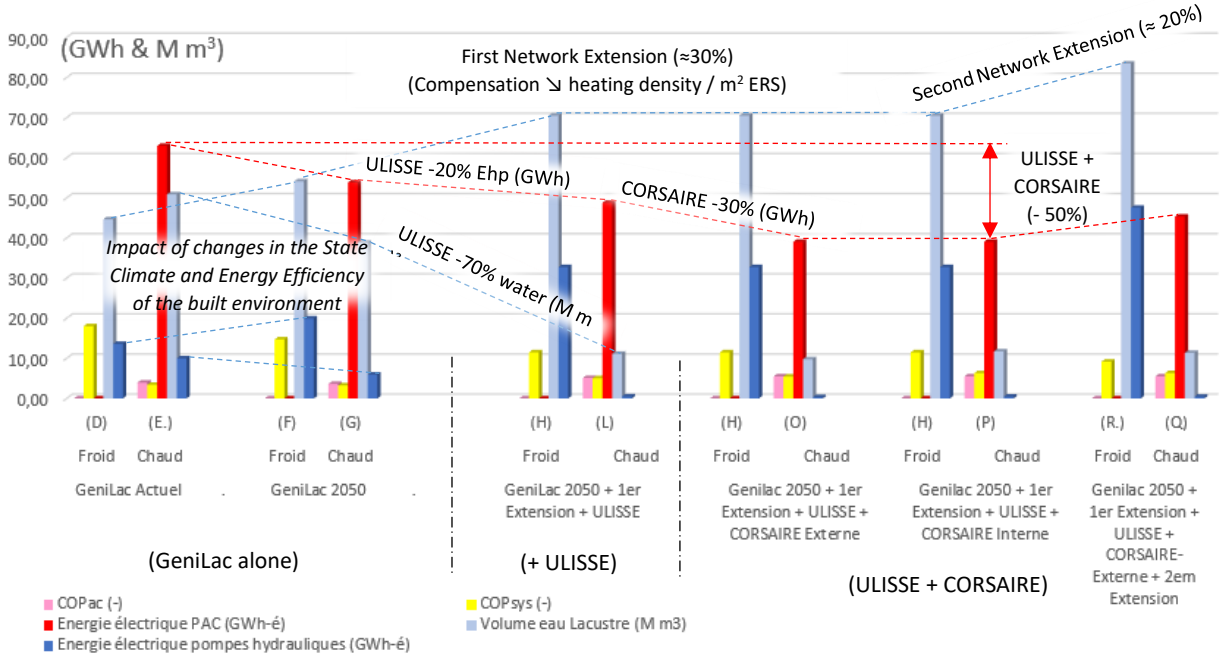

Fig. 5.13: Energy comparison of cooling (free-cooling) and heating (hot), associated with the volume of lake water (M m³) and electricity (GWh) from hydraulic and heat pumps (HP) applied to GeniLac alone and with ULISSE and CORSAIRE.

Concomitant with ULISSE in 2050, CORSAIRE *free heating* also contributes to efficiency gains. *From the* point of view of the TLN network, these gains depend on whether the *free heating is* provided either by an internal heat exchanger on the building's cold-water network (CORSAIRE *Internal to the TLN, Tab. 22, column P*), or by the urban DWN (CORSAIRE External to the TLN, **Tab. 5.12*, column O or Q***).

Irrespective of the input mode (Internal and External), for the CORSAIRE building the DHW requirement is reduced and the Room Heating relatively increased; the MixH/W rising from 55/45 to 63/37 (L-11 => O11). From the point of view of the TLN network and compared with ULISSE alone, the COPsys increases by 8% (L-19: **5.07 => 5.46**: O-19). From the point of view of the building as a whole (TLN + DWN), the COPbat (compared with L-19) is 25% higher (L-19: **5.07 => 6.33**: M-20 to Q-20).

Finally, for the first GeniLac Extension in 2050 (column I), the combination of ULISSE with CORSAIRE increases the COPbat by 100% (I-20: **3.18** => **6.33**: M/Q-20).

From the point of view of the energy performance of the building, the winter electrical energy of the TLN network (Esys) for Room Heating and DHW is reduced by 50% in 2050 thanks to the combination of ULISSE and CORSAIRE *free heating*, the latter External via the urban DWN or Internal to the building or to the TLN network with or without extension (I-38: 79 => 39 GWh: O-38)!

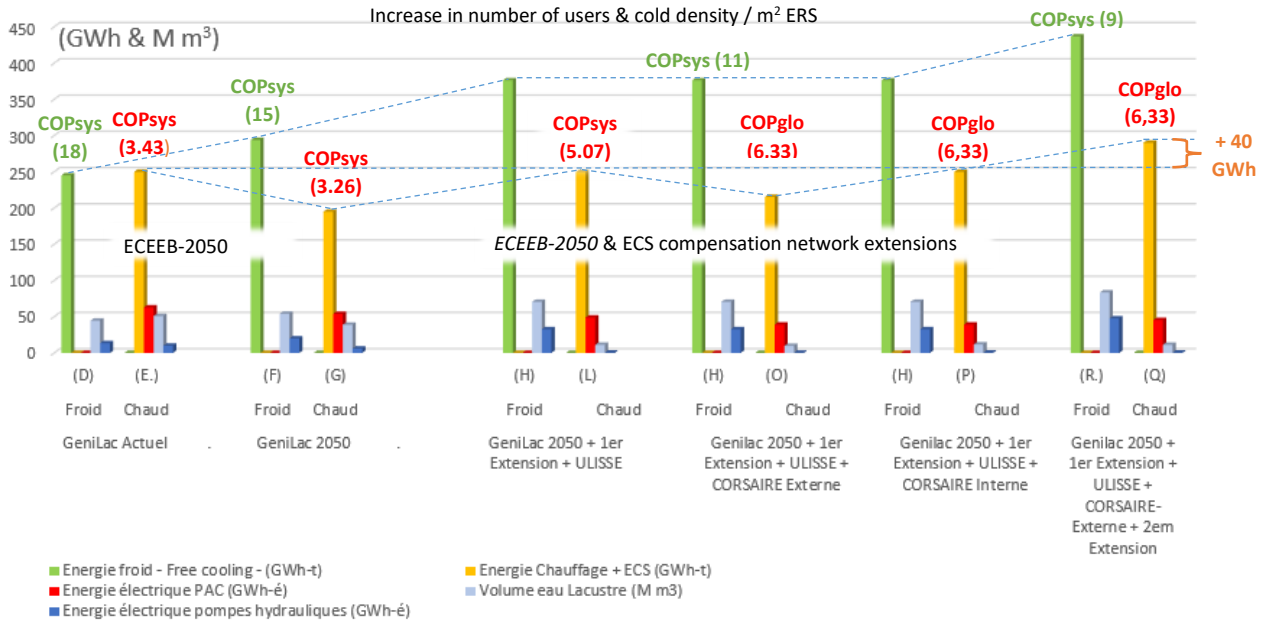

Figure 5.14: Comparison of energy flows (GWh) and circulating lake water (M m³) for cooling (free-cooling) and heating (hot), using the Thermal Lacustrine Network (TLN) applied to GeniLac - alone and with ULISSE + CORSAIRE (free-heating).

The electrical energy gain for the TLN networks has been calculated here (conservatively) with a moderate cold source at 19˚C; this is with the ULISSE reservoirs initially charged to 20˚C by lake summit water heated by the summer sun. The temperature at which the water is collected and stored may be higher (> 20˚C), or even come from the return of air conditioning (*free cooling*) or other sources of thermal waste (WTP, etc.).

In other words, ULISSE and CORSAIRE *free heating* can potentially reduce winter electricity consumption on TLN networks such as GeniLac by more than half.

Illustrated again in Figure 5.14, by 2050, with the increase in cooling demand (D-9 => R-9) and the second Extension of the GeniLac TLN network (+50%), the free cooling COPsys falls by half from 18 to 9 (D-19 => R-19). This is due to the 87% increase in volume (VL, D-26 => R-26) and lake pumping rate (DLM, D-24 => R-24). However, the significant concomitant increase (350%) in electricity consumption from summer hydraulic pumping for air-conditioning (EPH, D-35/38: 14 => 48 GWh: R-35/38) can be absorbed by excess photovoltaic production *(peak-saving)*.

For GeniLac and the Canton of Geneva, the integration of ULISSE into GeniLac represents winter electricity savings of 40 GWh-e, i.e., almost 20% of the winter production of the "Vebrois" hydroelectric power station on the Geneva Rhône River, or more than 133% of the 30 GWh winter electricity that would return to Geneva for the "Conflan" cross-border hydroelectric plant project downstream of the Verbois hydroelectric plant (cost of the "Conflan" plant: CHF 253 million in 2016) [6].

Based on the cost price of hydroelectric power in 2050 in the AES study [16], between a run-of-river and a storage power plant, respectively 190 and 320 k CHF/GWh, the financial savings of the 40 GWh avoided for the canton of Geneva would be between 7.6 and 12.8 million CHF/year.

5.6 Connection of the GeniLac TLN network to the ULISSE Reservoirs

The CORSAIRE process covers the entire DWN in the canton of Geneva (> 1,200 km). Its thermal source can also come from industrial thermal waste, e.g. the canton's main Wastewater Treatment Plant, the WTP d'Aïre ($2m^3/s$). CORSAIRE with Geneva's urban DWN could supply around 500 GWh net directly to all buildings during the winter months, i.e., twice as much as GeniLac, and virtually without any additional infrastructure [6]. The "internal" CORSAIRE contribution to the Genilac TLN network is limited.

To supply GeniLac's 250 GWh thermal during the winter semester, with ULISSE and CORSAIRE "internal" (the "free heating" heat exchanger placed at the start of the TLN or at the cold drinking water inlet to the connected buildings), the volume of tempered water required by the heat pumps is 12 M m^3 (Tab. 5.12, line 26, column J-Q). This corresponds to 6 ULISSE Reservoirs of 2 M m^3 each, with an average lake flow (DLM, 25-Q) of 0.75 m^3/s and a maximum of 1 m^3/s at the coldest point in winter (DLP, 24-Q).

The ULISSE Reservoirs are laid at a depth of around 65 m on the lake bed. In the Petit-Lac of lake Geneva, between the Versoix and Hermance diagonal, the depth varies between 60 and 75 m. A location for the 6 ULISSE Reservoirs would be possible near Anières, on the central axis of the Petit Lac (Geneva-Vaud border) (fig.5.15).

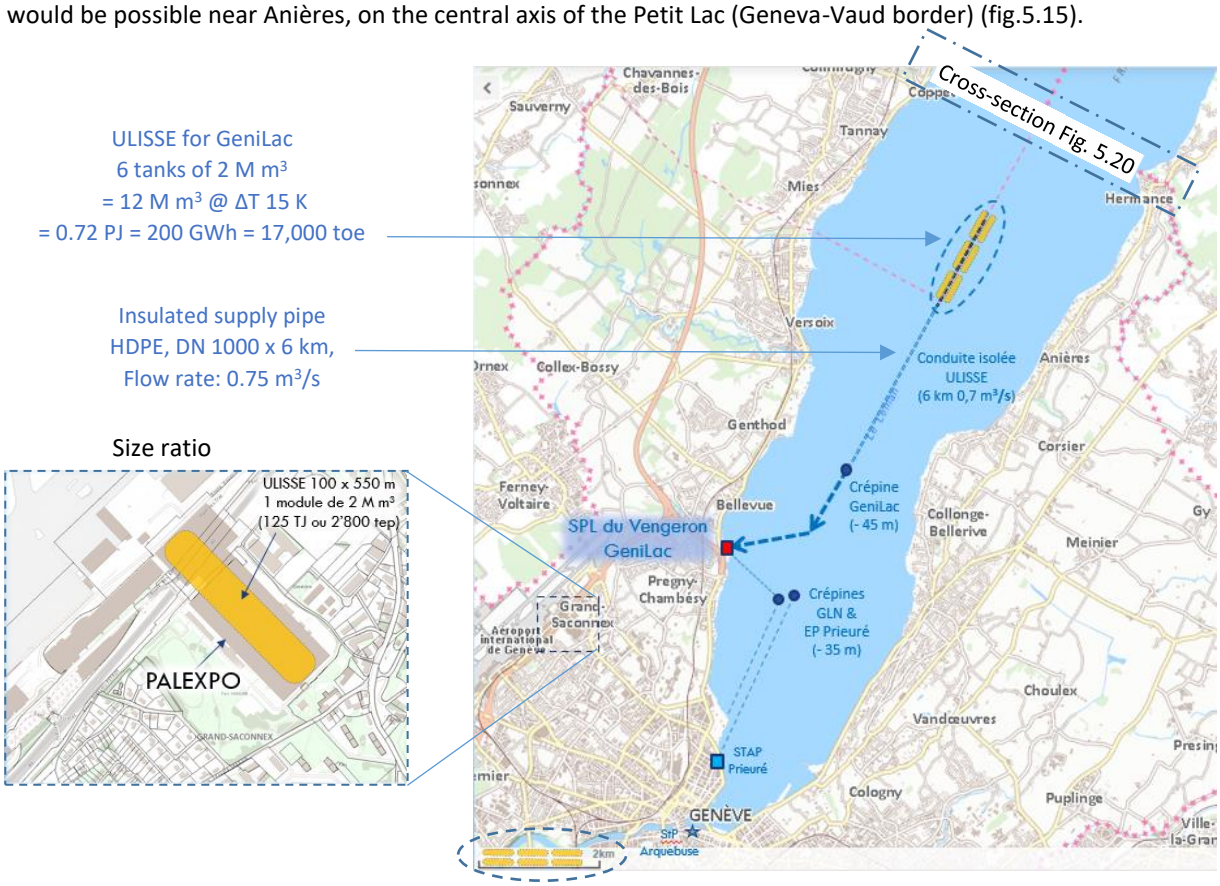

Figure 5.15: Location of the 6 ULSSE Reservoirs in the Petit-Lac Léman for GeniLac and in conjunction with the pump station.

The distance from the ULISSE Reservoirs to the GeniLac du Vengeron lake pumping station (SPL) is approximately 6 km, and 4 km from the GeniLac suction strainer. The supply pipe is therefore approximately 6 km long. With a nominal diameter (DN) of 1 m and a hydraulic flow rate (Dh) of 0.75 m^3/s, the hydraulic head losses in the HDPE (High Density Polyethylene) supply pipe are approximately 1 m w.c. or 10^{-4} Pa per km. Taking into account the 6 km length of the pipe, the fittings and elbows connecting it to the networks inside the Reservoirs and the suction strainers, the total pressure drop (Δp) in the hydraulic circuit is approximately 10 m w.c. (10^{-5} Pa or 1 bar). The hydraulic power (Ph) required to circulate the water in the supply pipe is the product of the pressure drop (Δp) and the hydraulic flow rate (Dh):

$$Ph = \Delta p * Dh = 10^4 \text{ kg/ m}^2 * 0.75 \text{ m}^3/\text{s} = \quad 7{,}500 \quad \text{[kg.m/s] or 73.5 [kW]} \qquad (56)$$

Hydraulic energy (Eh) is the product of power and time (4,380h), i.e., 0.32 [GWh] (57)

5.6.1 Thermal insulation of the connection pipe

The DN 1000 HDPE link pipe is a "COOL-FIT 4.0 de +GF+" pre-insulated pipe. This type of pipe is generally used for commercial and industrial refrigeration applications.

The PE base material makes it particularly resistant to corrosion and insensitive to contact with water. Its smooth surface gives it low pressure losses (Δp). The maximum size (Nominal Diameter) available for COOL-FIT 4.0 is currently DN 450 (mm). It has an insulation thickness (GF HE foam) of 4 cm with a heat transfer coefficient (λi) of 0.026 W/m.K (source GF). The standard unit length is 12 m. The various pipe sections are joined together by thermoelectric welding or bolted connections. A special version in DN 1000, possibly with a different insulation thickness, is essential.

Fig. 5.16: Pre-insulated HDPE pipe type COOL-FIT 4.0 from +GF

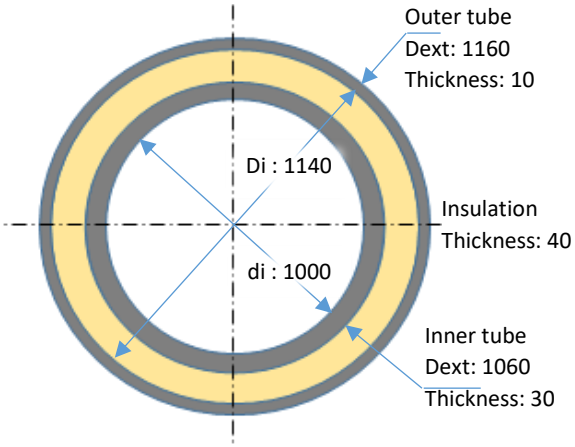

Fig. 5.17: Theoretical dimensions for DN 1000 pipe (mm)

5.6.2 Calculating heat loss from the supply pipe

The thermal power (Pt) dissipated by the supply pipe (DN 1000 x 6 km) is produced by the difference in temperature (ΔT) between that at the bottom of the lake (TL) and that of the water coming from the ULISSE reservoirs (TU). It is also a function of the circular conductivity (Kc) of the triple-layer pipe (PEint/Isol/PEext):

$$Pt = \Delta T * Kcl = (TU-TL) * Kcl = 15\ K * 17\ KW/K = 255\ [KW] \quad (58)$$

where $Kc = 2.\pi.L * \left(\lambda/\ln.(Rext/Rint)\right) \Rightarrow 2.\pi.L * \left((\ln. R2/R1)/\lambda pe) + (\ln. R3/R2)/\lambda i) + (\ln. R4/R3)/\lambda pe)\right) = 17$ [KW/K].

where R1 = di/2 = 0.5 m; R2 = dext/2 = 0.53 m; R3 = Di/2 = 0.57 m; R4 = Di/2 = 0.58 m

Thermal energy (Qt) is the product of power and time (4,380h), i.e., 1.12 [GWh]. (59)

5.6.3 Transporting, immersing and laying the supply pipe on the lake bed

Immersing and laying the supply pipe on the lake bed, at a depth of around 70 m, subjected it to a hydrostatic pressure of 7.10^5 Pa (7 bar). The HDPE is perfectly resistant to this pressure level, which is balanced on both sides of the internal/external walls. The thermal insulation (GF HE foam) is also subject to this compression pressure, which should be bearable, and is not normally exposed to water. However, water intrusion into the insulation would affect its thermal properties (λi), or even damage the base material in the long term.

One way of preventing the parasitic introduction of water, causing by a crack in the wall of the inner or outer HDPE casing, would be to apply a slight overpressure of air or nitrogen between the tubes in the insulation. This would follow the same principle of protection by air pressurisation (21-22) as for the enclosures of the submersible pump units of the summer loading system for ULISSE Reservoirs (Figure 7.6).

The procedure for laying the high-density polyethylene (HDPE) feeder pipe is very similar to that for the "Morges-Lac" (Lake Geneva) network or the Toronto DLWC[4] (Figs. 5.18 and 5.19 below) [**51, 52, 53**]. The pipe is assembled by thermoelectric welding and is simply floated onto the lake, with its concrete blocks already attached for ballasting on the lake bed. For the operation, the pipe is plugged at the ends to keep it empty of water. Once there, it is progressively filled with water and lowered to the lake bed.

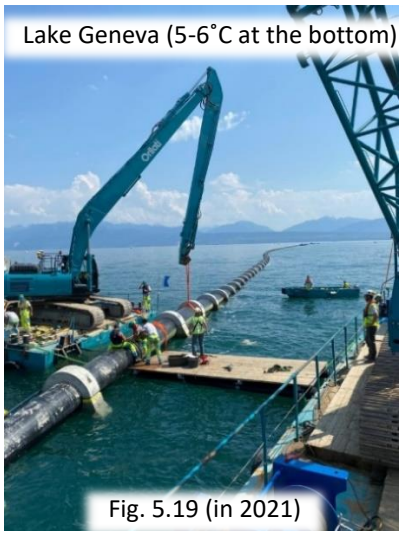

Fig. 5.18 Transport (Lake Ontario) of the HDPE pipe (Ø 1.6 m x 15 km!) for pumping and supplying water of the Deep Lake Water Cooling (DLWC) system in the Canadian city of Toronto (Enwave image)

Fig. 5.19: Laying of the 1,500 m HDPE pipe of the Morges-Lac network at a depth of almost 45 m at the level of the suction strainer (production: 3.3 GWh for heating and 1 GWh for cooling).

Laying 15 km of DN 1600 (!) pipes at a depth of 80 m in Lake Ontario in 2003 cost 50 million dollars. Transposed 20 years later, to the 6 km for GeniLac (DN 1000 x 6 km) in Petit Lac Léman (Fig. 5.15), this would represent proportionally CHF 12.5 million, or about CHF 2 million/km of pipe.

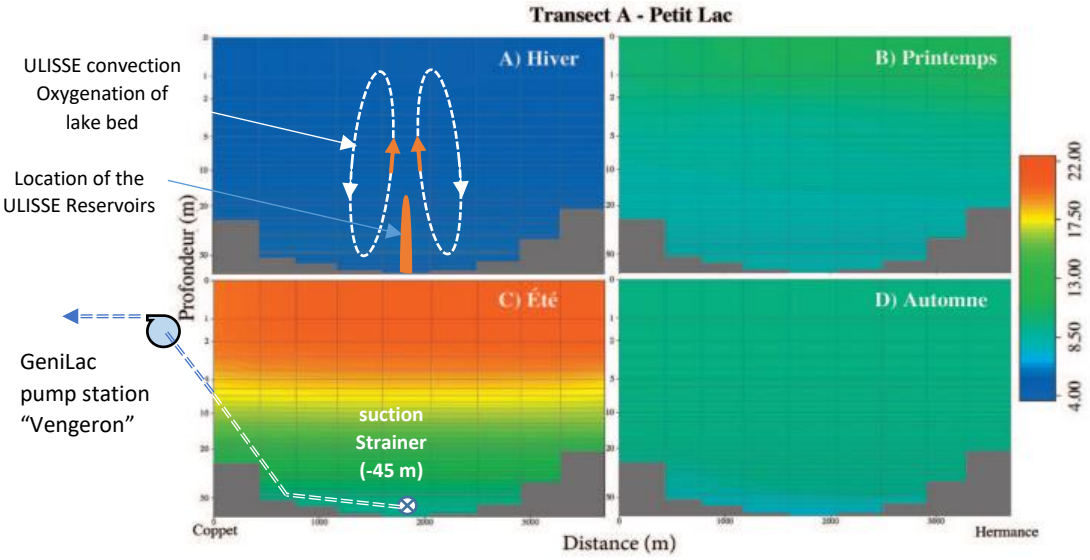

*Figure 5.20: Vertical distribution of water temperature (°C) in transect A (Fig.2), Petit-Lac (**Coppet - Hermance**): (A) winter (9 February 2005), (B) spring (20 April 2005), (C) summer (29 July 2005) and (D) autumn (26 November 2005). **The logarithmic depth scale (!)** is used to highlight the evolution of the thermocline. Source: Structure thermique et courantologie du Léman, Anh Dao LE THI 1, *, Francesca DE PASCALIS2, Georg UMGIESSER2 and Walter WILDI 1, Arch.Sci. (2012) 65 :65-80 |*[**23**]

[4] https://www.enwave.com/case-studies/enwave-and-toronto-water-tap-into-innovative-energy-source/

5.6.4 Sustained investment in GeniLac by ULISSE and CORSAIRE

In round figures, the annual CO_2 emissions of Geneva's building stock are 2 Mt CO_2 (2012 assessment)[5]. GeniLac represents an expected reduction of 70 kt CO_2 by 2035, or 3.5% of the canton's CO_2 "buildings" balance.

The reduction in CO_2 emissions at GeniLac is due to the use of fossil fuels for heating and DHW and, to a lesser extent, to the reduction in electricity consumption due to summer *free cooling*; this is because summer electricity is, in principle, less "carbon-intensive". The major climatic challenge of reducing greenhouse gas emissions and controlling electricity consumption is therefore essentially in the winter half-year.

In the Swiss building sector, heating energy requirements are higher than those for comfort cooling, with the exception of commercial refrigeration and technical processes, which are expanding rapidly (data centres, refrigerators, hospitals, offices, shops, etc.). The GLN system and its GeniLac extension, based on the lake's thermal capacity, are an effective large-scale solution for summer cooling using *free cooling* and for heating buildings using *heat* pumps as "*thermal lifts*".

However, for winter room heating and DHW production, it is more constrained by the cascade of technical and economic impacts (investment and operation), including a smaller temperature differential for extracting heat from the lake (ΔTh: 3 K) than for rejecting heat for *free cooling* (ΔTc: 5 K), implying large flows for extracting and circulating lake water and the use of energy-intensive heat pumps.

The investment for GeniLac is CHF 800 million, including CHF 110 million for the main lake pumping station (LPS) at Vengeron, with a nominal capacity of 10 m^3/s. A large part of the infrastructure and investment is attributable to the decentralised substations in the buildings (BSS), comprising mainly the heat exchangers for free cooling (summer) and the heat pumps (mainly winter).

With the evolution of *the Climate Efficiency Building Condition* (ECEEB), the limiting factor of the GeniLac TLN network is not the thermal capacity of the lake[6] , nor that of the LPS. By 2050, for an application of the ULISSE system combined with CORSAIRE internally with GeniLac, the capacity of the LPS would still be sufficient to provide air conditioning by summer free cooling, with a 25% peak reserve (DLP: 7.4 m^3/s). This is despite a 50% extension of the TLN network, in terms of length (30 => 45 km) and number of connections (300 => 450).

Since the heat discharged from the air-conditioning system, either into Lake Geneva or downstream into the Rhône, should be eliminated and introduced into the ULISSE Reservoirs, the flow rate and volume of water can be further reduced by increasing the temperature using the heat pumps available in summer.

To supply the 250 GWh of heat in the winter semester, with an average lake flow of 0.75 m^3/s (DLM, 25-Q) and a maximum of 1 m^3/s (DLP, 24-Q) at the coldest point in the winter, there is still a reserve of 90% of the capacity of the LPS and the primary supply network (TLN). In other words, thanks to ULISSE and CORSAIRE-Interne (on the TLN), GeniLac's basic infrastructure could potentially supply 2,500 GWh. Combined with the 500 GWh supplied by CORSAIRE-External free cooling (via the DWN), this would give a total of 3,000 GWh, or almost all the heating needs of the buildings in the canton of Geneva.

In addition, CORSAIRE free heating (external to GeniLac) benefits from a *windfall effect in the form of the* public drinking water network (DWN) connected to all the buildings in the urban area.

In the end, according to Loïc Quiquerez's 2017 thesis **[8],** depending on the scenario, total heat demand in the canton of Geneva in 2035 would already be between 4,150 GWh (BAU) and 3,368 GWh (EE+), and in any case lower than in 2014 (4,414 GWh/year). In 2014, thermal networks accounted for just 10% of the heating market (430 GWh). By tripling their market share by 2035 (in which GeniLac would initially account for around 28%) and through parallel measures, it would be possible to achieve the cantonal objectives for the thermal supply of buildings.

---

[5] CANTONAL CLIMATE PLAN - Part 2 of 20 December 2017 / page 6, Fig.2 : Carbon footprint and reduction targets

[6] Viquerat P-A. 2012. Utilisation de réseaux d'eau lacustre profonde pour la climatisation et le chauffage **[46]** Étude de cas : le projet GLN (Genève-Lac-Nations) à Genève, Thèse de doctorat n° 4448, Université de Genève.

6 National potential for installation and electricity savings by ULISSE and CORSAIRE

6.1 National potential of ULISSE and CORSAIRE "in-house" (via TLNs)

At the stage of this exploratory study, with fragmentary data on the state and evolution of demographics and the situation of urban agglomerations, the estimate of the potential of ULISSE and CORSAIRE can only be approximate, at best a target for 2050. This is not to say that there will be nothing left to do after 2050, or that climate change will stop. Nevertheless, we can categorise three scenarios and put forward hypotheses that will have to be validated later.

In 2050 (ECEEB), assuming widespread ambient heating and DHW production via TLN networks in the "*urban agglomerations of the 15 Great Lakes*" (1/4 of the Swiss population: Qc = 50 PJ/year of heat for a total of 200 TJ), the winter electrical energy (Esys) to power heat pumps (HP) and hydro-lacustrine pumps (PHL) would be 15.3 PJ (6.4 TWh, with COPsys = 3.26 => TAB. Fig. 22, G19).

Combining these TLN networks with ULISSE and CORSAIRE (Internal/External) would result in a gain of 50% with a COPbât = 6.34 (TAB. Fig. 22, O-20), i.e., a winter electrical energy saving of 2.1 TWh (ΔEsys):

$$\Delta Esys = (Qc / COPbât) - (Qc / COPsys) = (50\ PJ/6.34) - (50\ PJ/3.26) = \quad 7.45\ [PJ] \text{ or } 2.07\ [TWh] \qquad (52)$$

With a gain equivalent to the GeniLac TLN (≈ 40 GWh-e with 12 M m^3 of ULISSE Reservoirs), the 2.07 TWh would require 310 ULISSE Reservoirs of 2 M m^3 each:

Number of ULISSE Reservoirs (NUR @ 2 M m^3) = (2.07 TWh / 40 GWh) * 12 M m^3 = 621 M m^3 = 310 [NUR] (53)

The 310 ULISSE Reservoirs would total almost 17 km^2 of (invisible) surface area on the lake bed, i.e., 0.83% of the total surface area of the 15 large lakes (> 10 km^2). These large lakes have a total surface area of 2,024 km^2 of which 1,233 km^2 are in Switzerland. The 621 M m^3 of water stored in the 310 ULISSE Reservoirs represents a 30 cm thick layer of water spread over the 2,024 km^2 of these 15 largest lakes shown on the map of Switzerland in figure 6.1 below.

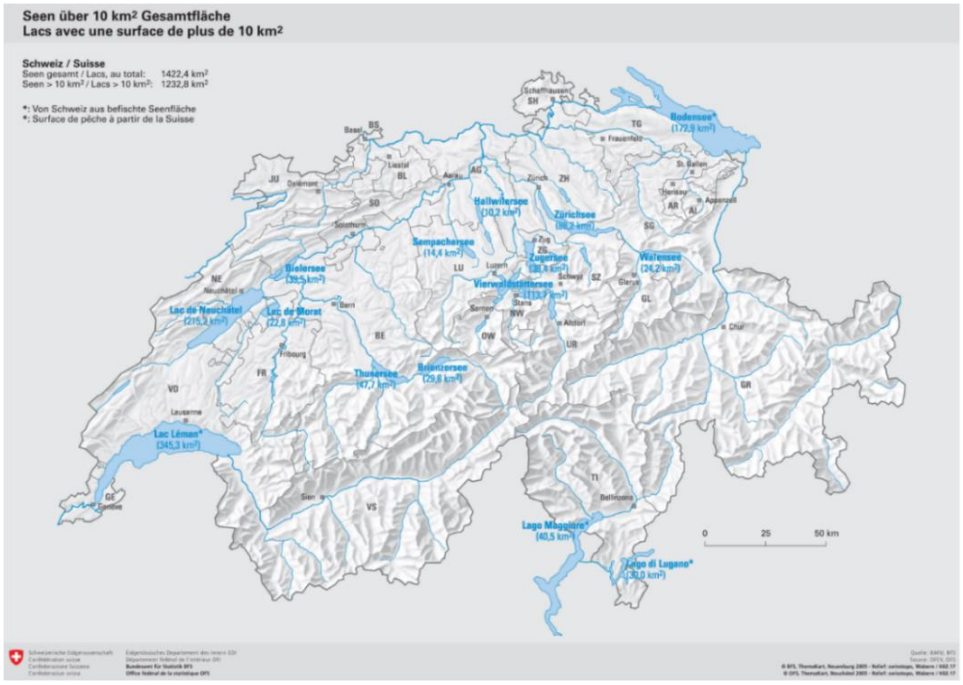

Fig. 6.1: The 15 largest Swiss lakes, with a surface area of more than 10 km^2, compatible for ULISSE Reservoirs (source: FSO)

To put this into perspective, the 17 km^2 of (invisible) right-of-way on the lake bed of 310 ULISSE Reservoirs (NUR) represent 11% of the 150 km^2 surface area of the 30 GW-p of photovoltaic panels still to be installed to supply the 30 TWh of additional electrical energy by 2050 (150 km^2 ≈ 1/4 of the 580 km^2 surface area of Lake Geneva).

A distribution of 310 ULISSE Reservoirs over the 15 largest Swiss lakes represents an average of approximately 21 Reservoirs/lake. More precisely, in Table 6.2 below, we can establish a first theoretical distribution of the Number of ULISSE Reservoirs (NUR) in proportion to the surface area of these 15 large lakes.

However, this is not necessarily a sufficient criterion. It also needs to be assessed in terms of the population living near the lakes and potentially benefiting from the ULISSE system, in particular through the TLN networks.

	Nom	Volume par lac (km^3)	Surface totale (km^2)	Surface Suisse (km^2)	Surface Suisse (% vs les lacs)	Répart. ULISSE (NRU/surf.CH. lac)	Répart. ULISSE (NRU / habitans)	Volume ULISSE (% vs lac)	Surface ULISSE (% vs lac)
1	Lac Léman (CH, FR)	89	580	345,3	28,7	87	?	0,20	0,81
2	Lac de Constance (CH, D, AT)	48	539	172,9	26,6	43	?	0,18	0,44
3	Lac de Neuchâtel	14	215	215	10,6	54	?	0,77	1,36
4	Lac Majeur (CH, IT)	37	212	40,5	10,5	10	?	0,06	0,26
5	Lac des Quatre Cantons	11,8	114	114	5,6	29	?	0,49	1,36
6	Lac de Zurich	3,9	88	88	4,3	22	?	1,13	1,36
7	Lac de Lugano (CH, IT)	6,5	49	30	2,4	8	?	0,23	0,83
8	Lac de Thoune	6,5	48	48	2,4	12	?	0,37	1,36
9	Lac de Bienne	1,1	40	40	2,0	10	?	1,80	1,36
10	Lac de Zoug	3,2	38	38	1,9	10	?	0,60	1,36
11	Lac de Brienz	5,2	30	30	1,5	8	?	0,29	1,36
12	Lac de Walenstadt	2,5	24	24	1,2	6	?	0,48	1,36
13	Lac de Morat	0,6	23	23	1,1	6	?	2,10	1,36
14	Lac de Sempach	0,7	14	14	0,7	4	?	1,07	1,36
15	Lac de Hallwil	0,3	10	10	0,5	3	?	1,80	1,36
	Totaux :	**230,2**	**2 024**	**1 233**	100,00%	310	310	0,20	0,83

Table 6.2: Distribution of the Number of ULSSE Reservoirs (NUR) in the 15 major lakes on a pro rata basis according to surface area ***(what about distribution according to the number of people living near the site?)***

As an example, for Lake Geneva, illustrated in figure 6.3 below, the bathymetric map shows that the lake bed has a surface area of 68 km^2 (green colour) where the depth is between 50 and 75 m, equivalent to 1,200 ULISSE Reservoirs with a unit right-of-way of 54,000 m^2 on the lake bed. The actual installation of 87 ULISSE Reservoirs in Lake Geneva (Table fig.6.2, line 1) would represent 4.7 km^2 or 0.8% of the lake bed (580 km^2) and 0.2% of the volume (89 10^9 m^3), invisibly and neutrally for navigation (e.g., CGN).

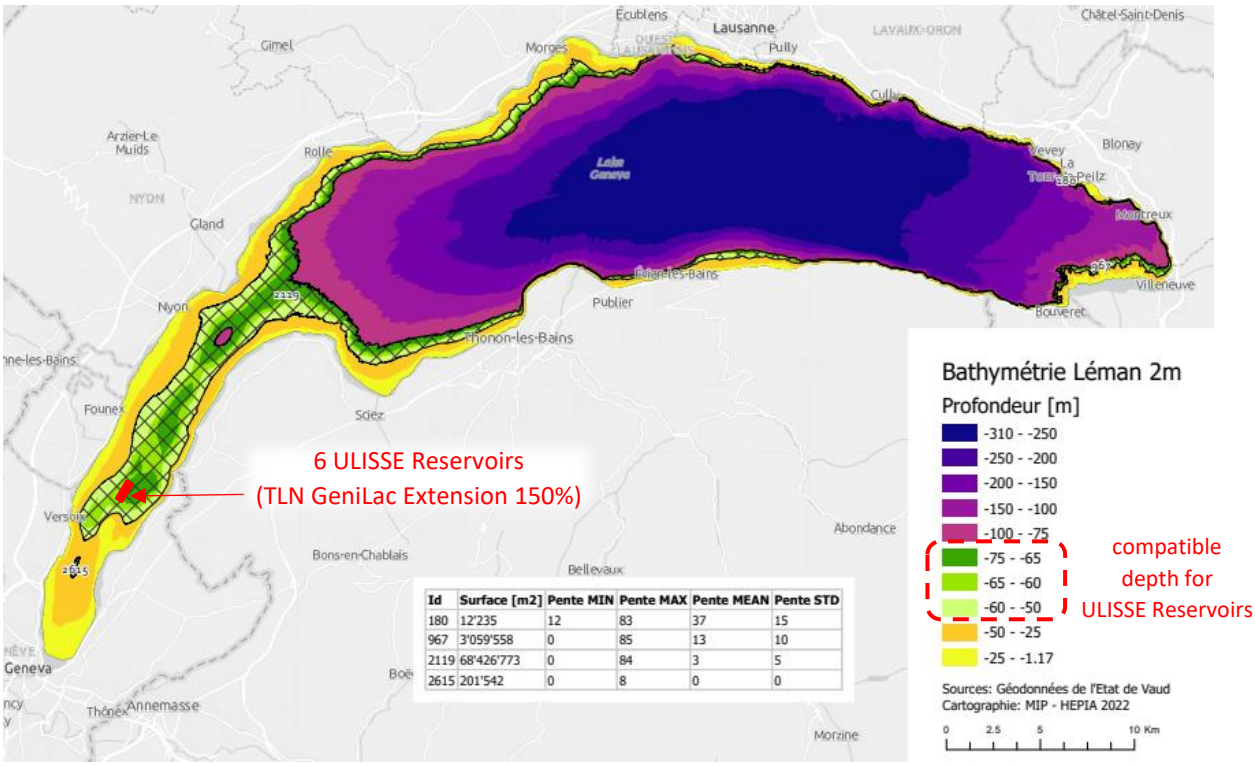

Id	Surface [m2]	Pente MIN	Pente MAX	Pente MEAN	Pente STD
180	12'235	12	83	37	15
967	3'059'558	0	85	13	10
2119	68'426'773	0	84	3	5
2615	201'542	0	8	0	0

Fig. 6.3: Bathymetry of Lake Geneva. Green zones (50-75m): depth compatible with the installation of ULISSE Reservoirs (green zone surface area: 68 M m^2 => 1,200 ULISSE Reservoirs @ 54,000 m^2) (source map: Prof. Alain Dubois, HEPIA 2022).

6.2 National potential for External CORSAIRE (via DWN excluding TLN or lake regions)

As described above, the CORSAIRE free heating process can exploit waste heat produced during the winter months, such as waste heat from wastewater treatment plants (WTPs) **[4].** The use of DWN by CORSAIRE upstream with heat from WTPs is therefore quite logical, especially as their respective flows are concomitant.

CORSAIRE free heating does not therefore necessarily require seasonal storage of the ULISSE type or infrastructure other than the existing DWN. It can therefore be used outside the regions of the large lakes and be accessible to all other urban agglomerations with a sufficient density compatible with the installation of the CORSAIRE heat exchanger on the urban DWN.

For a first estimate of the potential, we make the conservative assumption that in 2050 half (P1: 0.5) of the buildings are not connected or are unsuitable for the ULISSE and CORSAIRE systems, for various reasons (density too low, building too far away, insufficient or unsuitable heat source, etc.). If we deduct 1/4 (P2: 0.25) of the buildings already benefiting from ULISSE (lake regions), this leaves 1/4 (P3: 0.25 = 1 - P1 - P2) of the Swiss population benefiting from 30% (P5: 0.3) of the energy for DHW (Q-ECS3) via the CORSAIRE free heating and urban DWN.

While for the entire Swiss population, the heat demand for room heating and DHW (Qcn) in 2050 is 200 PJ, the demand for the part (P3) is: Qc3 = 0.25 * (Qcn) = 50 PJ. According to the MixH/W in Table 5.12, 45% (P4: 0.45) of the heat Qc3 is used for Q-ECS3 = 0.45 * Qc3 = 22.5 PJ. Finally, the CORSAIRE contribution (Q-cor) corresponds to 30% (P5: 0.3) of the heat for Q-ECS3.

$$Q\text{-cor} = Qcn * P3 * P4 * P5 = 200\ PJ * 0.25 * 0.45 * 0.3 = \quad 6.75 \quad [PJ] \qquad (54)$$

The 6.75 PJ of heat supplied by the CORSAIRE free heating system for DHW (Q-ECS3) would (without CORSAIRE) normally be produced by the heat pumps. With a COPhp-dhw of 2.73 (assumed to be identical to the TLN heat pumps in table 4.1, E-7), they would have absorbed 1.15 TWh electricity. This is therefore as much electrical energy saved (ΔEcor) by the net supply of Q-ECS3 in CORSAIRE free heating:

$$\Delta Ecor = 6.75\ PJ / 2.73) = \quad 2.47\ [PJ] \quad 0.69 \quad [TWh] \qquad (55)$$

6.3 National potential for electricity savings and investment by ULISSE and CORSAIRE

With these conservative assumptions (or objectives) for 2050, 1/4 of the Swiss population (lake regions) would benefit from ULISSE combined with free heating via the TLN networks (internal CORSAIRE) and another 1/4 of the population (outside lake regions) would benefit from CORSAIRE alone, with external free heating via the urban DWN.

Together, ULISSE (52) and CORSAIRE (55), by supplying 57 PJ of heat (i.e., almost 30% of national requirements), represent a “net” potential Winter Electricity Savings (WES) of 2.76 TWh.

$$EEH = \Delta Esys + \Delta Eecs = \quad 2.07\ TWh + 0.69\ TWh = \quad 2.76 \quad [TWh] \qquad (56)$$

Taking into account transformation and transmission losses of 10% (7% annual average), the “net” 2.76 TWh require a gross production of 3 TWh, i.e., 1/3 of the structural winter electricity deficit in 2050 (9 TWh). This is equivalent to the gross winter output of 2 Grande Dixence (CGD) hydroelectric storage complexes in 2050.

According to the AES study [16], the electricity cost of a storage power plant in 2050 will be 32 ct/kWh or 320 M CHF/TWh (Table 6.4 below). As a result, the production savings of 3 TWh would also represent an Annual Financial Savings (AFS) of CHF 1,312 M/year, roughly 3/4 of which would come from ULISSE (via the TLNs) and 1/4 from the "external" CORSAIRE free heating (via the urban DWN):

$$EFA = EEH * 32\ ct/kWh = \quad 3\ TWh * 320\ M\ CHF/TWh = \quad 960 \quad [M\ CHF] \qquad (57)$$

Furthermore, according to the same AES study, the Avoided Investment Cost (AIC) of the equivalent construction of 2 Grande Dixence Complexes is: AIC = 2 x 2,000 MW[7] x 4.75 M CHF/MW = 19 [G CHF] (58)

Coûts des constructions et des transformations en 2015, 2035 et 2050		
	Centrale au fil de l'eau	**Centrale à accumulation**
Coûts d'investissement [CHF/kW]	5300	4750
Exploitation et entretien par an	1% des coûts d'investissement	0,5% des coûts d'investissement
Redevance hydraulique [ct./kWh]	1,1	1,1
Coûts de revient [ct./kWh]	10–19	17–32

Table 6.4: Costs of new buildings and conversions in the various stages of the 2050 Energy Strategy (Source: Grande hydraulique, AES, July 2020) ***[16]***

The potential of ULISSE corroborates the *Position Paper* of May 2022 **[41]** of the *Forum Energy Storage* Switzerland (FESS), which shows that seasonal heat storage can not only reduce dependence on imported fossil fuels, but can also reduce, in theory, 4 TWh or 40% of the 10 TWh of additional electricity needs in winter (deficit)!

[7] Winter hydroelectric power & energy from the Grande Dixence Complex (CGD): 2 TW & 1.5 TWh.

6.4 Environmental and cohabitation aspects

The environmental issue inevitably arises when we consider "immersing a foreign body" in an aquatic environment such as a lake or even just using its water, for example for energy purposes (thermal impact). This is true even if the intention is “environmentally friendly”.

In the various chapters describing the ULISSE system, environmental and cohabitation considerations have been incorporated as the technological and construction choices are explained. Nevertheless, it may be useful to take them up again here, distinguishing them roughly into four interfering categories, as follows:

- Location and dimensions of underwater infrastructure
- Type and quantity of materials used
- Direct and indirect interactions with the aquatic environment
- Co-existence with lake users (boating, fishing).

6.4.1 Location

The large dimensions of a single ULISSE-type Reservoir (2 million m^3 of volume and 54,000 m^2 of projected surface area and footprint on the lake bed), require an ideal water depth of 65 to 75 m for the location. This automatically distances it from the *lake bed*. This zone, which extends from the shore towards the open sea, forms a gently sloping submerged coastal terrace. In Lake Geneva, it is home to seagrass beds that develop to a depth of around 10 m and are vital to the balance of the entire lake ecosystem **[60].** The meadows are already subject to numerous human-induced disturbances to their development, including the destruction of young macrophyte shoots by mooring buoys and boat chains moored in the open water [**56**].

6.4.2 Type and quantity of materials used

The ULISSE Reservoir is mainly made up of a semi-rigid/flexible "self-supporting" envelope (with no supporting structure). In addition to stainless steel cables, the shell is made up of a triple layer of type E fibreglass fabric sandwiched between cellular glass thermal insulation blocks. Beads of needled fibreglass or basalt felt are sandwiched between these blocks. The assembly is hydrophobic, inorganic, mineral and inert with respect to the aquatic environment (§ 7.1).

The ULISSE Reservoir is anchored by approximately 500 helical screw-in anchors aimed into the lake bed (§ 7.4). These anchors are installed in the lake bed from a boat, without a diver or robot, and have virtually no impact on or disturbance of the lake bed (Fig. 6.1 below).

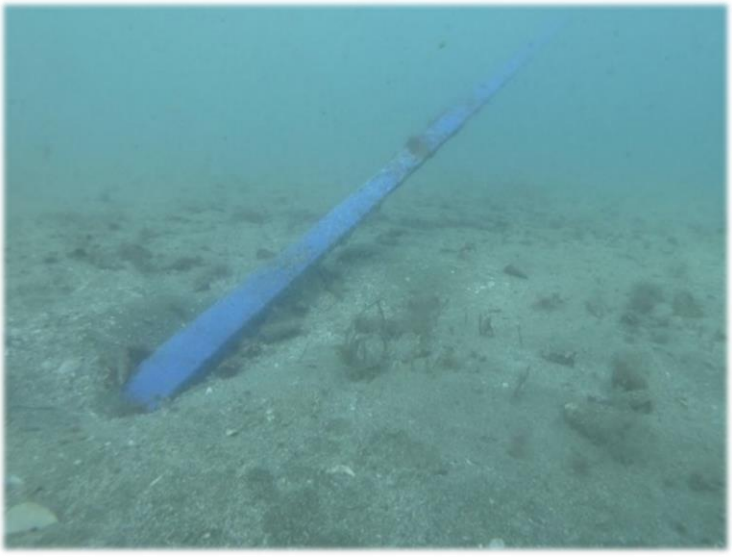

Fig. 6.1: Impact of a helical anchor aimed at the lake bed (Screw-in Anchor Technology, marinflex.com)

6.4.3 Interactions with the lake

1. In the configuration where **the ULISSE Reservoir is charged in summer with the return of tempered water from the TLN network**, the dilution of hot water discharged from the air-conditioning system directly into the lake is avoided, thus reducing the negative impact on the lake, which is already affected by global warming. In particular, global warming tends to modify the seasonal cycle(s) of mixing and thermal stratification of lakes, which influences their deep oxygenation, which is essential for these aquatic ecosystems **[28, 29].**

2. In the configuration where **the ULISSE Reservoir is charged in summer with temperate water from the upper layers of the lake** (Epilimnion), the selective capture device (phytoplankton filtration) makes it possible to regulate blooms (toxic algal blooms) if necessary and to recover the production of GHGs and CH_4 for energy use in the Reservoir (§ 7.3.4).

3. The 621 million m^3 of water confined in the 310 ULISSE Reservoirs constitute 39 PJ of heat and represent a 30 cm thick layer of water spread over the 2,024 km^2 of the 15 large lakes (§ 6.1).

Extracting the 39 PJ of heat from the epilimnion lowers the surface temperature of the lakes, **reducing water losses through evaporation by 17 million m^3** (latent heat of vaporisation of water: 2.3 GJ/m^3).

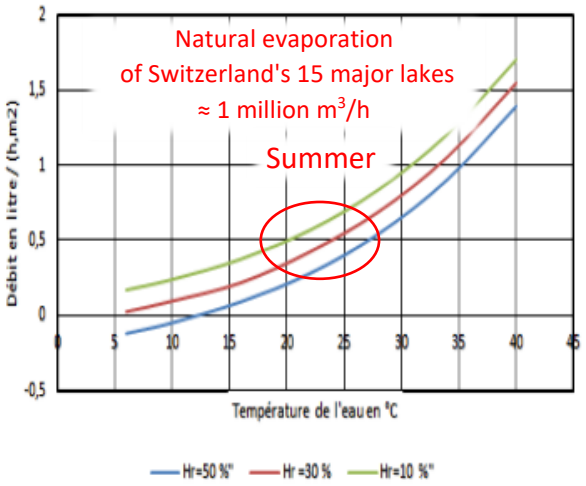

(Image : jcq2.fr/piscine)

Figure 6.2: Evaporation curves for a body of water (litre/h.m^2) as a function of water temperature (˚C)

While the 17 million m^3 of water loss potentially avoided by the ULISSE reservoirs may seem minimal compared with the natural evaporation from lakes (≈ 1 M m^3/h), it is nevertheless to ULISSE's credit and is more than the 14 million m^3 of water evaporated (0.75 to 1 m^3/s) taken from the Rhine River during the summer semester to cool the Leibstadt nuclear power plant, or the 10 million m^3 taken from the Aare River at the Gösgen nuclear power plant (§ 1.8.2).

On the other hand, lowering the temperature in the epilimnion and at the surface of lakes increases the solubility or dissolved oxygen content (O_2) in the water, which is beneficial and essential for aquatic life (fish).

Température de l'eau, (Celcius)	Concentration de l'oxygène, mg/L
0	14,6
5	12,8
10	11,3
15	10,1
20	9,1
25	8,5
30	7,6

Table 6.3: Dissolved oxygen content in water as a function of temperature

In addition, a greater quantity of oxygen is then also transported throughout the lake water column to the bottom by the mixing effect induced by the ULISSE Reservoirs (§ 4).

4. The external thermal convection currents induced by the ULISSE Reservoirs can improve the circulation of nutrients and oxygenation of the water layers at the bottom of the lake, thus protecting the aquatic ecosystem against eutrophication and Global Warming (§ 7.3.2). This thermal convection is illustrated by the numerical simulation of the ULISSE Reservoir carried out at HEPIA (figure 6.4).

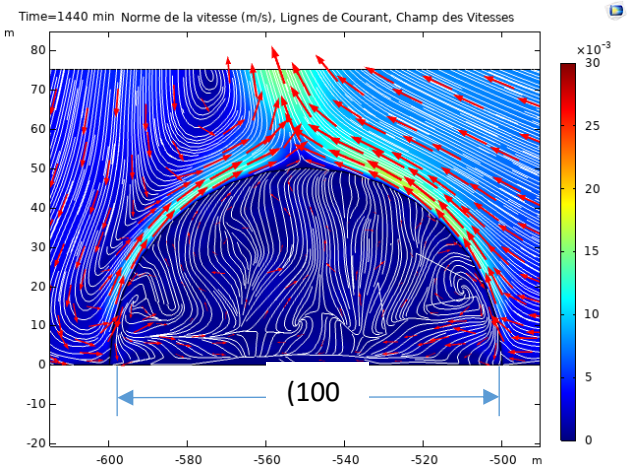

Fig. 6.4: Visualisation of *thermal convection (water velocity fields) inside and outside the ULISSE Reservoir* (cross-section *of the COMSOL digital simulation with the full-scale model of the Reservoir in the lake)*

5. The installation of ULISSE Reservoirs in homogeneous areas of the lake can diversify the "ecological niches" and enrich the lake fauna. In addition, the area where the Reservoirs are located (protected from fishing) can also constitute a protected area (a quiet zone) where the fauna can develop peacefully, replenish itself if necessary, and eventually spill over into the rest of the lake, resulting in an increase in the abundance and biomass of fish. This phenomenon is observed in Marine Protected Areas (MPAs) **[33, 34].**

Extract from the article: *https://reporterre.net/Les-aires-marines-protegees-le-mirage-de-la-preservation-des-oceans* [**34**] *"When there is a marine protected area, all the small fishing boats position themselves around it, because it spreads outwards",* explains Jean-Pierre Gattuso. "*When their levels of protection are high, they are beneficial not only for the ecosystems, but also for tourism, fishing, scuba diving... In most cases, users don't want to part with them",* adds Joachim Claudet...

6. The ULISSE Reservoir is subject to the internal movements of lake water masses, to varying degrees, which can threaten its structural integrity [**61**]. Its semi-flexible shell is light and can only deform under the action of water movements. At the very least, under the action of opposing masses of water (horizontal shear), the deformations of the envelope modify the (open) volume of the Reservoir and would cause it to lose some of the tempered water inside. Under no circumstances must the stresses on the Reservoir anchors exceed their holding limits in the lake soil (§ 7.4)!

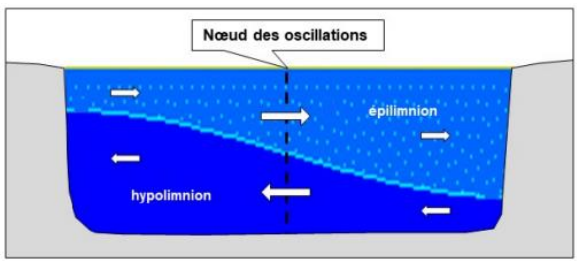

Figure 6.5: Due to thermal stratification, the currents generated by an episode of seiche and internal seiche are opposed between the epilimnion and hypolimnion. The strongest currents are created under the oscillation nodes.
(Figure taken from the preliminary analysis report on the risks associated with lake currents threatening the structural integrity of ULISSE, Zsolt Vecsernyes, LHA of HEPIA 2022), ***Appendix 4. [61]***

Under the action of the prevailing winds, water masses at the surface move and more particularly variable internal currents (seiches) towards the depths, depending on the thermal state of the lake (seasonal stratification). These internal seiches are generally located in the *thermocline* zone (metalimnion) and can form strong, oscillating counter-currents with a period of several hours **[61]**.

In conclusion, it is important to study the hydrodynamic phenomena and structural stability of ULISSE in an appropriate manner by specialists, in a hydraulics laboratory.

The location of the ULISSE Reservoir needs to be defined carefully. Its size (55 m high, 100 m wide, 560 m long) could have an impact on lake currents, especially if several units are installed in parallel. The reduction in the wetted area of the lake will increase the speed of the current, at least in the vicinity of ULISSE. These aspects will have to be analysed hydrodynamically by a specialist **[61].**

6.4.4 Co-existence with lake users (navigation, fishing)

1. Navigation: Anchored to the lake bed, the top of the ULISSE Reservoir is located approximately 10 to 15 m below the surface of the lake. It is therefore invisible from the surface and will not interfere with navigation. The water catchment device in the epilimnion zone, if used, does not come closer than 3 m below the surface. It is lifted out of the water only in the presence of a specialised maintenance boat, which is duly marked (§ 7.3.5).

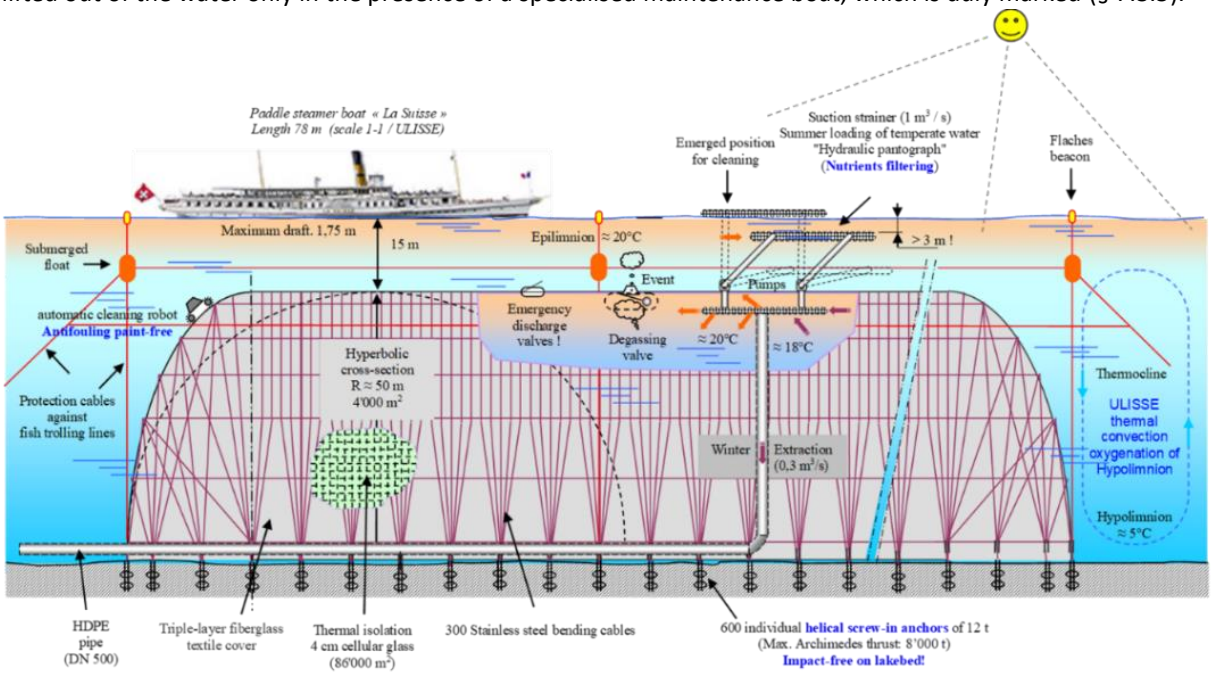

Figure 6.6: Schematic representation of the ULISSE type Reservoir, with signalling beacons (CGN boat to scale).

For example, the draught of the large CGN (Compagnie Générale de Navigation) boats on Lake Geneva is less than 2 m. Pleasure boats (sailboats) have a keel draught of barely 1.2 m.

Figure 6.7: CGN boat "La Suisse" on Lake Geneva, length 78 m, draught ≈ 1.7 m

2. Fishing: Fishing is probably the lake activity that can be most influenced/impacted by the presence of ULISSE Reservoirs **[60]**. However, this interference can be put into perspective, given the respective surface areas and lake volumes involved.

The potential installation of 310 ULISSE Reservoirs would total 17 km^2 of (invisible) right of way on the lake bed, which represents 0.8% of the 2,024 km^2 of the total surface area of the 15 large lakes (> 10 km^2), of which 1,233 km^2 are on Swiss territory (61%). For Lake Geneva, the potential of **87 ULISSE Reservoirs also represented the equivalent of 0.8% of the surface area and 0.2% of the volume of lake fishing.**

The 580 km^2 of surface area and 167 km of shoreline of Lake Geneva are shared between 150 professional fishermen (with still nets and fish traps) and around 8,000 amateur fishermen (with lines and trolls), catching around 1,000 tonnes/year of fish (≈ 10% by amateur fishermen). Source: http://leurres.ch/leman.html.

Amateur fishermen use lines and trolls, generally towed by a boat in motion or anchored in the lake. These lines, which can be up to a hundred metres long, are fitted with hooks that can potentially interfere with or even catch on the casing of the ULISSE Reservoir.

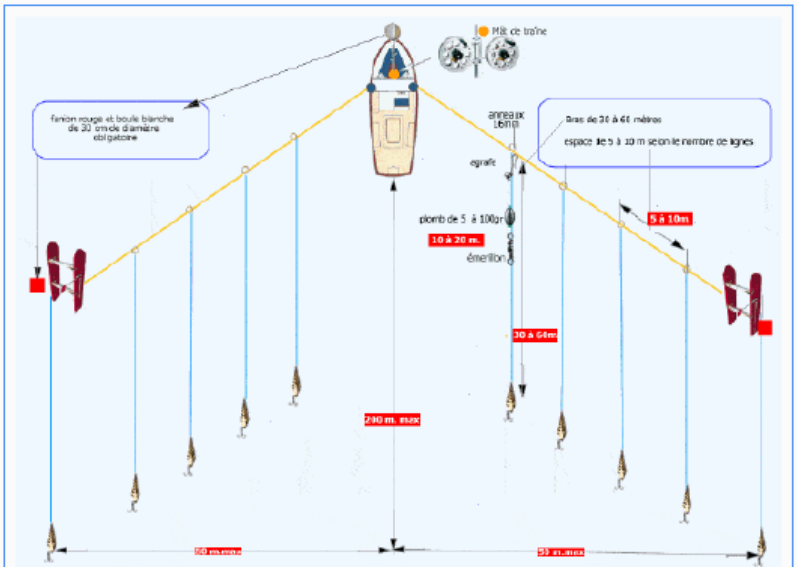

Figure 6.8: Diagram of troll fishing and spreaders (Fédération Internationale des Pêcheurs Amateurs du Léman, FIPAL)

In the same way as for professional fishing gear set or stretched in the water and anchored, **ULISSE Reservoirs can, in addition to being clearly mapped and geolocated, be marked with physical markers to help anglers avoid them.** The installation of ULISSE Reservoirs in large lakes should be carried out in consultation with anglers and by demonstrating their positive environmental impact.

7 ULISSE Reservoir: construction, operation and investment cost

7.1 Reservoir envelope

The ULISSE Reservoir consists mainly of a semi-rigid envelope forming a concave pocket with the opening pointing downwards and fixed close to the lake bed by means of non-invasive ad hoc screw-in anchors. It behaves like an "aquatic hot-air balloon" filled with water at a higher temperature and therefore less dense than the surrounding aquatic environment.

The shell of the Reservoir is thermally insulated with cellular glass *blocks.* Cellular glass has a low density (100 to 200 kg/m^3), withstands a hydrostatic pressure of 10 kg/cm^2 and is totally hydrophobic. In addition to reducing heat loss, the low density of these isolation blocks in relation to water ensures the structural stability that is essential for the self-supporting Reservoir, even when it only contains cold water identical to that surrounding the lake!

Illustrated in Figures 7.1 and 7.2, the configuration of juxtaposed but independent rigid blocks is required to give the overall mobility (semi-rigid/soft) and shape of the Reservoir envelope. The isolation blocks follow the transverse curvature of the envelope (R ≈ 50 m) and have a variable inclination of a few degrees between them.

Heat loss from the Reservoir is limited (15-20%), by the favourable ratio between the surface area of the hyperbolic envelope (88 10^3 m^2) and the large unit volume (2 10^6 m^3). The thickness of the cellular glass blocks is limited to a few centimetres (5 to 10 cm) and can vary according to depth in order to optimise quantity.

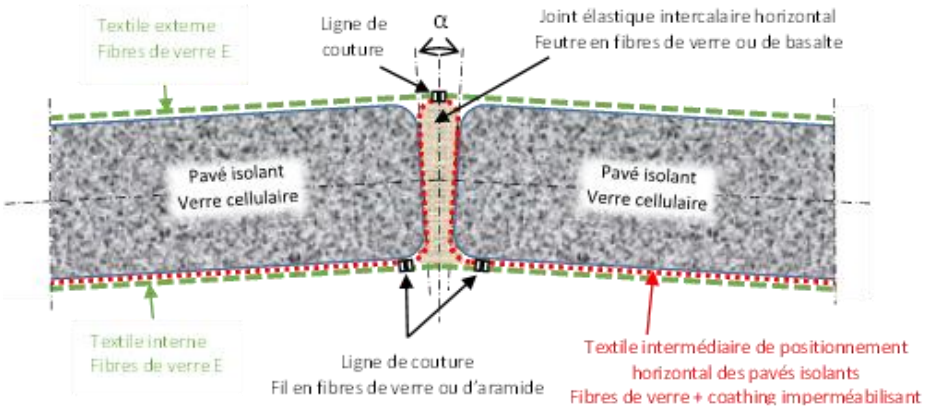

Figure 7.1: Cross-section of the ULISSE Reservoir shell (junction of insulating blocks)

The envelope consists of a triple layer of technical textile, made of type E glass fibre, which is also hydrophobic, inorganic, mineral and inert to the aquatic environment. The thermal insulation blocks are sandwiched between the outer textile layer and the inner layer. The blocks are held in place (against Archimedes' buoyancy) by an intermediate layer of fabric. The intermediate fabric used to position the blocks is attached to the inner and/or outer fabric by means of seams (glass fibre or aramid threads), forming a horizontal pocket in which the blocks are held in place.

Beads of needled fibreglass or basalt felt are sandwiched between the isolation blocks and around as an abrasion protection layer of the cellular glass (§ 8.4.7, layer not presented on the figures 7.a, 7.2). They reduce heat loss and water leakage at the interfaces. The latter is caused by the difference in hydrostatic pressure of the hot water under the envelope and can be eliminated by waterproofing the intermediate textile. In addition, the (permeable) textile layers are pressed against the isolation blocks and are therefore hydraulically obstructed by the impermeability of the cellular glass blocks.

The various sections of the Reservoir shell are arranged in wide transverse arch strips which are clamped together in symmetrical *jaws.* More precisely illustrated in Figure 7.2, at the edges of these strips, the three layers of textile surround a stainless-steel cable which together are clamped and held in the said jaws. These jaws are the same length as the height of the isolation blocks, so that they can follow the curvature of the envelope. To reduce thermal bridging, these jaws are covered with a mat of insulating felts.

The lower edges of the transverse strips of the envelope are also given a hyperbolic shape by the tension of a stainless-steel cable held in place by a similar clamp system. The cables are connected to low-impact targeted pile anchors (Marineflex Screw Anchor Technology).

The upward Archimedean thrust, which the anchor must retain as a minimum, totals 7,000 t. Half of this is constant, due to the apparent density of the shell insulation (-835 kg/m^3), and the other half variable, due to the quantity and temperature of the "hot" water in the Reservoir (-1.76 kg/m^3 @ ΔT: 15 K).

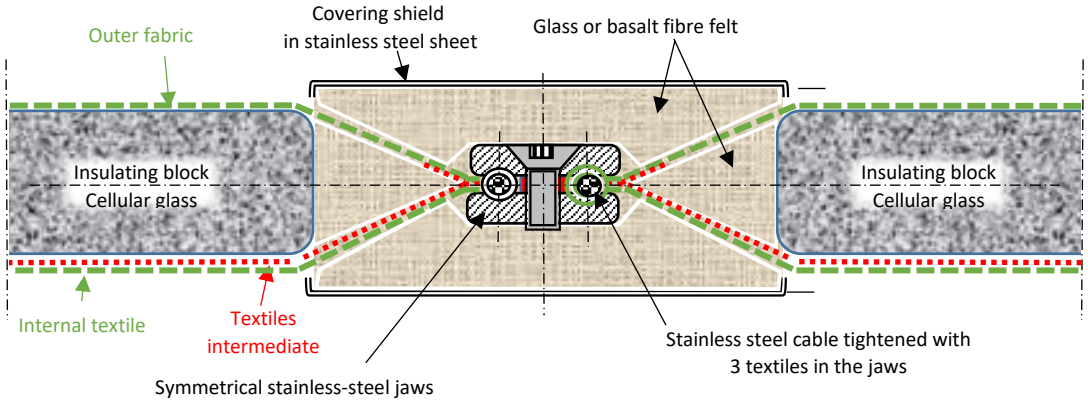

Figure 7.2: Junction of the transverse bands of the ULISSE Reservoir shell

7.2 Reservoir operation (loading & unloading cycle)

Operation of the Reservoir consists of an annual cycle of 4 distinct (seasonal) phases of different durations, comprising: 1 *Summer Loading of* tempered water (SL), 2 *Autumn Stagnation of* the full Reservoir (AS), 3 *Winter Discharging* (WD) of tempered water, 4 *Spring Stagnation* (SS) of the "thermally empty" Reservoir.

The durations of the various phases of annual operation influence the energy balance and are shown in Figure 7.3 below:

1.	Summer Loading (SL)	=>	2	months (1/3 workforce: 6h/day)
2.	Autumn Stagnation (AS)	=>	2	months
3.	Winter Discharging (WD)	=>	6	months
4.	Spring Stagnation (SS)	=>	2	months

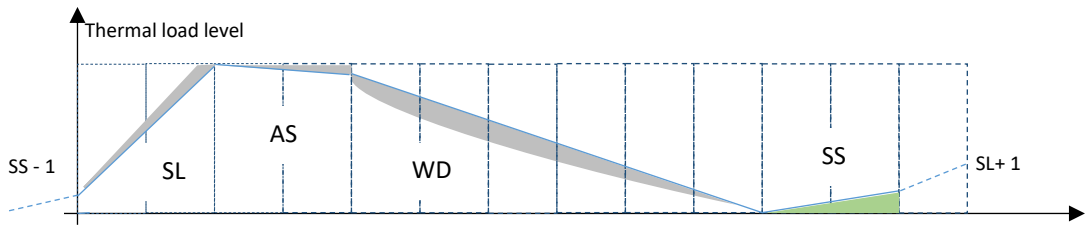

Figure 7.3: Dynamic operating phases of the ULISSE Reservoir (annual cycle)
*(Grey areas: **loss/gain**)*

7.2.1 Summer Loading process (SL)

Summer Loading process (SL) is carried out by (in principle) electric pumps **when sunshine and photovoltaic production are at their maximum**. To charge the 2 10^6 m^3 of an ULISSE Reservoir, during the 2 hottest months of the summer and at a rate of 6 hours/day (e.g., from 10 a.m. to 4 p.m.), i.e., over 365 hours, the **pumping rate is 1.5 m^3/s**.

During this loading process, each injection of tempered water (at temperature Ti) at the top of the Reservoir (at constant volume) also involves the evacuation of the same volume of cold water at its base (at temperature To). With a temperature gain ΔT = 15 K over the initial temperature (Ti) of the water in the Reservoir, the heat injected into the Reservoir is 125 TJ (@ ΔT = Ti-To = 15 K).

Ideally, there would be no heat loss, convection or advection inside the Reservoir, with the gradual establishment of perfect thermal stratification (without dilution or mixing between waters of different temperatures). This would amount to the formation of a "*flat-front thermocline*" at the interface between the upper volume of hot water and the lower volume of cold water inside the Reservoir. In this case, the temperature of the cold water at the lower outlet (To) would be constant and equal to the initial input temperature (Ti) until the end of summer loading (SL).

However, the tempered water (ΔT = 15˚K) injected tends to mix and partially dilute with the cold water already or still inside the Reservoir as well as with that which simultaneously emerges at its base. Depending on the dilution/mixing rate, more tempered water will therefore have to be injected than the actual volume of the Reservoir to fill it completely with tempered water. This is due to the advection or turbulence created by the water introduction jets as well as diffusion and thermal loss and convection.

This increase in the volume of tempered water can be provided by a higher flow rate and/or pumping time. In fact, the rate of thermal filling of the Reservoir will decrease as the temperature of the (diluted) water at the low outlet (To) increases until it approaches and reaches that at the inlet (Ti). In itself, this does not affect the initial or nominal thermal capacity of the Reservoir, as long as this is compensated for by the additional supply of tempered water during the Summer Loading phase (SL).

7.2.2 Winter Discharging process (WD)

The winter discharging phase (WD) concerns (or is intended to concern) the heating period, which averages 193 days in Geneva (average 1997-2007), i.e., 6 months, also known as the "winter or heating semester".

The opposite process to the SL phase also tends to occur during the WD phase. In winter or when buildings are being heated, the extraction of temperate water from the Reservoir is also compensated by the introduction of cold water at its base, with the same phenomenon of mixing and diffusion between the temperate and cold water; all induced by the deleterious trio of conduction-convection-advection.

7.2.3 Impact on throughput and performance of ULISSE with and without CORSAIRE

During WU, the gradual lowering of the residual temperature (ΔT ≈ 2K) of the water in the Reservoir means that, for the same heat extraction power, the pumping flow rate will have to be increased (due to the lowering of the volumetric energy density of the water, in J/m^3). In addition to an increase in the energy absorbed by the water circulation pumps in the distribution network (proportional to the square of the flow rate), the performance of the Heat Pumps (HP) decreases as the temperature of their "cold source" (ULISSE Reservoir) decreases and therefore negatively affects the efficiency or overall coefficient of performance of the system.

However, unlike Summer Loading (1.5 m^3/s x 365 h), Winter Reservoir Unloading is spread over the winter semester (6 months). For a supply to the urban DWN, intended for the room heating and DHW needs of buildings, the daily flow (day and night) is relatively continuous but changes according to the rigour of winter (atmospheric temperature). The average daily flow from the thermal discharge WU is therefore around 0.13 m^3/s (x 4,380 h), i.e., ≈ 8.5% of the flow from the SL.

The ULISSE tempered water supply flow rate, intended for winter de-icing of the public drinking water network (CORSAIRE external to the TLN), follows not only the initial seasonal (sinusoidal) change in the DHW temperature but also the diurnal/nocturnal variation in drinking water consumption. For simplicity's sake, we can consider full daily modulation, with a diurnal concentration of drinking water consumption. The (diurnal) flow from the WU of ULISSE Reservoir is then 0.25 m^3/s (x 2,190 h), i.e., 17% of the flow from the SL.

The continuous input (4,380 h) CORSAIRE internal to the TLN (without DWN) remains identical to the 0.13 m^3/s.

In the end, the water extraction rate (WD) from the Reservoir, being significantly lower than that for the CE, will produce proportionally fewer parasitic advection currents and therefore, a priori, better maintenance of stratification (*flat-front thermocline*) throughout the WD phase.

7.3 Collecting tempered water and loading/unloading the ULISSE Reservoir

7.3.1 Introductory issues

The ULISSE Reservoir is thermally charged during the summer period (SL) in two possible ways; one by the capture of tempered water from the upper layer of the lake (epilimnion zone) heated directly by the summer sun and the other by heat rejected from the *Thermal Lacustrine Network* (TLN) for air conditioning (indirect solar heat) and district heating (e.g., GeniLac).

7.3.2 Lake eutrophication

The eutrophication of aquatic environments (lake and sea) is characterised by excessive growth of plants and algae due to the high availability of nutrients and favourable thermal conditions. In addition to the coastal appearance of algal blooms (bloom), which can be nauseating and toxic, phytoplankton, which thrive on these nutrients, absorb large quantities of oxygen when they die and decompose. Its proliferation causes the depletion of the necessary oxygen and then the death of the aquatic ecosystem by "asphyxiation".

The problem of aquatic eutrophication is caused in particular by excessive inputs of nitrogen and phosphate, from nitrates in agriculture, wastewater and motor vehicle pollution. The situation is exacerbated by sunshine, temperature and global warming.

Limiting aquatic eutrophication means limiting the nutritional input (e.g., by banning phosphate in washing detergents, limiting fertilisers, etc.) and eliminating the algae and plants in question (e.g., by cleaning up beaches during green tides, etc.).

7.3.3 Fouling and clogging of lake water suction strainers

Generally, the water intake for various uses (drinking water, cooling water and/or lake hydrothermal heating) is located near the bottom (hypolimnion zone) to benefit from a low and more stable temperature than in the upper part of the aquatic environment (epilimnion zone).

Typically, suction strainers in pumping installations have a mesh size of less than 1 cm to filter out debris and prevent adult zebra mussels from being sucked in (an effective barrier to their proliferation in the system). Strainer openings are large enough to limit suction speed to a maximum of around twenty cm/s so that small fish (< 1 cm) can escape (*NYSDEC, 1998*)[8] [**8**]. Chlorine is generally injected to prevent the development of algae and zebra mussels in the system (source SIG, 2017).

Strainer cleaning is generally carried out annually using pressurised water jets, requiring the use of experienced divers and, failing that, extensive dismantling and lifting of the strainers in the open air.

Suctioning water from the upper part of the water body (epilimnion) during the summer semester, precisely at the height of the phytoplankton growth zone and period (bloom), would normally accelerate clogging of the suction strainer and would require (without any other prophylactic or curative measures) even more regular and tedious, if not prohibitive, cleaning.

7.3.4 Capture of phytoplankton blooms in the ULISSE Reservoir

The summer phytoplankton introduced into the ULISSE Reservoir, deprived of vital light, dies prematurely (compared with autumn-winter) and settles to the bottom where it is decomposed by heterotrophic bacteria, First the aerobic bacteria, which consume the free oxygen in the water (0_2), producing carbon dioxide (CO_2), then in the progressively anoxic environment, the anaerobic bacteria, producing mainly methane gas (CH_4).

Under the effect of the expansion pressure, these biogases migrate towards the top of the Reservoir and push the water through the bottom opening out of the Reservoir, increasing the Archimedean thrust and the resulting traction force on its anchors.

Nevertheless, the summer loading of the ULISSE Reservoir offers the opportunity to regulate the concentration of phytoplankton (by extraction or controlled filtration at the suction strainer) in order to prevent or cure the lake environment and subsequently to capture CO_2 and CH_4 in situ for energy purposes.

[8] Viquerat P-A. thesis, page 66/ A/Pumping and discharge

7.3.5 ULISSE temperate epilimnion water collection and storage system

Shown schematically in Figures 7.4/5/6 below, the ULISSE Reservoir's mobile lake water collection device consists of at least one suction strainer, divided into two parts or a pair of separate strainers operating in tandem (A-B). The tubular strainer (1) is mobile and adjustable in height (3 to 15 m from the surface of the lake) by means of joints (Xc, Xp) in the pipes (2) connecting it to the motor pumps (3-16). These are located at the top of the Reservoir and connected to the tempered water injection/extraction ramp, which is also tubular in shape.

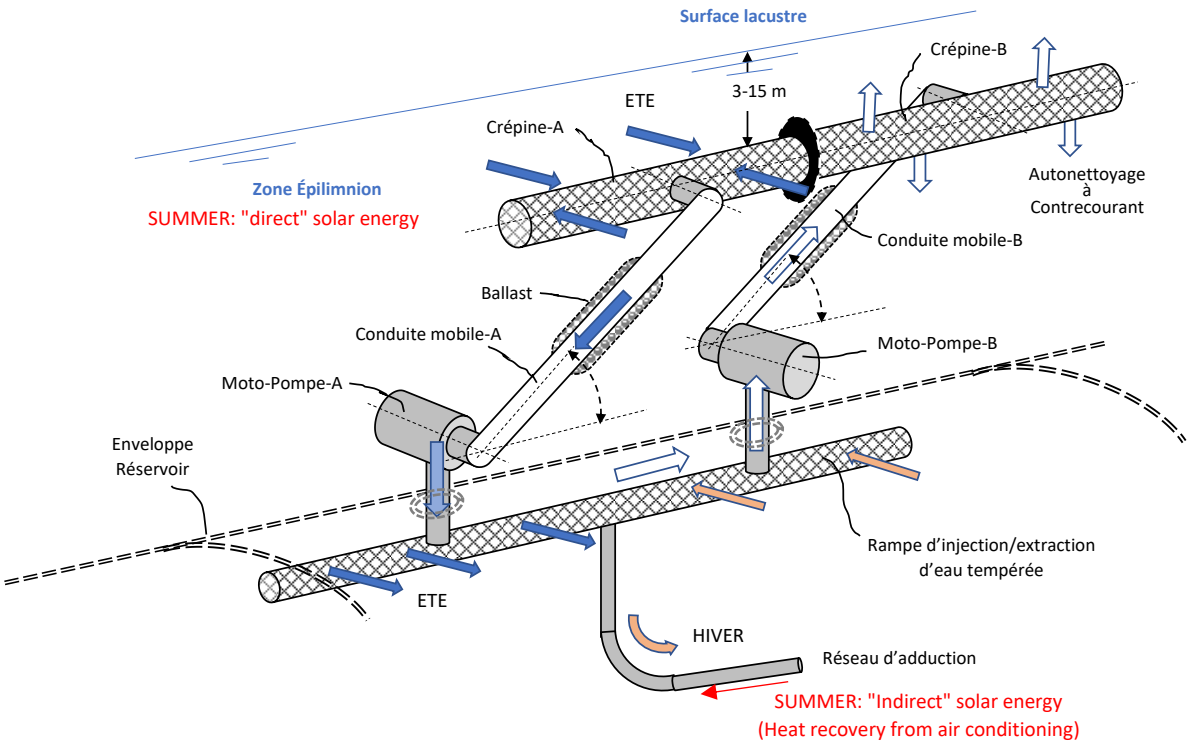

Figure 7.4: Schematic diagram of the mobile temperate lake water collection device (Epilimnion zone) Here the internal injection/extraction manifold is closed during the strainer self-cleaning process. The water sucked into the A-strainer is pumped back to the B-strainer for counter-current cleaning and vice versa.

Each part A/B or pair of strainers is fitted with a Distancing Grid (G) and a Filter (F) for micro-organisms (phytoplankton). The filters (F) can be retracted by remote control, either by translation or rotation (at 90˚) around the longitudinal axis of the Tubular Strainer (Fig. 3). This allows the filters to be placed in front of the suction ports as required, and thus regulate the quantity of phytoplankton captured per unit volume of water sucked in. The remote-controlled actuator, e.g., a jack or similar, is not shown to avoid unnecessarily overloading the drawing.

The articulated ducts 2-A/B form a deformable parallelogram (variable geometry), like a "hydraulic pantograph", which keeps the mobile strainer in a horizontal position whatever its height (h) from the lake water. The inclination of the connecting pipes takes the strainer from a low position (h-b), passing through the optimal height collection zone (h-m, from 3 to 5 m), to a high position (h-h) which allows the strainer to be lifted out of the water for maintenance in the open air.

The top of the Reservoir, located at a depth of around ten metres, is out of reach (draught) of boats, which can pass over it without difficulty. The connecting pipes therefore have a minimum length of 10 m to allow the strainer to emerge from the water in the upper position.

The water injection/extraction manifold is fitted with a tubular shutter for the side orifices, which can be moved or rotated by remote control. This allows water to be sent alternately from one pump to the other compartment of the screen, which is stopped for periodic self-cleaning in counter-current, possibly supplemented by an injection of compressed air for cleaning. When the pump is stopped, it has only a small head loss in the counter-current of water flowing through it.

A UV-C disinfection system can be installed inside the suction strainer and distribution manifold in the Reservoir. This reduces mussel colonisation in the pipes and pre-treats the water for use in the drinking water network (DWN).

Shown in more detail in Figure 7.5 below, the action of positioning the height (h-h) of the suction strainer can be achieved using a piloted ballast tank (18) which provides a modulating upward thrust on the device.

This ballast tank can be fixed directly under the suction strainer (1) or to any other moving parts (2), which would ensure its positioning action. The thrust of the ballast tank (18) is controlled by varying the ratio of the volume of water inside and the volume of compressed air (20) supplied from outside.

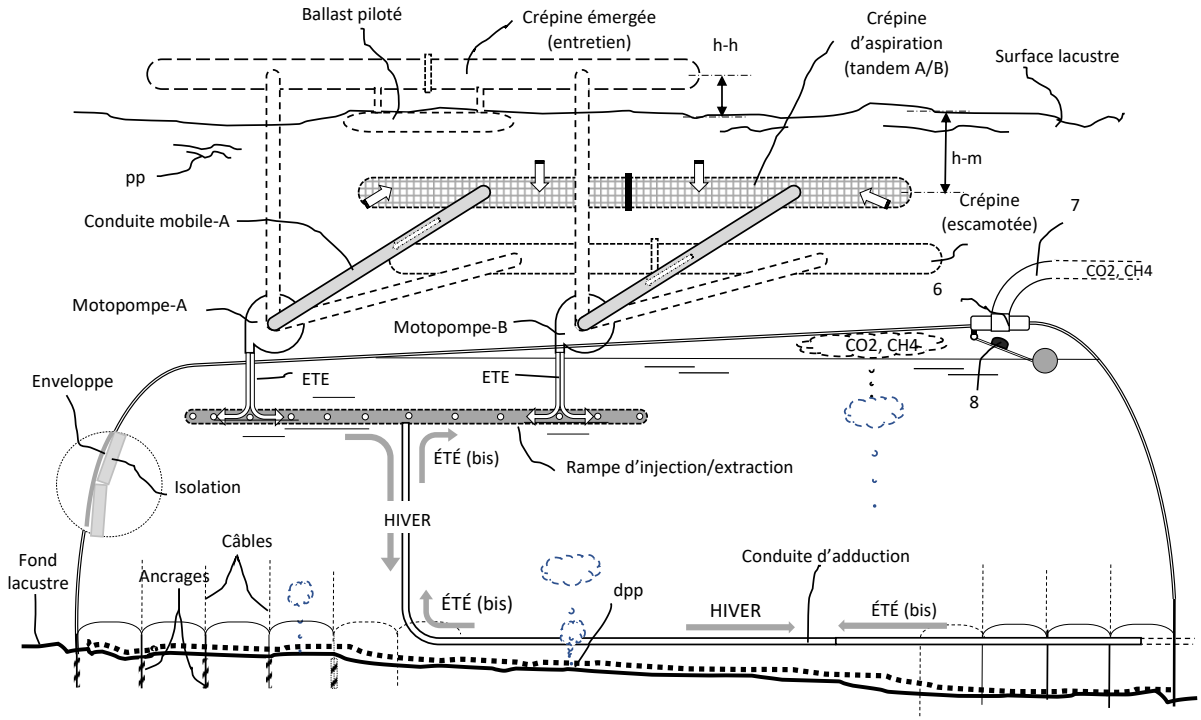

Figure 7.5: General diagram of the Summer Loading and Winter Discharging system for the ULISSE Reservoir (the different components are not to scale)

An alternative or complementary aid to this ballast tank (18) for positioning is, for example, a pneumatic cylinder (19), the intensity of whose lifting action force is produced by the pressure of compressed air (20) on the inner piston of the cylinder.

This solution has little effect on the apparent weight of the moving part and possibly avoids the need for a positioning locking system. The air pressure in the cylinder (19) determines the force of the piston in equilibrium with the reaction force due to the weight of the moving part as a function of its position. An offset counterweight or return spring may be used to complete the mechanism.

7.3.6 Power supply for pump units

The motors (16) of the pumps (3) are electric or pneumatic (compressed air) and are powered by a corresponding remote terrestrial generator source (17). The pump units are immersed and placed on the dome of the Tank by means of a fixing frame (23) which distributes the load of the assembly and are fitted as required with low-density supports, e.g., made of cellular glass.

In addition, these pump units are housed in a sealed enclosure (21) pressurised with compressed air to repel the parasitic introduction of water (22). In the case of an electric motor, cooling by removing heat from the enclosure is further facilitated by the greater density of the pressurised compressed air. The enclosure (16), filled with pressurised air (22), provides additional buoyancy which further reduces the weight of the pump units on the dome of the ULISSE Reservoir.

To balance the torsional forces on the joints, the connecting ducts (2) with the motor pumps (16-3) are mounted on either side of the Strainer (1). The motor pump units can also be mounted co-axially, which then requires a 90˚ elbow on their suction inlet to connect the lower joint (Xp) of the connecting ducts (2).

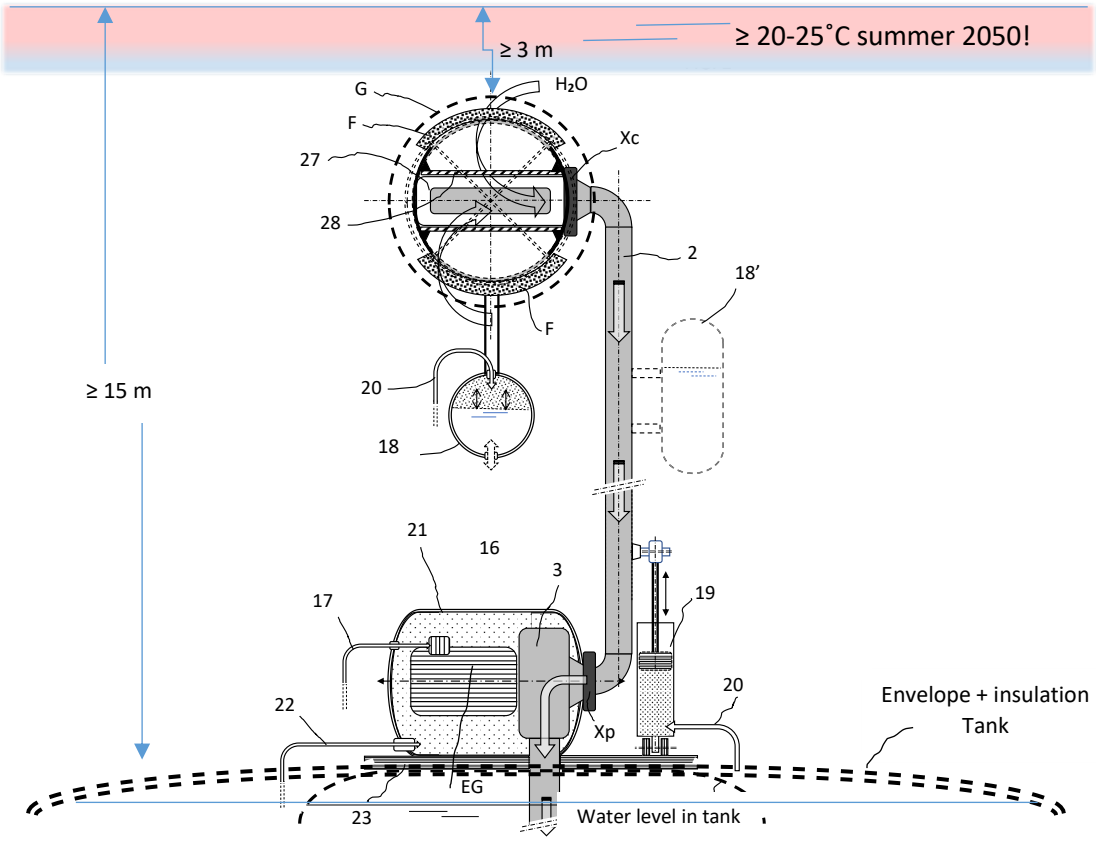

Figure 7.6: Schematic representation of the lake water suction strainer pump unit

7.3.7 Hydraulic shut-off and degassing valves

A rotary obturator device (27), fixed transversely in the strainer at the level of the joints Xc, covers the opening (28) in the water passage tube when the strainer descends into its low or rest position (Figures 7.4 and 7.5), which prevents any undesirable backflow of water towards the strainer from the Reservoir. The rotary obturator (27-28) being fixed to the strainer and the tube being fixed co-axially to the upper elbow of the connecting duct 2, together they form the rotary bearing of the joint Xc.

If necessary, a brake or detent between the two obturator tubes can be used to remotely lock the joint and therefore the height position of the strainer.

The curvature of the top of the Reservoir combined with its longitudinal inclination and the control of the extraction orifice (6) at the highest point of the Reservoir create a Degassing space (DS) where the biogas (CO_2, CH_4, thiols) produced during the decomposition by the bacteria of the dead phytoplankton dpp deprived of light in the Reservoir migrates naturally.

The water level ΔR in the Reservoir and therefore the volume of the Degassing Shpe (DS) are conditioned by the pressure Pg of the biogas inside. This pressure Pg is controlled by a pressure regulator and corresponds mainly to the hydrostatic pressure of the water column (Ph = ρ.g.Δh) with the surface of the water plane and added to the Archimedean pressure PA.

For example, with the top of the Reservoir 10 metres below the lake surface, the *hydrostatic pressure* (Ph) there is 1 kg/cm^2 or 1 bar. At this depth on the envelope, the differential Archimedean pressure (ΔPA = Δρ.g.h) results from the difference in density (Δρ) of the height (h) of the water column in the Reservoir and that of the surrounding lake. It is induced by the inside-outside temperature difference (ΔTi-o). For example, with ΔTi-o = 15K, Δρ = 1.8 kg/m^3, and h = 50 m => PA = Δρ.g.h ≈ 9 g/cm^2 ≈ 9 mbar, i.e., of the order of one hundredth of Ph.

The orifice (6) is fitted with a float valve (8) which maintains a minimum Degassing Volume (DV) and also prevents water from entering the pipe (7) of the biogas recovery and transport network, for "prophylactic" (GHG) and energy purposes.

A safety degassing valve (10) fitted with a float (11), located at a lower height Emax, limits the degassing volume (DV). This is to limit the Archimedean thrust on the ULISSE Reservoir. As DV increases, some of the insulation blocks at the top are no longer immersed and therefore no longer subject to buoyancy. However, this is negligible compared with DV.

7.3.8 Distribution of the ULISSE Reservoir water catchment system

Given a 2 10^6 m^3 unit volume of the ULISSE Reservoir and a Summer Loading (SL) concentrated over 365 hours (6 h/d x 2 months), the corresponding pumping rate is approximately 1.5 m^3/s.

The ULISSE Reservoir can be fitted with several mobile suction strainers with double compartments and motor-pump units. With a total length of the Reservoir of 560 m and a spacing of 100 m, it is possible to install and distribute 5 "double" Strainers, i.e., 10 motor-pump units. Each motor-driven pump (16-3), with its connecting pipe (2) and half-strainer (1), then has a flow rate of 0.15 m^3/s. Pressure losses remain relatively low.

The large total storage volume of the ULISSE system is made up of several underwater Reservoirs arranged in a network (12 M m^3, divided into 6 Reservoirs for the GeniLac network).

Water is extracted from the ULISSE Reservoirs in winter via the internal tubular strainers (injection/extraction ramps), which are then in suction mode from the Lake Pumping Station (LPS). The injection pumps, on the dome of the Reservoir, are then at rest and their respective water inlet ports closed by the rotation of the articulated pipes of the hydraulic pantograph (Figures 7.4/5/6).

The water is transported via a High-Density Polyethylene (HDPE) supply pipe with built-in thermal insulation (Figures 5.16/17).

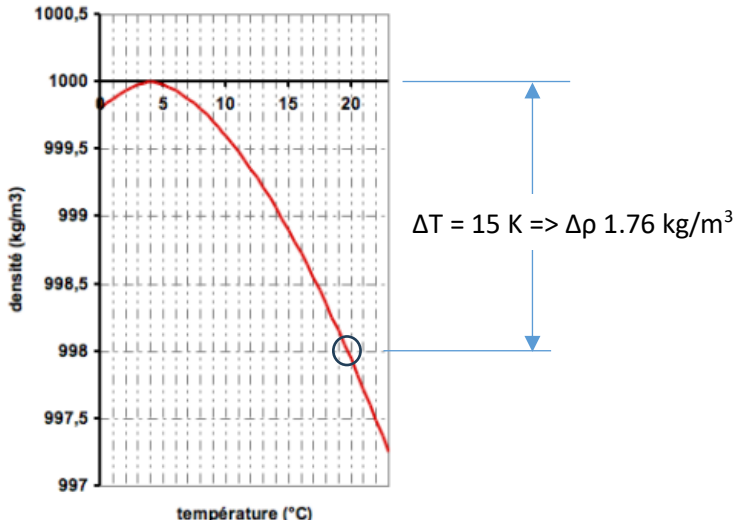

Figure 7.7: Variations in freshwater density with temperature at atmospheric pressure, calculated by the following empirical formula: ρ = (1-1.9549.10-5. |T -4| 1.68).1000 [Hostetler (1990), Heggen (1983)]. Source: Modélisation des températures de surface et de fond des plans d'eau, Camille Bouchez, 09.2010

7.4 Anchoring of the ULISSE Reservoir

The ULISSE Reservoir undergoes an Archimedes upward pull that reaches 7,000 t (eq.8.39), of which 3,500 t is due to the insulation (4,400 m^3 of cellular glass, $\Delta\rho g$ = -835 kg/m^3) and 3,500 t varies according to the temperature difference of the stored water (2 M m^3, $\Delta\rho w$ = -1.76 kg/m^3 @ ΔTw = 15 K). The Reservoir is anchored by means of **515 helical anchors screwed into the lake bed, distributed over 103 junction squares** and by cables connected around the circumference of 1,234 m (eq. 8.34) from the base of the Reservoir envelope.

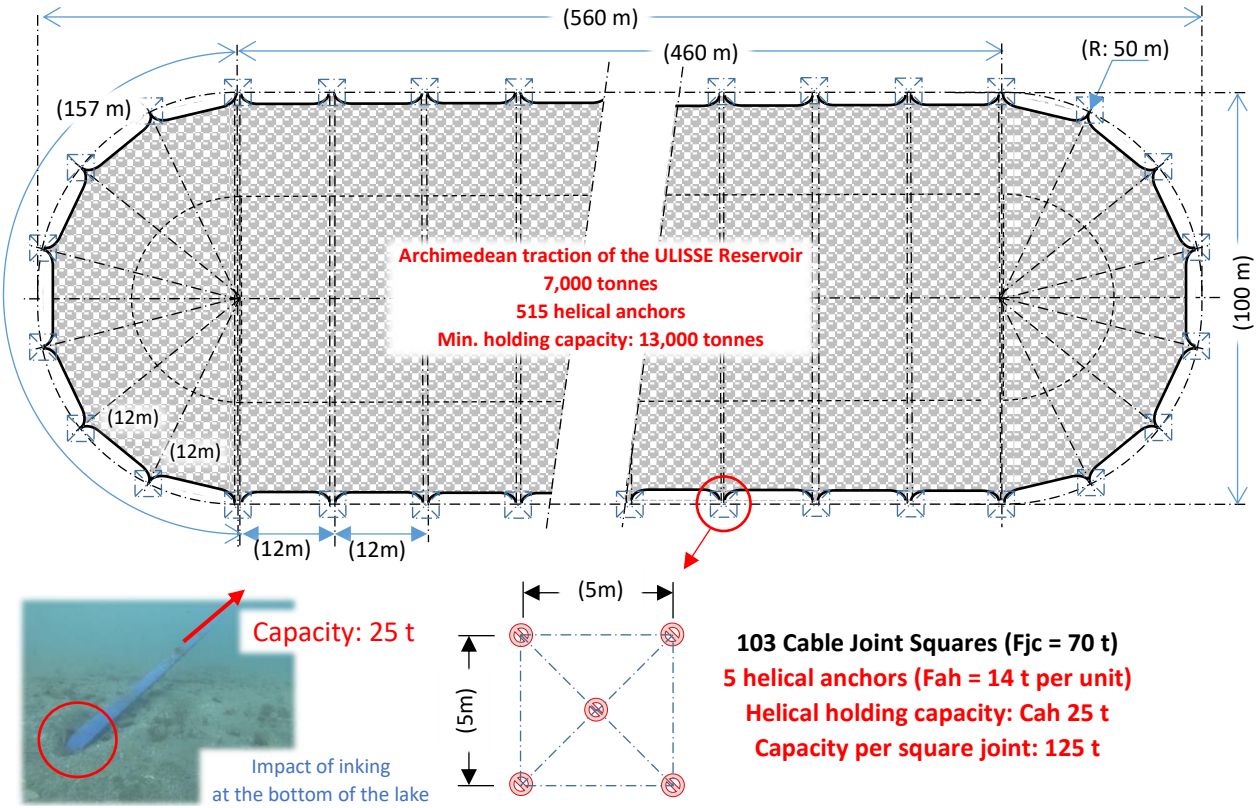

Fig. 7.7 bis: Principle of anchoring the ULISSE Reservoir on the lake bed with Marine Flex helical screw anchors

The lower edges of the transverse strips of the envelope are also hyperbolically shaped by the tension of a stainless-steel cable held in place by a similar clamp system. This lower part of the envelope is covered by a fibreglass textile skirt, which is presumably not insulated, touching the lake bed and closing off access to the Reservoir to the local fauna (fish, etc.).

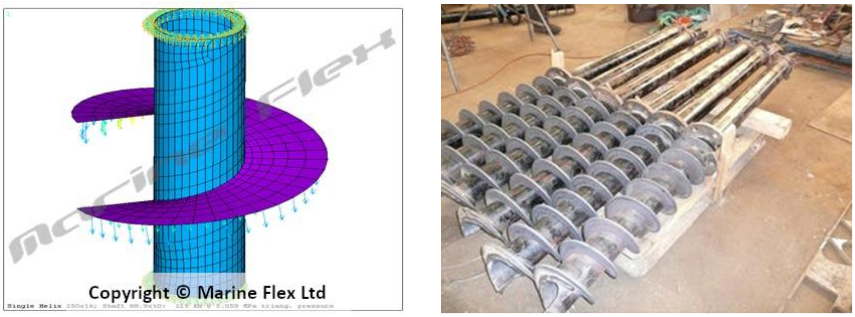

Figures 7.8: Spiral anchor for lake and seabed: Screw-in Anchor Technology (marinflex.com)

Helical anchors (Marine Flex, fig. 7.8) are characterised by a very high vertical holding capacity of up to 25 t (breaking load tested). They have virtually no impact on or disturbance of the lake bed. They are suitable for

different types of soil: silts, clays, sands, gravels, sandstones or weathered rocks (N=1 to 50). They are installed in the lake bed from the surface (boat) to depths of 100 m and more, with geolocation (accuracy < 10 cm).

7.4.1 Using Marine Flex helical anchors (40 years' experience)

No-dive, no-robot system: allows installation from the vessel economically, quickly and safely in very deep water, strong currents and sloping ground (fig.7.9). Typical installation time 35 to 50 minutes (≈ 10 anchors per 8-hour shift or per day). Cost per anchor and installation: € 1,500 to € 2,000 depending on volume and location (2022 prices).

Motion-compensated gantry system: higher productivity is achieved because the system allows work to be carried out in less clement conditions without which a vessel/work platform would have to cease operations (fig. 7.9). Licensed cost of ship installation equipment ≈ CHF 350,000.

Figure 7.9: Installation vessel from the surface (without diver or robot) with motion compensated gantry crane

	Anchor Weight (Kg)	Holding Capacity (T)
Marine Flex / N-Viro	75	12.5
Aqualine Fluke Anchor	700	14
Concrete block	5000	2.9

Table 7.10: Comparison of anchoring forces in concrete block and Marine Flex helical screw

DGPS positioning system: the installation point is determined with an accuracy of less than 10 cm, even at a depth of 100 metres.

Logging software: records precise installation position, water depth, torque, substrate penetration and anchor attributes.

Static load test method: safety system for rapid testing of up to 25 T vertical load capacity, checking both anchor capacity and geotechnical capacity before production anchors are installed.

Locating method: Developed to install anchors at "any" depth by adding extensions to the drive shaft.

Geotechnical sampling device: Soil characterisation can be carried out either in the pre-project phase for design and estimating purposes, or to check in more detail the homogeneity of the soil along the area during installation.

Empirically tested to destruction: all the anchoring components designed are adapted both structurally and geo-technically and are empirically tested with destructive tests. The tube used is of specific quality to facilitate installation while mitigating the risk of over-torque or cold-hardening failure during installation.

Shaftless anchors: shaftless anchors are at the cutting edge of load efficiency, with an unrivalled weight/load capacity ratio (table 7.10).

Optional plate anchoring system: allows installation in very difficult sites where the anchoring helix configuration can be quickly adjusted to cope with widely varying substrates.

Screw anchors for helical auger shafts: the optional Helix plate anchor system (HOPAS) built with high-quality tubular anchor shafts enables installation in difficult soil conditions, such as penetration of very hard substrates and transition from very soft to hard substrates.

Shaped helix: all anchors are constructed using true shaped helix plates, which guarantee the integrity of the weld, optimise the pitch depth per installation turn (critical for installation performance), anchor holding capacity and signature.

On the basis of initial data received from Marine Flex Ltd (New Zealand!), the cost of installing 515 Marine Flex helical anchors for a ULISSE-type tank could be between CHF 1 and 1.5 million, including installation equipment such as the gantry for the vessel (€ 350,000, under licence). Duration of work 51 days (10 anchors/d).

7.5 ULISSE Reservoir shell cleaning robot

Any surface immersed in water or even air is immediately colonised by living organisms. This is particularly true of boat hulls (Fooling). Algae and mussels will encrust and eventually cover the entire surface, to the point of increasing drag and even threatening buoyancy.

Algae need light and will not colonise surfaces in the dark. Mussels, on the other hand, will gradually do so, including the zebra mussel and the quagga mussel, which has been extremely invasive in Swiss lakes since 2015. The quagga mussel has overtaken the zebra mussel and is found at greater depths. The suction pipes and strainers at pumping stations are also invaded by these mussels.

The envelope of the ULISSE Reservoirs should not escape this phenomenon (2 x 90,000 m^2, external/internal, per Reservoir). Given that the Quagga mussel does not seem to like moving elements or a strong current of water [...], regular cleaning of the envelope could be done automatically by underwater cleaning robots/drones or ROVs (Remotely Operated Vehicles). The ROV, which cleans and inspects hulls, is connected to an 'umbilical' cable for remote control and visual feedback.

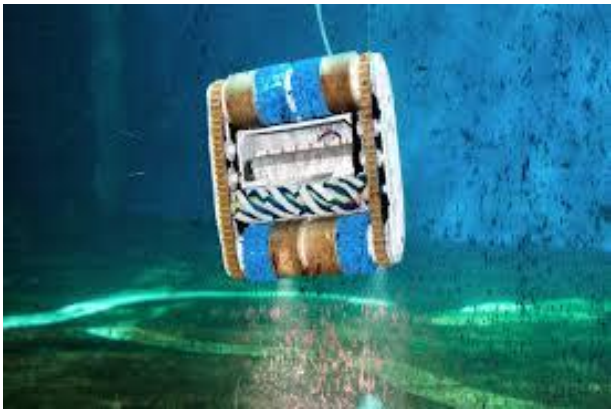

Figures 7.11: Example of an underwater cleaning drone, Keelcrab

The example of the Keelcrab drone (Fig. 7.11 above) is characterised by its plastic exoskeleton with a neutral hydrostatic balance. The suction force is generated by a central pump or turbine (propeller), driven by an electric motor, which performs the dual function of holding the drone against the hull and removing the algae that has formed. The movement is directed by rubber brushes on rails, which allow the drone to move in all directions. To improve the efficiency of vegetation removal, nylon bristle brushes of different lengths and diameters have been installed. The high-resolution IP68 underwater camera allows the robot to be steered via a wired remote control with real-time video display. In Switzerland, a team from the EPFZ is developing underwater or lake

robots with the **Téthys Robotics project [62].** It would be a good idea to work with them to develop an autonomous version dedicated to cleaning and inspecting ULISSE Reservoirs.

7.6 Financial investment cost of the ULISSE Reservoir

7.6.1 Comparison with large hydrothermal storage systems

At the stage of this exploratory study of the ULISSE project, it is difficult to establish the financial investment required for the construction of a completely new Reservoir, and what is more of several entire networks with almost 300 ULISSE Reservoirs potentially installed in the 15 large Swiss lakes. At best, on the basis of the dimensions of the typical Reservoir and the inventory of the main constituent materials, an order of magnitude can be given for the Material cost, but it is more difficult to give an order of magnitude for the cost of manufacture and installation on site (lake bed). The cost of the in-depth multi-disciplinary study phase and of producing a pilot prototype is also premature to establish in the present exploratory study.

Nevertheless, an analysis of the biggest projects in the field of solar heat storage gives an initial idea of the financial investment potentially required.

The difference in price between a prototype car and a production car is essentially due to the number of units and the method of production. This applies to just about every manufactured object. In the case of large structures (which are usually produced in smaller numbers), it is also and above all a question of size or dimensions (*economies of scale through size*) that will determine the unit and volume cost.

In this case, for the various hydraulic heat storage systems, size (m^3) has an inversely "*logarithmic*" effect on construction cost (CHF/m^3); however, this is independent of the unit thermal capacity (MJ/m^3), which depends on the excursion (useful variation) of the temperature of the water stored (or even under pressure). The geometric dimensions mainly determine the quantity of the various materials to be used, but also the spatial footprint of the structure.

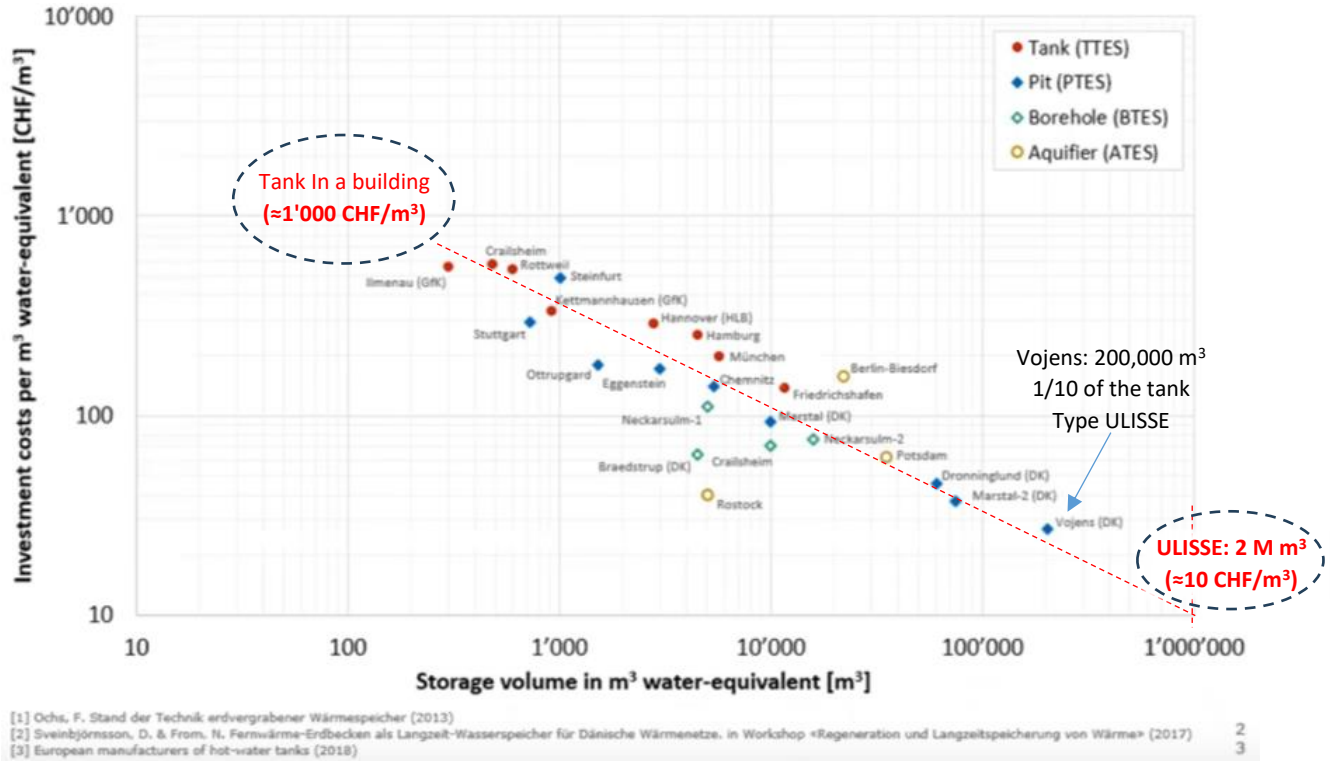

Figure 7.12: Investment costs for different types of hot water storage (source: HSLU Hochschule Luzern).
The effect of size (economy of scale) can be seen with a linear regression tending towards 10 CHF/m³ @1 M m³

The graph in fig. 7.12 above shows a broad distribution (factor 100) of the cost (CHF/m^3) according to the type of storage (*Tank, Pit, Borehole, Aquifer*) and according to the "water equivalent" volume. Each type of storage has its own range of effective implementation sizes. Pit storage covers the entire range.

For example, above-ground *tanks* typically cover volumes of between 200 and 10,000 m^3, with relatively high investment costs of between 650 and 150 CHF/m^3. Buried/covered basins and *pit and boreholes* cover a wider range in terms of the number of projects and the volume/cost ratio (700 m^3, 500 CHF/m^3 and 200,000 m^3 @ 24 CHF/m^3 for the largest storage facility at Vojens in Denmark).

Storage basins or pits have a large footprint (surface area lost for other uses) and require large volumes of excavation (fig. below) but not only. Waterproofing the basin (liner) using HDPE limits the loading temperature to a maximum of 90˚C and has a limited lifespan in is. Their **heat losses vs. energy discharged are between 9 and 24%** for commercial installations (14% for the Vojens storage basin vs. 16% for an ULISSE Reservoir). => § 10.6

Aquifer storage has been less successful (3), mainly because of the problem of controlling heat loss through the natural circulation of water underground. The volume and cost by volume of aquifer storage are a few tens of thousands of m^3 and around CHF 100/m^3 respectively. In addition, temperature can also pose health problems and restrictions for aquifers when they are used for drinking water.

Dry wells (*Borehole*) do not require any excavation or insulation, but can also be affected by "parasitic" water migration. The thermal performance of wells is influenced by the withdrawal capacity and by the proximity of neighbouring wells (*McDonald's syndrome,* by density with expansion).

What influences the cost of Hydro-Thermal Storage systems (HTS) is the structure of the container (including the volume of excavation/backfill, walls/liner, etc.) and the thermal insulation. The thickness and effectiveness of the insulation provided to the reservoir and buried tank (walls, floating insulation blanket) are highly dependent on the surface/volume ratio and favour large reservoirs.

Generally speaking, Graph 7.12 shows that the various heat storage systems are distributed globally along a diagonal by linear regression (logarithmic abscissa). This shows a downward trend (cost by volume vs size) towards the bottom right-hand corner of the graph (10 CHF/m^3 for 10^6 m^3). Such a hydraulic sensible heat storage system of 2 M m^3 water equivalent would represent a unit investment cost of around 20 M CHF (equivalent to the ULISSE type Reservoir).

7.6.2 Land area for the thermal collector field and storage basin

Seasonal storage systems are generally combined with a field of solar thermal collectors and a heat distribution network with heat pumps connected to the buildings. These solar thermal collector fields also require a significant amount of land (including the purchase and use of land).

Figure 7.13: Fields of solar thermal collectors for district heating in Vojens, Denmark, (70,000 m^2) next to the seasonal storage tank (210,000 m^3) under construction in 2014-15 (still without the insulating and floating cover).

(source: http://solarheateurope.eu/2020/05/19/vojens-district-heating/)

For example (Figure 7.14), the largest heat storage system in the world using solar thermal collectors for district heating is in the Vojens conurbation (DK). It covers a surface area of 144,000 m^2 or five (5) times that of his seasonal heat storage reservoir alone (27,000 m^2)!

By way of comparison, the projected footprint on the lake bed per unit of energy stored (m^2/TJ) of a ULISSE-type Reservoir is therefore almost eight times (7.6) smaller than the largest seasonal terrestrial solar heat storage system (Vojens).

The energy density (MJ/m^3) of ULISSE is admittedly lower (1/3) because it operates with a lower thermal excursion (ΔT full-empty = 15 K for ULISSE compared with 50 K for the Vojens basin). However, the ULISSE system does not need any land to capture the solar heat energy, as it draws it directly from the lake, or is charged by industrial or air-conditioning waste heat (=> TLNs).

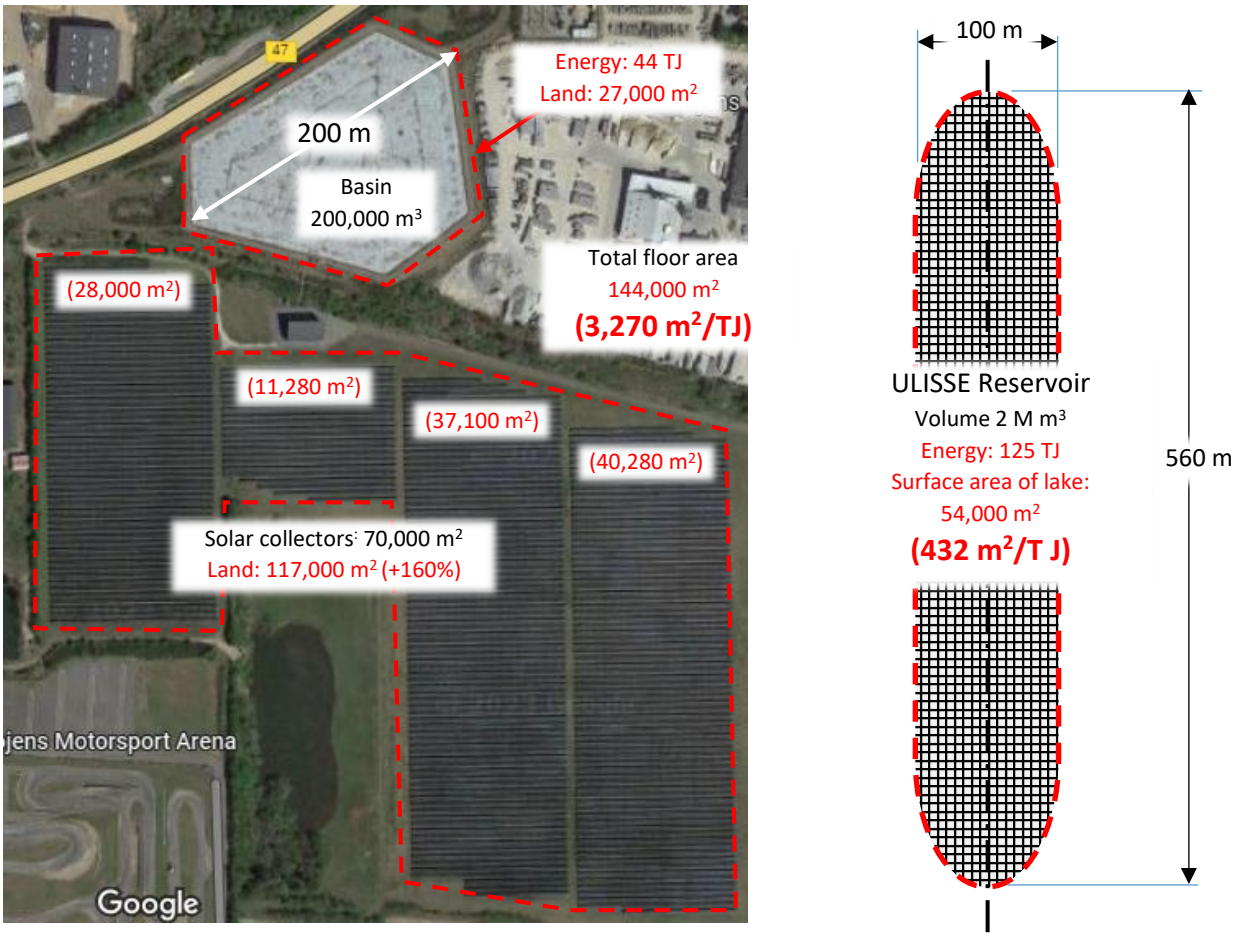

Figure 7.14: Total footprint: 144,000 m^2 (land) for the solar thermal collection infrastructure (70,000 m^2 of flat-plate collectors) and the seasonal storage basin (210,000 m^3 with its floating cover). of the urban area of Vosjens fjernvarme (DK) and comparison with a ULISSE Reservoir.

The financial cost of solar thermal collection can therefore be three times that of the storage system alone. For example, at Dronninglund (DK), the 62,000 m^3 covered storage basin cost ≈ 2.4 M € and the 37,000 m^2 solar thermal collector cost 6.1 M € in 2014 (165 €/m^2)! However, it is not specified whether these costs include the price of the land (one might logically assume that they do). Table 7.15 below shows clearly, for example between Vojens and Dronninglund, that the volume of storage has a direct impact on the volume price (38 compared with 24 €/m^3).

Note: Although "terrestrial solar" heating systems such as Vojens and Dronninglund require less energy from the heat pumps (2.5 to 3 kWh/MWh solar for Dronninglund) at higher temperatures from the district heating network, they cannot be used for air conditioning, particularly free cooling like the TLNs.

	Ottrupgård	Sunstore 2 Marstal	Sunstore 3 Dronninglund	Sunstore 4 Marstal	Vojens	Gram	Toftlund
Project type	Demonstration plants				Commercial plants		
Year of construction	1993-95	2003	2013	2011-12	2014-15	2014-15	2016-17
Size [m³ of water]	1,500	10,000	60,000	75,000	210,000	125,000	85,000
Cost [millions of EUR]	0.23	0.67	2.28	2.67	5.01	4.32	4.11
Price [EUR/m²]	150	67	38	36	24	34	48
Temperature range [°C]	35-60	35-90	10-89	17-88	40-90	20-90	20-90
Heat storage capacity [MWh]	43.5	638	5,400	6,000	12,180	12,125	6,885
(Dis)charge capacity [kW]	390	6,510	26,100	10,500	38,500	30,000	22,000
Total estimated heat losses [MWh/year]	85	402	1,602	2,475	5,500	4,024	1,900
Heat lost each year related to (dis)charges	22 %	6 %	6 %	24 %	14 %	13 %	9 %
Measured heat loss [MWh/year]	70	n/a	1,175	2,927	n/a	n/a	n/a

Key data on seven Danish pit heat storage systems. Figures are based on data points for 1998-2001 (pilot storage in Ottrupgård), 2013 (Marstal) and 2014 (Dronninglund).
Source: Technology Data for Energy Storage, March 2019 (see p. 46 of the attached PDF)

Table 7.15: Summary of the largest solar thermal installations
With onshore seasonal heat storage for district heating

7.6.2 What about a typical reservoir or a network of (300) new ULISSE Reservoirs?

Unlike the "conventional" solar thermal collection and seasonal storage systems described above, the ULISSE Reservoir (anchored to the lake bed) does not require its own thermal collection field (other than sub-lake water or waste heat), nor does it require the purchase of land or excavation work, nor does it have any visual impact on the landscape, nor does it hinder navigation. On the other hand, amateur fishing (with lines and trolls towed by boats) must take account of the presence of the sub-lacustrine Reservoirs so as not to snag their hooks! Mapping, geolocation and physical marking are therefore recommended.

The various aspects linked to these seasonal heat storage alternatives need to be put into perspective with regard to the ULISSE Reservoirs and their investment costs; in the end, this will cover part of the structural winter electricity deficit.

Furthermore, the cost of the urban TLN is not taken into account, as this is planned in Switzerland's Energy Strategy and ULISSE is "simply" a booster to improve energy efficiency of the TLNs.

The ULISSE Reservoir is characterised by a hyperbolic tunnel shape, with large unit volume of 2 M m^3, a relatively small surface area (88,000 m^2), a semi-flexible all-mineral structure (glass, basalt), 5 to 10 cm thick including the thermal insulation. On the other hand, it has no load-bearing structure due to the self-supporting nature of the apparent density of the insulation (cellular glass), with a hydrostatic resistance > 10 bars and a high tensile strength of the envelope made of a triple layer of E glass fibre textile fabric (30 t/m, safety factor 5). Anchoring

to the lake bed is carried out from a vessel (without a diver or robot) using invisible, virtually impact-free screw-in anchors.

Volume Réservoir ULISSE	Vr	m^3	2 000 000
Excursion thermique	ΔT	K	15
Capacité thermique	Ct	GWh ou TJ	35 ou 126
Longueur totale	Lo	m	560
Largeur	La	m	100
Rayon hyperbolique	Rh	m	50
Hauteur sommitale	Hs	m	55
Surface Enveloppe	Senv	m^2	88 000
Surface d'emprise au sol	Ssol	m^2	54 000
Epaisseur Isolation	Epi	m	0,05
Volume Insolation	Vi	m^3	4 400
Surface textiles env.	Stext	m^2	264 000
Epaissuer tri-couches	Etextile	m	0,003
Résistance enveloppe	Rte	t/m	30
Longueur câbles jonctions	Lcâbj	m	32 000
Longueur câbles pourtour	Lcâbp	m	2 000
Poussée Arch. Enveloppe	PAenv	t	3 674
Poussée Arch. eau temp.	PAenv	t	3 520
Poussée Arch. Totale	Pat	t	7 194
Nombre d'ancrages	Nanc	(-)	515

Figure 7.16: Main dimensions of the ULISSE type Reservoir and summary of the potential of the ULISSE project

7.7 Summary comparison of ULISSE with alternative solutions

TLN network infrastructure is not taken into account here, as it is planned as part of the general development (Switzerland, SES-2050) of heat networks, including those on lakes.

ULISSE system alone (without external CORSAIRE) Implementation in 2050 in the 15 major Swiss lakes:

- ⇨ Heat input via TLNs: Qh = 50 PJ/year (1/4 of the Swiss "lake" population = 50 GeniLac units: ≈ 1PJ).
- ⇨ Net winter electricity savings (EEH): 2.07 TWh
- ⇨ Financial cost Prototype reservoir including ULISSE study (2 M m^3): CHF 20 M (subject to confirmation)
- ⇨ **Cost 310 Reservoirs (621 M m^3): 3 billion CHF (≈ 50 % economy of scale vs. prototype).**

CORSAIRE contribution (via DWN and external to TLN)

- ⇨ Heat input (Q-cor): 6.75 PJ
- ⇨ Net winter electricity savings (ΔEcor): 0.69 TWh
- ⇨ **Financial cost of interconnection networks and heat exchangers: CHF 1 billion (assumption).**

Total (ULISSE & CORSAIRE)

- ⇨ Net electricity savings (EEHn): 2.76 TWh
- ⇨ Gross electricity savings (EEHb) (10% distribution losses in winter): 3 TWh
- ⇨ Accounts for 1/3 of the structural winter electricity deficit (9 TWh)
- ⇨ **Financial cost of ULISSE + CORSAIRE infrastructure: CHF 4 billion**
- ⇨ **Financial savings on electricity (320 M CHF/TWh): 960 M CHF/year (ref. Tab.6.4) [16].**

Alternative through additional electricity generation:

1. Gross electricity production equivalent to 2 Grande Dixence (GD) complexes: 3 TWh winter
- ⇨ **Capital cost of 2 GD Complexes ≈ 19 billion CHF (based on Table 6.4, cost of Large Hydro).**

Alternative by supplying thermal networks:

2. TLNs with solar thermal collectors and onshore seasonal storage: ≈ 57 PJ => § 7.6 (extrapolation from the Vojens, DK installation)
- ⇨ Surface of solar thermal collectors and associated land (160%): 35 km^2 & 56 km^2
- ⇨ Volume of seasonal thermal storage (≈ 85˚C) and surface area: 26 M m^3 & 35 km^2
- ⇨ Total surface area (collectors + storage): 91 km^2 (≈ the surface area of Lake Zurich)
- ⇨ Investment cost of solar collector field (excluding cost of land): ≈ 5800 M CHF

- ⇨ Investment cost of thermal storage (excluding land cost): ≈ 780 M CHF
- ⇨ **Total investment cost (collectors + storage): CHF 6580 million (excluding land purchase).**

8 Shape and dimensional analysis of the ULISSE Reservoir

8.1 Transverse hyperbolic shape of the envelope

The envelope of the ULISSE Reservoir is fitted with thermal insulation slabs of cellular glass approximately 5 cm thick. The low density of cellular glass (ρi = 165 kg/m^3 for e.g., Pittsburgh Corning's FOAMGLAS-F), immersed in water (ρe ≈ 1'000 kg @ 20˚C), represents an apparent density (Δρi) of approximately (-) 835 kg/m^3, which generates a volumetric (upward) Archimedean force (Fai), uniformly distributed over the said envelope.

$$Fai = \Delta\rho i = \rho i - \rho e = 165 - 1{,}000 = \quad -835 \quad [kg/m^3] \qquad (8.1)$$

Formally, this force Fai is the product of the "apparent" density of the insulator (Δmi), immersed in water, and the Earth's gravitational acceleration (g = 9.81 m/s^2), expressed in Newton per m^3.

$$Fai = \Delta mi.g = -835\ (kg/m^3).\ 9.81\ (m/s^2) = -8{,}191.35\ (kg/m^2\ s^2) \approx -8.2\ [kN/m^3] \qquad (8.2)$$

The sign (-) indicates that the force is indeed upward due to the apparent mass (negative).

This volumetric force (Fai) gives the envelope its characteristic "hyperbolic" transverse curvature. By analogy, it is also the (inverted) shape that a **chain suspended by its ends** (Fig. 8.1. below) takes under the effect of gravitational gravity. Mathematically, it corresponds to a transcendental plane curve with a *cosh* (hyperbolic cosine) function.

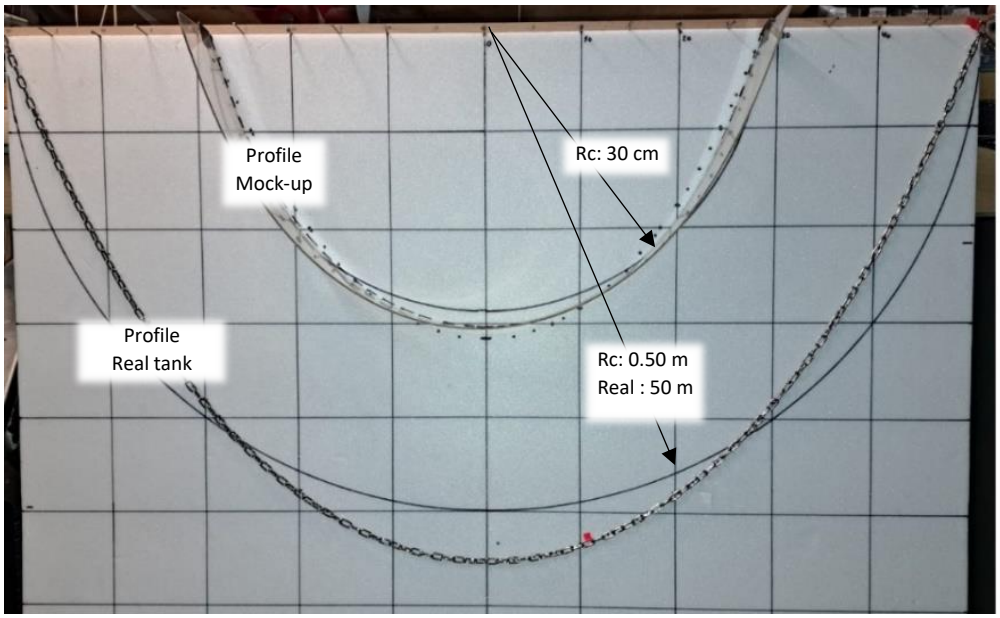

Figure 8.1. Similarity between the shape of the Reservoir envelope and a chain suspended between two horizontal points, distance (d) 1 m or 2Rc, Length (L) 1.57 m (L= π.Rc). Bottom grid: 10 x 10 cm.

The Archimedean force experienced by the submerged insulation results in a tangential **tension (T)** in the hyperbolic envelope. At the angle **α,** it is broken down into a vertical component T_V and a horizontal component T_H. The latter is constant at every point on the curve and therefore also at the base of the two anchor points (A, G), at Y(x = +/-Rc) at the angle **α** between **T** and T_H :

$$T_H = T \cos \alpha \qquad [kN] \qquad (8.3)$$

$$\text{with at base:} \quad \alpha = \arctan(hx/dx) = \quad 69.3 \qquad [^\circ] \qquad (8.4)$$

The vertical component T_V **= T** sin **α**, corresponds to the Archimedean force Fai (weight of the chain).

The Cartesian equation of the chain or envelope in the transverse plane is:

$$Y(x) = a \cosh (x/a) \qquad [m] \qquad (8.5)$$

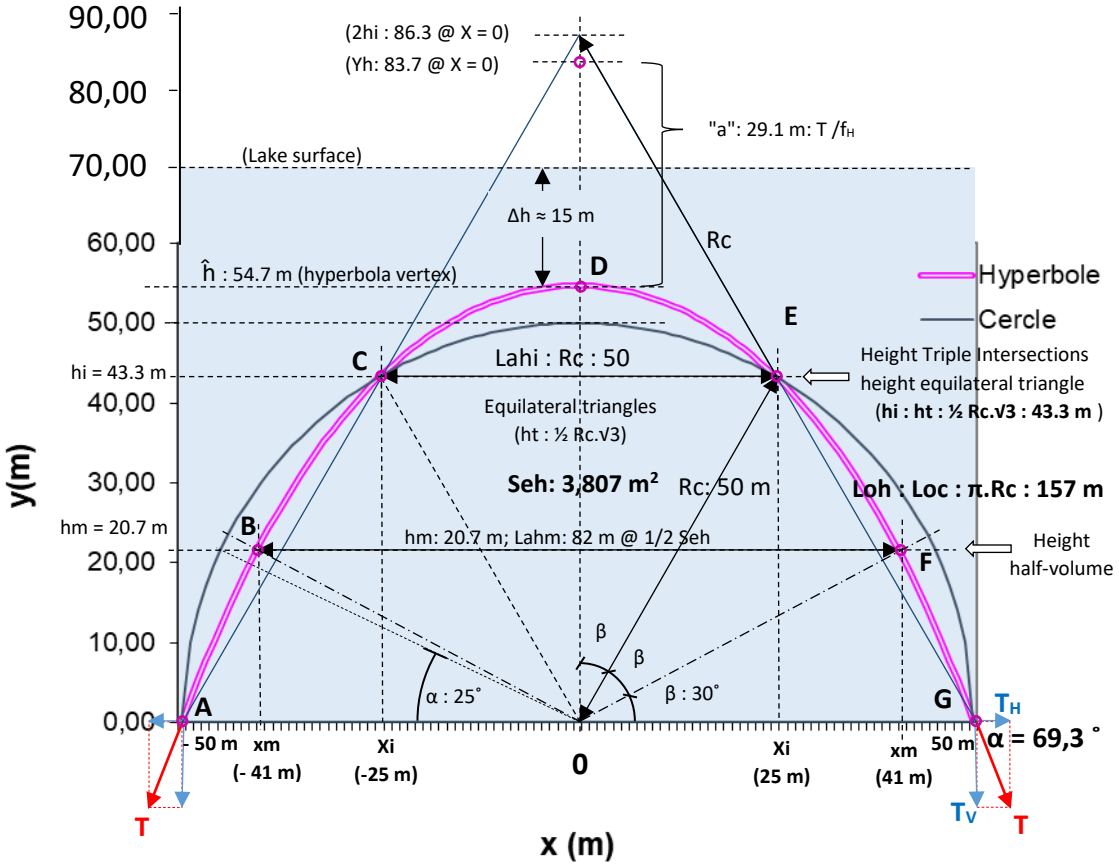

*Figure 8.2: **Hyperbolic** transverse curvature of the envelope compared with the arc of a circle*

By equating the length of the arc of a circle (Loc) of radius Rc = 50 m with that of the hyperbolic curve of the envelope (Loh), we can determine the value of the parameter "a" (29.1 m):

$$Loc = \pi Rc = Loh = 2 \sqrt{(2a\hat{h} + \hat{h}^2)} = \quad 157.1 \quad [m] \qquad (8.6)$$

$$a = ((Loh/2)^2 - \hat{h}^2)) / 2\,\hat{h} = \quad 29.1 \quad [m] \qquad (8.7)$$

Furthermore, the parameter 'a' = T_H **/ f**, where **f is** the linear force (Archimedean force per unit length of the hyperbolic curve). Parameter 'a' is dimensionally a length [m] and also corresponds to the distance of the vertex of the hyperbolic curve ($\hat{h}$) from its Cartesian origin [on the central axis of symmetry Y (x = 0)].

According to equation 8.8, with conditions 8.6 (Loh = Loc = 157.1 m) and 8.7 (a = 29.1 m), Y0 is:

$$Y0 = Y(x=0) = a \cosh (x/a) = \quad 83.8 \quad [m] \qquad (8.8)$$

The vertex of the hyperbola ($\hat{h}$) at point D on the axis of symmetry (Y) is then:

$$\hat{h} = Y0 - a = 83.8 - 29.1 = \quad 54.7 \quad [m] \qquad (8.9)$$

The **cross-section under the hyperbolic envelope (Seh)** corresponds to the integral of the elementary surfaces (ds = dy.dx) between x = -Rc and +Rc, i.e. the width of its base (Lahb = 100 m).

$$\mathbf{Seh = \int dy.dx = \quad 3,807 \quad [m^2]} \qquad \mathbf{(8.10)}$$

The **Width** of the hyperbola (Lah) varies with height [hx = F(x)]. At the base (h_b: x = 0, between the 2 anchor points), it simply corresponds to 2 radii of the arc:

$$Lah_b = 2Rc = \quad 100 \quad [m] \qquad (8.11)$$

At half the hyperbolic cross-section (Seh/2 = 1'903.5 m^2), the average width of the hyperbola (Lah_m) is 82 m and is located at points B and F, at a height of the average hyperbola (hh_m) of 20.7 m:

$$Lah_m = 2(X_m) = 2 \times 41 = \quad 82 \quad [m] \qquad (8.12)$$

$$hh_m = Y0 - Ym = [a \cosh (50/a)] - [a \cosh (41/a)] = 83.8 - 63.1 = \quad 20.7 \quad [m] \qquad (8.13)$$

The height of the hyperbola above hh_m is equal to:

$$\Delta h_m = \hat{h} - hh_m = 54.7 - 20.7 = \quad 34 \quad [m] \qquad (8.14)$$

Using equations 8.6, 8.7 (a), 8.9 ($\hat{h}$) and 14 (Δh_m), the length of the hyperbola Loh_m above the transverse half-section (Seh/2) is determined:

$$Loh_m = Loh_b - 2\sqrt{(2a\Delta hm + \Delta h_m^2)} = \quad 112 \quad [m] \qquad (8.15)$$

The hyperbolic length Loh is used to determine the hyperbolic surface (Suh) of the envelope and therefore also the volume (V) above the said level (h). This allows the heat loss of the hyperbolic envelope (Pte) to be calculated as a function of its "active" surface area (Suha) delimited by the level of the "*flat-front thermocline*" (Ntc), which separates the volume of "active" hot water (Va) from that of the cold water below.

8.1 Highlights (B, C, E, F)

Figure 8.1 shows *three small equilateral* and concentric *triangles* (O-A-C, O-C-E, O-E-G) in the arc of a circle which, together with a fourth (C-H-E) at the apex, form a *large equilateral triangle* (A-H-G) with a large base (A-G) equal to 2Rc (Lah_b).

Furthermore, at points C and E (with coordinates yi, -/+xi), a triple intersection of the hyperbola with the arc of a circle (and the large equilateral triangle) occurs symmetrically about the central axis Y. The width of the hyperbola (Lah_i) between its two points of intersection (C-E) is equal to half the width of the base (Lah_b /2) or equal to the radius Rc (50 m).

$$Lah_i = Rc = \quad 50 \quad [m] \qquad (8.16)$$

What's more, the height (hi) of the two points (C, E) of intersection corresponds precisely to the vertices and therefore to the height of the small equilateral triangles (ht).

$$h_i = h_t = \sqrt{3} \times Rc/2 = \quad 43.3 \quad [m] \qquad (8.17)$$

We can also obtain the value of h_i (or h_t), projected on the horizontal axis (X), at a distance (xi = Rc/2 = 25 m) from the central axis Y :

$$h_i = Y0 - Yi = [a \cosh (50/a)] - [a \cosh (25/a)] = 83.8 - 40.5 = \quad 43.3 \quad [m] \qquad (8.18)$$

Using the same procedure as (8.13) and (8.14), we determine the height of the hyperbola above the level of the two intersection points (Δh_i) and the length of the hyperbola above ($Loh_{\hat{i}}$):

$$\Delta h_i = \hat{h} - hi = 54.7 - 43.3 = \quad 11 \quad [m] \qquad (8.19)$$

$$Loh_{\hat{i}} = Loh - 2\sqrt{(2a\Delta h + \Delta h_{ii}^2}) = \quad 56.4 \quad [m] \qquad (8.20)$$

The part of the Hyperbolic Cross Section (Seh), respectively below Seh($h_{\check{i}}$) and above Seh($h_{\hat{i}}$) from the level of the intersection (hi) can be determined as follows:

with the double integration of the elementary half-surfaces (ds = dy.dx), between x = Rc to Rc/2,

$$Seh(h_{\underline{i}}) = hi \times Lai + 2\int dy.dx = (43.3 \times 50) + (2 \times 672.5) = \quad 3{,}510 \quad [m^2] \quad (8.21)$$

$$Seh(h\hat{i}) = St - St(h_{\underline{i}}) = 3'807 - 3'510 = \quad 297 \quad [m^2] \quad (8.22)$$

The hyperbolic section above the level of the Seh(hî) intersection represents 8% of Seh.

The points B and F corresponding to the level (hm), of half transverse section of the hyperbola (Seh/2), **are located on the bisectors O-B and O-F of the two small equilateral triangles**, O-A-C and O-E-F respectively. The bisectors with the base A-G on the abscissa X form an angle β (30˚).

The mean level of the hyperbola hh_m (B-F, at a height of 20.7 m) corresponds to its half transverse section and to the **centre of gravity at homogeneous temperature throughout the Reservoir**. The bisector angle (0-B-F) is equal to 4 β, i.e., 120˚. For the arc of a circle (Rc), the height of the "*homogeneous centre of gravity*" is substantially the same (hmc) but the angle α = 25˚ does not correspond to the said bisectors.

$$hmc = Rc \sin \alpha = \quad 21 \quad [m] \quad (8.23)$$

8.2 Half-hyperboloid ends of the Reservoir

The shape of the two half-shells at the ends of the Reservoir has the same hyperbolic curvature as that of the cross-section in its straight part. They therefore each have the **shape of a half-hyperboloid** of revolution (180˚) around the Y axis, with the radius Rc (50 m) at the base.

For a hyperbolic transverse length of the envelope (Loh = Loc = 157 m, starting hypothesis), the Surface of the two hyperboloid half-caps at the ends (Suc) remains equal to that of an equivalent half-spherical "cap" of radius Rc.

$$Suc = 2 \pi Rc^2 \quad = \quad 15{,}708 \quad [m^2] \quad (8.24)$$

However, the hyperbolic cross-section (Seh = 3,807 m^2) is slightly smaller (-3%) than that of the arc of a circle (Sac) with radius Rc :

$$Bag = 1/2 \pi Rc^2 = \quad 3{,}927 \quad [m^2] \quad (8.25)$$

The equivalent half-spherical volume (Vs) is simply equal to:

$$Vs = 2/3 \pi Rc^3 \quad = \quad 261{,}800 \quad [m^3] \quad (8.26)$$

Compared to the half-sphere, the volume of the hyperboloid caps (Vc) at the ends of the Reservoir is less than 8,000 m^3 (3%) in the ratio of the sections Seh and Sac (0.97):

$$Vc = Vs \times Seh/Sack = \quad 253{,}800 \quad [m^3] \quad (8.27)$$

With the volume of the hyperboloid caps at the ends of the Reservoir (Vc) and their surface area (Suc), we can associate them with an equivalent rectilinear length (Locéq):

$$Locéq = Vc / Suc = \quad 16.16 \quad [m] \quad (8.28)$$

8.3 Length, surface area and circumference of the ULISSE Reservoir

The volume of the Reservoir in its linear part (Vl) (without the caps) equal to its total volume (Vt: 2 10^6 m^3) minus that of the end caps (Vc):

$$Vl = Vt - Vc = \quad 1{,}746{,}200 \quad [m^3] \quad (8.29)$$

With the hyperbolic section of the Reservoir (Seh), its linear length (Lol) is equal to:

$$Lol = Vr / Seh = \quad 458.7 \quad [m] \quad (8.30)$$

The total length of the Reservoir (Lot) is then simply:

$$Lot = Lol + 2Rc = \quad 558.7 \quad [m] \quad (8.31)$$

Equations (8.6) and (8.30) are used to determine the linear envelope surface (Sul):

$$Sul = Loh \times Lol = 157.1 \times 458.7 = \quad 72{,}062 \quad [m^2] \qquad (8.32)$$

The total surface area of the hyperbolic envelope of the Reservoir (Sut) is then the sum of the linear part (Sul) and, according to equation (8.1), that of the end caps (Suc):

$$Sut = Sul + Suc = 72'062 + 15'708 = \quad 87{,}770 \quad [m^2] \qquad (8.33)$$

The length of the circumference (Locir) at the base of the Reservoir is:

$$Locir = (2\,\pi\,Rc) + 2Lorr = \quad 1{,}234 \quad [m] \qquad (8.34)$$

Right-of-way over the lake bed (Ssol): $Ssol = (Lol*2Rc) + (\pi Rc2) =$ 54,000 $[m^2]$ (8.35)

$\hat{h}$	**hyperbolic vertex of the ULISSE Reservoir**	**54.7**	**[m]**	**(8.9)**
hh_m	average height of hyperbola (half section)	20.7	[m]	(8.13)
hmc	average height of the base circle	21	[m]	(8.23)
Lah_b , m, i	**Base hyperbola width, average, intersection**	**100**	**[m]**	**(8.11)**
Loc	Length of the arc of the base circle	157.1	[m]	(8.6)
Locéq	Equivalent length of end cap	16.16	[m]	(8.28)
Locir	Circumferential length of the base of the Reservoir	1,234	[m]	(8.34)
Loh	Hyperbolic transverse length of the Reservoir	157.1	[m]	(8.6)
Lol	Linear length of the Reservoir	458.7	[m]	(8.30)
Lot	**Total length of the Reservoir**	**558.7**	**[m]**	**(8.31)**
Bag	Section of the base arc	3,927	$[m^2]$	(8.24)
Seh	**Hyperbolic cross-section of the Reservoir**	**3,807**	**$[m^2]$**	**(8.10)**
Suc	Surface area of the reservoir end caps	15,708	$[m^2]$	(8.14)
Sul	Surface area of the linear part of the Reservoir	72,062	$[m^2]$	(8.32)
Sut	Total hyperbolic surface area of the Reservoir	87,770	$[m^2]$	(8.33)
Soil	Surface area of the lake bed of the Reservoir	54,000	$[m^2]$	(8.35)
Rc	Radius of the arc of the base circle	50	[m]	(8.16)
Vc	Volume of the reservoir end caps	253,800	$[m^3]$	(8.27)
Vs	Basic half-spherical volume	261,800	$[m^3]$	(8.26)
Vl	Linear volume of the Reservoir	1,746,200	$[m^3]$	(8.29)
Vt	**Total volume of the Reservoir**	**2,000,000**	**$[m^3]$**	**(8.29.bis)**
Ct	**heat capacity @ ΔT: 15 K**	**126**	**[TJ]**	**(7.8)**
Fat	**Nominal total buoyancy @ ΔT: 15 K**	**≈ 7,000**	**[t]**	**(8.39)**

Table 8.3: Alphabetical summary table of (French) abbreviations, values, units and equation references

8.4 Impacts of water temperature and density on the ULISSE Reservoir

8.4.1 Archimedean and tensile forces on the envelope

The apparent density of the insulation (Δρi: - 835 kg/m^3), which gives the characteristic hyperbolic transverse shape of the ULISSE Reservoir (§ 8), generates a constant tensile force on the shell (Fti), proportional to the volume of insulation. The volume of insulation (Vi: 4,388 m^3) corresponds to the hyperbolic surface of the shell (Senv) multiplied by its thickness (ε = 0.05 m):

$$Fti = \Delta\rho i \times Vi = 835 \times 87{,}770 \times 0.05 = \quad 3{,}664 \quad [10^3\ kg] \qquad (8.36)$$

The difference in water density (Δρe), between that of the Reservoir (ρr) with that of the lake (ρl), is related to their temperature difference (ΔT). It generates a volumetric Archimedean force on the water in the Reservoir, which is variable (Fev). With a lake water temperature of 5 ˚C and a Reservoir at 20 ˚C, i.e., a ΔT of 15 K, it is worth:

$$Fev = \Delta\rho e = \rho r - \rho l = \quad -1{,}76 \quad [kg/m^3] \qquad (8.37)$$

With this difference in volume density (Δρe) of -1.76 kg/m^3, the Reservoir is subjected to a variable tensile force (Fte) at the level of its shell, proportional to its volume (V: 2.10^6 m^3):

$$Fte = \Delta\rho e \times V = \quad 1.76 \times 2.10^6 = \quad 3{,}520 \quad [10^3\ kg] \qquad (8.38)$$

Total buoyancy (eq.8.36 + 8.38): Fat = 7,184 [10^3 kg] (8.39)

In round figures, the envelope and anchoring of the ULISSE Reservoir must therefore resist more than 7,000 t of tensile forces (8.39). Half of this, i.e., 3,500 t generated constantly by the insulation (8.36) and between 0 and 3,500 t generated dynamically as a function of the hot water load rate inside the Reservoir (8.37).

The result is a linear tensile force (Ftl) distributed over the circumference of the envelope (Lcir, 8.34), which fluctuates between a minimum of 3 t/m and a maximum of 6 t/m:

$$Ftl\text{-}min = Fti / Lcir = 3'664\ 10^3 / 1'234 = \quad 2.97 \quad [10^3\ kg/m] \qquad (8.40)$$

$$Ftl\text{-}max = (Fti + Fte) / Lcir = 7'184\ 10^3 / 1'234 = \quad 5.82 \quad [10^3\ kg/m] \qquad (8.41)$$

8.4.2 Hydrostatic pressure on the envelope

Hydrostatic pressure is also a function of the height of the hot water column in the Reservoir. It increases towards the top and depends on the thermal filling of the Reservoir. The envelope curve then approaches a "*linear*" curve, or so-called "*bachette*" curve (by analogy with the hyperbolic chain), the curvature of which is proportional to the height and temperature of the hot water in the Reservoir.

The hydrostatic pressure difference (Δph) increases with the height of the water column in the Reservoir. It is maximum at the top, i.e., 10 mbar (1.76 kg/m^3 x 55 m ≈ 100 kg/m^2). The average Δph is located at the centre of gravity of the volume of water, 34 m from the top (1- 0.4244 Rc) and is therefore 60 kg/m^2 or 6 mbar.

As a reminder, a pressure of 1 mbar corresponds to 1 cm height of water column (@ 20°C). The average pressure on the envelope (Δph) therefore corresponds to around 6 cm of water column, which is relatively low. **It can nevertheless generate water leakage through the hydraulic permeability of the envelope**. In addition, the Δph produces a mechanical stress on the envelope that depends on its surface area and the longitudinal spacing (2m) between the cables taking up the forces through the anchors in the lake bed.

8.4.3 Properties of the materials making up the casing of the ULISSE Reservoir

The shell of the ULISSE Reservoir must fulfil two main functions: to contain the volume of water stored in the lake (hydraulic tightness) and to minimise heat loss (thermal tightness) over an extended period (seasonal heat storage).

The components that make up the envelope (textiles, insulation, cables, connectors, etc.) must meet a number of technical and environmental criteria: thermal insulating capacity, self-supporting, resistance to hydrostatic pressure (insulation), tensile strength and flexibility (textiles, cables), hydrophobic, vapour-tight, rustproof, rot-proof, biocompatible, minimum embodied energy and greenhouse gas emissions during manufacture, recyclable (circular economy).

To achieve this, the structure of the **envelope is made up of 3 layers of E-glass fibre textiles containing insulating cellular glass blocks.**

E-glass fibre is produced from boron oxide mixed with silica, lime, alumina and magnesia, melted at 800 ˚C and then refined at 1,500 ˚C. The tensile strength on density of E-glass fibre is greater than that of steel. The felt in the interlayer joints and around (abrasion protection layer) of the insulating pavers in the ULISSE envelope is made of E-glass (or basalt) fibre with has a low thermal conductivity (0.03 W/m.K). The fibre can withstand temperatures of over 600 ˚C, is **non-combustible, rot-proof and inorganic, and compatible with organic matrices (biocompatible).** Sources*: Final Advanced Materials Sàrl/GmbH*, *KLEVERS GmgH*.

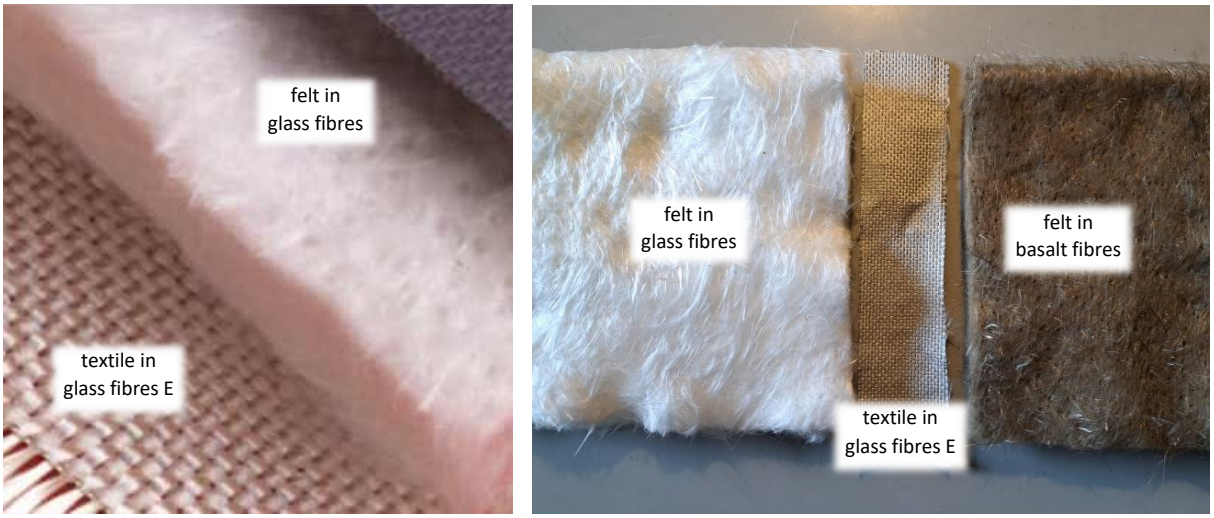

Figure 8. 4: Textile and felt made of type E glass fibres (photo final-materials.com), d. Glass and basalt fibres

Since 1930, technical textiles made from E glass fibres have been used mainly for their thermal resistance at high temperatures, in the fields of fire protection (fire and smoke curtains), thermal and acoustic insulation in the shipbuilding, automotive, aeronautics, metallurgy and furnace industries.

For example, KLEVERS GmbH in Germany produces E-glass fibre textiles (*KlevoGlass)* in grammages ranging from 160 to 1050 g/m^2, in thicknesses from 0.18 to 1.3 mm and widths up to 310 cm. These can be reinforced with stainless steel wires (V4A).

While resistance to very high temperatures (≥ 600 ˚C) is not a criterion for the ULISSE tank shell, tensile strength is crucial. It can reach 900 N/cm or **9 tonnes per metre of textile width** (according to the European standard: EN ISO 13934-1), which (according to eq. 8.5) is **1.5 times the maximum linear load of 6 t/m to which the ULISSE envelope is subjected**.

8.4.4 Thermal insulation of the hyperbolic shell of the ULISSE Reservoir

Some thermal insulation materials (e.g., extruded polystyrene) used in the building industry can withstand moderate compressive strength (floor slab insulation, etc.), but practically only cellular glass combines compressive strength with total watertightness. However, **the use of cellular glass in deep immersion under high hydrostatic pressure (≥ 7 kg/cm^2) is unprecedented.**

Cellular glass (made from around 60% recycled flat glass, windscreens and windows) is obtained mainly by oxidation (CO_2) and thermal expansion of additives such as sodium carbonate, dolomite, feldspar and a small amount of iron oxide.

The cellular glass manufacturing process was invented by the French engineer Bernard Long (Saint-Gobain patent 1934). It was sold in 1942 to the Pittsburgh Corning Corporation (USA), which continued its development and production. Initially cellular glass was used (marginally) as insulation and during the Second World War as **marine floats (protective beacons, rafts, lifeboats)**. In 1964, the first European production unit was set up in Belgium (Tessenderlo), followed by the Czech Republic (Klasterec) in 2008.

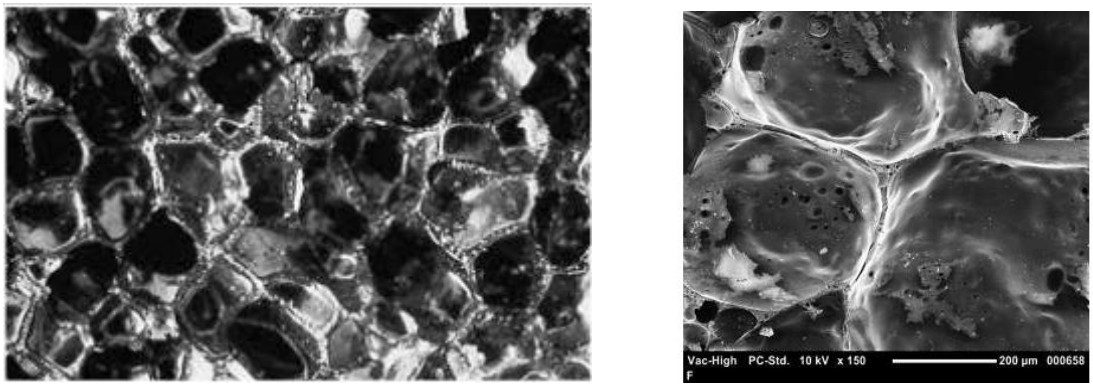

Figures 8.5: Microscope images of cellular glass cells (source FOAMGLAS)

Today, cellular glass is widely used for thermal insulation in buildings, particularly for its hygroscopic properties (complete water and vapour tightness) and resistance to compression (no deformation). These properties make it highly suitable for insulating flat roofs and heavily loaded (driveable) floors.

Cellular glass has very good compressive strength, from 500 to 1600 kPa, depending on its density (100 to 165 kg/m^3). However, the manufacturer (Pittsburgh Corning) was unable to provide values for water immersion under high hydrostatic pressure, as required for the insulation of the ULISSE Reservoir shell.

8.4.5 Procedure and organisation of hydrostatic insulation tests

This vital information, for the load-bearing insulation of the ULISSE Reservoir envelope, was obtained through tests carried out personally on a sample of a standard FOAMGLAS slab (type T3+, ρ: 100 kg/m^3, 80 x 600 x 450 mm) provided free of charge by the representative for French-speaking Switzerland (Mr Stanislas De Froment, Pittsburgh Corning Schweiz AG).

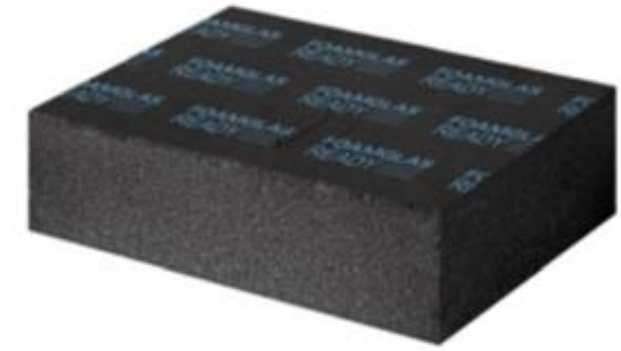

Figure 8.6: FOAMGLAS® T3+ cellular glass panel

Figure 8.7: Sample left: 165, right 100kg/m^3

According to figure 8.8 below, the hydrostatic test on the cellular glass sample is carried out using a reservoir-accumulator of a hydrophore sprinkler unit (volume +/- 10 litres). It is put under progressive hydrostatic pressure with a minimum of compressed air at the top of the Tank, minimising the potential expansion energy in the event of the Tank breaking (classic procedure for safe testing of Tanks under hydraulic pressure).

The choice of this pressurisation tank is motivated by its large closing lid (diameter of the opening: 10 cm), normally intended for the introduction of the rubber expansion "bladder" of the "*on de shelf*" commercial watering hydrophore pressurisation tank.

Figure 8.8: General layout of the FOAMGLAS® cellular glass hydrostatic test

The FOAMGLAS cellular glass sample (type T3+) is placed in a small transparent glass jar to collect any cellular glass particles that may detach from the sample in the event of crushing or crumbling under the effect of water pressure (Fig. 5). The jar is then sealed with a lid fitted with holes to allow air to escape. The whole assembly is inserted through the opening in the hydraulic pressurisation tank (accumulator vessel, Fig. 8.10).

The tank is closed by the cover (6 M8 bolts), which includes a connection with a valve to the drinking water network, a hydraulic and aeraulic drain valve, a compressed air connection and a pressure gauge (0 to 6 bar graduations). The tank is then completely filled with water (+/- 10 litres) via the water network, then pressurised (regulated) with compressed air supplied by the compressor (max. 8 bar).

The tests were carried out in January 2022. Pressure was gradually built up in stages, with intermediate checks on the integrity of the sample (dimensions, search for precipitated glass particles in the jar). The dimensions of the sample are 30 x 35 x 75 mm.

Fig. 8.9: Cellular glass sample and jar

Fig. 8.10: sample before immersion

Date	Start time	End time	(H)	Pressure (bar)	Observation
26/01/22			12	1,5	Sample idem
27/01/22			13		Sample idem
27/01/22	12h00	15h00	3	3,5	Sample idem
27/01/22	15h45	15h20 (28/01)	24	4	Sample idem
28/01/22	18h00	16h00 (29/01)	22	5	Sample idem
29/01/22	18h30	15h30 (30/01)	21	5,5	Sample idem
30/01/22	15h30	18h00 (30/01)	2,5	6	Sample idem
30/01/22	19h00	10h40 (01/02)	39	≥ 7	Sample idem
01/02/22	12h15	end of tests		≥ 7	Sample idem

Table 8.11: Table of pressure tests (gradual pressure build-up, with intermediate checks)

8.4.6 Conclusion of hydrostatic tests

The sample was not altered in any way at pressure levels up to 7 bar (the maximum available from the compressor). The cellular glass sample was taken from a standard "entry-level" FOAMGLAS slab, with a density of 100 kg/m^3 and a compressive strength of 500 kPa or 5 bar (EN 826 test). FOAMGLAS cellular glass type "F" has a density of 165 kg/m^3 and a compressive strength of 1,600 kPa (160 tonnes/m^2), which corresponds to a pressure of 16 bars or 160 metres of water column.

In the building sector, floor insulation is subjected to dynamic compression and deformation loads from traffic on the slab, for example on flat roofs, car parks, etc.

Conventionally, compression tests on insulating materials are carried out in accordance with the European standard EN 826, using only an axial force and in a dry environment (Figure 8). Under the effect of the unidirectional force, the material will at least deform or break.

The hydrostatic pressure on a body immersed in water is isotropic, which balances and distributes the (concentric) stresses on the matrix structure of the body and therefore increases its strength (Figure 9).

So, it's not surprising that the sample (advertised as having a compressive strength of 5 bar according to EN 826) is perfectly resistant to a hydrostatic pressure of 7 bar. Furthermore, hydrostatic pressure varies only with the depth of water. The ULISSE Reservoir shell would be progressively lowered to the required depth, so there would be no fluctuation in pressure on the cellular glass.

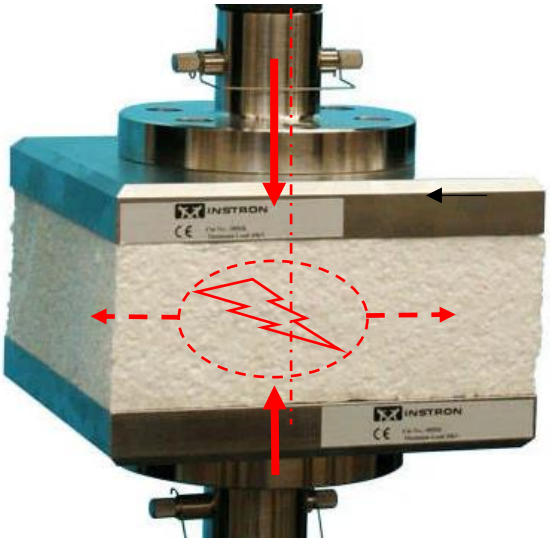

Fig. 8.12: Single-axis compression testing machine for thermal insulation panels to standard European EN 826 (photo instron.com)

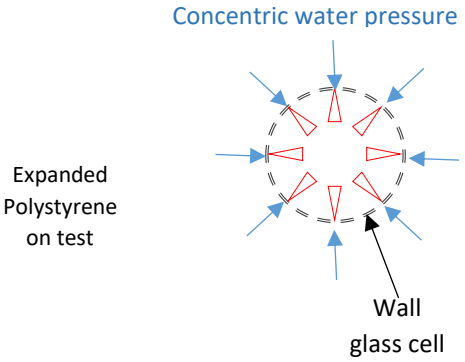

Fig. 8.13: Isentropic (concentric) hydrostatic pressure

8.4.7 Protection against cellular glass abrasion

T**he thin walls of cellular glass make it very abrasive and even brittle**. This is less the case as the density increases, due to the thickness of the walls (see Fig. 8.7). It is therefore essential to prevent the insulation blocks in the envelope from touching each other when they move!

Protection is therefore recommended, for example in the form of an individual wrapping (coat) using a sheet of fiberglass felt or basalt, identical to the intermediate joints. Also, for example, the 1200 x 600 mm FOAMGLAS® BOARD F panel is glass-fleece coated on both sides.


(Source : HKO.de)

Figure 8.13.1: Needle-punched glass felts stitched with glass sewing thread as anti-abrasion of cellular glass

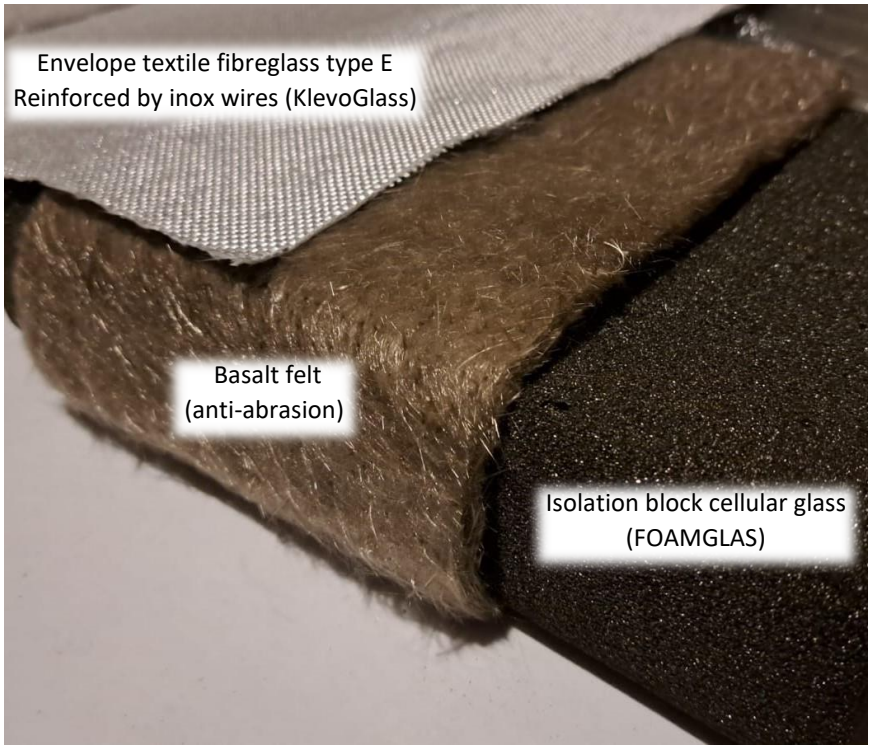

Figure 8.13.2: Example of an Intermediate arrangement of anti-abrasion Basalt felt layer for the cellular glass

Due to its relative incompressibility, cellular glass is rigid and insulating blocks or pavers are dimensionally stable. Their flexural strength is ≥ 550 kPa (EN 12089) and their tensile strength is ≥ 200 kPa (EN 1607). **Bending of the "semi-rigid/soft" envelope of the ULISSE Reservoir can only occur at the joints between the insulating blocks**.

8.5 Envelope joints

The joints between the insulating blocks or slabs allow the hyperbolic curvature of the envelope to be followed by the degrees of freedom of orientation (α) between the blocks, which are rigid (Fig. 8.14). The intermediate joints, whose Ctj is greater than that of the insulating blocks, will constitute "*thermal bridges*", in addition to those at the junctions of the envelope strips (Fig. 8.16).

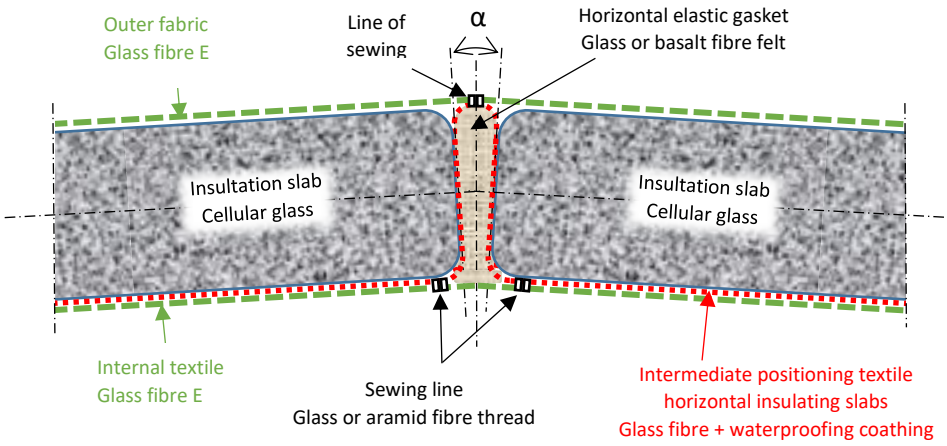

Figure 8.14: Partial cross-section of the envelope of the typical Reservoir (between the insulating slabs)

The shell of the Reservoir is subdivided into strips 12 m wide in *the* shape of a *hyperbolic arch*. The edges are parallel in the longitudinal section of the Reservoir and curved on the *hyperboloid half-shells* at either end. These envelope strips are joined together *by* symmetrical *jaws*.

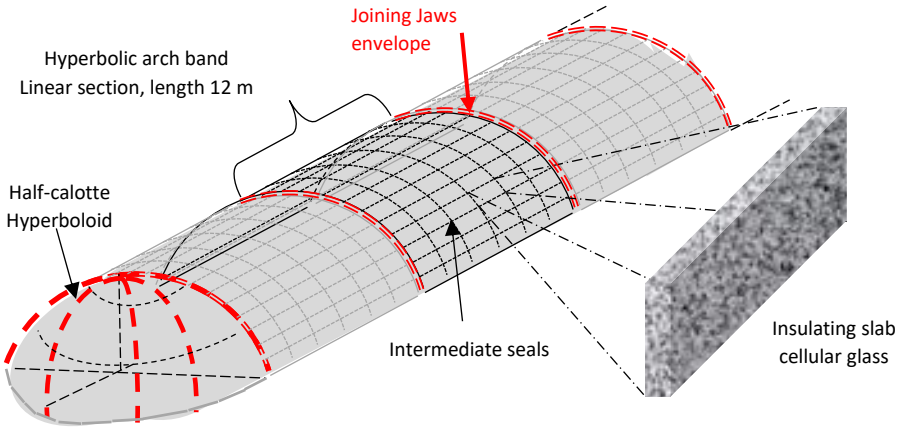

Figure 8.15: Typical Reservoir shell assembly diagram (components not to scale)

At the edges of the belts, the three layers of textile surround a stainless-steel cable, which together are clamped and held between the jaws (Fig. 8.16). A flat gasket is sandwiched inside to seal the joint between the strips.

The jaws are made up symmetrically of two stainless-steel flats (4 x 1 cm), spacing at approximately 5 mm and paired by tapered-head screws for central clamping (spacing between screws: 0.1 m). The flats are partially curved to surround and hold together the cables with the three layers of textiles.

Juxtaposed along the edge of the envelope strips, its junction jaws are individually equal in length to the height of the pavers, allowing them to follow the curvature of the envelope. Finally, to reduce thermal bridging, the junction is lined and covered with insulating felts, which are protected on each side by a stainless-steel sheet (*covering shield*).

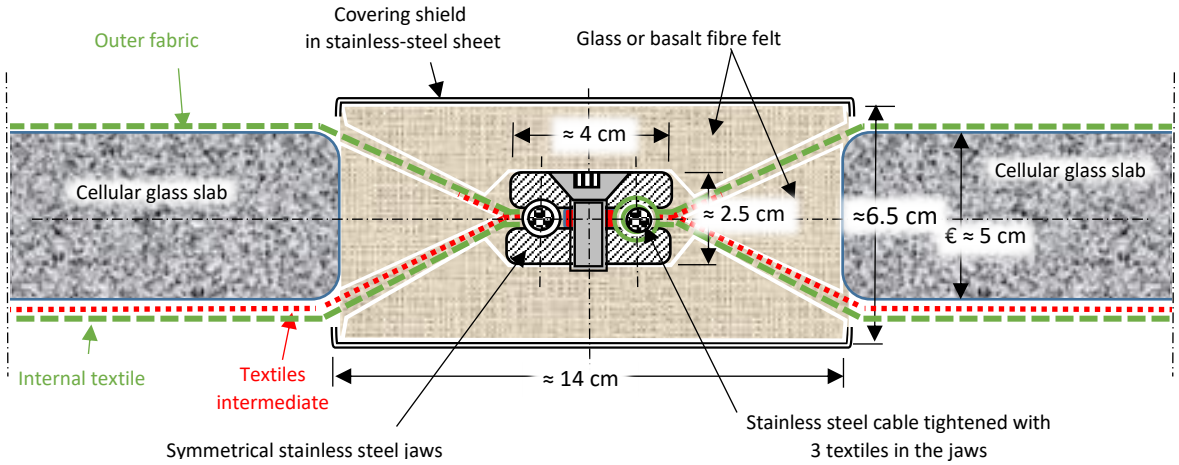

Figure 8.16: Perpendicular section at the junction of the envelope strips

8.6 Analysis of heat transfer through the ULISSE Reservoir shell

8.6.1 General information

The heat dissipative power (Q) through the envelope of the ULISSE type Reservoir is the product of the *heat transfer coefficient* U (W/m^2 K) with the surface area S (m^2) and with the temperature difference ΔT (K) between the Reservoir and the lake.

$$Q = U.S.\Delta T_{res\text{-}lac} \quad [W] \qquad (8.42)$$

U.S is the *Thermal Conductance* Ct (W/K) or the inverse of the *Thermal Resistance* Rt (K/W).

The efficiency of the long-term (seasonal) storage of hot water in the Underwater Reservoir, *ceteris paribus,* increases with the ratio between its Volume and the Surface Area of its shell, as well as with the *Thermal Resistance* (Rt) of the latter. The Rt or, conversely, the thermal conductance (Ct) of the envelope is essentially determined by the thermal conductance of the cellular glass insulating panels (Ctp), the thermal conductance of the *joints between the panels* (Ctji) and the thermal conductance of the *joints between* the strips of the envelope (Ctjb).

The thermal resistance of the thin stainless-steel sheets of the roofing shields (thickness 1 mm, λ_{inox}: 14 W/m.K) in the junction zones and of the 3 layers of fibreglass textiles (reinforced with stainless-steel wires) can be relatively neglected.

Apart from the fact that the textiles are also thin (≈ 1 mm) and have open meshes, free convection as well as water circulation currents (advection) around the Underwater Reservoir envelope, reduce the thermal resistance of the water (boundary layer) inside (Ri) and outside (Re) as much as possible. **We therefore make the conservative assumption that Ri and Re ≈ 0 (worst case). As** examples**:**

$$Ri = 1/(hi*S) \qquad (8.43)$$

-hi- being the heat exchange coefficient of the internal water in free convection = 100 - 900 Wm^{-2}K^{-1}

$$Re = 1/(he*S) \qquad (8.44)$$

-he- being the heat exchange coefficient of external water under free and forced convection due to circulation currents = 100 - 15'000 Wm^{-2}K^{-1}

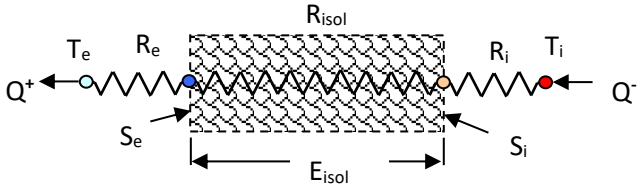

Figure 8.17: Representation of the simplified thermal model of the Reservoir envelope

8.6.2 Conductance of cellular glass blocks

The thermal conductance of an insulating block (Ctp) is determined by its thermal conductivity (λp: 0.05 W/m.K), surface area (S) and thickness (ε: 0.05 m). FOAMGLASS offers two standard sizes of cellular glass slabs (S_{-1}: 0.6 x 0.45 m = 0.27 m^2 and S_{-2}: 1.2 x 0.6 m = 0.72 m^2):

$Ctp\text{-}1 = S_{-1} (\lambda p / \varepsilon) = 0.27 (0.05/0.05) =$	0.27	[W/K]	(8.45)
$Ctp\text{-}2 = S_{-2} (\lambda p / \varepsilon) = 0.72 (0.05/0.05) =$	0.72	[W/K]	(8.46)

The surface thermal conductivity of the two sizes of the insulating blocks (S_{-1}, S_{-2}) remains equal to 1 W/m^2K.

The interlayer joints are made of a mat of E-glass or basalt fibre felts, with an uncompressed *density* (m) of 100 to 170 kg/m^3 for glass fibre and 120 to 137 kg/m^3 for basalt fibre. Filled with dry interstitial air, these materials have a low thermal conductivity (λ_f: 0.03 to 0.038 W/m.K) and are used in particular as thermal insulation in high-temperature applications (≈ 700 ˚C, source: *Final Advanced Materials*), a performance that is obviously not required for ULISSE.

However, when immersed in water, the interstitial space between the fibres is filled with water, whose CONVECTION-FREE thermal conductivity (λ_e: 0.58 W/m.K at 10˚C) is almost 30 times greater than that of dry air (λ_a: 0.02 W/m.K). The precise function of the fibre structure or matrix is to reduce the free convection of the "insulating or heat transfer fluid" (air, gas or water in our case) inside, and to do so with a minimum of structural mass (which is more conductive).

The same applies to synthetic insulating materials (XPS, EPS, phenolic foam, etc.) where the free space in the matrix is formed by the controlled expansion of cavities or bubbles enclosing the gas, like the CO_2 produced by oxidation of the carbon added to the molten glass bath during the manufacture of cellular glass. In this way, depending on the density of the cellular glass produced (100 to 200 kg/m^3), the thermal conductivity (λ_{vc}) varies from 0.04 to 0.06 W/m K.

According to figure 8.14, the joint is wedged between two insulating blocks, inclined at an angle of α. It has an average width (lj) of 1 cm (0.01 m) for a height (hj) equal to the thickness of the blocks (εp: 0.05 m). Illustrated in Fig. 8.18 below, the unit length (Luj) of the joint corresponds to half the circumference of a cellular glass block. The unit length then depends on the standard format of the FOAMGLASS slabs (S_{-1}, S_{-2}):

for S_{-1} (0.6 x 0.45 m = 0.27 m^2)	$L_{uj\text{-}1} = 0.6 + 0.45$ m =	1.05	[m]	(8.47)
for S_{-2} (1.2 x 0.6 m = 0.72 m^2)	$L_{uj\text{-}2} = 1.2 + 0.6$ m =	1.8	[m]	(8.48)

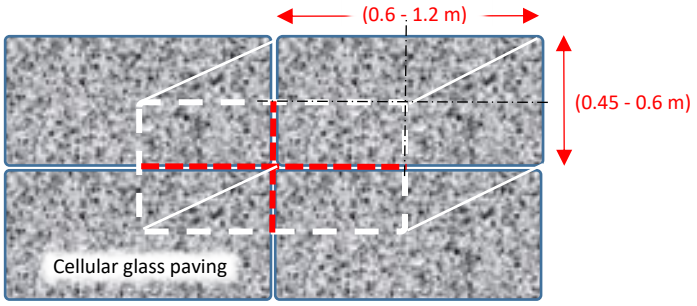

Figure 8.18: Unit length of interlayer joint (Luj) equal to half the circumference of a cellular glass block

The surface length of the joint (Lsj) per m^2 of paving is not equal to:

$L_{sj\text{-}1} = L_{uj\text{-}a} / S_{-1} = 1.05 / 0.27 =$	3.89	[m/ m^2]	(8.49)
$L_{sj\text{-}2} = L_{uj\text{-}b} / S_{-2} = 1.8 / 0.72 =$	2.5	[m/m^2]	(8.50)

The length of the joints decreases inversely with the size of the insulating blocks.

With a joint width (lj) of 1 cm (0.01 m), the surface area (Sj) is therefore also a function of the size of the cellular glass blocks (S_{-1}, S_{-2}):

$S_{j\text{-}1} = L_{uj\text{-}a}$ x 0.01 = 1.05 x 0.01 m =	0.0105	[m^2]	(8.51)
$S_{j\text{-}2} = L_{uj\text{-}b}$ x 0.01 = 1.8 x 0.01 m =	0.018	[m^2]	(8.52)

Depending on the density (ρ) of the uncompressed felt and that of the base material (ρ-glass: 2,500 kg/m^3 and ρ-basalt: 3,140 kg/m^3), the proportion (%) of the "net" volume of glass (Vv) or basalt (Vb) and that of water in the interstitial volume of the felt are in the ratio of the respective densities:

$Vv = m_{vj}$ / ρ-glass = (100 to 170) / 2,500 = 0.04 to 0.07 — 4 at 7 [%] (8.53)

$Vb = m_{bj}$ / ρ-basalt = (120 to 137) / 3'140 ≈ 0.04 — ≈ 4 [%] (8.54)

The water present in the interstices of the non-compressed felt therefore represents an average of 95% of the total volume of the gasket.

To maintain the spacing between cellular glass blocks, **uncompressed felt offers little resistance to compression**. This resistance can be increased by compressing the felt, for example by a factor of 5, which reduces the ratio of fibre and water volumes to approximately 1/4. The density of the (compressed) felt joint is then 500 to 850 kg/m^3 for glass fibre and 600 to 685 kg/m^3 for basalt fibre.

The surface area of the compressed interlayer joint (S_{jc}), which is a function of the size of the paving blocks (S_{-1}, S_{-2}), is therefore subdivided into 1/4 of the surface area (5 x 4% = 25%) for the fibres (Sf) and 3/4 for the interstitial water (Se).

For fibres, depending on the size of the paving blocks, we have:

$S_{f-1} = 1/4\ Sj = 1/4 \times 0.0105 =$ 0.0026 [m^2] (8.55)

$S_{f-2} = 1/4\ Sj = 1/4 \times 0.018 =$ 0.0045 [m^2] (8.56)

Similarly for water we have respectively:

Se-1 = 1/4 Sj = 3/4 x 0.0105 = 0.0079 [m^2] (8.57)

Se-2 = 1/4 Sj = 3/4 x 0.018 = 0.0135 [m^2] (8.58)

The thermal conductance of the fibre bundle alone (Ctf) is theoretically a function of its total cross-section (S_{f-1}, S_{f-2}), the thickness of the joint (εj: 0.05 m) and the material's own thermal conductivity (glass λ_v: 0.81 W/m K and basalt λ_b: 1.7 W/m.K).

For glass, depending on the size of the paving stones, we have:

$Ctv\text{-}1 = S_{f-1}\,(\lambda_v / \varepsilon_f) = 0.0026\ (0.81 / 0.05) =$ 0.042 [W/K] (8.59)

$Ctv\text{-}2 = S_{f-2}\,(\lambda_v / \varepsilon_f) = 0.0045\ (0.81 / 0.05) =$ 0.073 [W/K] (8.60)

For basalt we have respectively:

$Ctb\text{-}1 = S_{f-1}\,(\lambda_b / \varepsilon_f) = 0.0026\ (1.7 / 0.05) =$ 0.088 [W/K] (8.61)

$Ctb\text{-}2 = S_{f-2}\,(\lambda_b / \varepsilon_f) = 0.0045\ (1.7 / 0.05) =$ 0.153 [W/K] (8.62)

Similarly, the thermal conductance of water alone (Ctf) in the joint interstices is theoretically a function of the cross-sectional area (Se-1/-2), the thickness of the joint (εj = 0.05 m) and the thermal conductivity of non-convective water (λe: 0.58 W/m.K at 10˚C):

$Cte\text{-}1 = S_{e-1}\,(\lambda_e / \varepsilon_e) = 0.0079\ (0.58 / 0.05) =$ 0.092 [W/K] (8.63)

$Cte\text{-}2 = S_{e-2}\,(\lambda_e / \varepsilon_e) = 0.0135\ (0.58 / 0.05) =$ 0.157 [W/K] (8.64)

The thermal conductance of the compressed and immersed interlayer joint (Ctj) is then, as a first approximation, the sum of the Ctf of the fibres and that of the non-convective interstitial water (Cte):

$Ctj = Ctf + Cte$ [W/K] (8.65)

Depending on the materials and their respective surface areas, we obtain:

Ctjv-1 = Ctv-1 + Cte-1 = 0.042 + 0.092 = 0.134 [W/K] (8.66)

Ctjv-2 = Ctv-2 + Cte-2 = 0.073 + 0.157 = 0.23 [W/K] (8.67)

Ctjb-1 = Ctb-1 + Cte-1 = 0.088 + 0.092 = 0.18 [W/K] (8.68)

Ctjb-2 = Ctb-2 + Cte-2 = 0.153 + 0.157 = 0.31 [W/K] (8.69)

In compressed and immersed glass fibre, interstitial water represents 69% of Ctj and 51% in basalt fibre.

The thermal conductivity of the compressed and immersed felt (λf), according to the simplified model, is logically a function of the fibre material (glass, basalt):

λfv-1 = CtJ-1* ε_e / S_{j-1} = 0.134 * 0.05 / 0.0105 =	0.64	[W/m.K]	(8.70)
λfv-2 = CtJ-2* ε_e / S_{j-2} = 0.23 * 0.05 / 0.018 =	0.64	[W/m.K]	(8.71)
λfb-1 = CtJ-1* ε_e / S_{j-1} = 0.18* 0.05 / 0.0105 =	0.86	[W/m.K]	(8.72)
λfb-2 = CtJ-2* ε_e / S_{j-2} = 0.31 * 0.05 / 0.018 =	0.86	[W/m.K]	(8.73)

with (8.51) for S_{j-1} = 0.0105 m^2
with (8.52) for S_{j-2} = 0.018 m^2

This is 19 to 25 times the value of dry felt (λf-s ≈ 0.034 W/m.k) and 13 to 17 times that of cellular glass pavers (λvc ≈ 0.05 W/m.k), which is a real "bridge" for heat loss!

However, we have considered here (in a simplified way) that the joint is made up of two distinct, parallel resistances or thermal conductance's; one solid in fibre and the other liquid in water. Similar to an electrical circuit with two parallel resistors, the respective heat flows are continuous and do not interfere. Their individual and cumulative thermal conductivities (Ctf + Cte = Ctj) are therefore probably overestimated.

In reality, the thermal resistances are intimately intertwined, deformed (discontinuous) and the resulting heat flows disturbed, which consequently reduces the real thermal conductance of the joint (Ctjr). This is similar to the traffic capacity of a motorway compared with that of an equal surface area of secondary roads, but full of obstacles (traffic lights, junctions, speed bumps, etc.) ...

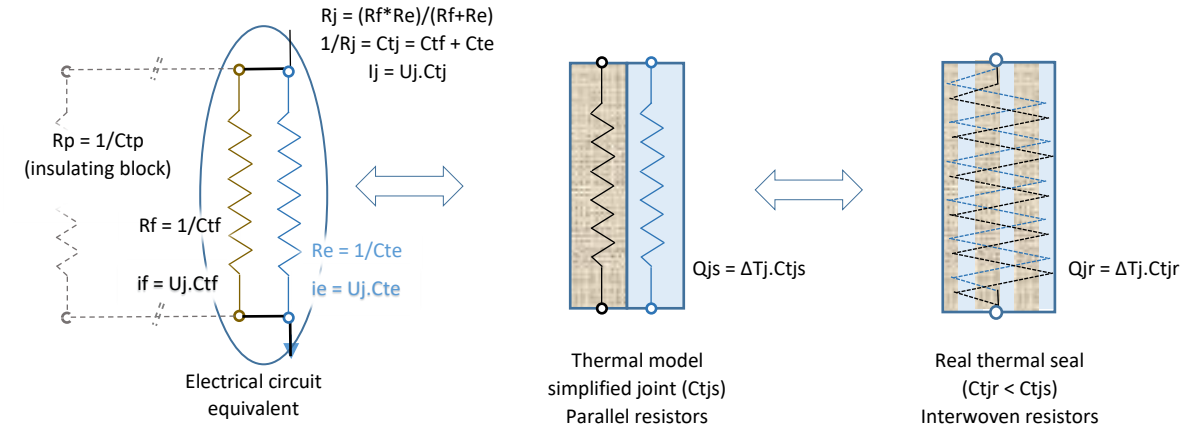

Fig. 8.19: Equivalent electrical circuit of the simplified and real thermal model of the seal

To verify this overestimation of Ctj, the simplified model can be applied to the thermal conductance of the uncompressed, dry, air-filled fibreglass joint (Ctjv-m) (λa: 0.022 W/m.K). This is done using the surface area of the joint Sj-1 (eq. 8.51) and the ratio between the volume of fibreglass Vv (eq. 8.53) and water Va (1 - Vv).

With the fibre surface:	Sf-1 = Sj-1 * Vv = 0.0105 * 0.04 =	0.00042 [m^2]	(8.74)
the air surface:	Sa-1 = Sj-1 * Va = 0.0105 * 0.96 =	0.01008 [m^2]	(8.75)

and according to (8.66), we obtain the Ctj-m of the simplified model (-m):

$$Ctjv\text{-}m = Ctv + Cta = Sf\text{-}1\ (\lambda v / \varepsilon f) + Sa\text{-}1\ (\lambda a / \varepsilon a) = 0.0108 \quad [W/K] \quad (8.76)$$

Comparatively, with the thermal conductivity of dry, uncompressed glass and basalt fibre felt (λf: 0.03 to 0.038 ≈ 0.034 W/m.k), the real thermal conductance of the joint Ctjv-r:

$$Ctjv\text{-}r = Sf\text{-}1\ (\lambda f / \varepsilon f) = 0.0105 * 0.034 / 0.05 = 0.00714 \quad [W/K] \quad (8.77)$$

The real thermal conductance is comparatively less than 1/3 of that obtained from the simplified model calculation (Ctjv-r / Ctjv-m = 0.66). We can therefore assign a ***corrective factor*** (**Fc = 0.66)** to approximate the physical behaviour of the insulating material **due to the intertwining of the fibres with the interstitial air.**

In this respect, it can be considered that the calculation, according to the simplified model, of the (real) thermal conductivity of the felt, compressed and immersed (λfr), respectively for the glass "(v)erre" and "(b)asalt" fibre, can therefore also be affected by the corrective factor (Fc):

for glass (with 8.70):	λfr-v = λf-v * Fc = 0.64 * 0.66 =	0.42	[W/m.K]	(8.78)
for basalt (with 8.30):	λfr-b = λf-b * Fc = 0.86 * 0.66 =	0.57	[W/m.K]	(8.79)

Similarly, the **thermal conductance of the** "unitary" (per block) **shper joint** (Ctj), made of glass fibres "(v)erre" or "(b)asalt" fibres and immersed in water, can also be affected by the correction factor (FC):

Ctjr = Ctjm * Fc		[W/K]	(8.80)
Ctjr-1v = 0.134 * 0.66 =	0.088	[W/K]	(8.81)
Ctjr-2v = 0.23 * 0.66 =	0.152	[W/K]	(8.82)
Ctjr-1b = 0.18 * 0.66 =	0.119	[W/K]	(8.83)
Ctjr-2b = 0.31 * 0.66 =	0.205	[W/K]	(8.84)

The cumulative thermal conductance (Ctp+j) of the cellular glass blocks (Ctp) with the proportion of the real joint (Ctjr), affected by the corrective factor (Fc), then also depends on the size of the cellular glass blocks (S_{-1} , S_{-2}) and the material of the joint in glass or basalt :

	Ctp+j = Ctp + Ctjr	[W/K]		(8.85)
with (9.3) for Ctp-1:	Ct_{p+j} -1v = Ctp-1 + Ctjr-1v = 0.27 + 0.088 = 0.358	[W/K]	**(+33%)**	(8.86)
with (9.4) for Ctp-2:	Ct_{p+j} -2v = Ctp-2 + Ctjr-2v = 0.72 + 0.152 = 0.872	[W/K]	**(+21%)**	(8.87)
	Ct_{p+j} -1b = Ctp-1 + Ctjr-1b = 0.27 + 0.119 = 0.389	[W/K]	**(+44%)**	(8.88)
	Ct_{p+j} -2b = Ctp-2 + Ctjr-2b = 0.72 + 0.205 = 0.925	[W/K]	**(+28%)**	(8.89)

It can be seen that the thermal conductance of the envelope, with the thermal bridge of the intermediate joints (Ctp+j) and in relation to the cellular glass blocks alone, **increases by 21 to 44%, depending on the size of the blocks (-2; -1) and the width (1cm) of the glass or basalt joints.** With double joint width (2 cm), the conductance of the envelope (Ctp+j) increases by **42 and 88%** respectively, and with it the heat loss of the envelope.

Note: In the calculation of the thermal conductance of the envelope, **we have deliberately neglected the insulating effect,** of the double layer of fiberglass or basalt, of the **anti-abrasion coat of the cellular glass pavers (§ 8.4.7)**.

8.6.3 Linear thermal conductance of the junction zone of the envelope strips (Ctjon)

In addition to the thermal resistance or conductance of the cellular glass blocks associated with the inter-layer joints, the junction of the envelope strips constitutes a *"linear" thermal bridge* (per metre of length). The connecting jaws (stainless-steel) are covered by a thermal insulation jacket consisting of several layers of fibreglass or basalt felt.

To determine the *linear thermal resistance* (Rt_L) or conversely the *linear thermal conductance* (Ct_L), the junction zone is divided into its various constituent elements, characterised by the width (L), thickness (ε) and thermal conductivity (λ) specific to the material of each element.

As shown in Fig. 8.20 below, these different elements are juxtaposed in width (B//A//B') and stacked in thickness (C + D + E), similar to a circuit of electrical resistors.

The equivalent linear thermal resistance (Rt_L) is as follows:

$$Rt_L: R_B \,//\, R_A \,//\, R_{B'} \Rightarrow Rt_L = 1 / [C_B + C_A + C_{B'}] = 1 / [\,(1/R_B) + (1/R_A) + (1/R_{B'})]$$

$$= 1 / [\,(1 / (R_{B\text{-}C} + R_{B\text{-}D} + R_{B\text{-}E})) + (1 / (R_{A\text{-}C} + R_{A\text{-}D} + R_{A\text{-}E})) + (1 / (R_{B'\text{-}C} + R_{B'\text{-}D} + R_{B'\text{-}E}))] \quad (8.90)$$

Note: to simplify the writing, the subscript "t_L" has been removed from the element names.

As the area where the strips meet is symmetrical, in width B/A/B and thickness C/D/E=C), the resistances R_B and $R_{B'}$ are identical and made up of three layers (C/D/E) of felt ($\lambda_f \approx 0.5$ W/m.K).

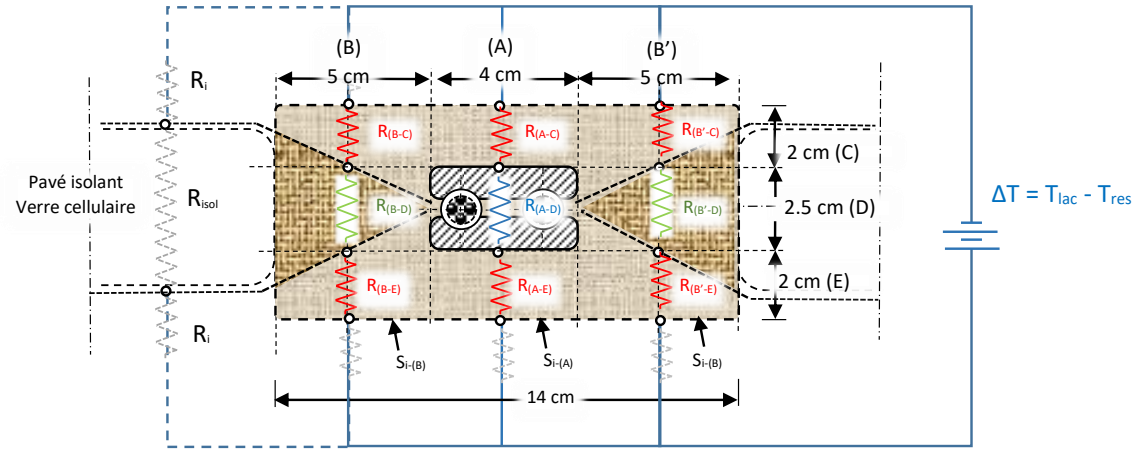

Figure 8.20: Cross-section of the junction zone of the envelope strips and its equivalent thermal circuit

According to (8.78 and 8.79), the thermal conductivity of **compressed and immersed** glass fibre **felt** ($\lambda_{f\text{-}v}$: 0.42 W/m.K,) and basalt fibre ($\lambda_{f\text{-}b}$: 0.57 W/m.K), is on average 0.5 W/m.K. This is 10 times that of cellular glass pavers (λ_{vc}: 0.05 W/m.K).

To simplify, we homogenise the three layers of felt, whose resistances R_B and $R_{B'}$, to form a single equivalent resistance $R_{B\text{-}B'}$. This, over the thickness $\varepsilon_{c\text{-}d\text{-}e}$ = 0.065 m, the width $2L_B$ = 0.1 m, and over a length of 1 m (linear), the surface $2S_B$ = 0.1 m^2; which gives for $R_{B\text{-}B'}$ and its inverse conductance $C_{B\text{-}B'}$:

$$R_{B\text{-}B'} = \varepsilon_{c\text{-}d\text{-}e} / 2S_b * \lambda_f = 0.065 / 0.1*0.5 = \quad 1.3 \quad [K/W] \qquad (8.91)$$

$$C_{B\text{-}B'} = 1/ R_{B\text{-}B'} = \quad 0.77 \quad [W/K] \qquad (8.92)$$

R_A is made up at the centre of the resistance of the connecting jaw (R_{AD}), which is made of stainless-steel (λ_{inox}: 14 W/m.K) and covered on each side (C, E) with the same layer of felt ($R_{A\text{-}C}$ = $R_{A\text{-}E}$). The equivalent resistance R_A and its inverse conductance are then as follows:

$$R_A = R_{A\text{-}C} + R_{A\text{-}D} + R_{A\text{-}E} = 2*(\varepsilon_{C/E} / S_A * \lambda_f) + (\varepsilon_D / S_A * \lambda_{inox}) \qquad (8.93)$$

$$= 2*(0.02/0.04*0.5) + (0.025/0.04*14) = \quad 1.04 \quad [K/W] \qquad (8.94)$$

$$C_A = 1/ R_A = \quad 0.96 \quad [W/K] \qquad (8.95)$$

The *linear* thermal resistance (per m linear) of the junction zone of the envelope strips (Rt_L) is therefore made up of the parallel resistances $R_{B\text{-}B'}$ and R_A or conversely (C_{tL}) the sum of their corresponding thermal conductance's $C_{B\text{-}B'}$ and C_A:

Rt_L: $R_{B\text{-}B'}$ // R_A => $Rt_L = 1/ (C_{B\text{-}B'} + C_A) = 1/ (0.77 + 0.96) =$ 0.58 [K/W] (8.96)

$Ct_L = C_{B\text{-}B'} + C_A = 0.77 + 0.96 =$ 1.73 [W/K] (8.97)

For the record, Rt_L is the *linear* thermal resistance - or Ct_L is the linear thermal conductance (per m) of the junction zone. The length of a junction (Lojo), between the strips of the envelope, is 157 m (hyperbolic arch Loh = πRc, eq.8.6).

The thermal resistance of the junction zone (Rtjon) and the conductance are then as follows:

$Rtjon = Rt_L / Lojon = 0.58 / 157 =$ 0.0037 [K/W] (8.98)

$Ctjon = Ct_L * Lojon = 1.73 * 157 =$ 272 [W/K] (8.99)

With a junction zone width (Lajon) of 0.14 m, the surface area is 22 m^2 (Sjon). The *surface* thermal resistance (per m^2) of the junction zone (Rtjons) and the conductance are then as follows:

Rtjons = Rtjon * Sjon =	0.0037 * 22 =	0.081	[K/W]	(8.100)
Ctjons = Ctjon / Sjon =	272 / 22 =	12.35	[W/K]	(8.101)

The parallel strips of the envelope (in the straight part of the Reservoir), 12 m wide, have a surface area of 1884 m^2 (Sbe = 12 x 157 m), including the cellular glass paving blocks, the glass or basalt felt interlayer joints and the junction jaws.

A strip comprises N paving blocks according to their size (S_{-1}, S_{-2}) with the thickness of the intermediate joint (0.01 m):

S_{-1} (0.61 x 0.451 m = 0.275 m^2)	=>	N_{-1} =	1884 / 0.275 =	6'851	[-]	(8.102)
S_{-2} (1.21 x 0.61 m = 0.738 m^2)	=>	N_{-2} =	1884 / 0.738 =	2'553	[-]	(8.103)

The thermal conductance of an envelope strip (Ctbe) is then the sum of the thermal conductance of the (N) pavers with their interlayers (Ctp+j) and that of the junction zone (Ctjo):

$$Ctbe = (N*Ctp+j) + Ctjo \quad (8.104)$$

Depending on the size and number (N) of the isolation blocks (9.60; 9.61) and the type of felt (glass, basalt), we obtain (9.44/45/46/47 for Ctp+j and 9.57 for Ctjo):

Ctbe-1v = (6'851*0.358) + 272 = 2'453 + 272 =	2'725	[W/K]	(8.105)
Ctbe-2v = (2'553*0.872) + 272 = 2'226 + 272 =	2'498	[W/K]	(8.106)
Ctbe-1b = (6'851*0.389) + 272 = 2'665 + 272 =	2'937	[W/K]	(8.107)
Ctbe-2b = (2'553*0.925) + 272 = 2'361 + 272 =	2'633	[W/K]	(8.108)

It can be seen that the thermal conductance of the junctions (Ctjon) represents approximately 10% of the total thermal conductance of the envelope.

Using the Ct values for the paving stones, the intermediate joints (1 cm thick) and the strip joint, the thermal conductivity of the envelope (λenv) is deduced for the large paving stone format and fibreglass (-2v):

$$\lambda env\text{-}2v = Ctbe\text{-}2v * \varepsilon / Sbe = 2'498 * 0.05 / 1884 = 0.066 \text{ [W/m.K]} \quad (8.109)$$

8.6.4 Using the thermal conductivity of the envelope:

This value (8.109) of the envelope thermal conductivity (λenv = 0.066 [W/m.K]) is used to calculate the **Reservoir vs Mock-up *Time Scale Factor*** [§ 18, (16.2)] and to calculate (theoretically) **the envelope heat loss of** the experimental Mock-up (0.077 m^3) and that of the typical full-scale ULISSE Reservoir (2 10^6 m^3).

Theoretical calculations of heat loss are carried out for phases representative of the annual operation (cycle) of the Reservoir, using two approaches.

One of the calculations is based on "mean values" of the temperature gradient on the "active" surface of the envelope:

- Specifically, for the *Autumn Stagnation* Phase (AS), the "active" surface area of the envelope and the volume correspond to the entire Reservoir and remain constant by definition,
- For the *Summer Loading* (SL) and *Winter Discharging (WD)* phases, the "average values" calculation is based on the average "mid-volume" of the Reservoir.

The other approach to the theoretical calculation is carried out, for the SL and WD phases, by 'integrating' the different 'steps' (of distinct volumes) that vary constantly during these phases.

9 ULISSE Mock-up

9.1 General layout of the Mock-up

The Mock-up reproduces the various operating phases of the ULISSE Reservoir in order to analyse and establish the efficiency of its sub-lacustrine seasonal energy-heat storage system. The *Autumn Stagnation* phase (AS) is used to establish the *Stagnation Heat Loss* (SHL) and *the cooling time constant* (Ctr). The Mock-up can also be used to reproduce and measure heat exchange flows during the 'dynamic' phases of *Summer Loading* (SL) of tempered water and *Winter Discharge* (DW).

The Mock-up represents a "linear slice" (1/5) of the shell of the Reservoir, at a reduced scale of 1/175. At the two longitudinal ends, the shell is "strongly insulated" (relatively a-thermal walls) by a 4 cm thick extruded polystyrene sheet ($\lambda \approx 0.035$ W/m k, => $U \approx 0.9$ W/m^2 K).

The hyperbolic envelope of the Mock-up is reduced to a thin (2 mm), transparent sheet of polycarbonate ($\lambda \approx 0.21$ W/m k, => $U = 105$ W/m^2 K). This sheet (62 x 90 cm = 5,580 cm^2) is curved in its large dimension (90 cm) and is fixed at the base between two stainless-steel threaded rods (M6) spaced 57 cm apart and a third located at the top. Two further M5 threaded rods are placed halfway up. These threaded rods are used to hold the envelope between the two insulating end plates. The resulting curvature is close to the hyperbola with an average radius of 30 cm (28.5 at the base and 31.3 at the top), giving a cross-section (x, y axes) of 1'238 cm^2 (≈ 97% of the equivalent half circle). Between the end plates, the length of the envelope being 62 cm (z axis), **the corresponding volume of the Mock-up is 77 litres.**

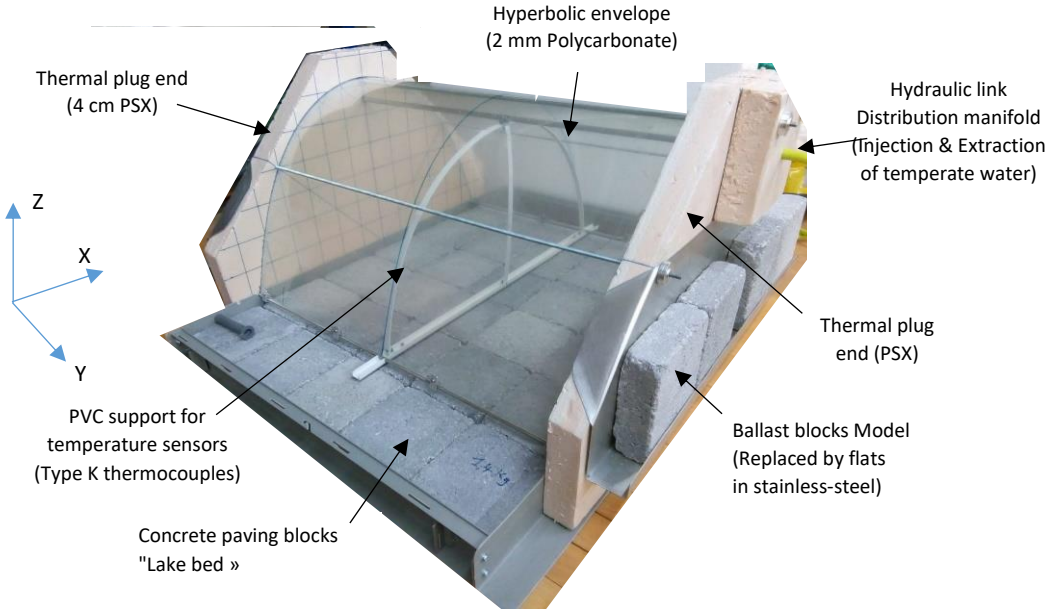

Figure 9.1 : ULISSE Mock-up

Taking into account the surface area of the end plates and that of the curved envelope, as well as their own thermal conductivity, the **"transverse" (x, y) specific heat flux (Ø) of the envelope is 236 times greater than that of the ends**: $Ø_{env} = 59$ W/K and $Ø_{ext} = 0.25$ W/K (thermal plugs).

As a first approximation, this allows the longitudinal heat loss of the Mock-up to be neglected and highlights the predominance of transverse heat loss from the envelope, including that from the lake bed, as well as free convection, which tends to reduce internal stratification, leading to Exergy losses.

The Mock-up is placed in a 1,000-litre plastic IBC tank with iron basket reinforcement, fixed on a plastic pallet (120 x 100 cm). The ratio between the volume of water in the IBC tank and the Mock-up is a maximum of 12.

A rectangular opening (100 x 80 cm) is made at the top of the IBC tank for the Mock-up to be inserted. The Mock-up is held on the bottom of the IBC tank (against the buoyancy of the PSX end plates) by a ballast made of 4 stainless-steel flats (10 kg gross weight) and by the support of two adjustable retaining rods from the IBC tank structure. The lower opening of the Mock-up is laid on two layers of concrete paving blocks (total thickness 8 cm) reproducing the conductivity and thermal capacity of the lake bed.

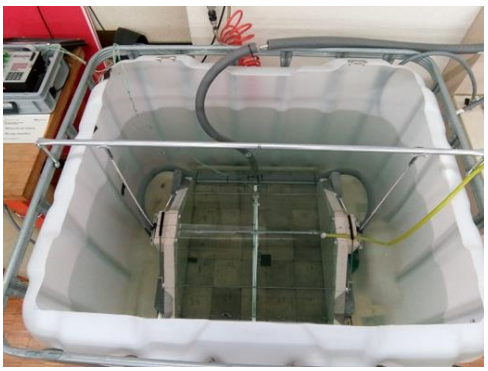

Figs. 9.2 & 9.3: ULISSE Mock-up *in the IBC test tank connected to the hydrothermal supply unite*

The IBC tank is located in a room in the basement of HEPIA (B I 23, formerly the "wood workshop"). The IBC tank is not insulated and is in thermal equilibrium with the room. To reduce the influence of room temperature, it can be covered with thermal insulation (e.g., 10 cm of glass wool). Its thermal stability depends on heat transfer from the Mock-up to the IBC tank (Q_{m-c}) and to the bottom slab (Q_{m-f}), as well as from the IBC tank to the room (Q_{c-l}). The IBC tank is also equipped with a water inlet at the surface and a lower extraction by overflow at a constant level, enabling the temperature inside to be regulated as required.

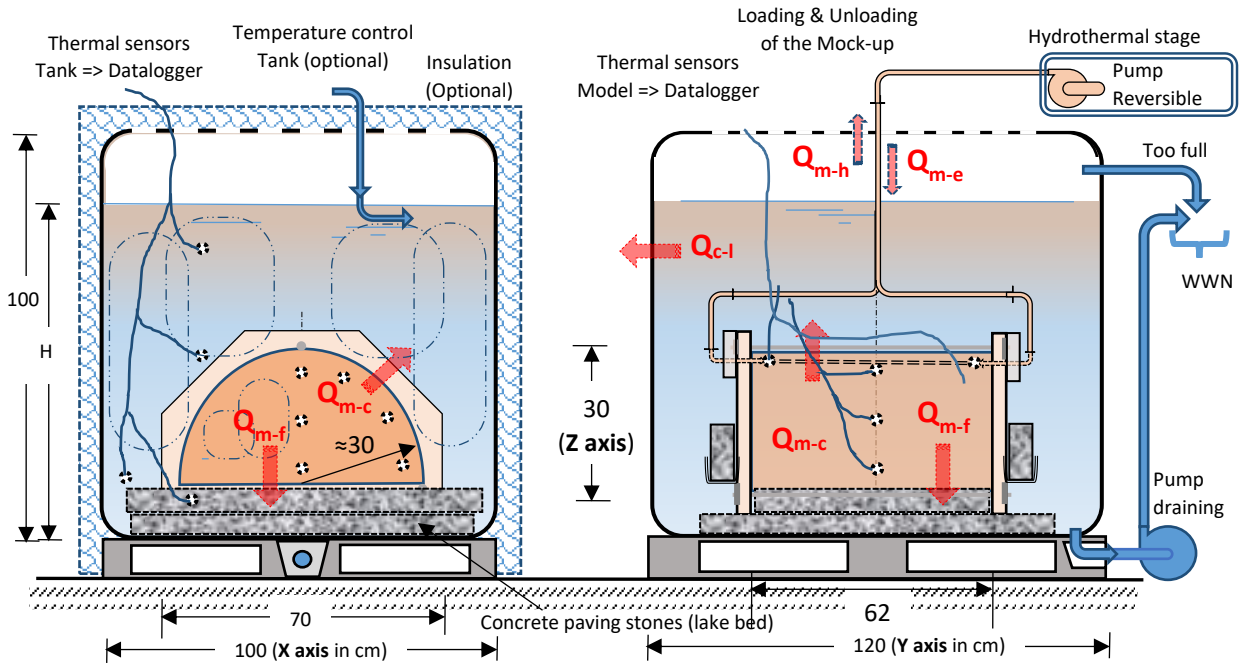

Figure 9.4: Diagram of thermal tests on the ULISSE Mock-up in the IBC tank *(scale 1/175)*

The temperature of the water in a full-scale ULISSE Reservoir is a priori around 20°C, whereas the temperature at the bottom of the lake is 5°C, i.e., a difference of 15˚K. **The experiments on the Mock-up are carried out with a supply from the domestic hot water (DHW) and cold water (CW) networks.** The temperature is regulated by a conventional shower mixer and an intermediate Thermal Stabilisation Tank (TST). For example, with a temperature difference of 15K and given the ratio between the volumes of water in the Mock-up and the IBC tank, the temperature of the IBC tank can gradually increase by about 1K if it is insulated and not cooled.

9.2 Hydrothermal supply unite for the Mock-up

Thermal loading and unloading of the model are carried out by means of a **Hydrothermal Supply Unite (HSU)**, comprising **a Membrane Pump (MP**) that can be reversed by opening and closing the Direction Valves (DV) that direct the water flow to and from the Mock-up. The membrane pump is supplied by a stabilised power supply for fine flow adjustment.

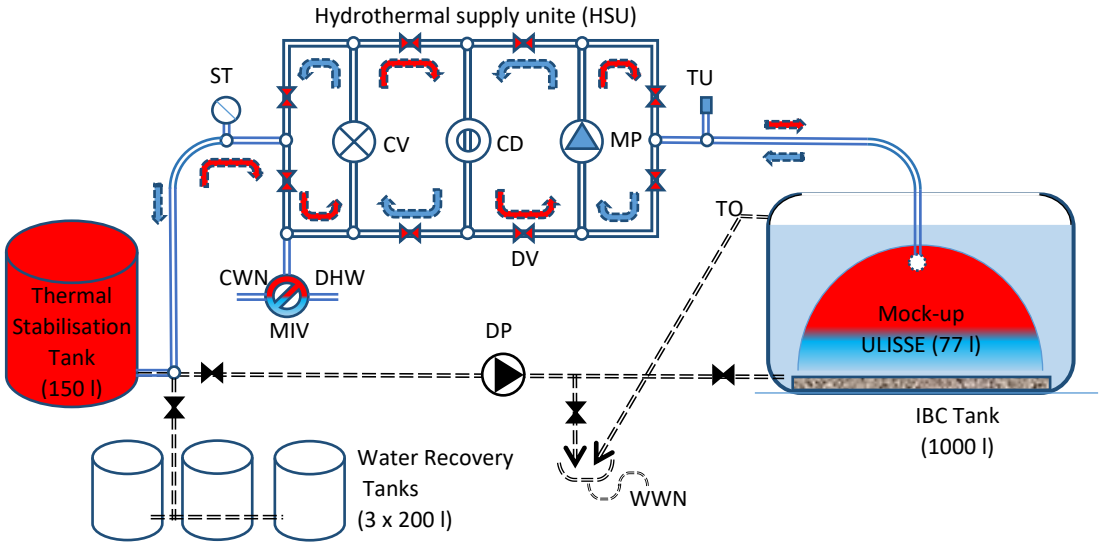

Figure 9.5: Hydraulic diagram of the ULISSE Mock-up
(direction of travel: **arrow - red = loading** / arrow **- blue = thermal unloading)**

CV:	Single-jet volumetric meter for domestic hot water (pre-equipped with pulse sensor)
CWN:	Cold water network
DHW:	Domestic hot water
DP:	Drainage pump, FLOTEC BIOX
DV:	Directional valves.
FM:	Flow meter 0.1-2 L/min (Teckflow, IR-OPFLOW)
HSU:	Hydrothermal supply unit
IBC:	Intermediate bulk container
MIV:	DHW/CWN temperature mixing valve (thermal pre-charging of the buffer tank)
MP:	Membrane pump (thermal loading/unloading of the Mock-up), 12V, 36W
ST:	Supply thermometer (Mock-up loading temperature stabiliser)
TO:	Tank overflow => WWN
TST:	Thermal stabilisation tank.
TU:	Supply thermocouple temperature sensor Mock-up
WRT:	Water recovery tanks
WWN:	Wastewater network

Table 9.6: Abbreviations for hydraulic circuit board components

The Mock-up is equipped at the top with a **tempered water injection and extraction ramp** (Fig. 9.7), enabling the reproduction of the Summer Loading (SL) of heat ($Q_{m\text{-}e}$ = 5.3 MJ or 1.47 kWh @ ΔT = 15˚K) and the Winter Discharge (WD) ($Q_{m\text{-}h}$).

The different water flow rates are provided by the membrane pump (MP) which is connected to both ends of the ramp, consisting of a brass tube with an internal/external diameter of 6/8 mm and fitted with 24 small holes (Ø 2 mm), diametrically opposed in two rows and with decreasing inter-distances (of 1 cm) towards the centre

of the tube. A **water flow distribution grid**, fitted with a fibreglass mat, is placed directly under the ramp (Figures 9.7 below).

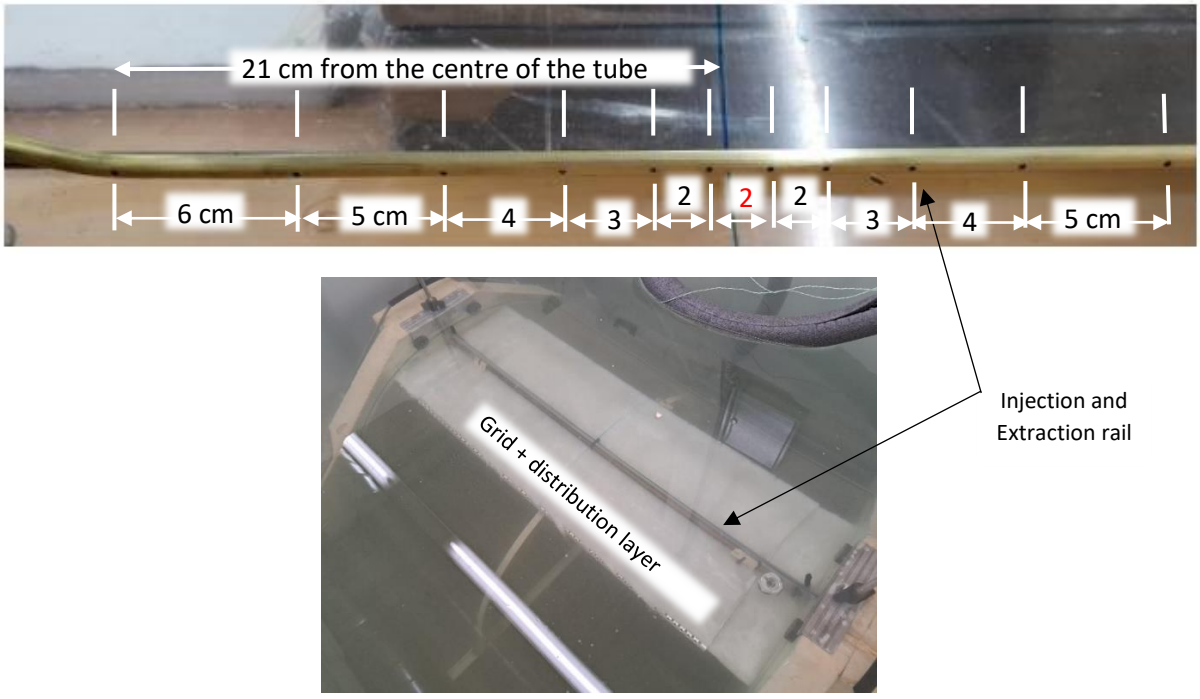

Figure 9.7: Summit ramp for summer injection (Q_{m-e}) and Winter extraction (Q_{m-h}) with a tempered water flow distribution grid

9.3 Thermocouples for temperature measurement

A temperature sensor (type K thermocouple, TC9/10) is fitted at each end of the manifold.) The connecting pipes are insulated from the influence of the water temperature in the tank by a foam sleeve. Measurements of the temperature and water flow rate at the ramp are used to quantify the heat energy introduced (Q_{m-e}) and extracted (Q_{m-h}) from the Mock-up over a complete cycle (pseudo-annual).

The measurements are mainly of a thermal nature, making it possible to determine the temperature and also to indirectly deduce the convective movements of water in the Mock-up and in the IBC tank (representing the lake).

Fig. 9.8: Type K thermocouples

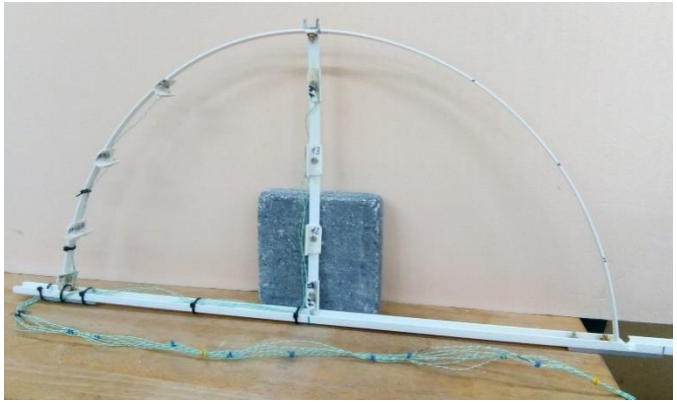

Fig. 9.9: Transverse support for thermocouples

The temperature probes (type K thermocouples, Fig. 9.8) are placed in the Mock-up on a PVC **transverse support** that can be moved longitudinally (Fig. 9.9), as well as on the **top** water distribution/extraction **ramp.**

Nine (9) thermocouples (TC) are placed, in pairs, at different heights on the transverse support; one on the central axis and the other on the lateral edge of the support as well as two (TC9/10) laterally (in opposite position or end) on the top ramp:

Location	***Support***	***Support***	***Support***	***Support***	***Support***	***Ramp***
Position/height	3 cm	8 cm	16 cm	23 cm	28 cm	30 cm
Central	TC11-B (T8)	TC12 (T12)	TC13 (T13)	TC14 (T14)	TC8 (T1')	-
Lateral	TC11-A (T11)	TC15 (T5)	TC15 (T5)	TC17 (T7)	-	TC9 (T9) & TC10 (T10)

Table 9.10: Thermocouple positions in the Mock-up

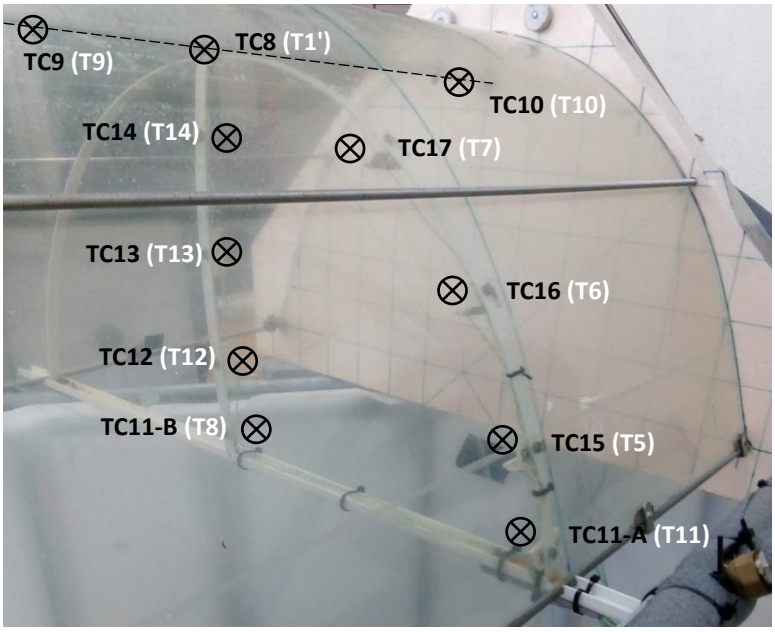

Figure 9.11: Detailed positions of the thermocouples on the Removable Support and the Ramp in the Mock-up

The thermocouples are connected to a Micrologger data acquisition and measurement interface (Campbell Scientific CR3000, Fig. 9.12). The Micrologger also records the flow rate/volume of hot water entering and leaving the model, via the pulse flow meter (FM) located on the hydrothermal supply plate (Figs. 9.3 and 9.5).

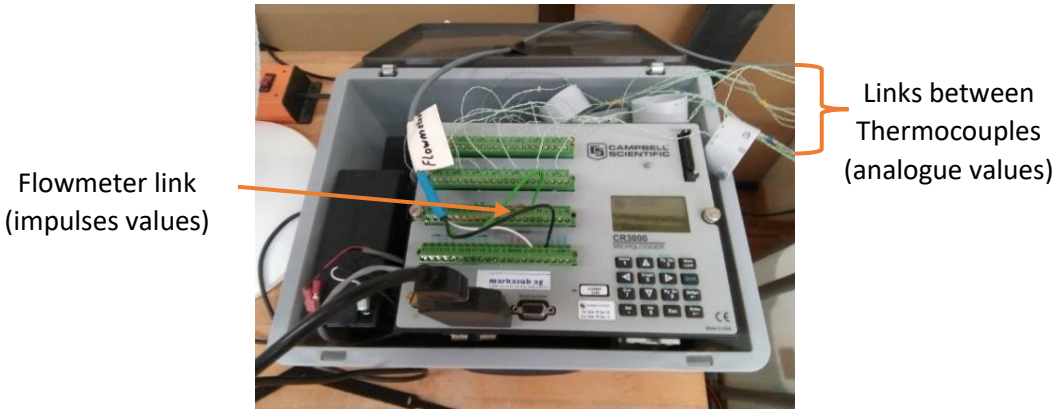

Figure 9.12 : Campbell Scientific Micrologger CR3000 data acquisition *unit*

Thermocouple		Milieu	
Numéro	**Position sur maquette**	**Humide / Sec**	**Symbole**
1	Rampe Alimentation gauche	H	RAG
2	Rampe Alimentation droite	H	RAD
3	Réservoir sommet centre	H	RSC
4	Réservoir sommet lateral	H	RSL
5	Réservoir milieu centre	H	RMC
6	Réservoir milieu latéral	H	RML
7	Réservoir fond centre	H	RFC
8	Réservoir fond latéral	H	RFL
9	Fond sur béton	H	FSB
10	Fond milieu béton	H	FMB
11	Fond béton cuve	H	FBC
12	Air sous cuve	S	ASC
13	Eau fond cuve	H	EFC
14	Eau paroi latérale cuve	H	EPL
15	Air paroi latérale cuve	S	APL
16	Cuve sommet réservoir	H	CSR
17	Eau sommet cuve	H	ESC
18	Air sommet cuve	S	ASC
19	Sortie Mitigeur Réservoir	S	SMR
20	Sortie Mitigeur Cuve	S	SMC
21	Evacuation basse Cuve	S	EBC

Table 9.13: List of thermocouples and their locations in the Mock-up and IBC tank

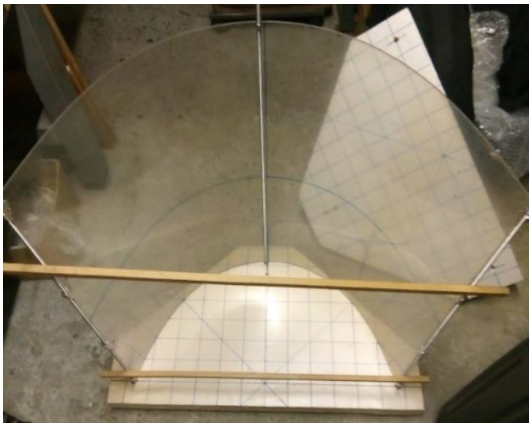

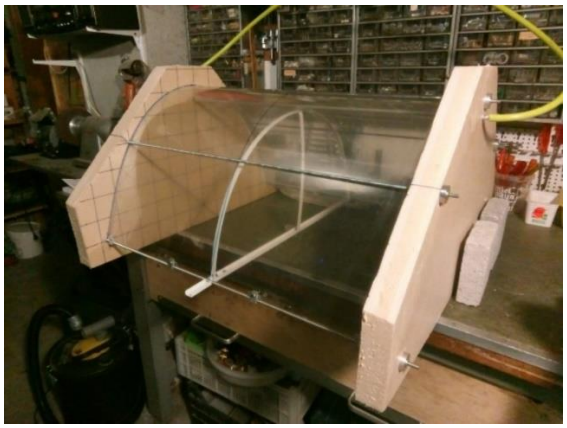

Figure 9.14.g: Construction of the Mock-up, hyperbolic bending of the polycarbonate (PC) envelope

Figure 9.14.d: Assembly and fixing of extruded polystyrene (PSX) end plates

Figure 9.15: Construction of the Mock-up, ballast support, concrete paving frame (lake bed)

9.4 Reproduction of heat loss at the base of the Reservoir (lake bed)

Installing the Reservoir close to the bottom of the lake is likely to benefit from its insulating properties. Heat loss in the soil at the bottom of the lake is "diffusive", like the propagation of heat in any type of soil. **Water immobilised in the soil matrix does not undergo convection.** In addition to the soil's own conductivity (λ: W/m K), we also benefit from its volumetric heat capacity (ρC: MJ/m^{3}K), which varies according to its composition.

Example for some types of rock:

Rocks -	**Conductivity λ (W/m K)** min - **typical** - max	**Capacity ρC (**MJ/m^3 **K)** min - max
Sedimentary		
Limestone	2.5 - **2.8** - 4.0	2.1 - 2.4
Marne	1.5 - **2.1** - 3.5	2.2 - 2.3
Sandstone	1.3 - **2.3** - 5.1	1.6 - 2.8
Non-consolidated		
Water-saturated gravel	approx. 1.8	approx. 2.4
Moraine	1.0 - **2.0** - 2.5	1.5 - 2.5
Water-saturated sand	1.7 - **2.4** - 5.0	2.2 - 2.9
Clay/water saturated loam	0.9 - **1.7** - 2.3	1.6 - 3.4
For comparison		
Water (tied up)	0.58	4.19
Ice (-10°C)	2.32	1.87
Concrete	0.9 - **1.6** - 2.0	1.8

Table 9.16: Comparison of Conductivity and Heat Capacity of rocks

The reproduction for the Mock-up of the lake bed is made with 4 large concrete slabs (40 x 40 x 4 cm) placed on the bottom of the tank and on top of that a layer of 35 small concrete paving stones (12.5 x 12.5 x 4 cm), held in a PVC frame, and possibly a layer of about 1 cm of sand. In this way, the characteristics of the lake bed are approximated, with a mix of sedimentary rocks and unconsolidated sedimentary materials. Thermocouples are placed between and on the concrete slabs (Figures 9.17 below).

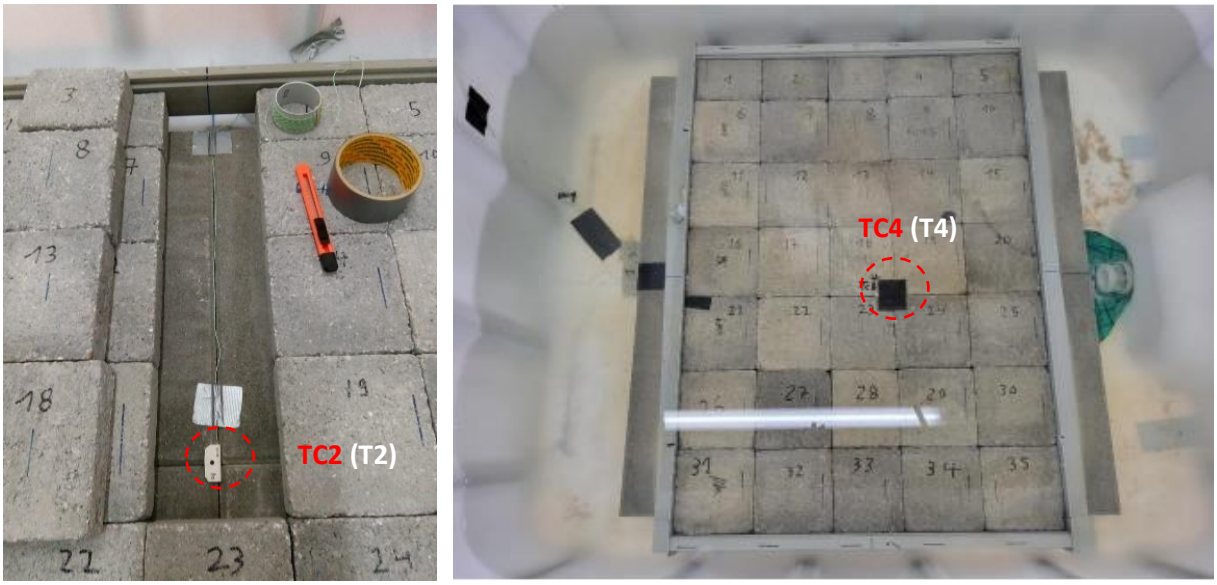

Figure 9.17: Reproduction of the lake bed in the IBC tank with concrete slabs and pavers
***Location of the thermocouples between (TC2) and on (TC4) the bottom slabs,** connected to the Datalogger terminals (T2) and (T4) respectively.*

9.5 Construction and calibration of type K thermocouples

9.5.1 Type K thermocouples and their mountings

Shown in Figure 9.18 on the left, the thermocouple measurement junction is formed solely by a tight, stripped twist, over a length of about 1 cm, of two type "K" conductor wires (diameters 0.18 mm, green positive terminal: nickel-chromium; white negative terminal: nickel-aluminium).

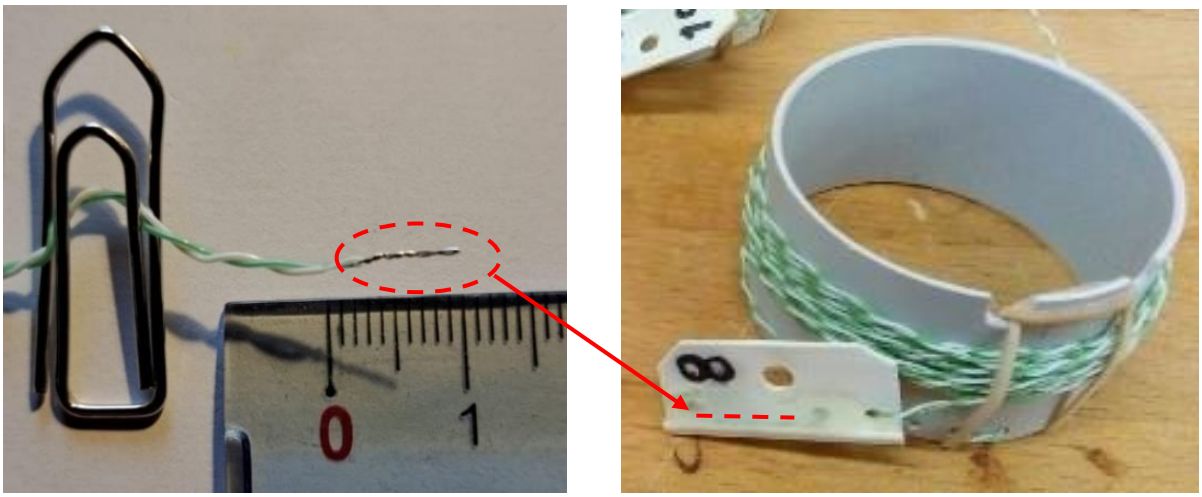

Figure 9.18: TC8 type K thermocouples, twisted junction mounted on the mounting plate before calibration

Visualised in Figure 9.18 right, **the said junction is placed in a narrow (1 mm) groove or cuvette on the edge of the mounting pad** (at the general probe support in the Mock-up). The junction is coated in the cup with a thin layer (≈1 mm) of transparent, flexible, water-resistant gel-glue (PATTEX). **This gel serves first and foremost, to electrically isolate the junction from water** and therefore from other thermocouples (avoiding interference). The twisted cable is blocked by the baffle holes in the plate.

The PVC plastic plate (25 x 10 mm) is about a millimetre thick and surrounds approximately half of the joint coating. **The other half of the joint coating is in direct contact with the water**. The thermal resistance between the joint and the water is therefore relatively low. In addition, with water circulating around the thermocouple junction, the thermal resistance of the water boundary layer should be negligible.

9.5.2 Response times of thermocouples with their mountings

The response time of the thermocouple measuring junction, to variations in water temperature (ΔTe), is mainly determined by the product of its heat capacity (Caj) and the thermal conductivity of the heat transfer interface (Coi) between the junction and the contacting water. It is characterised by its Time Constant (τrj) according to the following relationship:

$$\tau rj = Caj * Coi \qquad (9.1)$$

The distribution of heat in the junction depends on the intrinsic conductivity of the constituent material (Nickel-Aluminium for the type K thermocouple). Since the heat capacity is identical for all type K thermocouples, the time constant is only modified by the thermal conductivity of the junction-water interface (Coi).

The remote bowl of the mounting plate as well as the support of all thermocouples in the Mock-up has virtually no influence on the heat transfer between the surrounding water and the junction and therefore its response time (d˚C/dt). The screw-nut (M 2.5) connecting the stainless-steel plate to the support equilibrates in a few seconds with the temperature of the surrounding water.

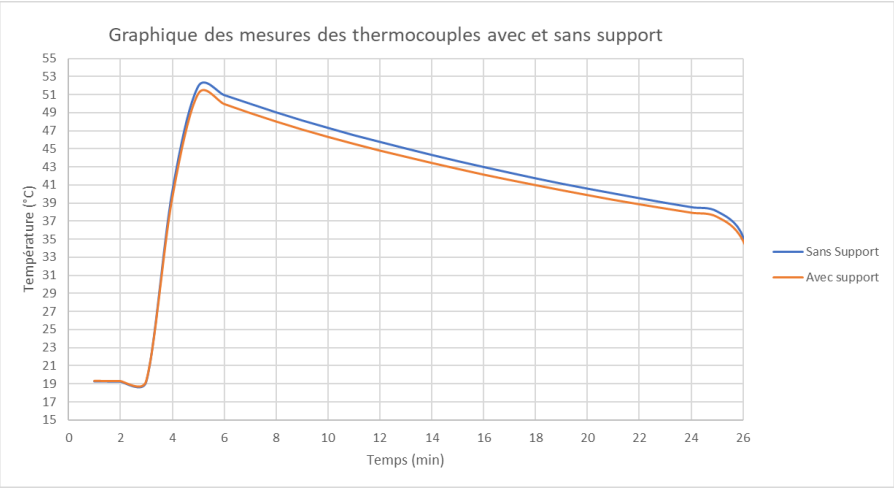

Figure 9.19: Thermocouple response time measured by Daniel Bello Mendes, master's thesis on the digital simulation of the ULISSE Mock-up

The response time of a thermocouple is reflected in the inclination (α = dT/dt, in ˚C/min) of the temperature rise or fall. A difference in response time (Δt) between two thermocouples results in a relative difference between their inclinations (Δα). The graph in Figure 9.19 above shows the time evolution of the temperature of two thermocouples (Type K) immersed simultaneously in a glass of hot water at nearly 52 ˚C. It can be seen that the temperature rise time (ΔT ≈ 33 ˚C) of the two thermocouples are identical (2 minutes) as well as their slopes (α) are superimposed, to simultaneously reach the nominal temperature of the glass of water.

A difference in temperature (ΔTd) peaks at 1.2˚C at the end of their maximum heating (in thermal equilibrium with the hot water). The discrepancy (ΔTd) is due to the disparity in response and intrinsic non-linearity between the two thermocouples. This shows the need to calibrate the thermocouples before using them.

9.5.3 Thermocouple calibration

Prior to the tests on the Mock-up, a calibration campaign for the thermocouples used took place during the summer of 2022, using a *laboratory reference thermostatic bath (JULABO)*.

9.5.4 Characteristics of the thermocouples used

Thermocouples have a disparity in response and intrinsic non-linearity. The tolerance of the thermocouples, type "K" used in the Mock-up, is +/- 1.5˚C in class 1 (between - 40 and + 375 ˚C). It is even +/- 2.5˚C in classes 2 and 3.

The **type K thermocouple**, generally called *Chromel/Alumel*, is designed mainly for general temperature measurements in the most common atmospheres (Tab. 9.20 below).

Type K - Données techniques

Thermocouple Type K Conducteurs		Variation approximative par degré de la f.e.m. générée jonction de référence a 0°C µV/°C à			Tenue en température de la jonction de mesure		Classes de Tolérances à IEC 60584-1			
Positif	Négatif	100°C	500°C	1000°C	usage continu	usage intermittent	Type	Classe 1	Classe 2	Classe 3
Nickel - Chrome Noms déposés: Chromel™, Thermokanthal KP*, NiCr, T1*, Tophel™	Nickel - Aluminium (magnetique) Noms déposés: Ni-Al, Alumel™, Thermokanthal KN™, T2™, NiAl™	42	43	39	0 à +1100°C	-180 à +1350°C	Domaine Valeur de tolérance Domaine Valeur de tolérance	–40°C à +375°C ±1.5°C 375°C à 1000°C ±0.004 · |t|	–40°C à +333°C ±2.5°C 333°C à 1200°C ±0.0075 · |t|	–167°C à +40°C ±2.5°C –200°C à –167°C ±0.015 · |t|

1. La tolérance est exprimée soit sous la forme d'une déviation, soit sous la forme d'une fonction de la température..
2. Les matériaux thermoélectriques sont normalement fournis pour répondre aux tolérances de fabrication spécifiées dans le tableau pour les températures supérieures à -40°C. Cependant, ces matériaux peuvent ne pas répondre aux tolérances pour les basses températures de la classe 3 pour les thermocouples type T, E, K et N. Si les thermocouples doivent satisfaire simultanément à la classe 3 et à la classe 1 ou 2, l'acheteur doit l'indiquer, une sélection des matériaux étant normalement nécessaire.

Table 9.20: Characteristics of the type K thermocouple, (source: TC SA.fr)

To obtain accuracy (to +/-10^{-2}) of the Temperature measured (Tmx) with a Thermocouple (TCx), its measured value (Vx) is affected by the **Calibration or Correction Factor (FC) of the thermocouple.**

$$Tmx = Vx*FC \quad (9.2)$$

The correction factor (Fc) of the thermocouple is obtained during calibration by comparing (quotient) the reference temperature (Tr) of the thermostatic bath and the measured temperature (Tc).

$$FC = Tr / Tc \quad (9.3)$$

Figure 9.21 : Thermocouple calibration setup

The thermocouples are inserted into the thermostatic bath, fixed together on a bar to prevent them from moving due to the (strong) stirring of the water inside. The measurements are recorded on the Fast Measurement Acquisition Unit or 'Micrologger' (*Cambell Scientific, CR 3000*).

The *Data/Micrologger* takes approximately 43 measurements (samples) per second (1/23 ms) of the temperature of the thermocouples, converts them (analogue/digital) to 16 bits, stores them in its memory (4 MB) and displays them as average values (Avg) over 1 minute (≈ 2,600 measurements or samples). The data is retrieved from the laptop for analysis.

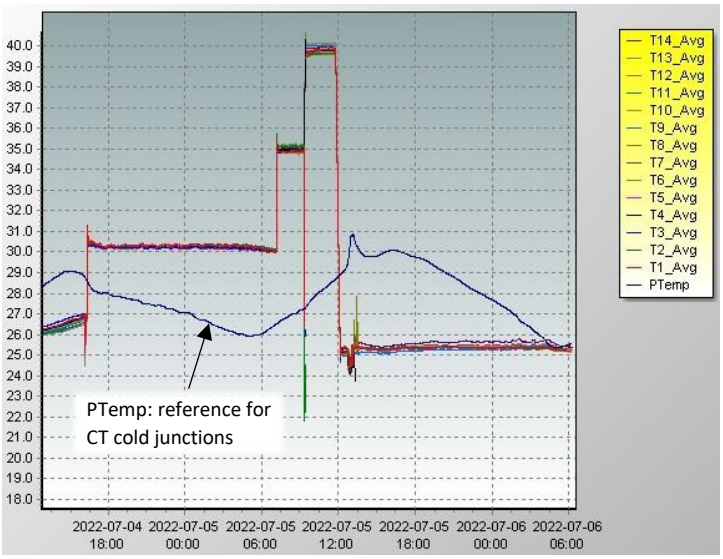

Figure 9.22: Calibration of the thermocouples for the ULISSE Mock-up*, using the reference thermostatic bath (JUMALO) from the HEPIA/LECEA laboratory. 1er Calibration between 4 and 22 July 2022. Observation of the relative disparity and temporal stability over the ranges, 25, 30, 35 and 40˚C and* ***the influence of PTemp****.*

To check the thermocouple's thermal linearity, calibration is carried out over several temperature *steps*, from P-5˚C to P-40˚C, in increments of 5˚C, over variable but relatively long timescales (several hours).

In Figures 9.22 above, the blue curve (PTemp) is the temperature of the *built-in* thermistor (accuracy: +/- 0.5-0.8˚C). This is used as a reference temperature for the junctions (or cold joins) of the thermocouples. Between the two junctions of the thermocouple a potential difference or voltages (Seebeck) is produced in relation to the temperatures of the two junctions (hot - cold).

It is this voltage (in µV) that is converted into a temperature in the Datalogger, based on a precise cold junction standard reference table equal to 0˚C. (*source TC SA.fr*). The reference temperature (PTemp) drives the cold junction compensation circuit located at the H/L terminals of the differential analogue terminals and to which the thermocouples are connected.

In Figure 9.22 we observe that PTemp varies periodically with an amplitude of 5 ˚C as a function of the temperature of the room where the Mock-up is located, peaking in the afternoon (31˚C) and declining until the early morning (26 ˚C at 5-6H). **The calibration takes place during the heatwave of July 2022**, with the ventilation of the basement room and the building shut down (summer closure of the school for students).

Deviations (tolerance) are also observed when measuring the temperature between the thermocouples, after a period of stabilisation or thermal equilibration (of the mass of internal metallic material) of the measuring junctions with the water in the thermostatic bath. This "stabilised" value is taken into account for the calibration and not the "transient" value of the thermal equilibration phase of the thermocouples with the bath water.

The values for TC1 to TC15 were obtained in steps from 10 to 40°C during calibration from 4 to 6 July 2022 and are shown in Table 9.23 below. The indication "NAN" means that the thermocouple is not connected for the corresponding measurement. Ptemp shows the "heatwave" period of the calibration. In the last line of Table 9.23, FC10-40 is the average correction factor over all the stages.

PTemp	Palier	TC1	TC2	TC3	TC4	TC5	TC6	TC7	TC8	TC9	TC10	TC11-A	TC11-B	TC12	TC13	TC14	TC15
˚C	˚C	˚C	˚C	˚C	˚C	˚C	˚C	˚C	˚C	˚C	˚C	˚C	˚C	˚C	˚C	˚C	˚C
28,20	10	NAN	NAN	NAN	NAN	NAN	NAN	NAN	10,66	9,99	10,74	10,42	10,76	10,15	10,07	10,60	10,70
	FC10								0,938	1,001	0,931	0,960	0,929	0,985	0,993	0,943	0,935
27,60	15	NAN	NAN	NAN	NAN	NAN	NAN	NAN	15,57	15,12	15,64	15,40	15,67	15,25	15,19	15,57	15,59
	FC15								0,964	0,992	0,959	0,974	0,958	0,984	0,987	0,963	0,962
26,45	20	NAN	NAN	NAN	NAN	NAN	NAN	NAN	20,33	20,12	20,40	20,24	20,43	20,22	20,20	20,42	20,35
	TC20								0,984	0,994	0,980	0,988	0,979	0,989	0,990	0,979	0,983
28,25	25	NAN	NAN	NAN	NAN	NAN	NAN	NAN	25,32	25,24	25,37	25,34	25,41	25,36	25,39	25,59	25,34
	FC25								0,987	0,991	0,985	0,987	0,984	0,986	0,985	0,977	0,986
27,01	30	30,30	30,33	30,20	30,21	30,20	30,27	30,17	30,27	30,32	30,18	30,16	NAN	30,26	30,27	30,20	NAN
	FC30	0,990	0,989	0,994	0,993	0,994	0,991	0,994	0,991	0,989	0,994	0,995		0,991	0,991	0,993	
26,94	35	34,88	35,14	34,86	34,98	34,98	35,20	34,94	34,81	35,10	34,82	NAN	34,84	35,12	35,19	35,01	NAN
	FC35	1,003	0,996	1,004	1,001	1,001	0,994	1,002	1,005	0,997	1,005		1,005	0,997	0,995	1,000	
28,11	40	NAN	NAN	NAN	39,76	39,79	40,11	39,75	39,59	40,01	39,60	39,81	39,64	40,01	40,11	39,92	39,62
	FC40				1,006	1,005	0,997	1,006	1,010	1,000	1,010	1,005	1,009	1,000	0,997	1,002	1,010
Moyenne :		TC1	TC2	TC3	TC4	TC5	TC6	TC7	TC8	TC9	TC10	TC11-A	TC11-B	TC12	TC13	TC14	TC15
FC10-40 :		0,997	0,993	0,999	1,000	1,000	0,994	1,001	0,983	0,995	0,981	0,985	0,977	0,990	0,991	0,980	0,975

Table 9.23: Calculation of Correction Factors (CF) for the 15 thermocouples (NAN = CT not connected)
(Useful test area on the Mock-up, ΔT: 15˚K)

A second calibration period was carried out between 19 and 22 July 2022 for TC16 to TC21 with temperature steps from 5 to 40°C (Fig. 9.24 below). The range of calibration temperature steps largely covers that used for tests on the Mock-up (20-35°C, ΔT: 15 K).

The "NOV" indication for thermocouple TC19 means that the measurement is invalid due to an unexpected displacement out of the water of the thermostatic bath. It can be seen that the Ptemp temperature rose again to over 31˚C during the 2nd "canicular" period of the calibration.

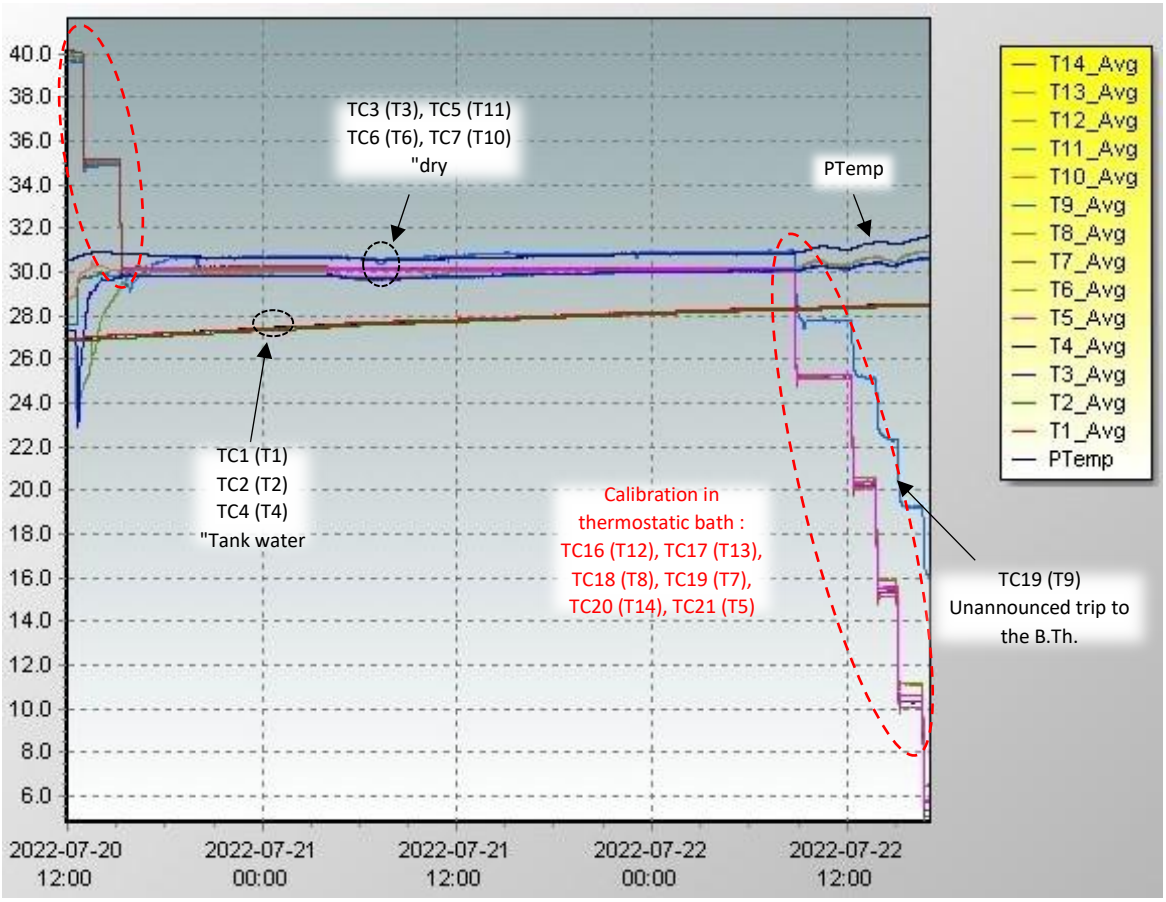

Fig. 9.24: Calibration of thermocouples TC16 to TC21 (from 19 to 22 July 2022)

9.5.5 Details of the TC16 to TC21 thermocouple calibration procedure

19.7.22 - 14 : 30 - **Connection TC16 on Terminal T12** => in Thermostatic Bath (TB) at 30°C
- Connection TC17 on Terminal T13 => in TB at 30°C
- 15 : 51 - LV stage at 35°C
- 16 : 47 - LV stage at 35°C

20.7.22 - 10 : 30 - **Connection TC18 on Terminal T8** => in TB at 40°C
- Connection TC19 on Terminal T9 => in TB at 40°C
- Connection TC20 on Terminal T14 => in TB at 40°C
- 12 : 3 0 - TC6 water outlet and TC7 (T10) tank outlet (fitted next to each other)
- TC3 (T3) water outlet and TC5 (T11) tank outlet (fitted sideways)
- 12 : 56 - TB stage at 35°C
- 15 : 14 - TB stage at 30°C
- 15 : 35 - **Connection of TC21 on Terminal T5** => in LV at 30°C

22.7.22 - 08 : 45 - TB stage at 25°C
- 12 : 14 - TB stage at 20°C
- 13 : 45 - TB stage at 15°C
- 15 : 00 - TB stage at 10°C
- 16 : 38 - TB level at 5°C
- 16 : 53 - End of 2nd calibration and recording period (TC16-TC21).

PTemp	Palier	TC16	TC17	TC18	TC19	TC20	TC21
°C	°C	°C	°C	°C	°C	°C	°C
31,61	5	5,07	5,78	6,46	NOV	5,31	5,76
	FC5	0,986	0,866	0,775		0,942	0,868
30,66	10	10,08	10,65	11,14	NOV	10,30	10,63
	FC10	0,992	0,939	0,898		0,971	0,941
31,29	15	15,16	15,58	15,89	NOV	15,36	15,56
	FC15	0,990	0,963	0,944		0,977	0,964
31,36	20	20,11	20,41	20,56	NOV	20,27	20,40
	FC20	0,995	0,980	0,973		0,987	0,980
31,05	25	25,14	25,30	25,31	NOV	25,25	25,28
	FC25	0,995	0,980	0,973		0,987	0,980
30,85	30	30,13	30,17	30,01	29,50	30,21	30,15
	FC30	0,996	0,994	1,000	1,017	0,993	0,995
30,83	35	35,14	35,07	35,00	34,89	35,19	NAN
	FC35	0,996	0,998	1,000	1,003	0,995	
30,76	40	40,09	39,91	39,85	39,66	40,10	NAN
	FC40	0,998	1,002	1,004	1,009	0,998	
31,05	**Moyenne**	**TC16**	**TC17**	**TC18**	**TC19**	**TC20**	**TC21**
	FC10-40	**0,993**	**0,965**	**0,946**	**1,009**	**0,981**	**0,955**

Table 9.25: Calibration of thermocouples TC16 to TC21 (19-22.07.2022)
(Useful test area on the Mock-up, ΔT: 15˚K)

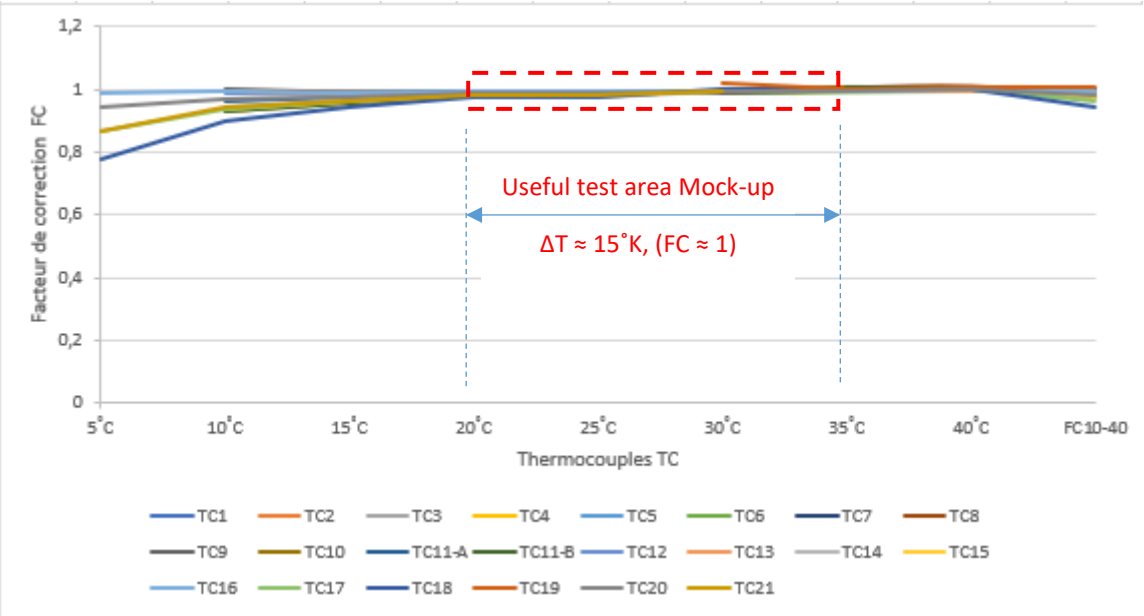

Figure 9.26: Correction factors (CF) for thermocouples as a function of temperature (from 4 to 22.07.2022)

10 Time Scale Factor (TSF) of the real Reservoir vs Mock-up

10.1 Dimensional analysis

A dimensional analysis is essential to establish a relationship between the characteristic time of the real ULISSE Reservoir and that of the Mock-up. The Mock-up represents a "linear slice" of about 1/5 of the real Reservoir (figure 10.1 below). The ratio of the volume of the slice of the Reservoir to that of the Mock-up (4.10^5 m^3 / $7.7\ 10^{-3}$ m^3) is $4.7\ 10^6$.

From certain points of view, two isomorphic objects can be considered to be identical, or at least indistinguishable, which makes it possible to transpose results and properties demonstrated for one to the other. In many cases, the interesting properties of one object will be shared by all the isomorphic objects in the category (source: Wikipedia/Isomorphism).

If the characteristic geometric ratios of the full-scale Reservoir envelope are the same as those of the Mock-up: [hyperbola of radius (R) at the base, with the length of curvature (Loh) in an identical ratio of (π = Loh/Rc) and the said base (2Rc) equals the longitudinal length (L) of the envelope], they can be considered as isomorphic and assigned a *form factor* (FF) equal to -1-.

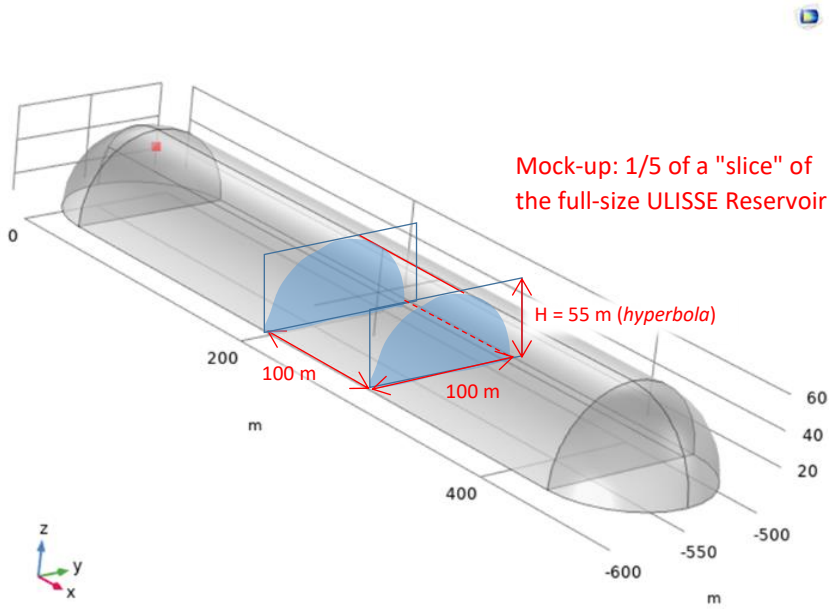

Figure 10.1: Approximate perspective representation with dimensions (m) of the real Reservoir (2 10^6 m^3) and the "slice" (1/5 = 400,000 m^3) corresponding to the Mock-up *(0.077 m^3)*
(Base figure: Roland Rozsnyo, HEPIA, COMSOL Multiphysics software, ULISSE numerical simulation)

However, in addition to their shape and size ratios (Rr/m, Lr/m), the respective materials and thicknesses of their envelopes are not the same (5 cm of cellular glass for the real Reservoir vs 2 mm of polycarbonate for the Mock-up).

In addition, the thermal conductivity of the envelopes (λenv: λr, λm) also differs because, unlike the Mock-up, the envelope of the real Reservoir includes, in addition to the cellular glass pavers, the **intermediate joints (Ctjin)** and the **junctions of the envelope strips (Ctjon).** These increase the total thermal conductivity of the shell of the real Reservoir compared with that of the blocks alone (λenv: 0.05 => 0.066 W/m.K, see § 10, eq. 9.67).

In order to be able to correctly interpret the results of measurements obtained experimentally (physical model) with those obtained by calculation (Excel, COMSOL digital simulation), we determine their appropriate *Time Scale Factor* (TSF) (dimensionless). This will correlate the different dimensional ratios and the characteristics of the materials making up the envelope of the two objects (full-scale Reservoir and reduced-scale Mock-up).

The dimensional analysis, not explained further here, shows a relationship between the characteristic time of the full-scale Reservoir and that of the Mock-up, which is referred to here as the Reservoir/Mock-up *Time Scale Factor* (TSF). With a Reservoir/Mock-up form factor equal to 1, we obtain the following TSF:

$$TSF = t_r / t_m = (FF) \,.\, (Rr / Rm).\, (Epr / Epm) \,.\, (\lambda m / \lambda r) \qquad [-] \qquad (10.1)$$

$$TSF = (1).\, (50 / 0{,}29) \,.\, (0{,}05 / 0{,}002) \,.\, (0{,}21/ 0{,}066) = \quad \mathbf{13'715} \quad [-] \qquad (10.2)$$

with:

t_r	the characteristic time of the full-scale Reservoir	
t_m	the characteristic time of the Mock-up	
FF	form factor Reservoir vs. Mock-up	(1)
Rr	the characteristic transverse radius of the actual Reservoir	(50 m)
Rm	the characteristic transverse radius of the Mock-up	(0.29 m)
Épr	thickness of the Reservoir shell (cellular glass insulation)	(0.05 m)
Epm	the thickness of the Mock-up envelope (polycarbonate)	(0,002 m)
λr	Thermal conductivity of the Reservoir shell	(0.066 W/m.K)
λm	Thermal conductivity of the Mock-up envelope	(0.21 W/m.k)

Clearly, the TSF = 13,715 means that **1 minute elapsed for the Mock-up corresponds to 13,715 minutes, or almost 229 hours or almost 10 days** of **elapsed time (t_r) for the real Reservoir!**

One complete cycle of a real year (t_r = 8,760 h) corresponds to 38.3 minutes of Mock-up time (t_m), i.e., **1 real month of Reservoir corresponds to 3.2 minutes of Mock-up time**.

The ratio (13,715) between the duration of the different operating phases over a real year (t_r) would then correspond for the Mock-up (t_m) to:

			Reservoir (t_r)		**Mock-up (t_m)**	
1.	Summer Loading	(SL)	2 months	<=>	6.4	minutes
2.	Autumn stagnation	(AS)	2 months	<=>	6.4	minutes
3.	Winter Discharging	(WD)	6 months	<=>	19.1	minutes
4.	Spring Stagnation	(SS)	2 months	<=>	6.4	minutes
Annual operating cycle			12 months (t_r)	<=>	38.3	minutes (t_m)

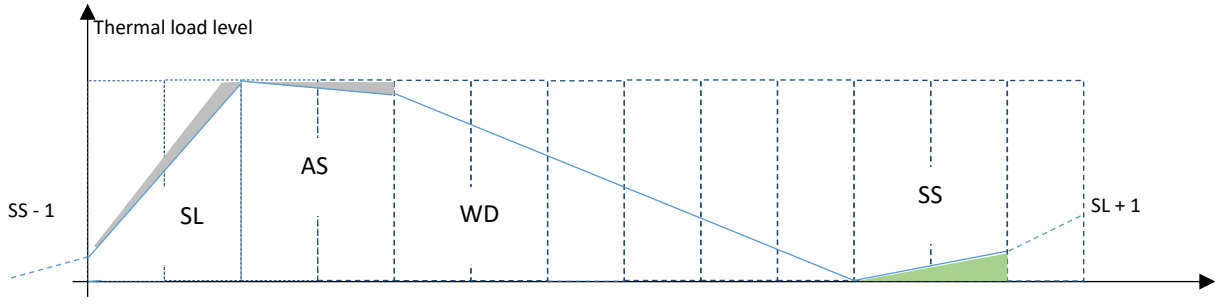

Figure 10.2: Dynamic operating phases of the ULISSE Reservoir (annual cycle)
*(Grey areas: energy **losses/gains**)*

According to this first approach, with a TSF = 13,715, between the real Reservoir and its reduced-size Mock-up, the temporal evolution of their internal temperatures and therefore also of their energy balances can be correlated.

10.2 Other approach: Time constant of the real Reservoir and the Mock-up

The heat loss from the envelope of the real Reservoir as well as from the Mock-up evolves in a **similar** way **to the discharge of an electrical capacitor (C) through a resistor (R)**. To be more precise, we would have to consider that the capacitor discharges, through the resistor, into a capacitor with a comparatively almost infinite capacity, which would represent the lake. In this way, the voltage across the capacitor (lake) remains almost constant and we can then consider only the potential difference (Lake-Reservoir temperature difference) across the capacitor (Reservoir) that concerns us.

The change in temperature of the Reservoir or Mock-up as a function of time [Tr(t)] is therefore, by analogy, the voltage [Uc(t)] across the electrical capacitor, which follows a characteristic decreasing exponential.

$$Uc(t) = E.e^{-t/\tau} \qquad [V] \qquad (10.3)$$

where τ **is the characteristic time constant of the electrical circuit (τ = RC),** expressed in [s] and "C" is the Capacitance of the capacitor (in Farad or [A.s/V]) and "R" is the Resistance (in Ω or [V/A]).

The voltage [Uc(t)], shown in graph 10.4 below, follows the "reduced" decreasing exponential curve (Uc/E), whose tangent at the origin intersects the abscissa (= 1) for t = τ. The voltage ratio across the Capacitor and Resistor is then:

$$Uc(\tau)/E = e^{-1} = 0 \quad .37 \qquad [-] \qquad (10.4)$$

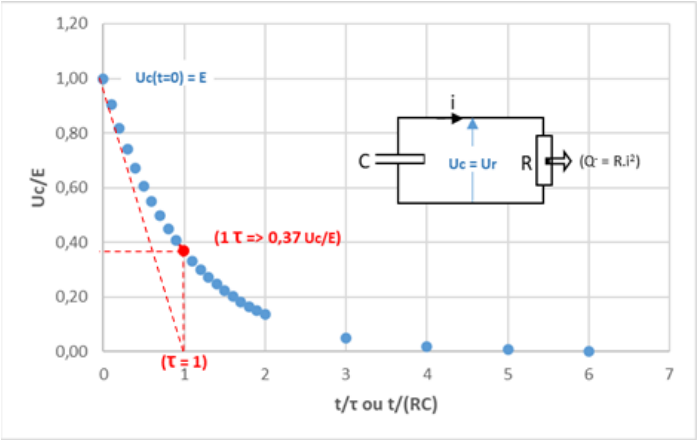

Figure 10.4: Decreasing exponential curve of capacitor discharge through the resistor

The corollaries of the electrical circuit for the Reservoir and the Mock-up are as follows:

- the *conductance* (1/Ro) of their envelope $Co = \lambda.S / \varepsilon$ [W/K] (10.5)

where "λ" is the conductivity in [W/m.K], "S" is the surface area in [m^2], and "ε" is the thickness in [m] of their respective envelope,

- heat *capacity* $Ca = Q / \Delta Tr\text{-}l$ [J/K] (10.6)

where "Q" is the energy-heat content in the Tank in Joules [J] and "ΔTr-l" is the temperature difference between the Reservoir and the lake, i.e., the temperature gradient across the shell. The heat load Q also depends on the active volume (Va) and the heat density of the hot water stored (ce = 4.18 $MJ/m^3.K$).

The "*thermal time constant*" (τ_r) of the Reservoir or the Mock-up (τ_m) with their respective envelope, is expressed as a time:

$$\tau = Ca.Co^{-1} \qquad [s] \qquad (10.7)$$

With the characteristics of the actual Reservoir, including the hyperbolic envelope and the level of the flat-front thermocline, we find the corresponding **Thermal Time Constant (τ_r)** expressed in years [y]:

Capacity Thermal	**Level Thermocline**	**Hyperbolic envelope**		**Envelope Hyperbolic**
(Ca) [GJ/°K]	 [m]	(Ro) [°K/KW]	(Co) [KW/°K]	($\tau r = Ca.Co)^{-1}$ [an]
672	Top	0,04	25,48	**0,84**
4 197	Environment	0,01	76,72	**1,73**
8 395	Low	0,01	109,96	**2,42**

Table 10.5: Thermal time constant (τ_r) of the real Reservoir depending on the level of the Thermocline

The same calculation can be made for the Mock-up (τ_m) with its own characteristics:

Capacity Thermal.	**Level Thermocline**	**Hyperbolic envelope**		**Envelope Hyperbolic**
(Ca) [KJ/°K]	 [m]	(Ro) [°K/KW]	(Co) [KW/°K]	($\tau m = Ca.Co)^{-1}$ [min]
28	Top	47,41	0,021	**22,49**
178	Environment	24,38	0,041	**72,29**
356	Low	17,07	0,059	**101,21**

Table 10.6: Thermal time constant (τ_m) of the Mock-up depending on the level of the Thermocline

Years" for the real Reservoir correspond to "minutes" for the Mock-up. The Factor (Tct) or the ratio between the thermal time constants, τ_r **and** τ_r (each expressed in hours), is as follows:

$$Fct = \tau_r / \tau_m = (2.42 \times 8'760\ h.y^{-1}) / (101.21/60\ min.h^{-1}) = \quad 12,566 \quad [-] \qquad (10.8)$$

This ratio is about 7% lower than the *time scale factor* (TSF) of 13,715 (§16). It is due to the *form factor* (FF) between the Reservoir and the Mock-up, which is not exactly equal to 1.

In fact, the result in table 10.5 is based on the actual shape of the Reservoir with its "*half-hyperboloid*" ends, whereas the result (16.2) considers as a first approximation a "slice" of 1/5 of the linear Reservoir. The Reservoir (in the shape of a tunnel) is 5.6 times longer than it is wide (eq. 7.3) and the heat flow is mainly transverse.

This transverse heat flow is 'channelled' into the model between the 4 cm polystyrene end plates, which are virtually 'athermal' (236 times less thermally conductive than the hyperbolic envelope (2 mm polycarbonate).

Since the TSF would be closer to the Fct, the 4 operating phases of the Mock-up would also increase by 7%, which does not fundamentally change the test results. For example, for the most significant phase, Winter Discharging, which lasts 6 months for the full-scale Reservoir, the duration for the Mock-up would increase from 19.1 to 20.9 minutes. However, adjusting the flow rate for the total unloading of the Mock-up (77 litres), within the time allowed, was not easy to achieve, despite the use of a stabilised power supply for the pump.

10.3 Actual observations on the Mock-up

Figure 10.7 (and 10.10) below shows the test (03.11.2022) of "passive" cooling (without water extraction) of the Mock-up, initially filled with water warmer than the IBC Tank ($\Delta Tm(t_0) = 15.8^{\circ}K$) and which is close to the typical difference for the real Reservoir at the end of Summer Loading. With this starting temperature deviation, we can deduce the cooling time constant (τ) :

$$\tau = 0.37\ \Delta Tm(t_0) = 0.37 * (Tm(t_0) - Tc)\ 0.37 * (37.28^{\circ}C - 21.52^{\circ}C) = 5.8^{\circ}K;\ Tm\ @\ t = 1\tau = 28.7\ [^{\circ}C] \quad (10.9)$$

It can be seen that the cooling time constant for the Mock-up τ_m is 109 minutes, 8 minutes longer than that calculated theoretically (τ_m: 101.21 min, Table 10.6, low thermocline). This longer time is partly related to **the (partial) insulation blanket that was removed (13 minutes after the end of loading), which partially and temporarily slowed down cooling and therefore proportionally increased the Mock-up's characteristic time constant.**

This can be clearly seen in graph 10.7 below, by the slower decrease (slope) in the temperature curve during the first 13 minutes. Without this delay in the experimental procedure, this first result converges with the result of the theoretical calculation!

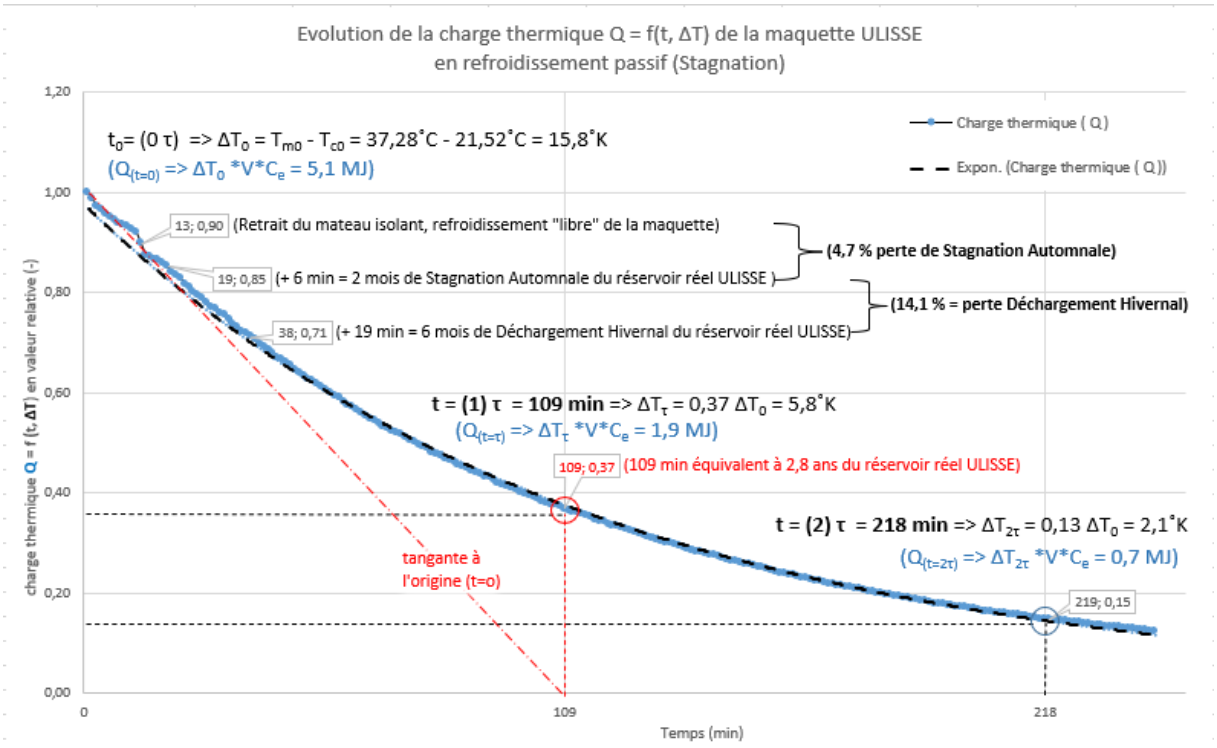

Fig. 10.7: Evolution of the thermal load (Q) or heat content of the Mock-up *during its passive cooling, following a decreasing exponential with a time constant* τ_m *of 109 min.*

In the end, with the TSF, the 109 minutes of the Mock-up correspond to the 2.8 years of the real Reservoir to lose "passively" (without winter discharge of tempered water) about 2/3 of the heat initially loaded (HIL).

Beyond graph 10.7, thermal equilibrium with the surrounding water is practically reached at 5τ; i.e., in 8.4 hours for the Mock-up and 12 years for the real Reservoir.

By way of comparison, graph 10.7 above also shows the proportional Autumn Stagnation phase of 6 minutes (2 months for the real Reservoir, loss 4.7%) and the Winter Discharging phase of around 20 minutes, equivalent to 6 real months (loss 14.1%).

10.4 Note: Removable temporary insulating jacket

During this test, over a long period of time (until thermal equilibrium is reached with the test tank), the model is pre-filled with tempered water using temporary, removable insulation on the envelope (Figs. 10.8 and 10.9). This is to minimise the change in temperature of the water in the test tank **and to approximate reality as closely as possible, given that the temperature of the lake does not increase as a result of heat loss from the Reservoir**.

Figure 10.8: Temporary insulation limiting heat loss from the Mock-up during loading

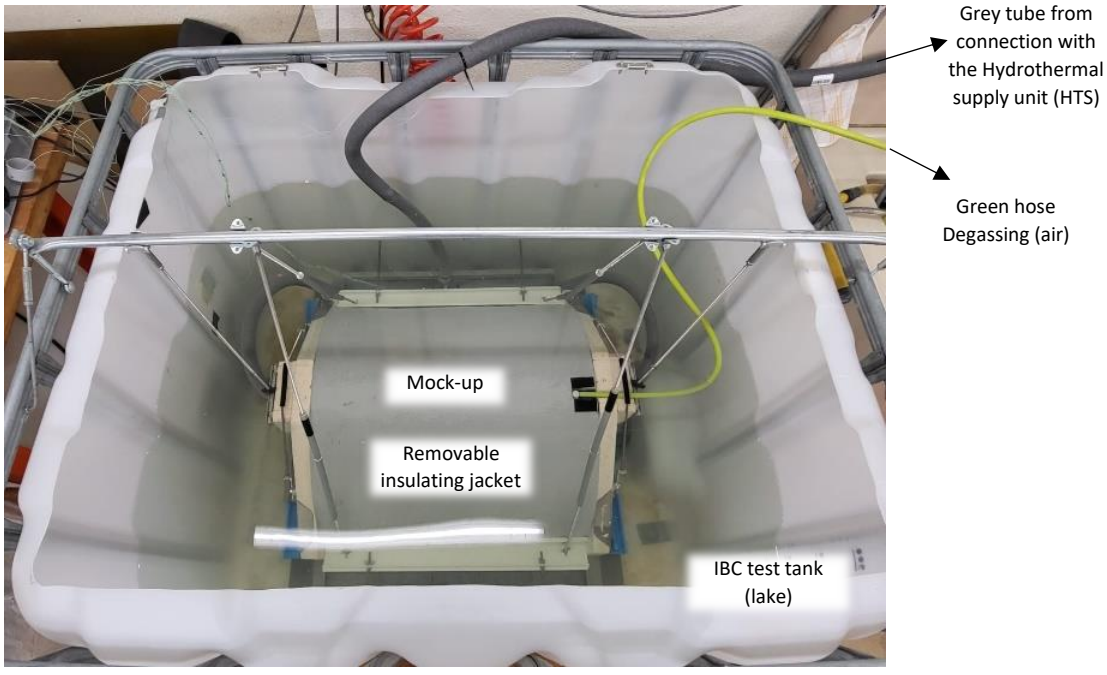

Figure 10.9: Mock-up with removable insulating jacket during thermal loading (test 3.11.2022)

After loading the Mock-up, the insulating jacket must be removed slowly so as not to disturb the water in the test tank (representing the lake). This was not done correctly, as can be seen from the sudden drop in temperature in the lower part of the model, without disturbing the rest of the Mock-up's internal volume (the upper thermal stratification remained unchanged).

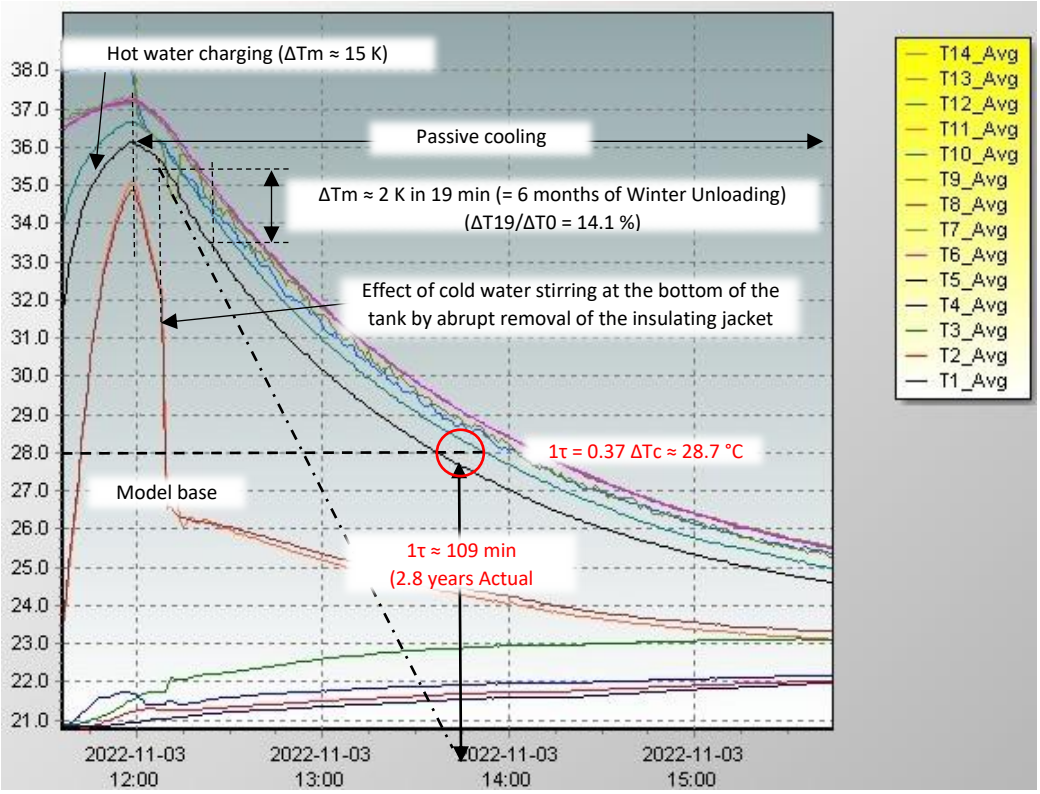

Figure 10.10: Temperature changes during passive cooling of the Mock-up (test 03.11.2022)

10.5 Example of a complete cycle on the Mock-up (test on 20.12.2022, Appendix 1.8)

This test includes a complete cycle on the Mock-up, with Summer Loading (**SL)**, Autumn Stagnation (**AS)** and the Winter Discharging phase (**WD**). To reduce or eliminate mixing during the injection of hot water at the top of the Mock-up, a distribution grid with a layer of fibreglass felt was placed under the injection bar (Figure 9.7). **Continued in Appendix 1.8.**

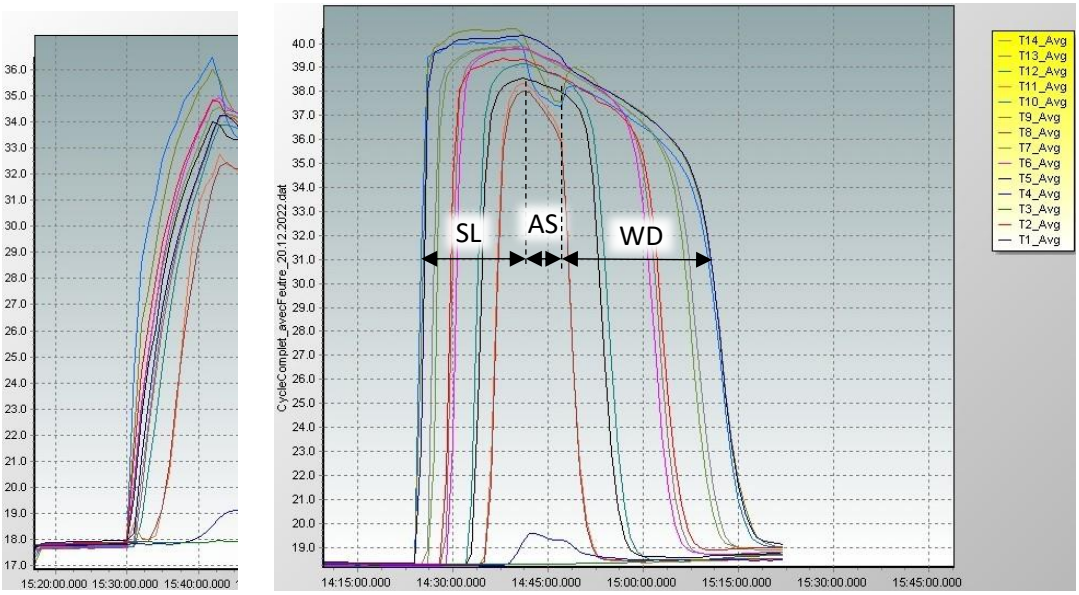

Figure 20: Comparison of stratification during the loading phase, without (fig. left) and with (fig. right) a grid + felt distributing the water injection flow (identical flow rate) via the top ramp of the Mock-up (tests 19 and 20.12.2022)

10.6 Energy balance for the real Reservoir and the Mock-up

10.6.1 Preliminary considerations

To establish the efficiency of the seasonal energy-heat storage of the ULISSE Reservoir, the heat losses of all the annual operating phases of the full-scale Reservoir and of its reduced-scale Mock-up were determined and accounted for. **In this energy balance, a clear distinction was made between *heat loss and summer loading***. In this way, we have defined, globally, the *Gross Heat Losses* - (GHT, including that of Autumn Stagnation, Winter Discharging, - and - Summer Loading,) and the *Net Heat Losses* - (NHL, without SL).

Its justification lies in the fact that **the *Summer Heat Loss* (*SHL)* of the ULISSE Reservoir is not a major issue,** as the electrical energy used to power the pumps would essentially come from photovoltaic (PV) sources. Furthermore, with the massive development of PV, the summer loading of the ULISSE Reservoirs would reduce the potential and paradoxical recourse to "peak-shaving" (capping excess summer electricity production by shutting down PV installations).

Incidentally, the Summer Heat Loss of the ULISSE Reservoir is the sum of the heat loss from its shell and the excess water injected above its volumetric capacity. The latter results from the partial compensation of the shell loss and the modification of the internal thermocline of the Reservoir (by thermal diffusion and multiple mixing). The establishment of the energy balance or storage efficiency of the ULISSE Reservoir and the Mock-up therefore starts from the thermal capacity or the **Net or Nominal Summer Load (NSL)**.

10.6.2 Heat losses are calculated using 3 different approaches:

- 1. by calculation using a **theoretical model** of the Mock-up and the full-scale Reservoir, taking into account the *"active" surface area* (Sa) and the *thermal conductivity* (Cot) of the insulating envelope as well as the difference (ΔTr-l) between the average temperature of the Reservoir (Tr) and that of the surrounding lake (Tl). Specifically, for the dynamic phases, by integrating the evolution of the heat loss as a function of the filling of the Reservoir or the level of the thermocline ("active" volume of hot water).

- 2. calculations based on actual physical data (temperatures, flow rates) acquired from **experience on the Mock-up,** reproducing the main part of the annual operating cycle, which includes the "dynamic" phases (*summer loading, winter discharging*) and the "static" *autumn stagnation* phase.

- 3. **numerical simulation** (COMSOL Multiphysics) of the Mock-up and the real Reservoir.

Before carrying out the experiments on the model, ***the Time Scale Factor (TSF)* between the full-scale Reservoir and the Mock-up** was determined (section 10). In order to check the consistency between the Mock-up, the real Reservoir (theoretical model) and the numerical simulation, we compared the ***Characteristic Time Constant*** *(τ_r) of their* respective *passive cooling.* This makes it possible to validate the consistency (convergence) between the results of the three approaches.

10.6.3 Theoretical model

The theoretical model makes the conservative assumption that there is no temperature gradient in the water of the active part of the Reservoir and that of the surrounding lake (the IBC test tank for the Mock-up). This implies that the thermal gradient across the shell (internal/external) and therefore the steady-state heat loss will be maximal (Ri and Re ≈ 0), i.e., the most unfavourable case (absence of an insulating boundary layer).

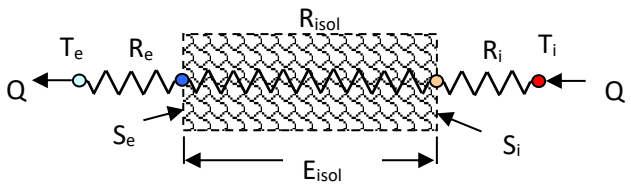

Figure 10.11: Simplified thermal model of the ULISSE Reservoir envelope

As a result of free convection and water circulation currents (advection), around the shell of the Reservoir, the thermal resistance of the water inside (Ri) and external (Re) are reduced to a maximum (Ri and Re ≈ 0):

$$Ri = 1/(hi*S) \qquad (10.10)$$

with hi the heat exchange coefficient of the internal water in free convection = 100 - 900 W m^{-2} K^{-1}

Inside the Reservoir, apart from free convection, there are in principle no water circulation currents other than those for injection and extraction of water from the top (distribution ramp).

$$Re = 1/(he*S) \qquad (10.11)$$

where he is the external water heat exchange coefficient for free and forced convection due to circulation currents = 100 - 15,000 W m^{-2} K^{-1}

According to Figure 10.12 below, the theoretical model considers that the active surface (Sa) and the active volume (Va) of the Reservoir or Mock-up change with each period of time and that the concomitant heat loss is exclusively located in the "active" (hot) part through the active surface of the Reservoir shell.

The theoretical model also makes the admittedly simplified assumption of a **homogeneous mean temperature in the active volume** (through convection and advection). Thermal stratification in the Reservoir is then reduced to a ***flat-fronted thermocline***, which separates the "active" (warm) upper part from the "passive" lower part (cold or at the same temperature as the surrounding lake).

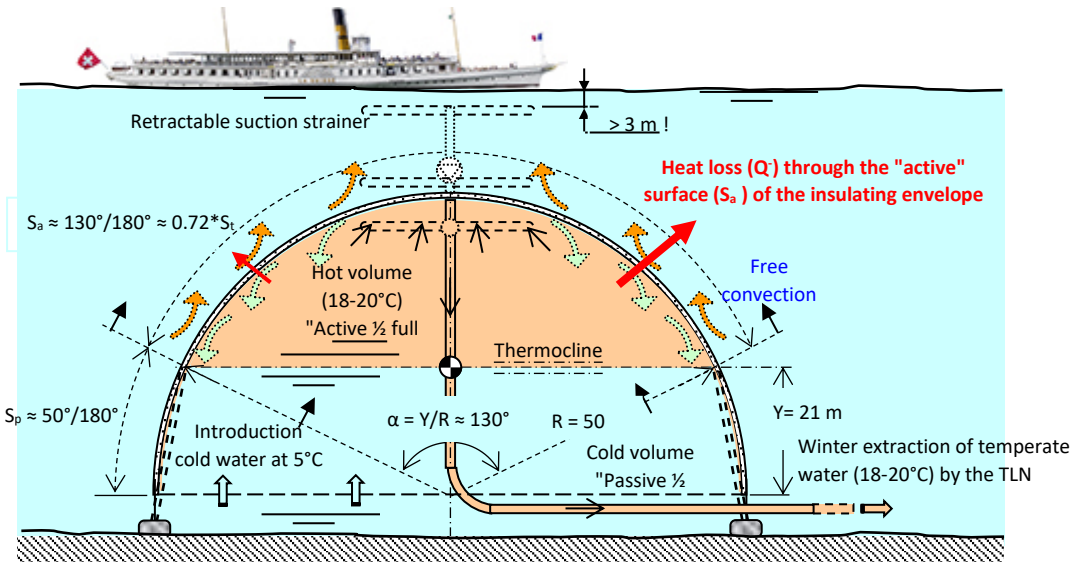

Figure 10.12: Theoretical model of heat loss (Q-) from the sub-lacustrine Reservoir, shown as an average value at half volume, during the Winter Unloading phase for heating buildings via the distribution network

10.6.4 Theoretical calculations for the ULISSE Reservoir

The truncated table 10.13 below corresponds to the theoretical calculations of heat loss from the hyperbolic envelope of the real ULISSE Reservoir; this is for the "static" Autumn Stagnation (AS) phase lasting 2 months (line 23, grey background), followed by the "dynamic" Winter Discharging (WD) phase lasting 6 months.

More precisely, the WD phase is calculated here using two approaches: one based on "*mean values at mid-active volume*" (line 26, blue background) and the other by "*integration*" of jumps in the level of the flat-front *thermocline* or the interface between the hot and cold-water volumes (lines 31-81, green background).

	A	B	C	D	E	F	G	H	I	J	K	L	M	N
1	**Calculs théoriques de l'enveloppe hyperbolique du Réservoir ULISSE : 1) en Phase de Stagnation Automnale (plein volume "actif"),**													
2	**2) en phase de Déchargement Hivernal (par valeurs moyennes à mi-volume "actif" et par intégration des niveaux de la thermocline)**													
3	La stratification thermique du réservoir est constituée d'une "**Thermocline à front plat**", séparant le volume "actif" (chaud) du volume "passif" (froid =Tmoylac)													
4	La déperdition thermique est calculée en valeur moyenne sur le volume "actif" et sur la durée respective des 2 phases (2 et 6 mois)													
5	Rayon de courbure hyperbolique à la base :			Rhb	**50**	m		Volume total calotte hyperboloïde :				Vcal	253 800	m3
6	Longueur hyperbolique transversale :			Lht	157,08	m		Volume total réservoir :				Vres	**2 005 020**	m3
7	Longueur hyperbolique longitudinale :			Lhl	460	m		Epaisseur Isolant (verre cellulaire) :				Eiso	0,05	m
8	Longueur totale réservoir :			Ltr	560	m		Conductivité totale enveloppe :				λenv	0,066	W/mK
9	Surface calotte hyperboloïde d'extrémités :			Scal	15 708	m2		Conductivité enveloppe surfacique :				λenvs	1,32	W/m2K
10	Surface totale enveloppe :			Senv	87 965	m2		Chaleur volumique eau douce :				Cve	1,163	kWh/m3 K
11	Section hyperbolique transversale :			Sht	3 807	m2		Ecart densité eau stock-lac (ΔT = 15 °K) :				Ds-l	-1,76	kg/m3
12	Température Hivernal du Lac = température minimale réservoir :				Thlac	5	°C			Débit de Déchargement Hivernal:			457,77	m3/h
13	Température de Contact du Lac avec le réservoir :				Tcontlac	7,5	°C					(constant)	0,13	m3/s
14	Température nominale du stock à la fin du Chargement Estival :				Tnomrés.	**20**	°C							
15	Ecart maximum Température réservoir-lac :				ΔTmax.r-l	**15**	°K			**Charge therm. nominale (Qtn) :**			**34,98**	**GWh**
16														
17	Niveau	Longueur	Section	Surface	Volume	Conductance	Temps	Gradiant	Gradiant	Charge	Perte	Perte	Chute	Température
18	hauteur	hyperbole	transvers	enveloppe	enveloppe	enveloppe	différentiel	thermique	thermique	thermique	thermique	thermique	Température	final
19	Thermocline	"active"	"active"	"active"	"active"	"active"		début Réservoir - Lac	final Réservoir - Lac	résiduelle	enveloppe	enveloppe	Réservoir	Réservoir
20	Ntc	Loha 2*√(2ah+h2)	Seta	Sura	Vola	Conda	td	ΔTdr-l	ΔTfr-l	Qtr	Pte	Pte	ΔTr	Tfr
21	[m]	[m]	[m2]	[m2]	[m3]	[KW/K]	[h]	[°K]	[°K]	[GWh]	[GWh]	[%]	[°C]	[°C]
22	**Phase (statique) de Stagnation Automnale (plein volume "actif")**													
23	0,00	157,09	3 807	87 965	2 005 020	116,11	1 460	12,5	11,79	32,98	**2,00**	**5,71**	0,714	19,28596
24														
25	**Phase (Dynamique) de Déchargement Hivernal (calculs par valeurs moyennes à mi-volume "actif")**													
26	**20,66**	112,00	1 977	62 715	**1 041 383**	82,78	4 380	11,79	10,50	31,17	**3,81**	**10,89**	1,283	18,00274
27														
28	**Phase (Dynamique) de Déchargement Hivernal (calculs par Intégration des niveaux de la thermocline)**													
29	Ntc	Loh	Seca	Sura	Vola	Conda	td	ΔTdr-l	ΔTmr-l	Qtr	Pte	Pte	ΔTr	Tmr
30	[m]	[m]	[m2]	[m2]	[m3]	[KW/K]	[h]	[°K]	[°K]	[GWh]	[GWh]	[%]	[K]	[°C]
31	2,65	151,42	3 544	84 791	1 866 745	111,92	302	11,79	11,65	32,59	**0,39**	1,19	0,141	**19,14526**
32	5,21	145,93	3 306	81 717	1 740 909	107,87	275	11,65	11,53	32,24	**0,34**	1,05	0,114	**19,02308**
33	7,67	140,61	3 080	78 739	1 622 170	103,94	259	11,52	11,41	31,94	**0,31**	0,95	0,110	**18,91312**
34	10,04	135,46	2 867	75 855	1 510 200	100,13	245	11,41	11,31	31,66	**0,28**	0,87	0,099	**18,81409**
35	12,33	130,47	2 667	73 061	1 404 687	96,44	230	11,31	11,22	31,41	**0,25**	0,79	0,089	**18,72492**
36	14,53	125,64	2 478	70 353	1 305 329	92,87	217	11,22	11,14	31,18	**0,22**	0,72	0,080	**18,64464**
37	16,65	120,95	2 301	67 728	1 211 841	89,40	204	11,14	11,07	30,98	**0,20**	0,65	0,072	**18,57239**
38	18,69	116,41	2 134	65 183	1 123 947	86,04	192	11,07	11,01	30,80	**0,18**	0,59	0,065	**18,50741**
39	**20,66**	112,00	1 977	62 715	**1 041 383**	82,78	180	11,01	10,95	30,64	**0,16**	0,53	0,058	**18,44898**
40	22,54	107,72	1 830	60 322	963 896	79,62	169	10,95	10,90	30,49	**0,15**	0,48	0,052	**18,39650**
79	54,66	2,00	149	1 120	78 529	1,48	0	10,49	10,49	29,36	**0,00**	0,00	0,000	**17,99316**
80	54,68	0,00	149	0	78 538	0,00	**4 208**	10,49	10,49	29,36	**0,00**	0,00	0,000	**17,99316**
81										**29,36**	**3,62**	**10,34**	**1,285**	
82	[m]	[m]	[m2]	[m2]	[m3]	[KW/K]	[h]	[°K]	[°K]	[GWh]	[GWh]	[%]	[°C]	[°C]
83	Ntc	Loha	Seta	Sura	Vola	Conda	td	ΔTdr-l	ΔTfr-l	Qtr	Pte	Pte	ΔTr	Tfr

Table.10.13: - Truncated theoretical calculations of heat losses from the hyperbolic envelope of the ULISSE Reservoir, for the Autumn Stagnation and Winter Discharging phases

The upper frame, columns-lines A1 to N15, shows the parameters of the Reservoir (dimensions, physical characteristics) and those of the operation between the Reservoir and the lake (temperatures, flows and thermal load of 35 GWh @ ΔT: 15˚K - after - the Nominal Summer Loading (NSL).

→ 35 GWh thermal or 126 TJ corresponds to the annual production of 70,000 m^2 of flat-plate solar thermal collector (@ 500 kWh/m^2-year).

At the end of Summer Loading, the value of the temperature gradient between the Reservoir and the lake (I23: ΔT_{dr-l} = 11.79˚K, green background) is taken at the start of the Winter Discharging phase (H26 and H31).

The nominal end EC temperature is 20˚C (H14, orange background). Column N (orange background), includes the temperature end SA (N23), end DH (N26) and at each level of the Reservoir thermocline (N31-80).

→ **The temperature (variable between 20 and 18˚C) of the Winter Discharge conditions the efficiency of the Heat Pumps (HP)** for heating and the production of Domestic Hot Water (DHW) in buildings served by the Thermal Lacustrine Networks (following the example of GeniLac from SIG)!

Column G23 to G80 shows the time interval (in hours) of each phase, including that of each level of the WD Winter discharging thermocline (lines 31 to 80). Line 39 (green background) corresponds to the singular stage where the thermocline is at a height of 20.7 m above the base of the Reservoir, i.e., exactly half its volume (§ 5, eq. 5.13).

Table 10.13 also shows:

- Line 23 (grey background), the autumn stagnation phase (1,460 hours or 2 months, G23), has a Stagnation Thermal Loss (STL) of 2 GWh, i.e., 5.71% of the Net or Nominal Summer Load (NSL: 35 GWh or 126 TJ).

- Line 26 (blue background), the Winter Unloading phase (4,380 h or 6 months, G26), calculated by "*average values at half active volume*", is subject to a Discharging Thermal Loss (DTL) of 3.81 GWh, i.e., 10.89% of the NEC.

- Finally, between column lines 31K-L and 81K-L, the Winter Unloading phase, which is identical but calculated by "*integrating the jumps in the thermocline level*", incurs a Discharging Thermal Loss (DTL) of 3.62 GWh, i.e., 10.34% of the Nominal Summer Load (NSL).

Initial 'theoretical' conclusions:

- The two methods for the theoretical calculation of the Reservoir Winter Discharging phase are logically identical.
- According to theoretical calculations, **the *Net Thermal Loss* (NTL)**, being the sum of the AS and WD phases, **represents almost 16% of the NSL of the ULISSE Reservoir.**

10.6.5 Theoretical model calculations

The Excel table below (10.14) corresponds to the theoretical heat loss calculations for the hyperbolic envelope of the model; this is for the "static" Autumn Stagnation (AS) phase lasting **6 minutes** (2 real months), followed by the "dynamic" Winter Discharging (WD) phase lasting **19 minutes** (6 real months).

More specifically, the WD phase is only calculated here using the "*mean values at mid-active volume*" approach. The other method using "*integration of jumps in the thermocline level*" is not used, as the results of the two theoretical calculation methods are identical (previous conclusions for the Reservoir).

The arrangement of the Model parameters, in box A1 to N15 of Table 17.4, are identical to those of the Reservoir in Table 17.3. As for the Reservoir, at the end of Summer Loading, the value of the temperature gradient (I23: $\Delta T_{dr\text{-}I}$ = 11.81˚K, green background) between the Mock-up and the IBC tank (representing the Lake), is taken at the start of the WD Winter Discharging phase (H26). Columns G23 to G26 show the time (in hours) of the AS Autumn Stagnation and WD phases.

Table 10.14 also shows:

- Line 23K-L (grey background), the Autumn Stagnation phase (0.1065 hours: 23G) incurs a Stagnation Thermal Loss (STL) of 0.07 GWh, i.e., 5.49% of the Net Thermal Load (NTL: 1.34 kWh or 4.8 MJ).

- Line 26K-L (blue background), the Winter Discharging phase (0.3194 hours: 26G), calculated by "*average values at half active volume*", incurs a Discharging Heat Loss (DHL) of 0.14 kWh, i.e., 10.46% of the Net Heat Load (NHL).

	A	B	C	D	E	F	G	H	I	J	K	L	M	N
1	**Calculs théoriques de l'enveloppede hyperbolique de la Maquette ULISSE :**													
2	**1) en Phase de Stagnation Automnale (plein volume "actif"), 2) en phase de Déchargement Hivernal (par valeurs moyennes à mi-volume "actif")**													
3	La stratification thermique de la maquette est constituée d'une "**Thermocline à front plat**", séparant le volume "actif" (chaud) du volume "passif" (froid =Tmoylac)													
4	La déperdition thermique est calculée en valeur moyenne sur le volume "actif" et sur la durée respective des 2 phases (6 et 19 minutes)													
5	Rayon de courbure hyperbolique à la base :				Rhb	**0,285**	m			Volume total calotte hyperboloïde :		Vcal	0	m3
6	Longueur hyperbolique transversale :				Lht	0,9	m			Volume Maquette :		Vres	0,077	m3
7	Longueur hyperbolique longitudinale :				Lhl	0,62	m			Epaisseur Isolant (verre cellulaire) :		Eiso	0,002	m
8	Longueur totale réservoir :				Ltr	0,62	m			Conductivité totale enveloppe :		λenv	0,21	W/mK
9	Surface calotte hyperboloïde d'extremités :				Scal	0	m2			Conductivité enveloppe surfacique :		λenvs	105	W/m2K
10	Surface totale enveloppe :				Senv	0,56	m2			Chaleur volumique eau douce :		Cve	1,163	kWh/m3 K
11	Section hyperbolique transversale :				Sht	0,12	m2			Echelle de temps Réservoir/Maquette :		(Tr/Tm) =	13 715	-
12	Température Hivernale Maquette = température minimale Maquette :						Thlac	5	°C	Débit de Déchargement Hivernal:			0,241	m3/h
13	Température de Contact de la Cuve avec la Maquette :						Tcontlac	7,5	°C			(constant)	4,018	Lit/min
14	Température nominale du stock à la fin du Chargement Estival :						Tnomrés.	**20**	°C					
15	Ecart maximum Température entre maquette et cuve :						ΔTmax.r-l	15	°K	**Charge thermique initiale (Qti) :**			**1,34**	**kWh**
16														
17	Niveau	Longueur	Section	Surface	Volume	Conductance	Temps	Gradiant	Gradiant	Charge	Perte	Perte	Chute	Température
18	hauteur	hyperbole	transversale	enveloppe	enveloppe	enveloppe	différentiel	thermique début	thermique final	thermique	thermique	thermique	Température	finale
19	Thermocline	"active"	"active"	"active"	"active"	"active"		Maquette-Cuve	Maquette-Cuve	résiduelle	enveloppe	enveloppe	Maquette	Maquette
20	Ntc	Loha 2*√(2ah+h2)	Seta	Sura	Vola	Conda	td	ΔTdr-l	ΔTfr-l	Qtr	Pte	Pte	ΔT	Tfr
21	[m]	[m]	[m2]	[m2]	[m3]	[KW/K]	[h]	[°K]	[°K]	[kWh]	[kWh]	[%]	[K]	[°C]
22	**Phase (statique) de Stagnation Automnale (plein volume "actif")**						(6 min)							
23	0,00	0,90	0,12	0,56	0,08	0,06	**0,1065**	12,5	11,81	1,27	**0,07**	**5,49**	0,686	19,31430
24														
25	**Phase (Dynamique) du Déchargement Hivernal**						(19 min)	(calculs en valeurs moyennes à mi-volume "actif")						
26	**11,33**	0,64	0,09	0,40	0,04	0,04	**0,3194**	11,81	10,58	1,20	**0,14**	**10,46**	1,236	18,07829

Table 10.14: Theoretical calculations of heat losses from the hyperbolic envelope of the Mock-up, for the Autumn Stagnation and Winter Discharging phases (average values)

According to the theoretical calculations in table 10.14 above, **the Net Heat Loss (NHL) of the Mock-up**, being the sum of the heat losses of the AS (5.49%) and DH (10.46%) phases, **represents almost 16% of the Net Summer Load (NSL)**, i.e., a Net Storage Efficiency (NSE) of 84%.

Given the Time Scale Factor (TSF), this theoretical result is **identical to that of the ULISSE Reservoir.** In other words, it seems to indicate that the same net storage efficiency can be obtained between the Reservoir and the Mock-up, provided that the correct TSF (13,715) is respected.

10.6.6 Theoretical and experimental heat losses for the Reservoir and the Mock-up

The upper frame (A1 to N23) of table 10.15 below shows (in columns C to N), the times, flow rates and temperatures of the phases, SL (green background), AS (grey background) and WD (blue background); this (according to lines 6 to 18) for the various Tests on the Mock-up and Theoretical Calculations with the Reservoir and the Mock-up.

The lower frame (A20 to N38) shows the Gross and Net Loads and Heat Losses, and conversely the Net Storage Efficiency, NSE (yellow background), for the Reservoir and the Mock-up.

The Winter Heat Loss (WHL, blue background) is logically proportional to its duration. This is particularly true for the Test on 24.11.2022, where the WHL is 18.44% (K26) of the NHL (D26), given a duration of 41 minutes (F6), i.e., more than twice the time normally required (19 min) to comply with the TSF.

The WHL of all the other tests, including the theoretical calculations on the Reservoir and the Mock-up, are between 9.65% (K27) and 12.71% (K29). The Stagnation Heat Loss (SHL) is 5 to 6%.

Finally, the Net Storage Efficiency (NSE) for the Reservoir and the Model ranges from 74.80% (N30) to 89.06% (N37), with an average of almost 83% (N26-N38).

	A	B	C	D	E	F	G	H	I	J	K	L	M	N
1			Temps	Temps	Temps	Temps	Débit	Débit	Températ.	Températ.	Maquette	Gain	Chute	Chute
2			Charge	Stagnat.	Décharge	Décharge	Charge	Décharge	Lac	Lac	Début	Températ.	empératur	empératur
3					(100% Vol)	(total Q)	(moyenne)	(moyenne)	(Fond)	(moyenne)	Décharge	Chargemen	Stagnation	Stagnation
4	Type	Date	tc	ts	tdv	tdq	dc	dd	TLF	TLM	TDD (TFS)	ΔTC	ΔTS	ΔTS/ΔTC
5	Essai/Calcul	[j:m:a]	[min]	[min]	[min]	[min]	[Lit/min]	[Lit/min]	[°C]	[°C]	[°C]	[K]	[K]	[%]
6	Essai Maq.	24.11.2022	14	-	32	41	2,01	2,26	19,7	20,01	35,48	16,17	-	-
7	Essai Maq.	19.12.2022	14	6	19	27	6,07	3,91	17,9	17,98	33,35	16,06	0,83	5,17
8	Essai Maq.	20.12.2022	17	6	25	33	6,21	2,94	18,3	18,69	38,37	21,15	1,29	6,10
9	Essai Maq.	21.12.2022	14	6	19	22	6,12	3,83	18,68	21,6	38,72	21,00	1,21	5,76
10	Essai Maq.	21.12.2022	24	6	19	22	6,15	3,87	20,52	23,02	39,59	19,98	1,13	5,66
11	Essai Maq.	05.01.2023	16	6	19	22	6,02	3,64	13,2	14,68	33,07	20,37	1,04	5,11
12														
13	Cal. Maq.	"Moyenne"	-	6	19	19	-	4,02	5	7,5	19,31	15	0,69	4,60
14	Méthode:	"mi-volume"	[min]	[min]	[min]	[min]	[Lit/min]	[Lit/min]	[°C]	[°C]	[°C]	[K]	[K]	[%]
15														
16	Cal. Rés.	"Moyenne"		[h]	[h]	[h]		[m3/h]	[°C]	[°C]	[°C]	[K]	[K]	[%]
17	Méthode:	"mi-volume"	-	1460	4380	4380	-	457,77	5	7,5	19,28	15	0,71	4,73
18	Cal. Rés.	Intégration	-	1460	4380	4380	-	457,77	5	7,5	19,28	15	0,71	4,73
19														
20			Charge	Charge	Perte	Perte	Perte	Perte	Energie	Perte	Perte	Pertes	Pertes	Efficacité
21			Thermique	Thermique	Thermique	Thermique	Thermique	Thermique	Thermique	Thermique	Thermique	Thermique	Thermique	Stockage
22			Brute	Nette	Chargemen	Chargemen	Stagnation	Stagnation	Déchargée	Déchargem	Déchargem	Nettes	Nettes	Nette
23			CTB	CTN	PTC	PTC	PTS	PTS	ETD	PTD	PTD	PTN	PTN	ESN
24	Type	Date			(CTB-CTN)	(PTC/CTB)		(PTS/CTN)			(PTD/CTN)	(PTS+PTD)	(PTN/CTN)	(ETD/CTN)
25	Essai/Calcul	[j:m:a]	[MJ]	[MJ]	[MJ]	[%]	[MJ]	[%]	[MJ]	[MJ]	[%]	[MJ]	[%]	[%]
26	Essai Maq.	24.11.2022	5,78	5,21	0,57	9,89	-	-	4,25	0,96	18,44	0,96	18,44	81,56
27	Essai Maq.	19.12.2022	6,98	5,18	1,80	25,84	0,27	5,14	4,47	0,50	9,65	0,77	14,79	86,40
28	Essai Maq.	20.12.2022	9,77	6,82	2,95	30,24	0,42	6,10	5,69	0,71	10,42	1,13	16,52	83,48
29	Essai Maq.	21.12.2022	13,85	6,77	7,08	51,11	0,39	5,78	5,16	0,86	12,71	1,25	18,50	76,29
30	Essai Maq.	21.12.2022	12,67	6,44	6,23	49,16	0,36	5,65	4,82	0,82	12,70	1,18	18,35	74,80
31	Essai Maq.	05.01.2023	9,05	6,57	2,49	27,49	0,33	5,09	5,37	0,77	11,76	1,11	16,85	81,75
32														
33	Cal. Maq.	"Moyenne"		(kWh)			(kWh)	[%]	(kWh)	(kWh)	[%]	(kWh)	[%]	[%]
34	Méthode:	"mi-volume"	-	1,34	-	-	0,07	5,22	1,20	0,14	10,45	0,21	15,67	89,55
35														
36	Cal. Rés.	"Moyenne"	(GWh)	(GWh)			(GWh)	[%]	(GWh)	(GWh)	[%]	(GWh)	[%]	[%]
37	Méthode:	"mi-volume"	35	35	-	-	2,00	5,71	31,17	3,81	10,89	5,81	16,60	89,06
38	Cal. Rés.	Intégration	35	35	-	-	2,00	5,71	29,36	3,62	10,34	5,62	16,05	83,89

Excel Table 10.15: Heat loss balance for the full-scale ULISSE Reservoir and the reduced-scale Mock-up (based on calculations using the theoretical model and experimental measurements on the Mock-up)

This initial energy balance, the results of which are consistent, shows that the *Time Scale Factor* (TSF), the *theoretical model of* the Reservoir and the Mock-up, and their *thermal time constants* ($\tau_{r/m}$), validated by experiment on the Mock-up, are well-founded.

However, this preliminary energy balance is based on the assumption that the full-scale Reservoir behaves exactly like the Mock-up, which has yet to be demonstrated with the full digital simulation (COMSOL).

10.7 Numerical simulation of the ULISSE Reservoir and the Mock-up

10.7.1 General information

Numerical simulation, using COMSOL Multiphysics software, is the third approach for determining the heat losses or conversely the efficiency of the seasonal energy-heat storage of the ULISSE Reservoir and for **validating the theoretical calculation model and the experimental Mock-up**.

At the current end of the ULISSE project's exploratory study, this has already been done in part for the full-scale Reservoir and in part for the Mock-up. The latter was done as part of Mr. Daniel Bello Mendes's final year *Master of Science in Engineering thesis* at HEPIA under the supervision of Professor Roland Rozsnyo.

The Mock-up was used to physically reproduce, on a reduced scale, the annual seasonal operating cycle, with and without summit water injection and extraction, distinguishing between a "static" phase (autumn stagnation) and two "dynamic" phases (summer loading and winter discharging).

On the basis of data from the real ULISSE Reservoir and the Mock-up, the interactions with the outside (IBC test tank vs. lake) were modelled and numerically simulated. The modelling and numerical simulation, using finite elements, should make it possible to compare the thermal evolution and heat dissipation of the Reservoir. In particular, this comparison was made with the data collected from temperature and flow measurements actually carried out in the laboratory on the physical Mock-up.

Prior to this student work, Professor Rozsnyo explored a first modelling approach directly from the full-scale Reservoir located in the lake (Figures 10.16 and 10.17 left).

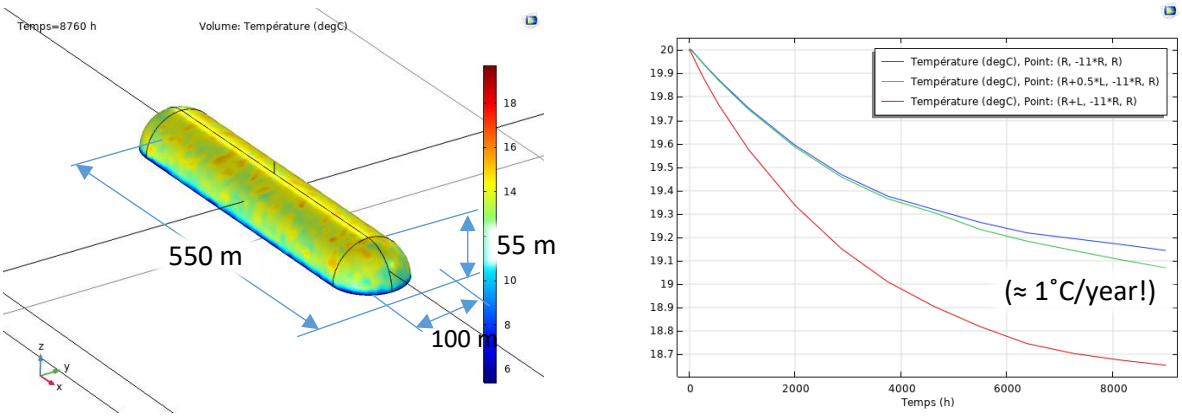

Figure 10.16: first modelling and numerical simulation of the full-size ULISSE Reservoir (2 M m³) and graph of temperature measurement points during "passive" cooling (without water injection or extraction) (≈ 1˚C/year!)

From the initial results of the numerical simulation, we can see the phenomenon of thermal convection inside the Reservoir and especially outside, i.e., the lake (fig. 2 left). This phenomenon can also be seen on the Mock-up (fig. 2 right). It clearly shows that heat loss from the ULISSE Reservoir would induce convection currents in the lake throughout the water column around the perimeter of the Reservoir.

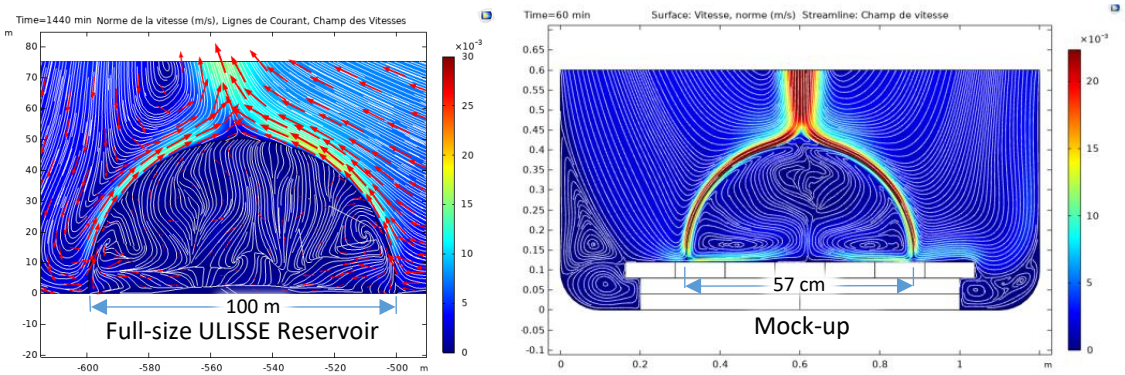

Figures 10.17: Cross-section showing thermal convection (water velocity fields) inside and outside the full-scale ULISSE Reservoir (left) and the Mock-up in the IBC tank (right).

Although heat loss is a determining factor and should be minimised from an energy point of view, it can also be a beneficial environmental aspect in terms of promoting mixing and the vital oxygenation of the lake bed; a subject taken up again in the chapter on the environmental impact of ULISSE (§ 6.4.3.4).

10.7.2 Method and mesh for numerical simulation

The COMSOL solver uses the finite element method. In the finite element method, space and time are generally discretised separately: space is subdivided into geometric elements known as meshes. Assuming that the solution is known at the nodes of a mesh element, then the numerical solution on this element is obtained by interpolating the known values at the nodes. This is why the solutions depend on the quality and size of the mesh.

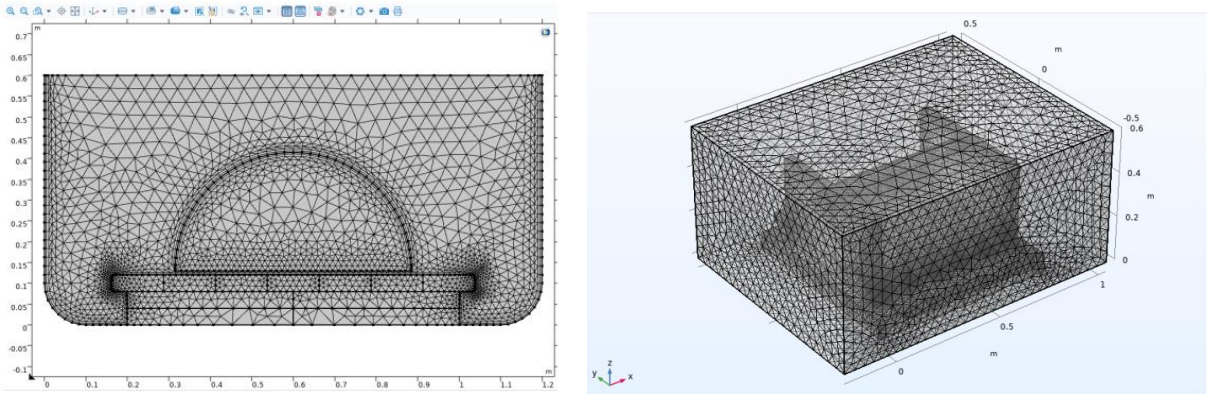

Figures 10.18: Automatic construction of the 2D (left) and 3D (right) mesh by COMSOL for the ULISSE Mock-up

COMSOL offers automatic mesh construction based on the physics used. The user can then modify the size of the elements in order to refine (or not) the results obtained. For most of the cases studied, this automatic meshing method is used. Alternatively, certain physical cases may require you to construct the mesh yourself. This is useful, for example, for obtaining greater accuracy at specific points in the domain.

In order to reduce the calculation time for the 3D simulation, a quarter of the Mock-up has been modelled, which should not influence the results due to the double symmetry of X and Y.

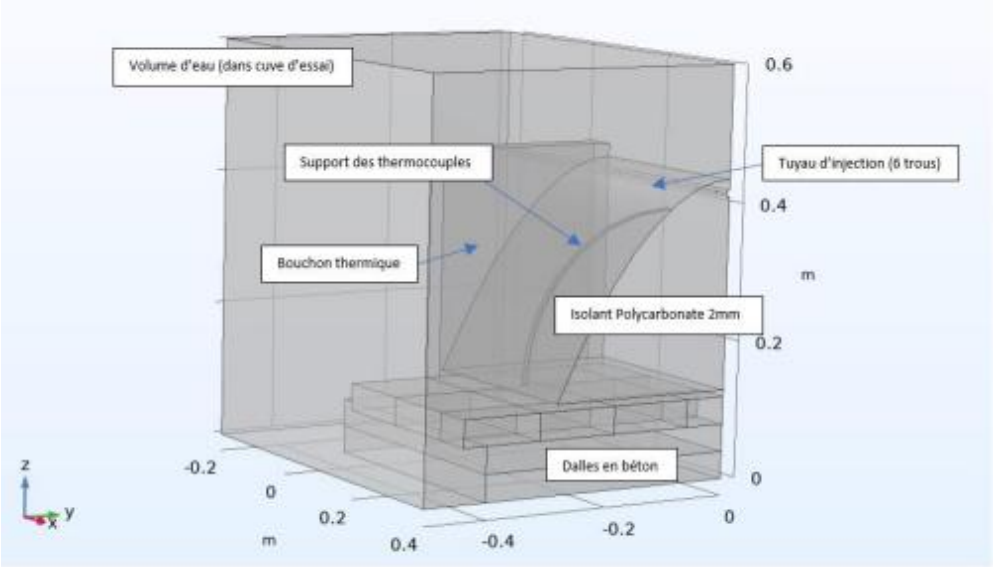

Figure 10.18: 3D digital geometry of the Mock-up for hydrothermal loading.
Only a quarter of the Mock-up is represented (double symmetry)

10.7.3 First results of the numerical simulation of the Mock-up

The initial results of the numerical simulation of the Mock-up show relatively good consistency with the experimental measurements. The simulation was carried out on a quarter of the Mock-up (18.103 litres) for a complete volume of 72.4 litres. The loading time is admittedly much too long (64 minutes instead of the normal 6 minutes required for 2 months of summer loading). This was taken to be similar to the first tests for comparison (with a total flow rate limited to 2.2 litres/min) and because of the limited initial capacity of the loading pump.

Normally, to fill the Mock-up in 6 minutes, a flow rate of 12 litres/min would have been required. However, this has no real influence on the net energy balance (without loading heat loss). The heat loss in the SL phase is less crucial because, for the full-scale Reservoir in the lake, it can be compensated for "at lower cost" by increasing the flow rate or the pumping time, fuelled by the surplus photovoltaic electricity, which will probably be in excess capacity in the summer.

On the other hand, the times for the Autumn Stagnation (AS) phase of 6 minutes and the Winter Discharging (WD) phase of 19 minutes are well respected and important for establishing the losses during the AS and WD phases. The latter is simulated numerically with an extraction flow rate of around 0.95 lit/min (3.8 lit/min for the full volume of the Mock-up).

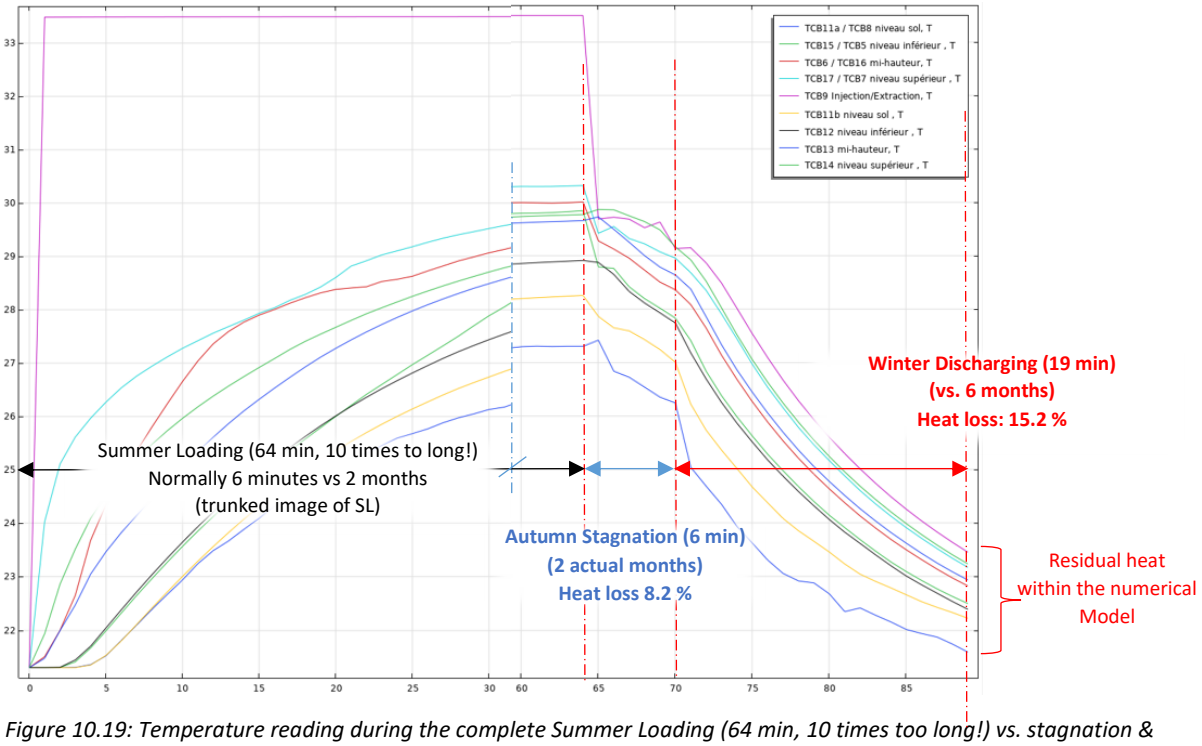

Figure 10.19: Temperature reading during the complete Summer Loading (64 min, 10 times too long!) vs. stagnation & discharging cycle obtained by numerical simulation of the ULISSE Mock-up (net storage efficiency 76.7 % for extraction equivalent to the volume of the Mock-up in 19 min.). There's still some heat left in the Mock-up!

At the start, the IBC tank (lake) and the Mock-up have a common temperature of approximately 21.3˚C. At the end of Summer Loading the Mock-up contains approximately 2.79 MJ of net heat energy (0.697 MJ for 1/4 of the Mock-up). At the end of the stagnation phase (6 min or 2 months in real life) the internal energy has fallen to 0.615 MJ, giving a heat loss of 8.2% (compared with 5.1 to 6.1% for real-life tests on the Mock-up). At the end of the unloading phase (19 minutes or 6 months), the residual internal energy was still 0.202 MJ.

Taking into account the energy extracted of 0.461 MJ for 1/4 of the Mock-up (1.843 MJ for the whole Mock-up), the net storage efficiency is 76.7%. This result is within the range of the results of the actual tests on the Mock-up, which are between 74.8% and 86.4%. (Table 10.15). An increase in the extraction flow rate or volume would make it possible to increase the recovery rate still further and approach the upper value of the said heat storage efficiency window.

Graph 10.19 shows that stratification is maintained even after 19 minutes of extraction equivalent to the volume content of the Mock-up. This can also be seen in figure 10.20 below. During the Winter Discharging phase there is a flow of heat both downwards and from the concrete slabs representing the lake bed (clearly visible colour gradient). These have stored heat during the loading and stagnation phases. In the present simulation, the loading phase was 10 times too long (64 instead of 6 minutes), which led to disproportionate thermal loading of the concrete bottom.

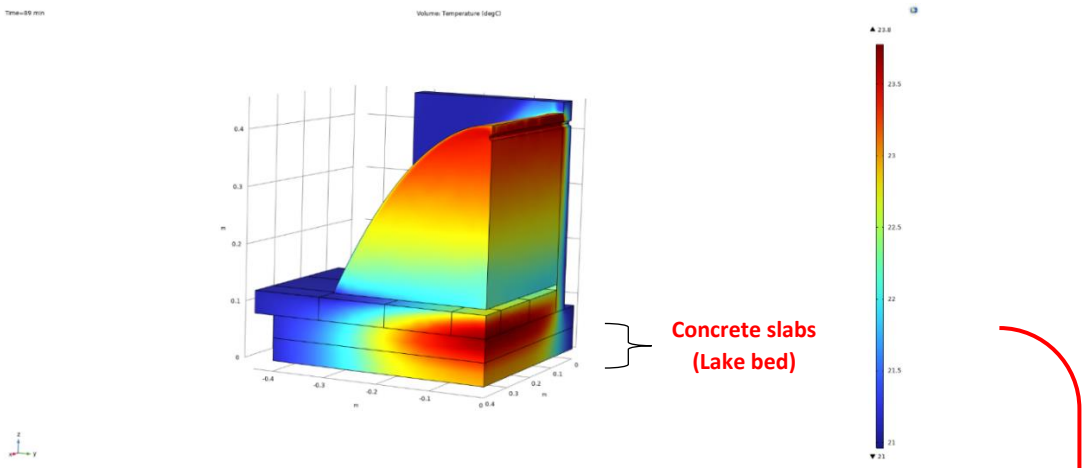

Figure 10.20: Graph representing ¼ of the Mock-up from the numerical simulation. It can be seen at the end of unloading (19 minutes) the equivalent of the volume of water in the Mock-up that there is still a temperature gradient in the Mock-up as well as in the ground (lake bottom). This indicates that the Mock-up still contains heat energy.

The warming of the bottom slab can also be seen in Figure 10.21 below, which corresponds to the last test on the real Mock-up on 5 January 2023.

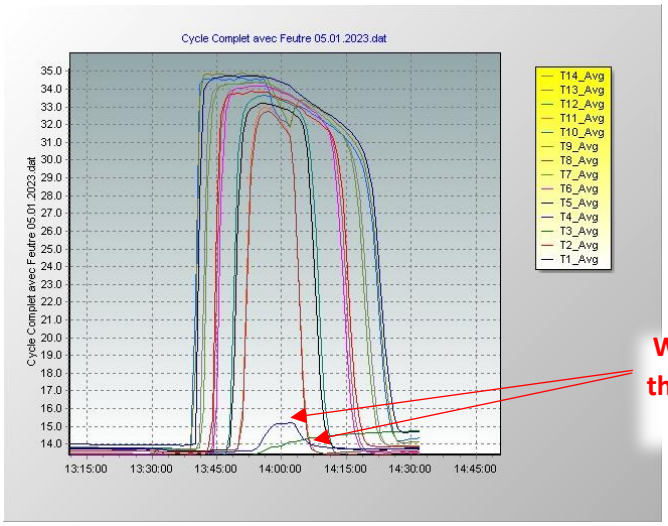

Figure 10.21: Last physical test on Mock-up (complete cycle) on 5 January 2023

In conclusion, given the current state of progress of the numerical simulation and taking into account the simplifications introduced for the purposes of numerical modelling, it shows relatively good consistency with the actual tests carried out on the physical Mock-up. This applies both to heat losses during the stagnation phase and the discharging phase, as well as to the efficiency of seasonal thermal storage. For the real full-scale Reservoir, the simulation has not yet been completed. The numerical simulation work will have to be continued in the next stage, after this exploratory study of the ULISSE project.

=> Appendix 5: Simulation of an Under Lake Infrastructure for Capture and Storage of Solar Energy (ULISSE), COMSOL Conference Munich 2023 [66]

11 Next Step: ULISSE & CORSAIRE project roadmap

The ULISSE project, in conjunction with the CORSAIRE free heating system, is in line with Switzerland's energy strategy 2050. It will enable the development of thermal networks and seasonal heat storage, reducing the structural winter electricity deficit, as encouraged by the aeesuisse *Swiss Energy Storage Forum* (FESS). [**41**]

The positive potential of seasonal heat accumulators has been studied by the *Swiss Competence Centre for Energy Research* (SCCER) and is currently being pursued as part of the SWEET-DeCarbCH project.

It is precisely in association with or within this SWEET-DecarbCH framework that the ULISSE project could also be advantageously pursued, along the following two lines:

A. For the ULISSE section:

1. Continuing the numerical simulation (COMSOL) of the Mock-up and the full-scale simulation of the Reservoir.
2. Analysing the real potential for installing ULISSE Reservoirs (2 M m^3) in the 15 major Swiss lakes.
3. Carry out an in-depth environmental impact assessment for the lakes concerned.
4. Carrying out an in-depth study of the hydrodynamic behaviour of the Reservoirs in relation to lake currents; in particular, the structural integrity of the Reservoirs in relation to the internal seiches causing adverse internal shear currents in large lakes (Appendix: 3).
5. Development of an autonomous drone for cleaning the shell and inspecting the standard Reservoir.
6. Development of a first prototype of the Intermediate Reservoir for an initial behaviour study in a closed basin or lake.
7. Production and installation in a real-life situation of a test pilot of typical size (2 M m^3) with observation of the physical and environmental behaviour in relation to the receiving lake.

Proposal

The ULISSE Pilot and Demonstration Reservoir (P+D) could advantageously be installed in Lake Geneva opposite EPFL and UNIL and connected to the new Pumping Station (SPP) on both campuses, for cooling and heating with lake water and the new heat pumps (HP) located in the EPFL thermal power station (CCT)!

The ULISSE Pilot Reservoir could be located near the EPFL-UNIL suction strainer, which is only 900 m from the shore where the SPP is located and 75 m deep (ideal for a typical ULISSE Reservoir). Its connection to the CCT would make it possible to test the energy impact on the performance of the heat pumps.

Figures 11.1: Proposed installation in Lake Geneva and connection of the ULISSE pilot to the heating and cooling infrastructure (SPP + CCT) at EPFL-UNIL, with environmental and physical observation by the LéXPLORE platform.

Objectives

One of the objectives of the ULISSE exploratory study project is to study its impact on the heating system (100% thermo-lacustrine since 2022) of the EPFL (main site in Ecublens) as well as that of the UNIL in 2025 **[59].**

The EPFL-Ecublens heating system is being upgraded mainly at the Pierrettes Lake Pumping Station (SPP) and the Central Heating Plant (CCT), with 4 new heat pumps totalling 24 MW of thermal power, plus 4 MW from the data centre above the CCT **[58]**.

Based on EPFL's Energy Master Plan 2015-2045, in 2014 the Ecublens site's heating requirement was 34 GWh. Nearly 70% (24 GWh) of the heat was extracted from Lake Geneva, with the remaining 30% supplied by heat recovery from the oil-fired turbines. By 2045, the heating needs of the EPFL's Ecublens site will have risen to 50 GWh-t/year (up 50% on 2014), supplied since 2022 by water from Lake Geneva and 4 new heat pumps. With a predicted annual COP of 5.5 for the heat pumps, their electricity consumption should reach almost 10 GWh to extract 40 GWh thermal/year from Lake Geneva and supply them at a maximum of 67 ˚C to the heating network.

UNIL also plans to switch entirely to heating its buildings using the same lake system as EPFL by 2025 (Figure 11.2 below). For all the EPFL + UNIL + Vortex heating, lake water requirements in 2030 and 2050 will be 1.7 and 2.35 m^3/s respectively, compared with the 2.5 m^3/s capacity of the new Pierrettes Pumping Station (SPP).[9]

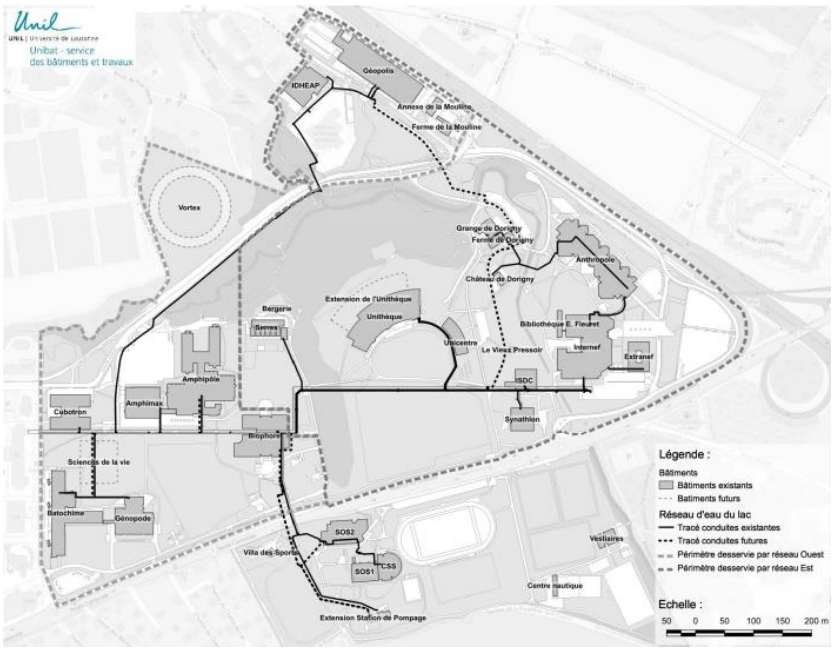

Figure 11.2: Map of the Dorigny campus, with the pipes to be added as part of the project to extend the pumping station and adapt the network dotted in black (source: Canton de Vaud, EXPOSE DES MOTIFS ET PROJET DE DECRET - pour financer l'agrandissement de la station de pompage et l'adaptation du réseau de distribution d'eau du lac alimentant le Campus de Dorigny, July 2019).

With these lake water flows and an identical heat pump COP (5.5) for EPFL and UNIL, the thermal energy for heating the two universities could reach 60 GWh-t @ 1.7 m^3/s in 2030 and 80 GWh-t @ 2.35 m^3/s in 2050.

Electricity consumption by the heat pumps will also reach 11 and 15 GWh respectively. To this must be added that of the SPP's primary circulation pumps, for the increase in the mass of water pumped: 0.8 GWh for 14 M m^3 in 2030 and 1 GWh for 19 M m^3 in 2050, as well as the pressure losses (?) in the hydraulic network between the water suction strainers, the evaporator of the heat pumps and up to the point of discharge into the Sorge river.

Main thermal parameters EPFL-UNIL without and with ULISSE:

Temperature (winter) cold spring of Lake Geneva (T_f): 5 to 6 °C
Temperature (winter) source ULISSE (T_u): 18 to 20 °C
Water discharge temperature at the heat pump evaporator outlet (T_r): 2 to 4°C
Temperature difference on the evaporator of ULISSE heat pumps (without) ($\Delta T_{f\text{-}r}$): 3 K
Temperature difference on the evaporator of ULISSE heat pumps (with) ($\Delta T_{u\text{-}r}$): 15 K
Maximum water distribution temperature at heat pump outlet (heating network): 67 ˚C

As a first approximation, based on the ULISSE impact study on GeniLac (§ 5), which indicates a potential gain of 50% on the COPsys, the heating system for the EPFL + UNIL + Vortex campuses could benefit from a 50%

[9] 159 TextCE crédit SPP campus UNIL.pdf (Canton of Vaud, July 2019)

reduction (6 to 8 GWh/year) in electricity consumption (SPP + CCT), to supply 60 to 80 GWh heat (2030/2050). This would have a fivefold positive energy impact:

1. Reducing (by a factor of 5 or -80%) the volume/mass and therefore the flow of water to extract the heat required for EPFL's heating needs from the lake,
2. 95% reduction in pressure losses (proportional to the square of the flow rate) and the corresponding energy required to pump lake water through the heat pump evaporators,
3. Reduction (-80%) in the potential energy of the water mass rising from the lake towards the HPs,
4. Increase (+50%) in the Coefficient of Performance (COP) of heat pumps, or reduction in the corresponding electrical energy absorbed,
5. Reduction in demand and heat losses for drinking water consumption during the heating season using CORSAIRE free heating: 125 to 175,000 m^3 @ $\Delta T_{ep} \approx 10$ K, => free-heating supply (without heat pump) = 1.5-2 GWh (2030-2050).

Physical and environmental observation of the ULISSE pilot Reservoir

Physical observations of the Underwater Reservoir and its environmental impact could be advantageously carried out using the LéXPLORE research platform. Since 2018, the LéXPLORE platform has been anchored for 8 years (110 m deep, 570 m from the shore) on Lake Geneva opposite the port of Pully (VD), 6 km from the Lausanne campus.

Photo https://lexplore.info/fr

Figure 11.2: The LéXPLORE platform for lake research on Lake Geneva, currently anchored opposite the port of Pully (VD)

B. For free heating CORSAIRE:

As mentioned in section 2.1 above, **the CORSAIRE project was included in the Geneva Cantonal Energy Master Plan (2001-2005) [46].** In November 2005, Part 1 of the multidisciplinary impact study began on a **pilot residential building made available by the City of Geneva**. Unfortunately, it was suddenly halted 3 months later due to an unforeseen budgetary restriction (reduction in the Confederation's funding for the OCEN, whereas the CORSAIRE "Phase-1" was entirely financed by the OCEN).

And as a reminder (§ 2.1), since that time (2006), the City of Toronto has been **applying (only in summer, by absence of heat in winter) exactly the same CORSAIRE free heating** on its drinking water network, using the 360 MW of heat rejected from the air conditioning of **more than 80 buildings in the city centre, including hospitals, government buildings, data centres, universities, commercial and residential towers**! **[51, 51, 52].**

As part of Switzerland's Energy Strategy 2050 and in response to the SFOE's call for SOUR projects, the ULISSE project, combined with the integration of the CORSAIRE free heating process, should take over the entire CORSAIRE project, which was officially registered and initiated in Geneva but has been on hold since 2005.

The *Services Industriels de Genève* (SIG) is both responsible for the public drinking water network (DWN) in the canton of Geneva and fully involved in the GeniLac project, the "*flagship*" of TLNs in Switzerland. The following points need to be addressed:

1. The basic study (master's thesis by W. van Sprolant EPFL 1995).
2. A study of heat loss from the public drinking water network (DWN).
3. A study of the physical integrity of the DWN (under winter free heating).
4. Study of the sanitary integrity of drinking water under winter temperature correction.
5. Psychosociological study of public acceptance of winter changes to the temperature of drinking water at the tap.
6. **The CORSAIRE free heating impact study(s) on a pilot and demonstration building (P+D)**.

Proposal

In order to carry out an effective **multidisciplinary study of the impact of the CORSAIRE free heating system on a building stock that is representative of an urban conurbation**, a large group of buildings should be chosen, at least equivalent to a residential area with a variety of shops (large number of different drinking water users).

To simultaneously test the transfer of heat from the source of thermal waste to the DWN, it would be useful for it to be close to the buildings concerned. This would also make it more practical to conduct multidisciplinary studies within a limited area. The Cité du Lignon, with its 2,780 homes, 6,500 inhabitants, various businesses and just a few hundred metres from the Aïre WWTP, could be an ideal pilot and demonstration site.

Figure 11.3: The Cité du Lignon "the longest building in Europe" (1 km)

Initially, under a mandate from ScanE (OCEN), the impact study(s) planned for 2005 on the City of Geneva building (87 rue de la Servette) was the first of 8 stages in the CORSAIRE project [**46**]. **For the purposes of experimentation and energy observation, the pilot building was** to be instrumentalised at the overall level of the building's energy installation and communal equipment (laundries), but also more individually on a number of representative flats, including water and energy meters on household appliances (dishwashers, washing machines).

In the absence of a suitable source of heat rejection, the temperature of the cold drinking water at the entrance to the building was corrected in the building's boiler room (for the Cité du Lignon, this would be done in the Aïre WTP). The energy measurements were planned to be carried out over two winter semesters on a comparative basis (with/without free heating). It was also planned to test a "daily alternation" procedure, i.e., to artificially correct the temperature of the cold water every other day, in order to statistically eliminate external variables such as heating degree days, changes in tenants, etc. The energy monitoring was carried out by Amstein. **Energy monitoring** was carried out by *Amstein+Walthert SA* & *CvS énergies sàrl*.

At the same time as the energy experiment on the building, **the quality of the drinking water was monitored during the experiment** (microbiological analyses) by the AMICO Lab SA laboratory in Geneva (Carouge), under the supervision of the *Hygie Europe Foundation*.

Similarly, a **psychosociological study** conducted by the company *Et Alii* in Geneva was planned on an exploratory basis (outside the building, representative sample of the Geneva population) and as an internal observation within the building with users in the situation; in order to assess the acceptability of "captive" consumers of the public drinking water network.

Finally, a **communications strategy** was also planned by *TerraWatt* (Vessy), to ensure that information was communicated to tenants in the pilot building and to SIG (in the event of a telephone call from a "diverted" tenant).

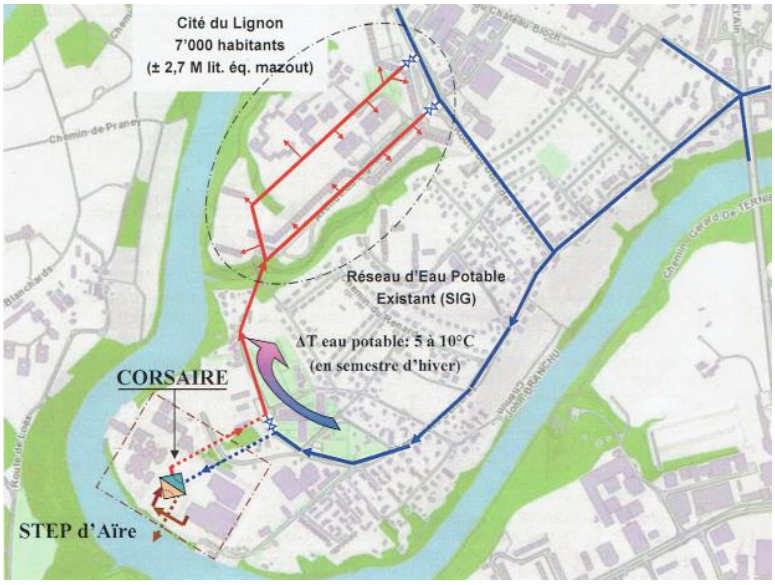

Figure 11.4: Proposal for the Cité du Lignon in Geneva connected to the Aïre WTP as Pilot for the multidisciplinary study of the impact of CORSAIRE free heating

WTP Aïre

The main wastewater treatment plant in Geneva, if not in Switzerland, the Aïre WTP, with its 140,000 m^3/d and 2 m^3/s, is a perfect example of an ideal source of low-temperature waste heat for CORSAIRE free heating **[65].** Insofar as the wastewater network is "separate" from the rainwater network, and in addition to the capacity of the wastewater tanks, the wastewater is logically in phase with the consumption of drinking water. After treatment, the temperature of this water is still higher than that of the drinking water network (DWN) in mid-winter, especially as the Aïre WTP tanks are completely covered. Heat can then be transferred to the DWN simply by *free heating* (without a heat pump) using a heat exchanger coil. The distance from the Aïre WTP is only a few hundred metres from the REP loop that supplies the Cité du Lignon (Fig. 11.4 above).

For History

Before the development of electricity networks, **Geneva's** emblematic "**Jet d'eau"** was the source of a co-supply of water and mechanical energy from the drinking water network (Eau motrice) to power the machines of Geneva's craftsmen from 1886 to 1960. In a way, the free heating CORSAIRE, by co-supplying heat through the public drinking water network, could reconnect Geneva with its industrial and craft history...

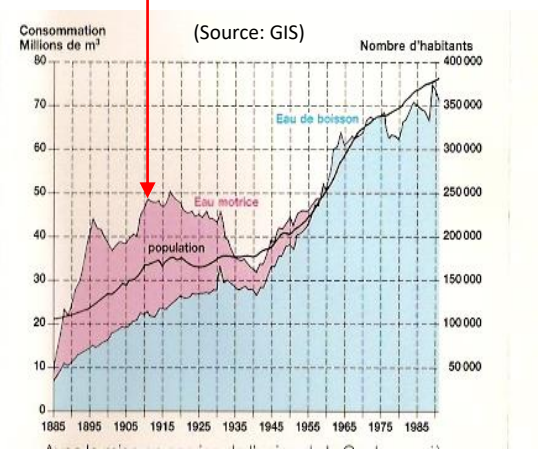

Figure 11.5: Geneva's first water jet at the site of the Coulouvrenière factory
Book "Genève - Passé et présent sous le même angle" by Nicolas Crispini and Jean-Claude Mayor

12 General conclusions and next steps

This final report concerns the exploratory study of the ULISSE (***Under Lake Infrastructure for capture and Storage of Solar Energy***) system/project. The study was subsidised by the Swiss Federal Office of Energy (SFOE), following the "SOUR Call 1-2021" (*SWEET Out the box Rethinking)* call for projects as part of Switzerland's Energy Transition 2050. The study took place at the host institute HEPIA, Geneva University of Applied Sciences for Landscape, Engineering and Architecture, from September 2021 to the end of May 2023.

Report

In the face of climate change, **the *Swiss Energy Strategy* (SES-2050),** which aims for "double *neutrality*": *Nuclear & Carbon*" (2035-2050), **forecasts a structural deficit of 9 TWh of electricity in the winter semester in less than 30 years' time; equivalent to the national hydroelectric storage capacity**.

This situation results from the planned withdrawal of nuclear power in 2035 and the increase in demand for electricity for air conditioning, electric mobility and heat pumps for heating buildings (replacing fossil fuels).

The major challenge of the SES-2050 is therefore to have enough "doubly *neutral*" electricity available in winter, with a foreseeable shortage of imports, either through increased domestic production (with seasonal storage) or by reducing demand (in particular by improving the efficiency of its use).

Increased annual production of undifferentiated electricity could amount to a "headlong rush":

- Adding even more photovoltaics to the 34 TWh already planned for 2050, while naturally only having 30% of annual production available in the winter months, would only accentuate the risk of having to resort to the paradoxical summer "*solar peak shavings".*

- Further development of hydroelectric storage capacity is limited by the number of acceptable potential sites. Added to this is the problem of summer loading of dams with water under water stress due to Global Warming. Generally speaking, the requirement to increase "residual flows" will reduce hydroelectric productivity. The potential for developing annual hydroelectricity production between now and 2050 is between 1 and 3 TWh (equivalent to the Grande Dixence complex), except that availability during the winter half-year is only half that at best, i.e., around 1.5 TWh...

- Maintaining nuclear power would further exacerbate the water stress on rivers already impacted by Global Warming. For technical and economic reasons, a nuclear power plant generally operates as a "ribbon" throughout the year, and therefore also during the summer months (≈ 4,000 h) **[18, 19**]. During the summer semester alone, the Swiss nuclear power plant at Leibstadt discharges 14 million m^3 extracted from the Rhine in the form of steam (32 PJ of heat equivalent to its annual electricity production of 9 TWh). The Gösgen nuclear power plant is not to be outdone, with almost 10 million m^3 of water evaporating from the Aare at the same time. As the summer drought worsens, exacerbated by more recurrent heatwaves, the increased need for water for other uses, particularly agriculture, will (already has) become critical. As a result, thermoelectric power plants (nuclear as well as fossil-fired, coal, fuel oil and gas), which will not be able to operate without cooling water losses (by recovering their thermal waste through cogeneration), will be forced to shut down or drastically reduce their production in the summer semester, and will therefore no longer be economically "competitive", let alone present in the winter semester. France and Germany, Switzerland's main importers of winter electricity, face the same problem of electricity availability and climate commitment...

Proposal

The ULISSE system/project, supported by the CORSAIRE *free heating* system, is proposed here as part of a potential solution to this multifactorial problem. In support of the Swiss Energy Strategy 2050, **ULISSE aims to optimise (boost) the hydrothermal networks of Switzerland's major lakes while protecting them from the effects of Global Warming**. This will be achieved by improving the electrical efficiency of heat pump heating and *free cooling*, and by combining this with CORSAIRE *free heating* to reduce the negative energy impact of the winter drop in the temperature of the public drinking water network (*2 ways of capturing, storing and using solar thermal energy and waste heat*).

The ULISSE system proposes firstly to supply a winter lake heat source of around 20°C, higher than the usual 5-6°C, which will double the efficiency of the heat pumps (HP) and halve their electricity consumption, as well as reducing by 95% the energy required to pump and circulate the water in the said TLN networks.

This ULISSE heat source consists of large tunnel-like Reservoirs (length 560 m x 50 m hyperbolic transverse radius), anchored to the lake bed, with a unit storage volume of 2 million m^3 and a thermal capacity of 125 TJ each. In summer, these ULISSE Reservoirs are charged with tempered water, either from the upper layer of the lake (*Epilimnion*) heated by the sun, or from industrial and air-conditioning waste heat. The charging pumps are powered by photovoltaic electricity, which absorbs the summer production peaks of photovoltaic (PV) installations and avoids their so-called *peak-shavings*.

The second way of using the tempered water supplied by the ULISSE Reservoirs or other thermal discharges is, using the CORSAIRE process, to correct (de-ice +5 to +10˚C) the winter temperature of the public drinking water networks (DWN). The DWNs concerned are those adjacent to TLNs as well as those not served by an TLN. Like free cooling for air conditioning, CORSAIRE free heating uses only a heat exchanger as a thermal "slide". It can supply 30% of the energy for DHW via DWNs and increase the electrical efficiency of TLNs, as well as all heat pumps for DHW, even outside TLN networks.

The ULISSE concept/project, with around 300 Reservoirs distributed invisibly across the 15 major Swiss lakes and in association with the CORSAIRE *free heating system* (including outside the lake regions), could supply almost 60 PJ or 30% of the 200 PJ of national heat requirements for room heating and domestic hot water. This would save 3 TWh of gross electricity in the winter semester (1/3 of the 9 TWh winter electricity deficit or the equivalent of twice the winter production of the Grande Dixence hydroelectric complex: 1.5 TWh).

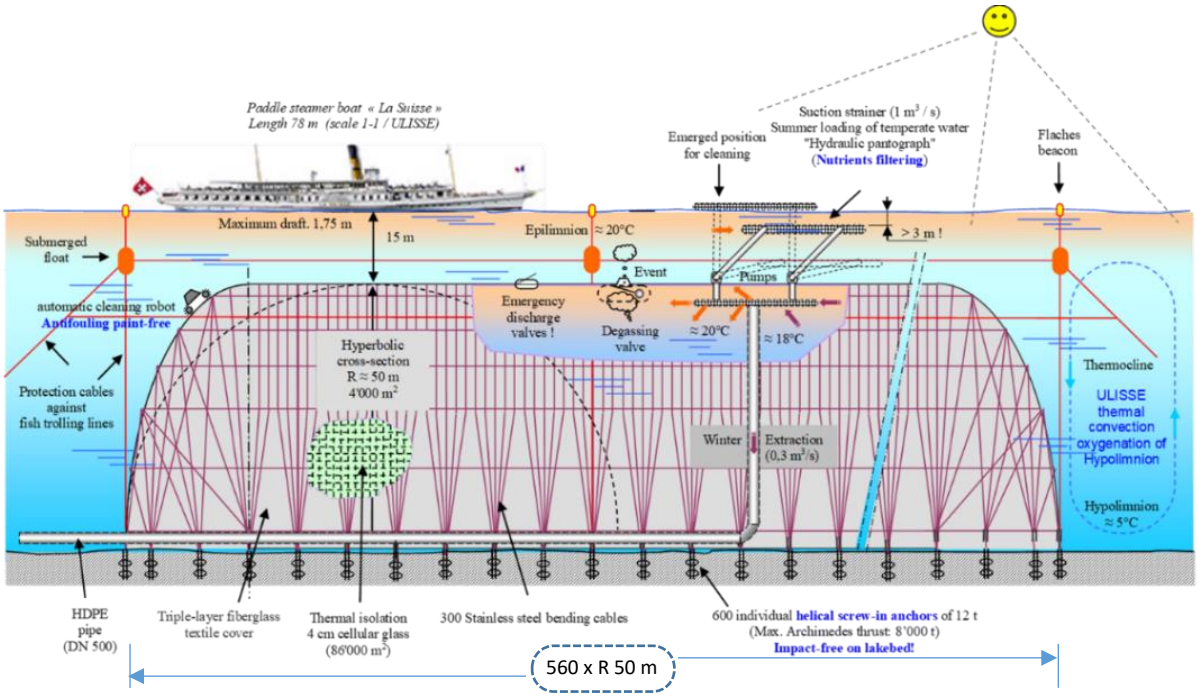

Fig. 2.1: Truncated longitudinal diagram of a typical ULISSE Reservoir of 2 M m^3 (CGN boat to scale)

The external thermal convection currents induced by the ULISSE Reservoirs can improve the circulation of nutrients and oxygenation of the lake bed, **protecting the aquatic ecosystem from eutrophication, which is exacerbated by Global Warming**. In addition, the presence of reservoirs can create ecological niches that are protected from fishing, thereby encouraging the development of aquatic fauna. Selective capture (filtration of phytoplankton) would make it possible to regulate blooms (toxic algal blooms) if necessary, and to recover greenhouse gases and CH_4 (for energy use). Containing the heat captured in the ULISSE Reservoirs would lower the surface temperature of the lakes, thereby reducing water loss through evaporation and increasing the oxygen dissolved in the water.

Approach, methodology and results of the ULISSE exploratory study

Following an analysis of Switzerland's Energy Strategy 2050 and a presentation of the ULISSE project, including the background to the initial concept (CORSAIRE-ULISSE), the workings of the Thermal Lacustrine Network (TLN) and the urban Drinking Water Network (DWN) were developed. The whole was then applied and quantified on the largest TLN network in Switzerland, "GLN - GeniLac" and the DWN in the canton of Geneva.

To establish the impacts, we have taken into account climate change and changes in the energy efficiency of buildings between now and 2050 (ECEEB-2050**). In the long term, we have also considered the (essential) widespread use of domestic hot water (DHW) for household appliances. It** has been observed that this changes the heat expenditure index for room heating and DHW and opens up the economic prospect of extending TLNs.

The application for GeniLac showed that supplying 250 GWh of heat in the winter semester would require (instead of 60 M m^3 at 6.5˚C) only 1/5 or 12 M m^3 of lake water at 19˚C, coming from 6 ULISSE Reservoirs anchored at the bottom of the *Petit lac* Léman 6 km from the LPS lake pumping station at the Vengeron. In combination with CORSAIRE *free heating*, the winter electricity consumption of the TLN GeniLac network for room heating and DHW is reduced by 50%. For GeniLac and the canton of Geneva, this corresponds to winter electricity savings of 40 GWh, or almost 20% of the winter production of the Verbois hydroelectric power station on the Rhône.

In the third stage, the exploratory study analysed more precisely the shape and structure of the main shell (biocompatible textile- and cellular-glass) of the ULISSE Reservoir, as well as its *screw-in* anchoring with very low impact on the lake bed. The efficiency of the ULISSE Reservoir's seasonal heat storage was determined using 3 approaches: 1) calculations using a theoretical model of both the full-size Reservoir and a Mock-up, 2) laboratory measurements on the Mock-up, and 3) a numerical simulation. The *Temporal Scale Factor* (TSF = 13,715) between the Mock-up and the real full-size Reservoir was established beforehand, making it possible to determine the duration of the various phases of the annual cycle of their respective operations.

The results of the three approaches converge with very few differences (a few %). **The energy efficiency of the Net seasonal Heat Storage (NHS) of the ULISSE Reservoir is around 84%.** It starts from the end of *Summer Loading* (SL: 2 months of real Reservoir vs. 6 minutes of Mock-up), the *Autumn Stagnation* phase (AS: 2 months vs. 6 minutes) and that of *Discharging in the Winter semester* (WD: 6 months vs. 19 minutes).

The convergence of the results also confirms the good value of the TSF and that the average temperature supplied to the TLN networks by the ULISSE Reservoirs could be at least 19-20˚C (initial loading at 20-23˚C compared with a lake summit temperature: ≥ 25˚C in the summer of 2050). This determines the effectiveness of the TLNs with ULISSE.

The financial cost of the ULISSE & CORSAIRE system for Switzerland has been estimated with reservations, given the absence of a precedent. However, this exploratory study has made it possible to sketch out an order of magnitude **of CHF 3 to 4 billion**, based on the world's greatest achievements in the field of seasonal storage of sensible heat of water. The cost of the ULISSE system should be put into perspective with alternative solutions (insofar as they are feasible), which would be CHF 19 billion for an additional winter hydroelectric production capacity of 3 TWh or around CHF 7 billion for a supply of 60 PJ of solar thermal energy via heat networks, comprising 35 km^2 of flat thermal collectors, 26 M m^3 of covered seasonal storage basins and 91 km^2 of land surface (= surface area of Lake Zurich).

From this exploratory study of the ULISSE system, it appears that the environmental impact is probably not neutral but could potentially even be positive, in particular by offering protection against the negative effects of global warming. With regard to the cohabitation of ULISSE Reservoirs anchored on the lake bed, with the "inhabitants" and users of the lakes, it can be considered that there is practically no impact on navigation and that the loss of 0.8% of the fishing area can be compensated for by the environmental protection provided by the ULISSE Reservoirs (development of fish).

Next Step

Finally, this exploratory study of ULISSE, associated with the CORSAIRE *free heating*, proposes a 'roadmap' for further development and validation of the project, with two main milestone objectives: a **pilot ULISSE Reservoir** (linked to the TLNs on the EPFL-UNIL campuses with observations by the LéXPLORE floating laboratory) and a **pilot CORSAIRE** (Cité du Lignon, 6,500 inhabitants and shops with the Aïre WTP in Geneva).

13 References

Swiss Energy Strategy 2050

[1] Perspectives énergétiques 2050+, Rapport succinct, Office fédérale de l'énergie (DETEC/OFEN 2020)

[1.1] Energie Panorama Office fédéral de la statistique, mars 2020

[1.2] Stratégie Chaleur Suisse 2050, OFEN

[2] Monitoring Stratégie énergétique 2050, Rapport de monitoring 2021 https://www.bfe.admin.ch/bfe/fr/home/versorgung/statistik-und-geodaten/monitoring-energiestrategie-2050.

[3] ClimaBau – Planen angesichts des Klimawandels, Bundesamt für Energie BFE, Hochschule Luzern 2017

[4] Potentiel d'exploitation des stations d'épuration des eaux usées en tant que source d'énergie thermique, OFEN, 23.11.2022

Canton of Geneva's energy strategy and studies on the GLN and GeniLac thermal lacustrine networks

[5] PLAN CLIMAT CANTONAL – Volet 2 du 20 décembre 2017 / page 6, Fig.2 : Bilan carbone et objectifs de réduction

[6] Réponse du Conseil d'État de Genève sur la Réalisation d'un barrage transfrontalier à Conflan, QUE 523-A, 5 octobre 2016

[7] Valorisation thermique des eaux profondes lacustres : le réseau GLN et… J. Faessler et. al., UNIG, Arch. Sci. (2012) 65 :215-228

[8] Viquerat P-A. 2012. Utilisation de réseaux d'eau lacustre profonde pour la climatisation et le chauffage … Étude de cas : le projet GLN (Genève-Lac-Nations) à Genève, Thèse de doctorat n° 4448, Université de Genève.

[9] Réseau thermique Genève-Lac-Nations (GLN), Étude de cas D. Crochet et al. SIG, SuisseEnergie, 18.10.2017

[10] De GLN à Genilac, 10 ans d'apprentissage dans la valorisation thermique des eaux du Léman, Sophie Durandeux, SIG, ARPEA-27.09.19

[11] Enjeux et développement des réseaux thermiques basse température à Genève, Fabrice Malla, SIG, 14.11.2019 https://www.cuepe.ch/html/enseigne/pdf/semin-19-20-5.pdf

Heating networks

[12] Décarboner le système énergétique à l'aide des réseaux de chaleur ; État des lieux et scénarios prospectifs pour le canton de Genève. Thèse de doctorat Loïc QUIQUERAZ, UNIG 2017, no. Sc. 5056

[13] Potentiel des installations de chauffage et de refroidissement à distance, Rapport du Conseil fédéral, Bern 17.12.2021. Ref. BFE-042.16-127/5

[14] Charta zur Beschleunigung des Ausbaus Themischer Netze, August 2022 (www.uvek.admin.ch)

Hydropower

[15] Étude sur le potentiel hydroélectrique de la Suisse 2019, OFEN https://www.newsd.admin.ch/newsd/message/attachments/58260.pdf

[16] Grande hydraulique, AES, juillet 2020

[16.1] Complexe Grande Dixence : https://www.alpiq.ch/fr/production-denergie/centrales-hydroelectriques/centrales-a-accumulation/grande-dixence

Solar Energy

[17] Installations solaires de préchauffage de l'eau chaude sanitaire pour immeubles locatifs de 10 à 200 logements, C. Macherel et G. Ktrebs, Ville de Genève, Les cahiers du Service du chauffage, No. 3, juin 1990

[17.1] Production d'électricité en hiver grâce au photovoltaïque. Rapport du Conseil fédéral en réponse au postulat 19.4157 Reynard du 25 septembre 2019, Berne, 23 juin 2021

[17.2] Le plan Solaire et climat, Roger Nordmann, 2019, Edition Favre

Cooling impacts of nuclear power plants

[20] Dynamique du système lacustre, Philippe Zahner et Jean-Pierre Vernet

[21] Température et mouvements des eaux des lacs, Bosset, Eric, Bulletin de la Société Vaudoise des Sciences naturelles, 1962-1964

[22] Courantologie lémanique, Lemmin, Ulrich, Archives des Sciences 1998

[23] Structure thermique et courantologie du Léman, Anh Dao Le Thi et al. Archives des Sciences (2012)65 :65-80

[24] Seasonality modulates wind-drive mixing pathways in a large lake, Beito Fernandez castro et al. Communications earth & environment (2012)2 :215

[25] Vagues Kelvin dans le lac Léman, D. Bouffard, U. Lemmin, 2013, Journal de recherche sur les Grands Lacs

[26] Program « Thermische Netze » Nutzung von Oberflächengewässer für thermische Netze, B. Schaffner, K. Niederberger, EnergieSchweiz, BFE, 09.2017

[27] Utilisation thermique des eaux superficielles, Potentiel des lacs et rivières suisses A. Gaudard; M. Schmid, Eawag; A. Wüest, Eawag et EPFL, AQUA & GAS N° 6. , 2018

[27.1] https://opendata.swiss/fr/dataset/potenzial-der-seen-und-flusse-fur-warmeentzug-und-warmeeinleitung

[28] The vulnerability of lakes to climate change along an altitudinal gradiant, L. Raman Vinna, I. Medhaug, M. Schmid, D. Bouffard, Communications earth & enviroment, 2021

[29] Model-based data analysis of the effect of winter mixing on primary production in a lake under reoligotrophication. S. Krishna et al. Ecological Modelling 440 (2021) 109401

[30] OFEV (éd.) 2022 : Eaux suisses. État et mesures, Office fédéral de l'environnement, Berne. État de l'environnement No 2207 : 93 p.

[31] Water column dynamics control nitrite-dependent anaerobic methane oxidation by Candidatus "Methylomirabilis" in stratified lake basins, G. Su et al. ISME 20.02.2023, Springer Nature

[32] Règlement d'application de l'Accord entre le Conseil fédéral suisse et le Gouvernement de la République française concernant la pêche dans le Lac Léman, RS 0.923.211, fedlex.admin.ch

[33] Les Aires Marines Protégées, un précieux allié pour la biodiversité, juillet 2020 https://planktovie.biz/actualites/les-aires-marines-protegees-un-precieux-allie-pour-la-resilience-de-la-biodiversite/

[34] Les aires marines protégées le mirage de la préservation des océans https://reporterre.net/Les-aires-marines-protegees-le-mirage-de-la-preservation-des-oceans

[35] Le changement climatique asphyxie les lacs, Manon Meyer-Hilfiger, NATIONAL GEOGRAPHIC, 19.07.2021,**https://www.nationalgeographic.fr/environnement/2021/07/le-changement-climatique-asphyxie-les-lacs**

Seasonal heat storage

[36] The Role and Economics of Different Types of Energy Storage, Margen Consult, 1984, Nyköping, Sweden

[37] Guide to Seasonal Heat Storage, Jean-Christophe Hadorn, SORANE SA, 1987 OFEN

[38] The cold store for a pumped thermal energy storage system, T.R.Davenne et al. Journal of Energy Storage 14 (2017) 295-310

[39] A review and evaluation of thermal insulation materials and methods for thermal energy storage systems, Willy Villasmil, Ludger J. Fischer, Jörg Woslitschek, Renwable and Sustainable Energy Reviews 103 (2019) 71-84

[40] Energy storage technologies, Overview 2021, Dr. Stefan Oberholzer SFOE 06.12.2021

[41] *Winterstrombedarf und saisonale Wärmespeicher - mit Sommerwärme Strom im Winter sparen.* Positionspapier des Forums Energiespeicher Schweiz Bern. Position paper on seasonal heat storage from the Swiss Forum for Energy Storage (FESS), May 2022, aeesuisse.ch

CORSAIRE

[42] Un ingénieur veut chauffer Genève avec de l'énergie gaspillée, W. van Sprolant, Tribune de Genève 30.11.1992, article de Pierre Ruetschi.

[43] Travail de Master EPFL, W. van Sprolant (1995) *Valorisation des rejets thermiques du CERN dans la Correction saisonnière de la température du réseau public d'eau potable du canton de Genève*.

[44] *Proposal for the CORSAIRE energy projet as part of a sustainable develoment effort*, W. van Sprolant, EPS 10 Trends in Physics, 10th General Conference of the European Pysical Society, September 9-13, 1996, Sevilla (Spain)
[45] Le Projet CORSAIRE à l'Expo 2001, W. van Sprolant, CvS énergies sàrl, 1997
[46] **Plan directeur cantonal de l'énergie de Genève**, (dans le cadre de la Conception générale de l'énergie CGE 2001-2005), rubrique Planification énergétique territoriale, Objectifs chiffrés : **Démarrage du projet CORSAIRE.**
[47] Winter temperature correction of the public drinking water mains by industrial waste heat mass recycling (CORSAIRE process), W. van Sprolant, World Engineers' Convention, 4-9 September 2011, Geneva
[48] From toxic releases to damages on human health : A method for life cycle impact assessment, with a case study on domestic rainwater use. P. Crettaz, Thèse no. 2212 (2000) EPFL 2021.
[49] Traitement de potabilisation des eaux de surface désinfection, Eau de Paris, Conf2006/64.
[50] Référentiel d'analyses du contrôle sanitaire des eaux, ANSES/LHN/REF-CSE - Version 3 Septembre 2020.
[51] Deep Lake Water Cooling (DLWC) https://www.enwave.com/case-studies/enwave-and-toronto-water-tap-into-innovative-energy-source/
[52] https://www.washingtonpost.com/climate-solutions/interactive/2021/toronto-deep-latke-water-cooling-raptors/
[53] https://deepresource.wordpress.com/2020/12/18/database-european-large-scale-solar-heating-plants/
[54] Quelle est la température de l'eau froide du réseau des SIG ? Archive Interroge-Question/réponse Bibliothèques municipales de Genève, 27.08.2015
[55] Bâtiments résidentiels locatifs à haute performance énergétique : objectifs et réalités. J.-M. Zgraggen, Thèse no. 4218 UNIG 2010
[56] Les températures du sol, G.P Williams ; L.W. Gold, février 1977 Archives des publications du CNRC Canada
[57] Les aspects liés à la température de l'eau potable Santé Canada, Ottawa (Ontario) 2021

ULISSE miscellaneous

[58] Centrale de Chauffe par Thermopompes, Domaine Ir et Infrastructures EPFL, CCT /J. SCHMID, 21.04.2015
[59] Plan directeur des énergies 2015-2045, Domaine Ir et Infrastructures EPFL, décembre 2015
[60] Analyse environnementale préliminaire du projet ULISSE, Jean-François Rubin, hepia-inTNE, 2022
[61] Analyse préliminaire des risques liés aux courants lacustres menaçant l'intégrité structurale d'ULISSE, Zsolt Vecsernyes, Laboratoire d'hydraulique appliquée LHA de HEPIA 2022
[62] Robot sous-marin/lacustre suisse de Tethys Robotics https://www.tecindustry.ch/fr/actualites/plonger-avec-proteus.html
[63] Pompes à Chaleur TRANE RTSF, type eau/eau à compresseur à vis www.tranebelgium.com
[64] Bâtiments résidentiels locatifs à haute performance énergétique : objectifs et réalités, Jean-Marc Zgraggen, Thèse 2010 UNIG.
[65] Le procédé CORSAIRE ou Comment réduire de 5 à 10 % l'énergie des immeubles d'une Ville (entière) ? William van Sprolant, CvS énergies sàrl, 01.12.2018
[66] Simulation of an Under Lake Infrastructure for Capture and Storage of Solar Energy (ULISSE) D. Bello-Mendes, R. Rozsnyo (HEPIA), W. van Sprolant CvS Énergies sàrl, COMSOL Conference Munich 2023

Appendix 1: Real experiments on the ULISSE Mock-up

1) 29 July 2022: First hot water injection test in the Mock-up

The volume of the Mock-up is 77 litres (Vm). The loading time is 16 minutes (**water flow rate: 4.7 litres/min**). During loading, the temperature of the mains hot water supply mixer tap is 44°C (measured on the CMM DT-21 multimeter at the outlet of the hydrothermal unit). Figure 1 below shows air bubbles entrained with the water jets at the outlet of the injection and extraction distribution manifold located at the top of the Mock-up. Under the effect of the flow rate or ejection speed, the jets are not perpendicular but at an angle, directed towards the middle of the water column.

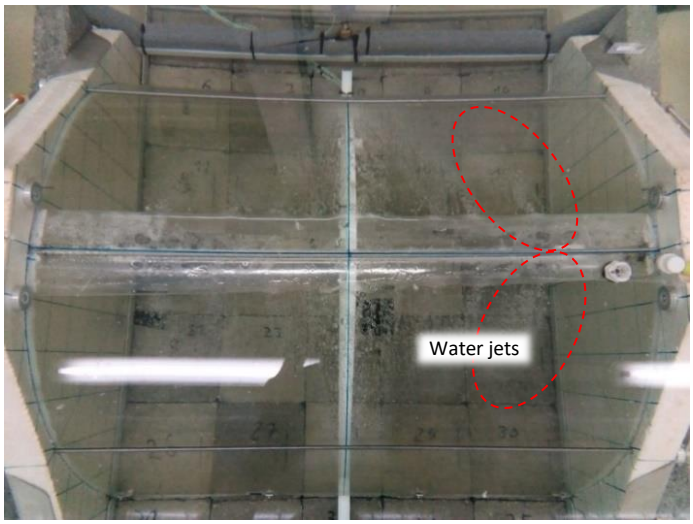

Figure 1: Water jets at the outlet of the distribution ramp of the Mock-up when loaded at 4.7 litres/min.

Graph 2 below shows the temperature measurements by the 14 thermocouples (TCs) distributed throughout the Mock-up. **The recording period extends over 5 days**, from 29 July to 3 August 2022, and covers the long asymptotic cooling to thermal equilibrium with the vessel at around 26˚C.

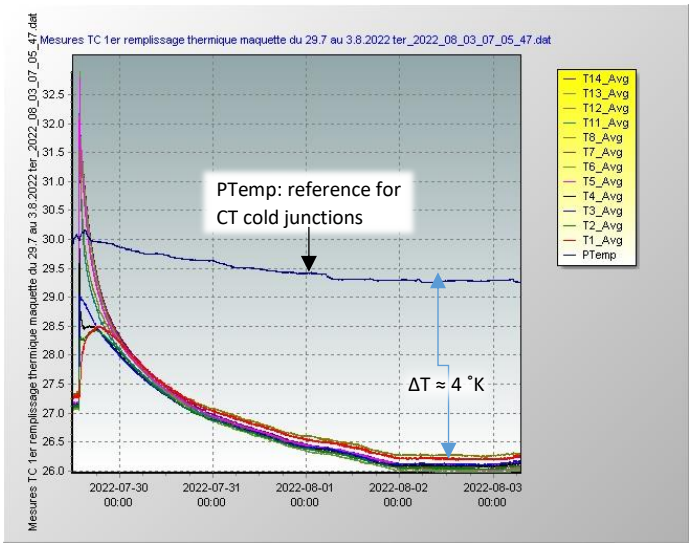

Figure 2: visualisation of hot water loading followed by cooling in the ULISSE Mock-up

Also noteworthy is the large discrepancy of 4 ˚K, between the temperature of the water in the IBC tank (26˚C) and "PTemp" which is the reference temperature of the "cold junctions" of the CTs in the Datalogger. It is close to the temperature of the room during the heatwave in the summer of 2022.

2) Test on 03 August 2022: "Slow" thermal loading of the ULISSE model

The loading time was 97.5 min, with an average flow rate of 0.79 litres/min (77 litres/97.5 min). During charging, the temperature at the outlet of the network's hot water supply mixer fluctuated between 38.5 and 44°C (upstream multimeter CMM DT-21) and was visible on TC9 & TC10 (38-35.5°C). In Figure 15.4, this can also be seen at the top of the model (TC14 & TC17) but not in the centre (TC13 & TC16). To avoid this disturbance, an intermediate thermal stabilisation tank was subsequently used for the hot water which is injected using the diaphragm pump on the hydrothermal unite (HTU).

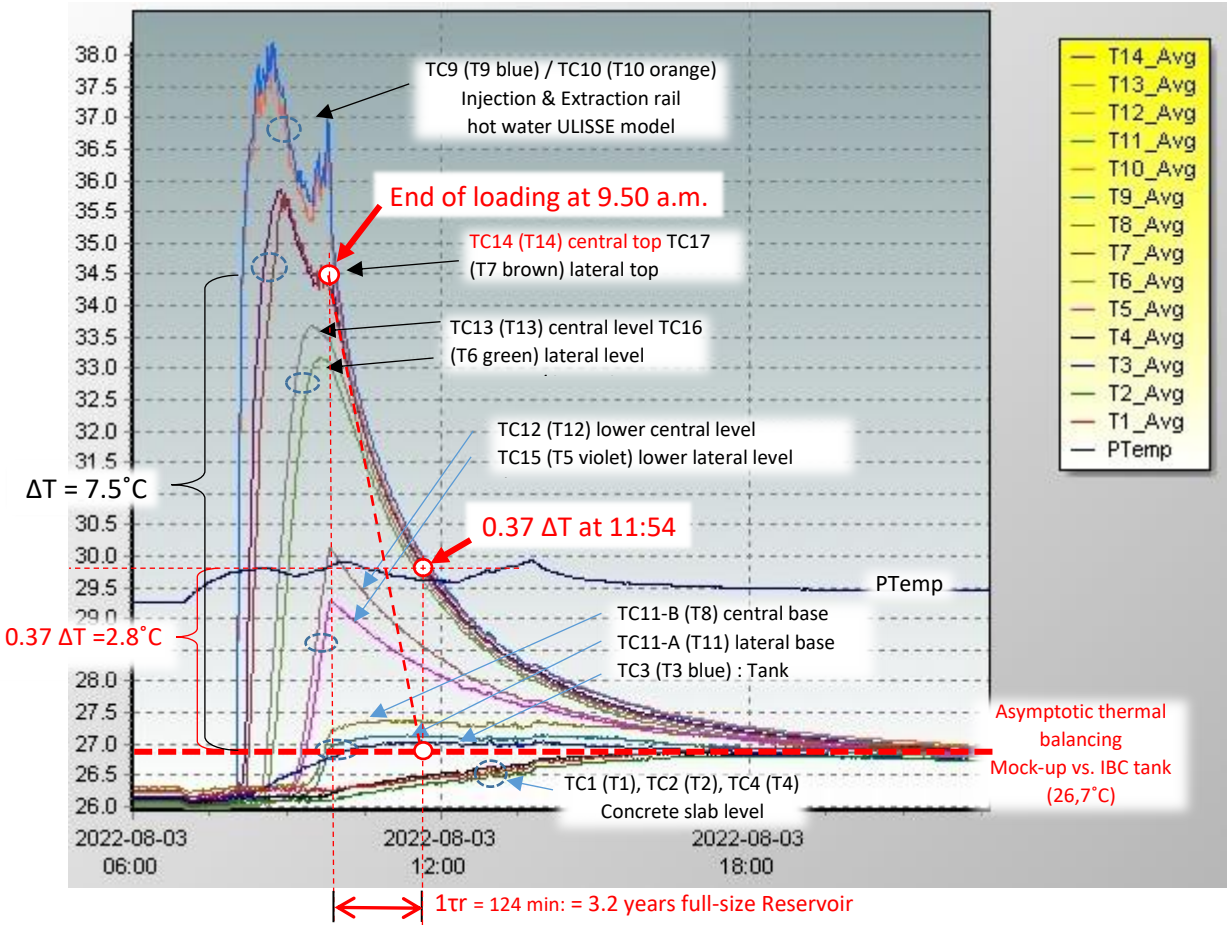

Graph 3: (Slow) loading of hot water into the ULISSE Mock-up followed by asymptotic cooling towards thermal equilibrium with the vessel and with a time constant of 124 minutes (τr).

Graph 3 also shows the (desired) phenomenon of **thermal stratification, with** the temperature curves clearly separated in time by "pair" of thermocouple CTs. Each pair of thermocouples is located at a different level in the model and is distributed horizontally (central thermocouple & lateral thermocouple). With filling from the top of the model (TC9/TC10), the hot water gradually spreads out, horizontally (similar temperatures per pair of thermocouples) and vertically, gradually replacing or pushing down the cold water out of the Mock-up (visualised by the time lag between the pairs of thermocouples), until it reaches the bottom of the IBC tank (concrete slabs).

Heat dissipation through the shell of the ULISSE Mock-up in the IBC tank, as well as in the concrete slabs at the bottom, occurs quite naturally asymptotically at around 26.6°C (IBC test tank temperature). The **cooling time constant *(τr)* is 124 minutes, corresponding to almost 3.2 years for the real ULISSE Reservoir with a volume of 2 million m³.**

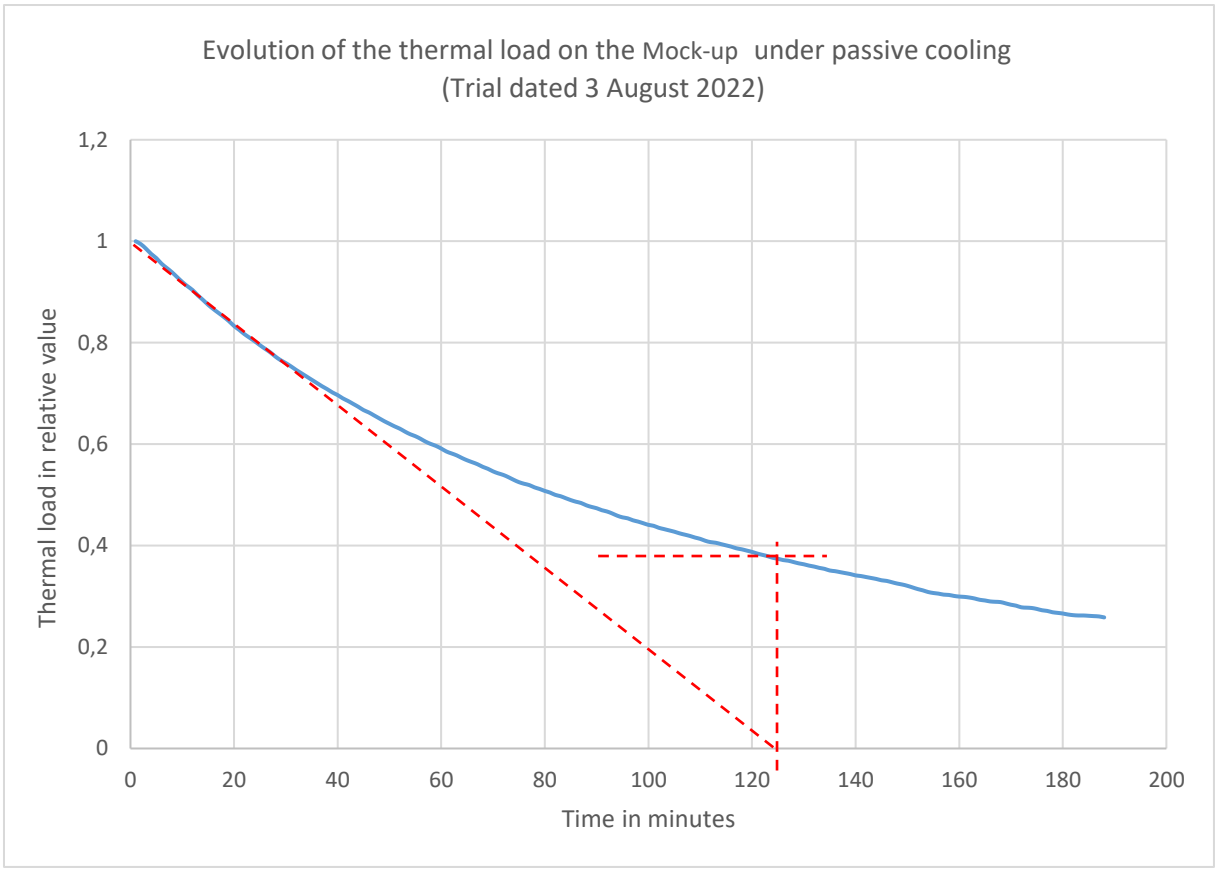

Figure 4: Changes in passive cooling at the top of the Mock-up (average T7, T14) in relative terms

3) Trial on 27 September 2022: (start of Daniel Bello's master's thesis)

To enable the students to familiarise themselves with the numerical modulization of the Mock-up and subsequently the full-size ULISSE Reservoir, we demonstrated the operation of the experimental installation on the Mock-up. In the absence of hot water (the building's domestic hot water system being temporarily out of order), we carried out "reverse" filling (loading), with cold water being introduced from the bottom of the Mock-up by suction at the top of the water via the injection/extraction ramp.

The IBC tank, in which the Mock-up is placed, is first filled with water, via the tank's drain valve, with around 200 litres of cold water taken directly from the Cold-Water Network (CWN). This means that the Mock-up is under about 10 cm of cold water at its base, i.e., 1/3 of its height. For the real Reservoir (in the lake), this corresponds to a stratified layer of cold water of almost 18 m from the bottom of the lake.

Using the diaphragm pump, the water is "*sucked*" out of the Mock-up from above. The water initially in the Mock-up is in thermal equilibrium with that in the rest of the IBC tank (22°C). The extraction of this cold water from the top is therefore progressively replaced by cold water entering from the base of the Mock-up.

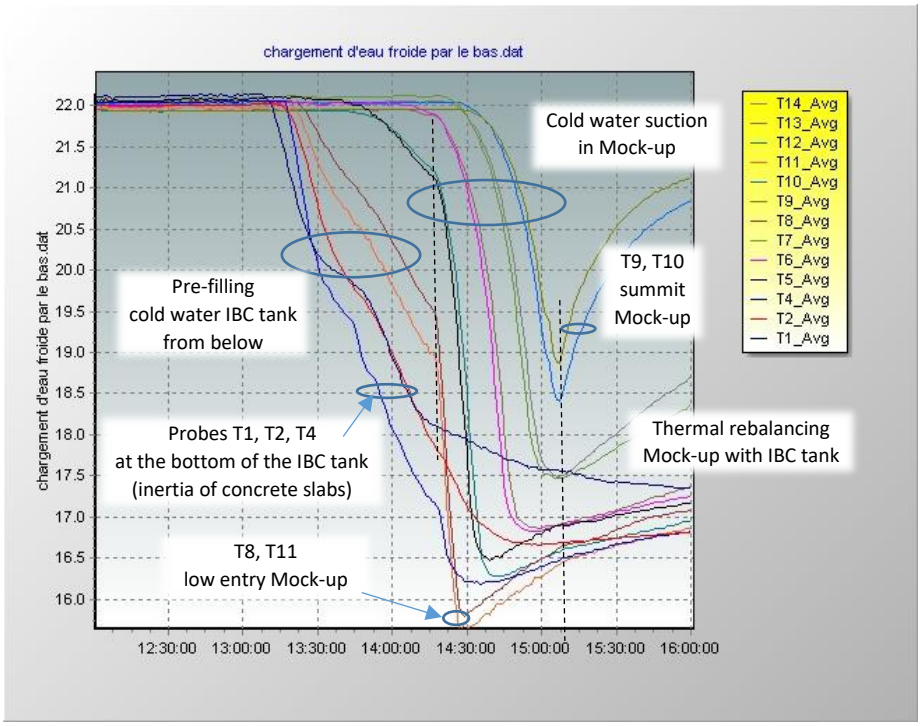

Figure 5: Mock-up cold water filling tests (test on 27.09.2022)

It is clear from graph 5 above that the cold water remains relatively separate from the warmer upper layer (stratification). Since the temperature in the Mock-up is lower than that in the IBC tank at the start of the experiment, the thermal gradient and heat flow through the envelope are reversed, moving naturally from the IBC tank to the Mock-up, which gradually warms up. This phenomenon occurs during the Spring Stagnation (SS) phase, just after the Winter Discharging phase (at the end of the building heating semester), when the ULISSE Reservoir is thermally empty or at its minimum level.

4) Test on 03 October 2022

With domestic hot water restored, we were able to reproduce on the experimental Mock-up a **complete (annual) operating cycle for the ULISSE Reservoir**, comprising: Summer Loading (SL), the Autumn Stagnation phase (AS), Winter Discharging (WD), followed by Spring Stagnation (SS).

Prior to thermal loading of the Mock-up, the (insulated) thermal stabiliser canister was filled with 100 litres of water at 37°C, which was then injected into the model (SL) using the membrane pump. Water extraction (WD) is carried out in reverse (Mock-up => canister).

Figure 6: Hot water cylinder (glass wool insulation all round)

The stagnation phases (AS, SS) on the Mock-up lasted 6 minutes (2 months in reality), while the loading and discharging phases took place over an hour (60 min), with a water flow in the Mock-up (1.4 lit/min, or 850 Hz on the flow meter). The Time Scale Factor (TSF) between the real Reservoir and the Mock-up is 13,715. As a result, the temperature drop is "overestimated" (over-expressed) on the Mock-up, compared with the real Reservoir, given that the 60 minutes on the Mock-up actually correspond to 1 year and 8 months for the real Reservoir in the lake.

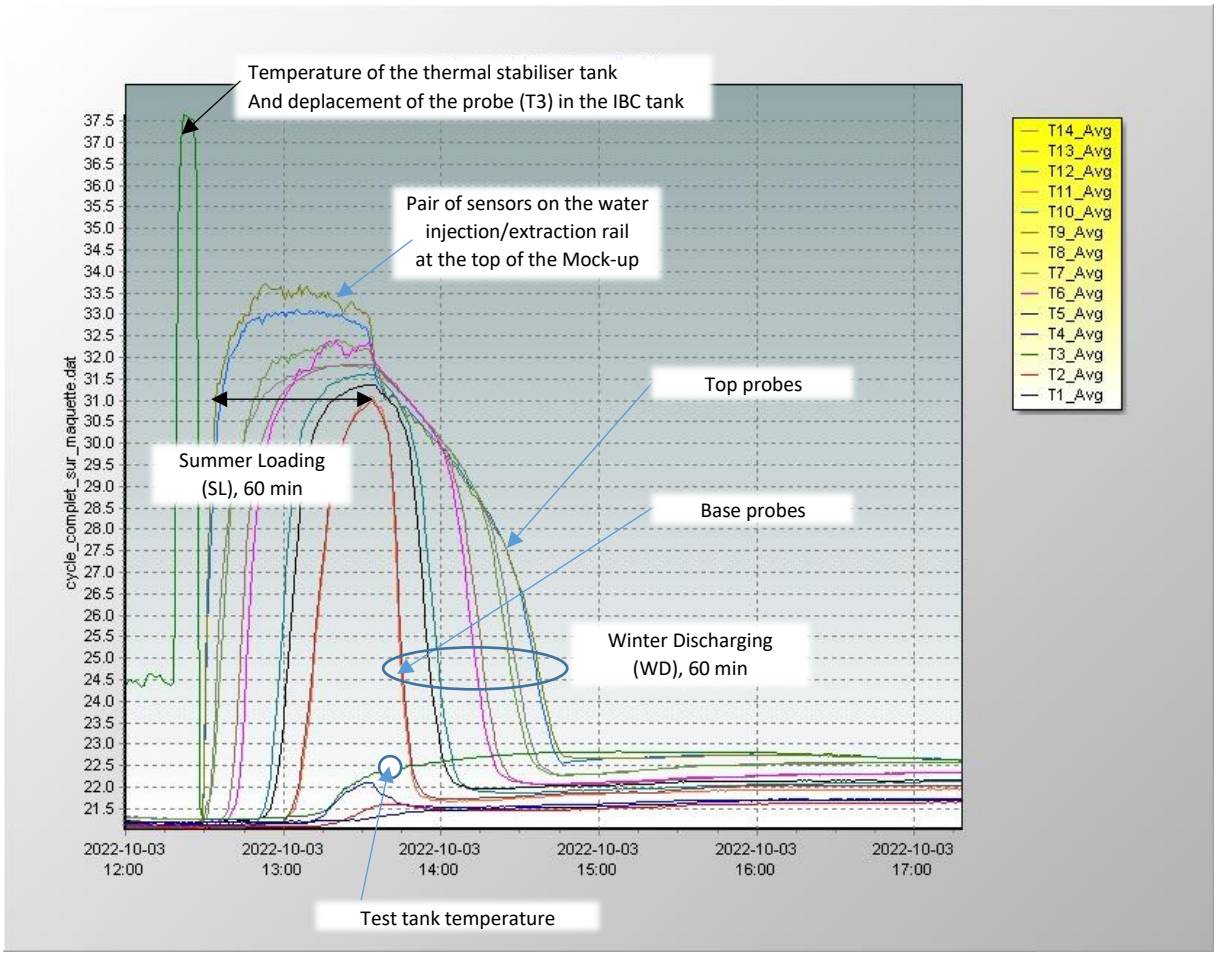

Figure 7: Graph showing temperature readings from the thermocouples in the Mock-up (test 03.10.2022)

During this experiment, we observed a **marked thermal stratification** during the loading and unloading of water from the Mock-up (temporal shift in temperatures between pairs of thermocouples located at the same height). In particular, the water temperature at the extraction point falls last.

Furthermore, at the end of the "reduced" time for unloading the Mock-up, probes T9 and T10 on the extraction ramp at the top indicate a temperature that is still higher than that of the tank. This means that the Mock-up still contains a certain amount of heat compared with the temperature of the IBC tank (lake). This is because the *flat-fronted thermocline* tends to straighten out and partially dilutes the upper hot water with the lower cold water. The result is that **to extract all the heat from the Mock-up, more water would have to be pumped out than the initial volume of the Mock-up, and this obviously also applies to the real ULISSE Reservoir in the lake**!

It can also be seen that the temperature at the TC14 thermocouples at the top-central and -lateral TC17 is about 1˚C lower than when hot water (TC9 and TC10) is injected into the Mock-up. The reason for this is that during hot water charging, heat loss takes place simultaneously.

5) Test on 03 November 2022 (loading with insulating jacket)

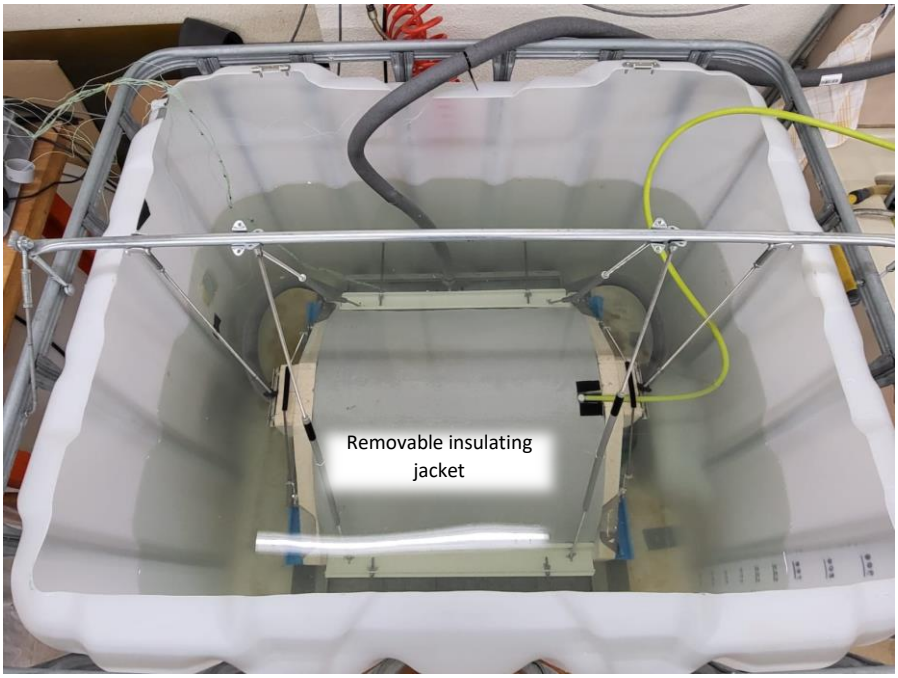

Figure 8: ULISSE Mock-up with removable insulating jacket during thermal loading (test 03.11.2022)

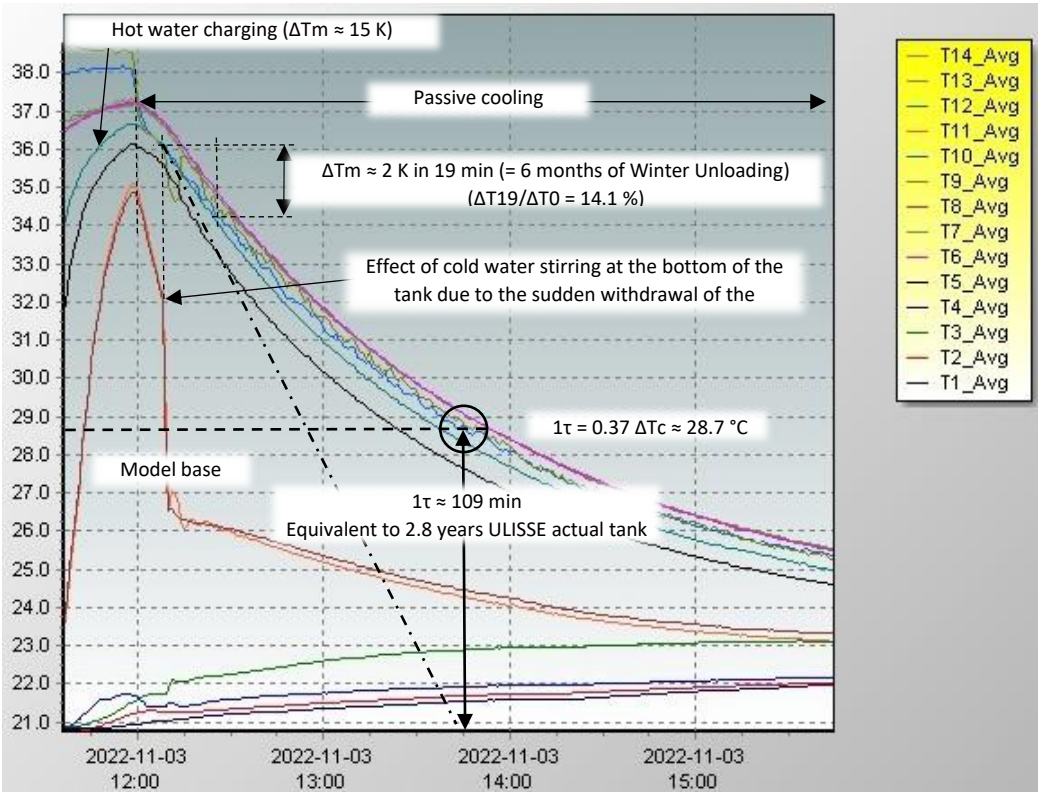

Figure 9: Temperature trends in the Mock-up after thermal loading (with insulating jacket) and passive cooling without jacket (test on 03.11.2022)

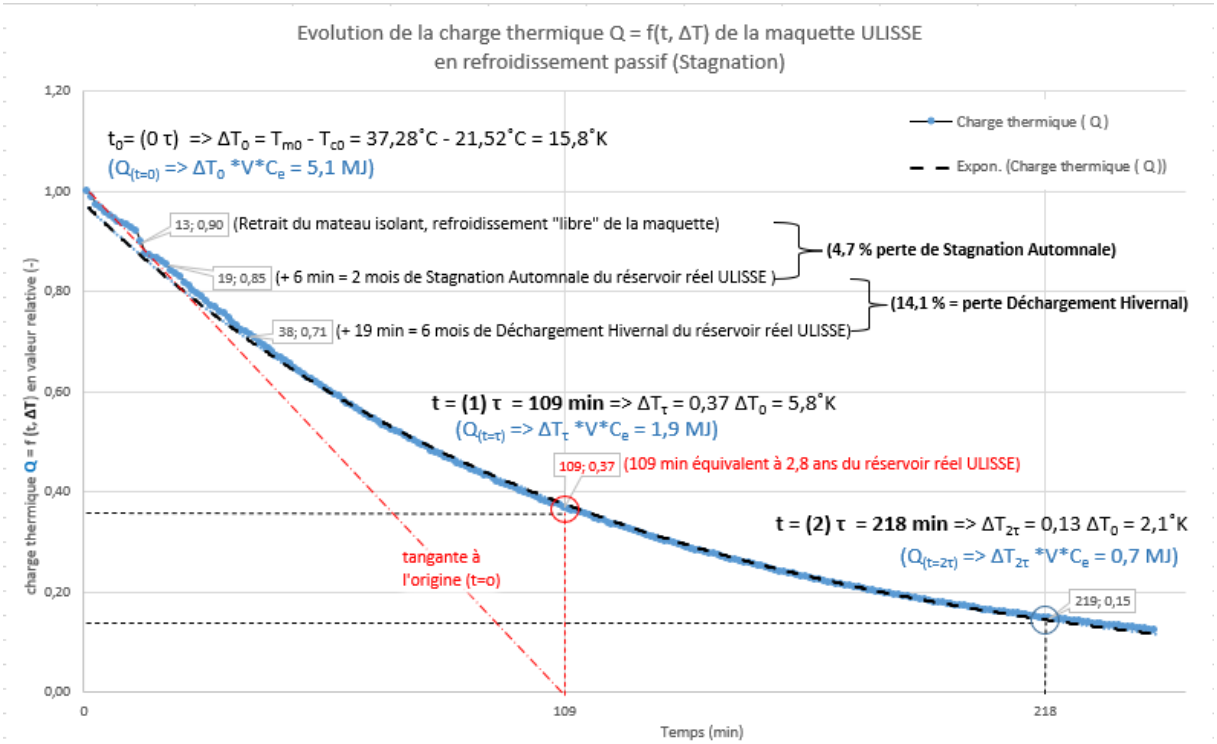

Graph 10: Evolution of the thermal load (Q) or energy-heat content of the Mock-up during its passive cooling, following a decreasing exponential with a time constant τ *= 109 min)*

1τ = 0.37 ΔTm(t0) = 0.37 *(Tm(t0) - Tc) 0.37 *(37.28˚C - 21.52˚C) = 5.8˚K; Tm @ t=1τ = 28.7 ˚C

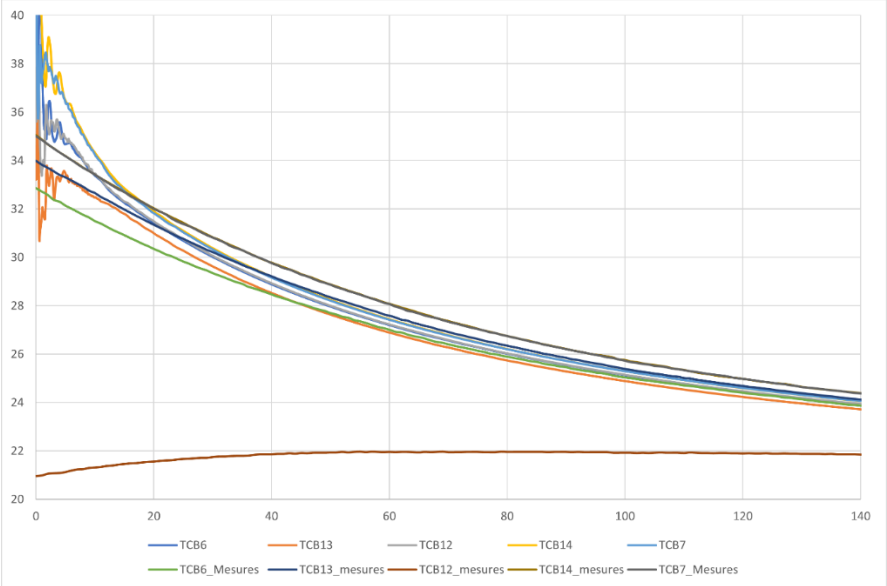

Figure 11: Comparison of the results of cooling measurements during the stagnation of the Mock-up after half a thermal load, with those of the numerical simulation (COMSOL).

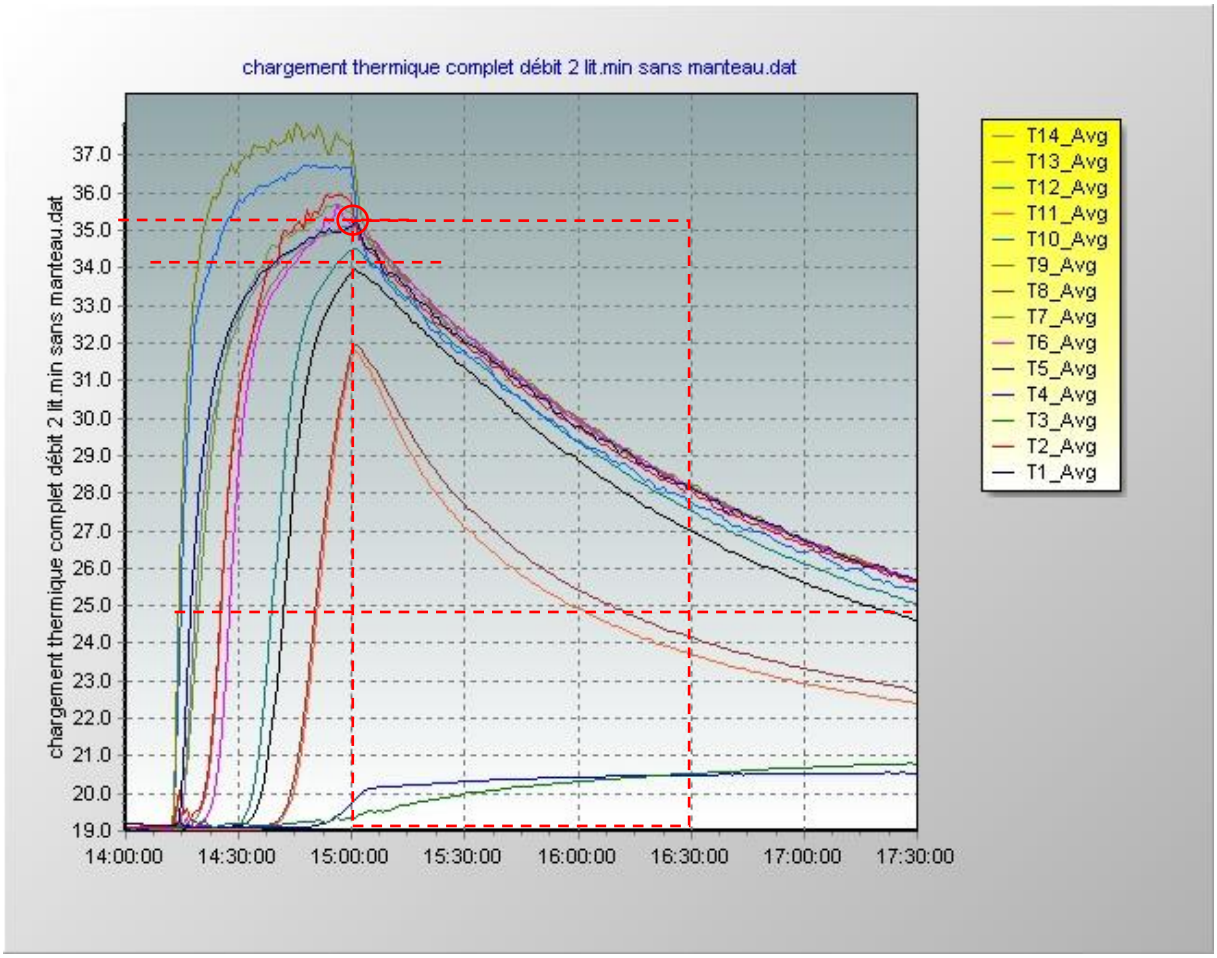

Figure 12: Complete loading and cooling Mock-up without insulating jacket, 22 November 2022

Preliminary modifications to thermocouple probes:

Place TC8 thermocouple on top of probe support and connect to Datalogger channel T1. Place TC5 thermocouple on probe support (next to TC16 for control of the latter) and connect to Datalogger channel T2.

6) Test on 24 November 2022: Full thermal load and discharge of the Mock-up

The Mock-up (with a volume of around 77 litres) was (over)charged in 36 minutes with 80 litres (104%) of water at a temperature of around 38 ˚C, i.e., at an average flow rate of 2.2 litres/min. The hot water injected in excess of the Mock-up 's capacity (3 litres) automatically "overflows" into the IBC tank.

After one minute (hydraulic switching of the pump), the Mock-up was discharged of its hot water with a flow rate slightly increased to about 2.3 lit/min (instability?) and prolonged for 43 minutes, i.e., 84 litres. The discharge was extended beyond the volume of the Mock-up (109%) until the temperature of the extracted water reached that of the IBC tank (≈19˚C), so that all the heat energy had been extracted (in thermal equilibrium with the IBC tank).

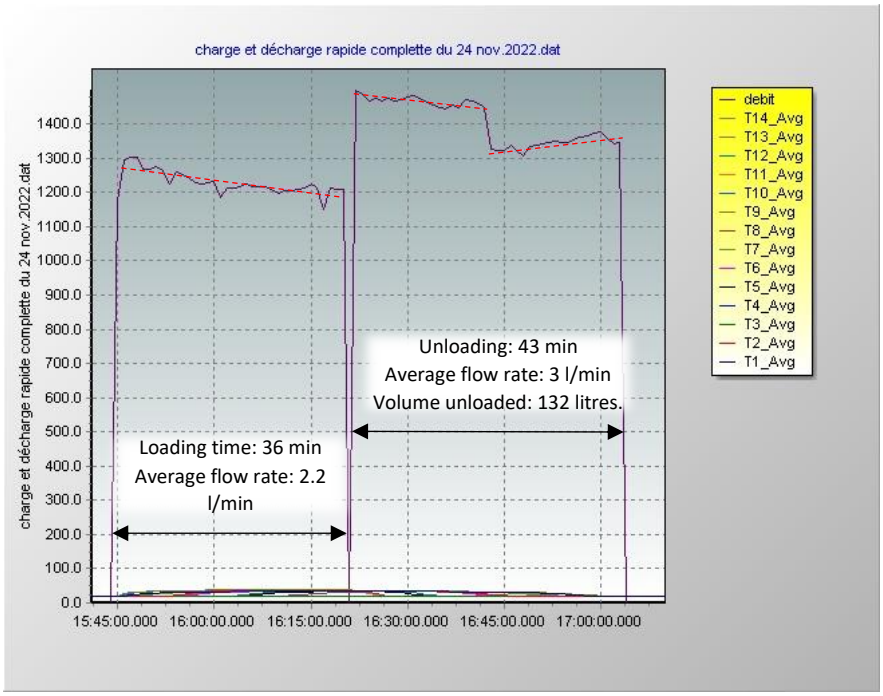

Figure 13: Flow profile (Hz) for thermal loading and unloading of the Mock-up (test 24.11.2022)

We can see that the temperature in the Mock-up changes gradually over time and almost in parallel at all levels. This indicates that a vertical and durable thermal stratification is created in the Mock-up, i.e., there is virtually no thermal mixing between the hot water injected from above and the colder water pushed downwards out of the Mock-up, and vice versa throughout the unloading process.

The temperature of the **TC9 and TC10** thermocouples **shows a curvature that does not correspond exactly to the temperature of the water injected into the Mock-up** (constant at nearly 38˚C). This is due to the fact that the thermocouples in question are fixed to the outer wall of the water injection and extraction manifold. The latter is made of brass and is immersed in the water inside and at the top of the Mock-up, which means that the T9 and T10 thermal probes are influenced (close to) by the surrounding temperature. This would lead to an error in the calculation (underestimation) of the introduction of heat into the Mock-up based on the continuous recording of T9 and T10, and consequently to an underestimation of the heat loss during loading!

During the 36 minutes of loading, the Mock-up loses heat through its envelope to the IBC tank (Qp). This can be seen in the figure by the fact that at the end of the charge, at all levels of the Mock-up, the temperature is lower than at the start (T9 and T10).

Given the hyperbolic cross-sectional shape of the envelope, the volume of water involved increases as you go down into the Mock-up. In other words, the lower temperature sensors are associated with a progressively larger volume of water. The average temperature of the hot water stock in the Mock-up therefore corresponds a priori to that between T12 and T13 (at half volume), i.e., approximately 35˚C. This represents a loss (ΔTpc) of 3˚K on an initial loading of 19˚K or nearly 16%.

During the 43 minutes of the unloading phase, the "extraction" temperature (T9 & T10) also varies continuously due to the accumulation of heat losses throughout the loading and unloading processes. However, the temperature displayed by T9 and T10 corresponds to the temperature of the water sucked out of the Mock-up by the pump.

It should be noted that, given the Time Scale Factor (13'715) between the full-size ULISSE Reservoir in the lake and the Mock-up, the loading (36 min) and unloading (43 min) times in the Mock-up are proportionately disproportionate (600 and 230% respectively). All other things being equal, the heat losses are therefore a priori also overestimated.

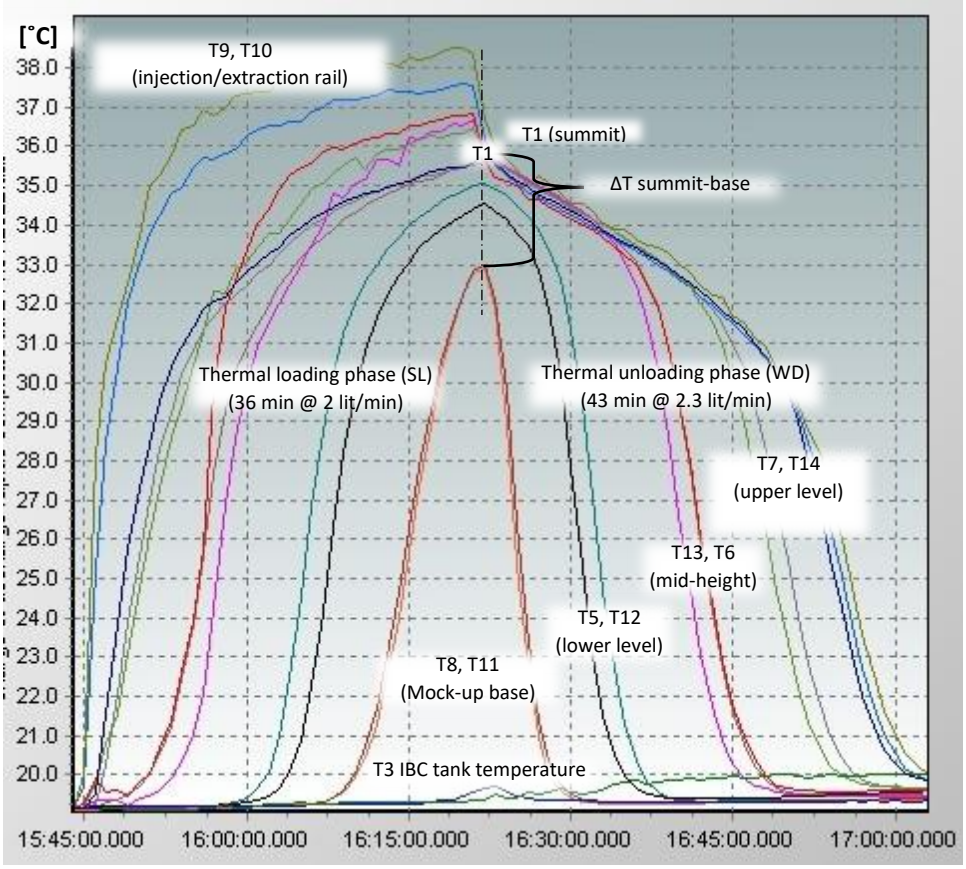

Figure 14: Temperature profile at different levels in the ULISSE model during a thermal loading and unloading cycle (test 24.11.2022)

To comply with this time scale factor (TSF), the loading time of the Mock-up should be reduced to 6 minutes for the 77 litres of its volume and the corresponding flow rate should be increased to 13 litres/min. The associated heat loss would also have to be reduced by a factor of 6 and therefore be limited to around 3%.

However, the energy issue (electricity savings) is less crucial in the summer loading phase than in the winter discharging phase or the building heating period.

Similarly, to comply with the time scale factor, the time and flow rate for unloading the Mock-up should be increased to 18.5 min and 4.3 l/min respectively (limited to the 77-litre volume of the Mock-up) or for a complete thermal drain of 98 litres, i.e., a flow rate of 5.3 l/min. Here too, the corresponding heat losses should be reduced in the same proportion.

The useful energy extracted from the Mock-up (Q-ext) can be determined by integrating, during the unloading period, the product of the flow rate (D) with the temperature difference between the water extracted from the Mock-up and that in the IBC tank (ΔTm-c) and the heat density of the water (c_e):

$$Q\text{-ext} = \int dD_* \, \Delta Tm\text{-}c_* \, c_e = \quad 3.43 \quad [MJ] \quad 0.95 \quad [kWh] \quad (...)$$

With the Datalogger recording the flow rate and the temperatures of T9, T10 (extraction), T3 (IBC tank temperature), the Excel calculation gives the value of Q-ext equal to 3.43 MJ or 0.95 kWh.

The ratio between the energy-heat extracted (Q-ext) and that introduced (Q-int) gives an initial estimate of the gross storage efficiency (GSE) of the Mock-up:

$$GSE = Q\text{-ext} / Q\text{-int} = 3.43 \text{ MJ} / 5.78 \text{ MJ} = 0.59 \quad 59 \quad [\%]$$

Given the length of the loading and unloading cycle (36 + 43 = 79 min), the loss of heat (Q-P = Q-int - Q-ext = 2.35 MJ) represents 41% of Q-int. It is logically proportional to the length of the cycle in question. Consequently, by reducing the cycle time to 24.5 min (6 + 18.5 min) compared with 79 min, in order to respect the time scale factor, the heat loss (Q-pr) should be reduced to 0.73 MJ, or 13% of Q-int:

$$Q\text{-pr} = Q\text{-p} * (24.5 \text{ min}/79 \text{ min}) = \quad 0.73 \text{ [MJ]} => 13 \text{ \% of Q-int}$$

7) Test on 19 December 2022: Full thermal load and discharge of the Mock-up

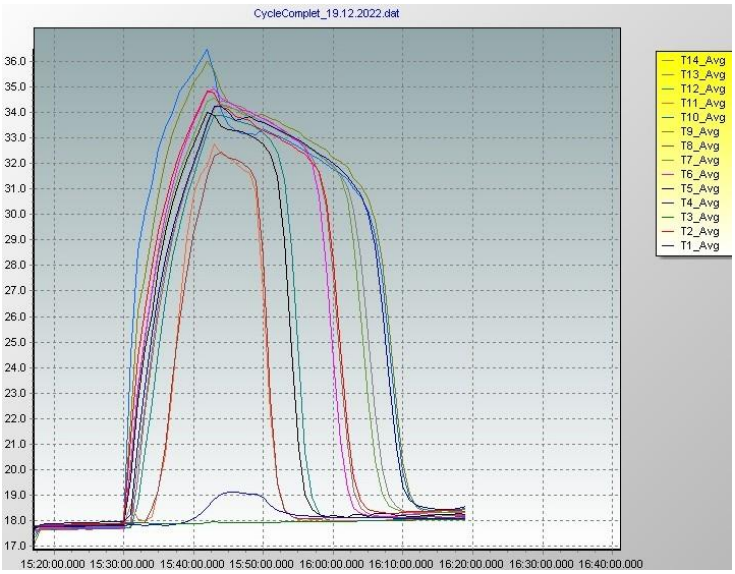

Figure 15: Temperature profile at different levels in the ULISSE Mock-up during a complete thermal loading, stagnation and unloading cycle (test 19.12.2022)

Summer Loading Phase (SL)

The Mock-up (with a volume of approximately 77 litres) is charged in 14 minutes with 91 litres (118%) of water at a temperature of approximately 36 ˚C, i.e., an average flow rate of 6 lit/min. Based on the actual injection temperature (≈ 36˚C) and that of the IBC tank (≈ 18°C), i.e., a ΔT = 18.3 K, the Gross Injected Heat (GIH) is nearly 7 MJ (1.94 kWh). Taking into account heat dissipation during the thermal loading phase, the increase in average temperature in the Mock-up compared with the IBC tank temperature (TC3) is 16.06 K and the Net Thermal Load (NTL) is approximately 5.18 MJ (1.44 kWh), which corresponds to a Loading Thermal Loss (LTL) of 1.8 MJ (0.5 kWh) or 26% of the GIH.

19/12/2022									Cumul		Volume
Temps	débit	Cum volume	ΔT9 (°K)	ΔT10 (°K)	ΔTmoy-9-10	Q	Q max	P max	QBC	QBC	Maquette
(min)	(Lit/min)	(lit)	(°K)	(°K)	(°K)	(KJ)	(KJ)	(KW)	(KJ)	(%)	(%)
1	5,05	5,05	-0,13	-0,08	-0,10	-2,22	386,89	6,45	386,89	5,5%	6,6%
2	3,21	8,26	-0,11	-0,06	-0,09	-1,14	246,17	4,10	633,06	9,1%	10,7%
3	6,65	14,91	-0,12	-0,06	-0,09	-2,51	509,97	8,50	1 143,03	16,4%	19,4%
4	6,28	21,19	4,08	6,58	5,33	140,19	481,85	8,03	1 624,88	23,3%	27,5%
5	6,38	27,56	8,31	10,65	9,48	252,98	488,88	8,15	2 113,76	30,3%	35,8%
6	6,28	33,85	9,67	12,16	10,92	287,01	481,73	8,03	2 595,49	37,2%	44,0%
7	6,35	40,20	11,41	13,34	12,38	329,03	487,09	8,12	3 082,58	44,2%	52,2%
8	6,36	46,55	12,84	14,68	13,76	366,04	487,35	8,12	3 569,93	51,1%	60,5%
9	6,36	52,91	14,22	15,49	14,86	395,59	487,86	8,13	4 057,79	58,1%	68,7%
10	6,40	59,31	15,26	16,12	15,69	420,12	490,54	8,18	4 548,34	65,1%	77,0%
11	6,38	65,69	16,01	16,95	16,48	440,36	489,52	8,16	5 037,86	72,2%	85,3%
12	6,32	**72,01**	16,61	17,31	16,96	448,57	484,54	8,08	5 522,40	79,1%	93,5%
13	6,36	**78,37**	17,29	17,68	17,49	465,26	487,48	8,12	6 009,87	86,1%	101,8%
14	6,33	84,69	17,64	18,18	17,91	474,19	485,05	8,08	6 494,92	93,0%	110,0%
15	6,35	91,05	18,08	18,56	18,32	487,09	487,09	8,12	6 982,02	100,0%	118,2%
15	**6,07**	**91,05**	**Chargement Thermique Brute (CTB) :**			**6 982,02**	(KJ)	**1,94**	(kWh)	100%	(CTB)
Temps	**Débit moy.**	Total	**Chargement Thermique Nette (CTN) :**			**5 177,83**	(KJ)	**1,44**	(kWh)	74%	(CTN/CTB)
(min)	(lit,/min)	(Lit)	**Perte Thermique Chargement (PTC) :**			**1 804,18**	(KJ)	**0,50**	(kWh)	26%	(PTC/CTB)

Table 16: Thermal loading phase of the Mock-up (test 19.12.2022)

Autumn Stagnation phase (AS)

The Autumn Stagnation phase (AS) of the Mock-up is 6 min (2 months of full-scale ULISSE Reservoir). The temperature at the beginning (33.97˚C) and end of stagnation (30.68˚C) is the average of the 13 thermocouples located in the Mock-up. The result is an average Stagnation Temperature Drop (STD: ΔTs = 0.83˚C), which corresponds to a Stagnation Thermal Loss (STL) of 266.18 KJ or 0.07 kWh i.e. 3.8% of the Net Thermal Load (NTL at the end of summer loading); this is based on the 77 litre volume of the Mock-up (Vm) and the specific heat by volume of the water (c_{ev} = 4.186 KJ/lit.K):

$$STL = \Delta Ts * \Delta Tsm * c_{ev} = \quad 266.18\ [KJ] \text{ or } 0.07\ [kWh] \quad (...)$$

	Phase de stagnation automnale														
19/12/2022	TC8	TC5//TC16	TC3	TC4	TC15	TC16	TC17	TC11-B	TC9	TC10	TC11-A	TC12	TC13	TC14	débit
	Sommet	Contr. TC16	Eau Cuve	Fond béton	ifférieure laté	milieu centra	ommet latér	base central	Injection /	Extraction	base latéral	ifférieur cent	milieu latéra	ommet centr	(Hz)
15:43:00	34,22	34,74	17,95	18,86	33,88	34,91	34,54	32,3	35,65	35,53	32,75	33,86	34,16	34,15	0
15:44:00	34,22	34,21	17,93	19,03	33,45	34,55	34,28	32,45	34,82	34,02	32,36	33,87	34,45	34,32	0
15:45:00	34,01	34,1	17,91	19,12	33,33	34,38	34,18	32,19	34,38	33,53	32,25	33,79	34,39	34,25	0
15:46:00	33,69	33,84	17,91	19,12	33,28	34,23	34,1	32,18	34,25	33,28	32	33,67	34,26	34,13	0
15:47:00	33,75	33,76	17,91	19,1	33,22	34,09	33,93	31,99	34,04	33,18	31,76	33,6	34,18	34,01	0
15:48:00	33,82	33,67	17,92	19,06	33,1	34,03	33,82	31,76	33,81	33,15	31,61	33,5	34,01	33,9	0
	-0,14	1,43	-0,01	-0,52	1,02	0,93	0,79	0,16	2,12	3,36	1,01	-0,2	-0,29	-0,28	
	ΔTC8 (°K)	ΔTC5 (°K)	ΔTC3 (°K)	ΔTC4 (°K)	ΔTC15 (°K)	ΔTC16 (°K)	ΔTC17 (°K)	ΔTC11-B (°K)	ΔTC9 (°K)	ΔTC10 (°K)	ΔTC11-A (°K)	ΔTC12 (°K)	ΔTC13 (°K)	ΔTC14 (°K)	

Température moyenne Début Stagnation (TDS) :	33,97	(°C)	<= Température moyenne Fin Chargement (TFC)		
Température moyenne Fin Stagnation (TFS) :	33,35	(°C)	Durée Phase Stagnation (DPS) : 6 minutes		
Chute Température moyenne Stagnation (CTS) :	0,83	(°C)		2,4%	(CTS/ATC)
Perte Thermique moyenne Stagnation (PTS) :	266,18	(KJ)	0,07	(kWh)	3,8% (PTS/CTN)

Table 17: Stagnation phase, change in temperature in the model (13 thermocouples) (test 19.12.2022)

Winter Discharging Phase (WD)

The Mock-up was "thermally" discharged of its hot water at a relatively stable rate of 3.9 lit/min for 19 minutes (100% of the Mock-up's 77 litre volume) and this was extended to 27 minutes or 109.5 litres. The discharge was extended beyond the volume of the Mock-up (142%) until the temperature of the extracted water reached that of the IBC tank (≈ 18˚C) in order to extract all the heat (in thermal equilibrium with the IBC tank).

The useful heat extracted from the Mock-up (Q-ext) or the heat of the Net Thermal Discharge (NTD) can be determined by integrating, during the discharge period, the product of the flow rate (D) and the difference (ΔTm-c) in temperature between the water extracted from the Mock-up (Tm) and that in the IBC Tank (Tc):

$$\text{NTD} \quad Q\text{-ext} = \int dD * \Delta Tm\text{-}c * c = \quad 4.47 \ [MJ] \quad 1.24 \ [kWh] \quad (...)$$

With the Datalogger recording the flow rate and the temperatures of T9, T10 (extraction), T3 (IBC tank temperature), the calculation (summation) with Excel gives the value of Q-ext (NTD) equal to 0.95 MJ or 0.95 kWh.

Given the volume (Vm) of the Mock-up, the Initial Discharging Capacity (IDC) is 77 litres, and the actual heat capacity (Q-cap) is only 5.9 MJ. The rest is expelled from the Mock-up:

$$IDC = Vm * \Delta Tm\text{-}c * C = 77 \text{ lit.} * 18.3°C * 4.186 \text{ MJ/lit.} = 4.97 \ [MJ]$$

The ratio between the heat extracted from the [MJ] (Q-ext, NTD) and that Initially Discharged (IDC) after stagnation heat loss (STL) gives the Discharge Efficiency (DE):

$$DE = NTD/IDC = 4.47 \text{ MJ} / 4.97 \text{ MJ} = \quad 90 \ [\%] \quad (...)$$

The heat loss during the Discharging phase (DHL) is 0.49 MJ (0.14 KWh).

The actual Storage Efficiency of the Mock-up is then:

$$\text{Mock-up SE} = Q\text{-ext} / Q\text{-cap} = 4.63 \text{ MJ} / 5.9 \text{ MJ} = 0.78 \quad 78 \ [\%]$$

19/12/2022		Cumul						Cumul		Volume
Temps	débit	Volume	ΔT9 (°K)	ΔT10 (°K)	ΔTmoy-9-10	QND	PND	QND	QND	Maquette
(min)	(Lit/min)	(lit)	(°K)	(°K)	(°K)	(KJ)	(KW)	(KJ)	(%)	(%)
1	3,89	3,89	15,95	15,19	15,57	253,53	4,23	253,53	5,7%	0,1%
2	3,95	7,84	16,00	15,44	15,72	259,93	4,33	513,46	11,5%	10,2%
3	3,94	11,78	15,83	15,27	15,55	256,57	4,28	770,03	17,2%	15,3%
4	3,91	15,69	15,72	15,13	15,43	252,36	4,21	1 022,39	22,9%	20,4%
5	3,98	19,67	15,53	15,02	15,28	254,38	4,24	1 276,77	28,5%	25,5%
6	3,78	23,44	15,41	14,85	15,13	239,09	3,98	1 515,86	33,9%	30,4%
7	3,89	27,33	15,27	14,68	14,98	243,74	4,06	1 759,60	39,3%	35,5%
8	3,91	31,24	15,04	14,51	14,78	241,93	4,03	2 001,53	44,7%	40,6%
9	3,90	35,15	14,87	14,36	14,62	238,70	3,98	2 240,22	50,1%	45,6%
10	3,90	39,04	14,70	14,19	14,45	235,72	3,93	2 475,94	55,3%	50,7%
11	3,88	42,92	14,57	13,98	14,28	231,55	3,86	2 707,49	60,5%	55,7%
12	3,91	46,83	14,26	13,80	14,03	229,83	3,83	2 937,32	65,7%	60,8%
13	3,86	50,70	14,11	13,64	13,88	224,39	3,74	3 161,71	70,7%	65,8%
14	3,92	54,62	13,87	13,39	13,63	223,85	3,73	3 385,56	75,7%	70,9%
15	3,83	58,45	13,43	13,05	13,24	212,27	3,54	3 597,82	80,4%	75,9%
16	3,84	62,29	13,12	12,68	12,90	207,54	3,46	3 805,36	85,1%	80,9%
17	3,87	66,16	12,65	12,16	12,41	200,79	3,35	4 006,15	89,6%	85,9%
18	3,91	70,06	11,77	11,22	11,50	187,90	3,13	4 194,05	93,8%	91,0%
19	3,92	73,98	10,16	9,48	9,82	161,00	2,68	4 355,05	97,4%	96,1%
20	3,96	**77,94**	7,51	6,78	7,15	118,39	1,97	4 473,44	100,0%	**101,2%**
21	3,93	81,87	4,59	3,97	4,28	70,41	1,17	4 543,85	101,6%	106,3%
22	3,98	85,85	2,31	1,94	2,13	35,42	0,59	4 579,27	102,4%	111,5%
23	3,94	89,79	1,01	0,88	0,95	15,59	0,26	4 594,86	102,7%	116,6%
24	3,94	93,73	0,48	0,52	0,50	8,25	0,14	4 603,11	102,9%	121,7%
25	3,90	97,63	0,33	0,42	0,37	6,12	0,10	4 609,23	103,0%	126,8%
26	3,94	101,57	0,29	0,38	0,34	5,53	0,09	4 614,75	103,2%	131,9%
27	3,95	105,52	0,29	0,39	0,34	5,61	0,09	4 620,37	103,3%	137,0%
28	3,99	109,50	0,29	0,37	0,33	5,51	0,09	**4 625,87**	**103,4%**	142,2%
	3,91	**Total (Lit)**		Temps ≈ 100 % volume maquette: 19 minutes						
	Débit moy,	(lit,/min)		Temps ≈ 142 % volume maquette : 27 minutes						
		Charge thermique Initiale de Déchargement (CID) :			**4 972,89**	(kJ)	**1,38**	(kWh)	**100,0%**	(CID)
		Déchargement Thermique Nette (DTN) :			**4 473,44**	(kJ)	**1,24**	(kWh)	**90,0%**	(DTN/CID)
		Perte Thermique Déchargement (PTD) :			**499,45**	(KJ)	**0,14**	(kWh)	**10,0%**	(PTD/CID)
							Perte Exploitation Nette (PEN) :		9,65%	(PTD/CTN)

Table 18: Thermal discharging phase of the Mock-up (test 19.12.2022)

8) Test on 20 December 2022: Full charge and discharge of the Mock-up with grid

During this cycle, in order to reduce or eliminate mixing when hot water is injected at the top of the Mock-up, a distribution grid with a layer of fibreglass felt is placed under the injection bar.

Figure 19: Felt layer under the injection rail in the Mock-up (water injection flow distributor)

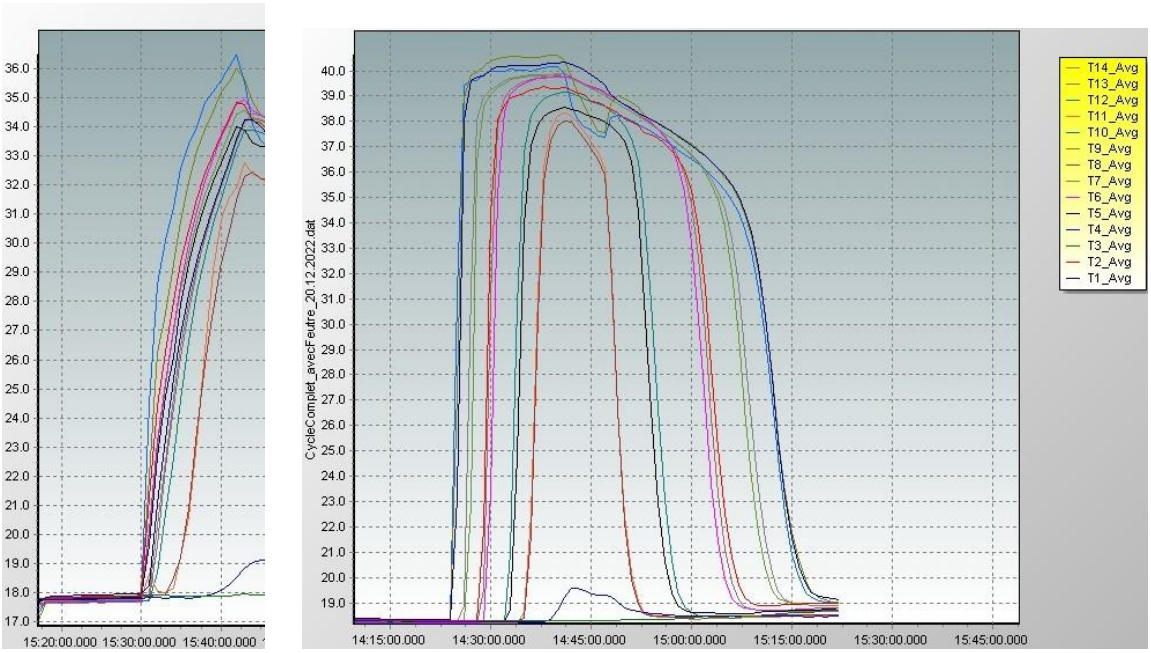

Figure 20: Comparison of stratification during the loading phase, without (left-hand diagram) and with (right-hand diagram) a grid + felt distributing the water injection flow (identical flow rate) via the top ramp of the Mock-up.

Thermal Summer Loading phase (SL):

The Mock-up (with a volume of 77 litres) is (over)charged (136%) in 17 minutes with an average flow rate of 6.21 lit/min, i.e., 106 litres (Vi) of water at an injection temperature of 40˚C. Relative to the IBC tank temperature (≈ 18°C), i.e., a ΔTc = 22.1K, the gross heat energy (GHE) injected into the Mock-up is 9.8 MJ (2.7 kWh).

$$GHE = Vi.c.\ \Delta Tc = 106*4.186*22.1 = \quad 9.8\ [MJ] \quad 2.7\ [kWh] \quad (...)$$

Temps (h:m:s)	débit (Lit/min)	Cum volume (lit)	ΔT9 (°K)	ΔT10 (°K)	ΔTmoy-9-10 (°K)	Q (KJ)	Q max (KJ)	P max (KW)	Cumul Q (KJ)	Part Q (%)	Part volume maquette (%)
14:24:00	6,46	6,46	-0,09	-0,03	-0,06	-1,62	597,64	9,96	597,64	6,1%	8,3%
14:25:00	6,20	12,66	9,09	12,85	10,97	284,78	573,59	9,56	1 171,23	12,0%	16,3%
14:26:00	6,13	18,79	20,65	21,12	20,89	535,91	566,96	9,45	1 738,19	17,8%	24,2%
14:27:00	6,28	25,08	21,55	21,31	21,43	563,65	581,14	9,69	2 319,33	23,7%	32,2%
14:28:00	6,19	31,27	21,65	21,32	21,49	557,00	572,82	9,55	2 892,15	29,6%	40,2%
14:29:00	6,17	37,44	21,85	21,52	21,69	559,62	570,20	9,50	3 462,35	35,4%	48,1%
14:30:00	6,18	43,62	22,10	21,69	21,90	566,41	571,59	9,53	4 033,94	41,3%	56,1%
14:31:00	6,20	49,82	22,17	21,70	21,94	569,44	573,59	9,56	4 607,53	47,2%	64,0%
14:32:00	6,25	56,07	22,21	21,68	21,95	574,44	578,37	9,64	5 185,90	53,1%	72,1%
14:33:00	6,24	62,31	22,27	21,77	22,02	575,33	577,29	9,62	5 763,19	59,0%	80,1%
14:34:00	6,18	68,49	22,27	21,73	22,00	568,67	571,12	9,52	6 334,31	64,8%	88,0%
14:35:00	6,23	**74,71**	22,26	21,72	21,99	573,17	575,90	9,60	6 910,21	70,7%	**96,1%**
14:36:00	6,15	**80,86**	22,21	21,70	21,96	564,75	568,35	9,47	7 478,56	76,5%	**103,9%**
14:37:00	6,21	87,07	22,23	21,77	22,00	572,04	574,52	9,58	8 053,08	82,4%	111,9%
14:38:00	6,10	93,17	22,27	21,81	22,04	562,32	563,72	9,40	8 616,80	88,2%	119,8%
14:39:00	6,24	99,40	22,31	21,86	22,09	576,72	576,98	9,62	9 193,78	94,1%	127,8%
14:40:00	6,24	**105,64**	22,32	21,87	22,10	576,98	576,98	9,62	9 770,76	100,0%	135,8%
	6,21	**Total (Lit)**	Temps : 17 minutes		8 496,46	(KJ)	2,36	(kWh)	<= Avec inerties T9 et T10 !		
	Débit moy.	(lit./min)									
		Chargement Thermique Brute (CTB) :			**9 770,76**	(KJ)	**2,71**	(kWh)	100%	(CTB)	
		Chargement Thermique Nette (CTN) :			**6 832,96**	(KJ)	**1,90**	(kWh)	70%	(CTN/CTB)	
		Perte Thermique Chargement (PTC) :			**2 937,81**	(KJ)	**0,82**	(kWh)	30%	(PTC/CTB)	

Table 21: Parameter readings during the loading phase of the Mock-up

The loading time, 17 minutes, is greater (265%) than the 6.4 minutes required to meet the time scale factor (13'715) between the full-size ULISSE Reservoir and the Reduced Scale Mock-up. This is mainly due to the insufficient capacity (6.2 lit/min ≈ 50%) of the hot water flow through the supply system available in the laboratory.

Normally, the flow rate required to fill the Mock-up should be 12 litres/min (77 litres/6.4 min). Given that heat loss from the Mock-up is proportional to time, the loss observed is also 50% disproportionate. The temperature and flow rate readings (averaged per minute) show, in the Excel table (Fig. 21), that the heat loss during the *loading phase* (PC) is 30% (2.94 MJ or 0.82 kWh). It should therefore normally be around half (15%) of the gross heat energy (GHE).

The *Loading Heat Loss* (*LHL) is* the sum of the loss through the envelope (Qenv) and that of the excess volume of water injected (Vex) above the volume capacity of the Mock-up (Vex ≈ 106 - 77 = 29 litres). The latter simply passes through and carries some of the heat (Qex) out of the Mock-up. It results both from the partial compensation of the envelope loss Qenv and from the thermal de-stratification linked to the downward flow of heat by diffusion, convection and advection (thermal dilution by multiple mixing).

However, in the real-life situation of the ULISSE Sub-Lacustrine Reservoir, **the *Loading Thermal Loss* (LTL) can be partially compensated for by a higher injection rate**. This is all the truer as the electrical energy used to power the pumps would be of photovoltaic origin. The latter will be largely in surplus during summer loading, and using it to (over)load the ULISSE Reservoirs would reduce the peak-shaving of the photovoltaic installations.

Autumn Stagnation Phase (AS):

The Autumn Stagnation phase (AS) lasts 6 minutes and respects the real time scale of 2 months before the Winter Discharging Phase (WD). **The *Stagnation Thermal Loss* (STL*)*** in the Mock-up is about 416 MJ (0.12 kWh), i.e., **6% of the *Net Thermal Load*** (NTL ≈ 6.8 MJ or 1.9 kWh). It is mainly linked to heat transfer through the envelope but also to the bottom slab of the Mock-up (lake bed). For the Mock-up, this translates into an average temperature drop of 1.3˚C

Température Début Stagnation (TDS) :	**39,45**	(°C)	**<= Température moyenne Fin Chargement (TFC)**			
Température Fin Stagnation (TFS) :	**38,37**	(°C)	**Durée phase de Stagnation (DPS) : 6 minutes**			
Chute Température Stagnation (CTS) :	**1,29**	(°C)			6,1%	(CTS/ATC)
Perte Thermique de Stagnation (PTS) :	**415,80**	(KJ)	**0,12**	(kWh)	**6,1%**	(PTS/CTN)

Table 22: Autumn stagnation phase

Winter Discharging phase (WD):

Between 14:47 and 15:20, the time taken to unload the Mock-up was 33 minutes (tdm). Normally it should be 19 minutes (tr) to respect the real time scale of 6 months corresponding to the winter semester. The flow rate is limited by the pump's capacity to the required 3/4 (≈ 3 lit/min instead of 4 lit/min). At 3:12pm, i.e., in 26 minutes, the 77 litres of the Mock-up's volume content were extracted and 88.7% of the *Initial Discharge Heat Load* (IDL).

During this period, as during loading, the downward flow of heat by diffusion, convection and advection transfers some of the residual heat to the cold water, which enters from the bottom of the Mock-up, replacing the hot water extracted from the top. As a result, the average temperature of the cold water in the Mock-up rises to 1.64 ˚C above that of the IBC tank and still represents 218 MJ (0.06 kWh) of heat energy (3.4% of the Initial Discharging Capacity IDC). This residual quantity of energy-heat is extracted, between 15H12 and 15H20, i.e., in 8 minutes, by pumping 23 additional litres until the temperature of the tank is practically reached (18.69˚C). The Mock-up *Discharging Heat Loss* (DHLm) is 0.51 MJ (0.14 kWh), or 11.3% of the IDC.

Graph 23: Thermal loading and unloading rate (rate expressed in Hz; 1 kHz = 1.67 lit/min)

Temps (h:m:s)	débit (Lit/min)	Cumul Volume (lit)	ΔT9 (°K)	ΔT10 (°K)	Tmoy-9-1((°K)	Q (KJ)	P (KW)	Cumul Q (KJ)	Part Volume Part Q (%)	Part Volume Maquette (%)
14:47:00	3,02	3,02	19,23	19,06	19,15	241,76	4,03	241,76	3,8%	3,9%
14:48:00	3,01	6,03	20,37	19,85	20,11	253,38	4,22	495,14	7,7%	7,8%
14:49:00	2,97	8,99	20,69	19,95	20,32	252,20	4,20	747,34	11,6%	11,7%
14:50:00	2,97	11,96	20,57	19,82	20,20	251,21	4,19	998,56	15,6%	15,5%
14:51:00	3,01	14,97	20,39	19,67	20,03	252,38	4,21	1 250,93	19,5%	19,4%
14:52:00	2,99	17,96	20,21	19,53	19,87	248,56	4,14	1 499,49	23,4%	23,3%
14:53:00	2,89	20,85	19,89	19,39	19,64	237,18	3,95	1 736,67	27,1%	27,0%
14:54:00	2,98	23,82	19,73	19,25	19,49	242,85	4,05	1 979,53	30,8%	30,9%
14:55:00	2,99	26,82	19,58	19,07	19,33	242,01	4,03	2 221,53	34,6%	34,8%
14:56:00	3,00	29,81	19,42	18,90	19,16	240,21	4,00	2 461,75	38,4%	38,6%
14:57:00	2,99	32,80	19,21	18,72	18,97	237,24	3,95	2 698,98	42,1%	42,5%
14:58:00	2,96	35,76	19,08	18,51	18,80	233,01	3,88	2 931,99	45,7%	46,3%
14:59:00	2,99	38,75	18,90	18,34	18,62	233,18	3,89	3 165,17	49,3%	50,2%
15:00:00	2,99	41,74	18,69	18,11	18,40	230,04	3,83	3 395,21	52,9%	54,1%
15:01:00	3,00	44,74	18,46	17,90	18,18	228,30	3,81	3 623,52	56,5%	58,0%
15:02:00	3,00	47,74	18,23	17,69	17,96	225,54	3,76	3 849,06	60,0%	61,9%
15:03:00	2,99	50,73	17,97	17,42	17,70	221,60	3,69	4 070,66	63,4%	65,7%
15:04:00	2,97	53,70	17,71	17,13	17,42	216,82	3,61	4 287,47	66,8%	69,6%
15:05:00	2,98	56,69	17,36	16,83	17,10	213,37	3,56	4 500,84	70,1%	73,5%
15:06:00	2,97	59,66	17,06	16,49	16,78	208,67	3,48	4 709,51	73,4%	77,3%
15:07:00	2,94	62,60	16,54	15,97	16,26	200,16	3,34	4 909,67	76,5%	81,1%
15:08:00	2,94	65,54	15,92	15,31	15,62	192,17	3,20	5 101,84	79,5%	84,9%
15:09:00	2,91	68,45	15,04	14,39	14,72	179,35	2,99	5 281,19	82,3%	88,7%
15:10:00	2,90	71,35	13,65	12,91	13,28	161,40	2,69	5 442,59	84,8%	92,5%
15:11:00	2,90	74,25	11,75	10,92	11,34	137,44	2,29	5 580,03	87,0%	96,2%
15:12:00	2,92	**77,17**	9,48	8,55	9,02	110,00	1,83	**5 690,03**	**88,7%**	**100,0%**
15:13:00	2,90	80,06	7,01	6,17	6,59	79,95	1,33	5 769,99	89,9%	103,8%
15:14:00	2,90	82,96	4,78	3,93	4,36	52,78	0,88	5 822,76	90,7%	107,5%
15:15:00	2,89	85,84	3,17	2,30	2,74	33,03	0,55	5 855,79	91,3%	111,2%
15:16:00	2,88	88,72	2,10	1,40	1,75	21,07	0,35	5 876,86	91,6%	115,0%
15:17:00	2,87	91,59	1,28	0,79	1,04	12,41	0,21	5 889,28	91,8%	118,7%
15:18:00	2,87	94,45	0,83	0,57	0,70	8,40	0,14	5 897,67	91,9%	122,4%
15:19:00	2,87	97,32	0,56	0,43	0,49	5,95	0,10	5 903,62	92,0%	126,1%
15:20:00	2,86	**100,19**	0,42	0,34	0,38	4,55	0,08	**5 908,18**	**92,1%**	**129,8%**
	2,94	**Total (Lit**	Temps total : 33 minutes			Fin du déchargement : T9 et T10 = température cuve				
	Débit mo	(lit./min)	Temps 100 % volume maquette: 25 minutes							
rge thermique Initiale de Déchargement (CID) :						**6 417,16**	(kJ)	**1,78**	(kWh)	**100,0%** (CID)
Déchargement Thermique Nette (DTN) :						**5 690,03**	(kJ)	**1,58**	(kWh)	**88,7%** (DTN/CID)
Perte Thermique Déchargement (PTD) :						**727,13**	(KJ)	**0,20**	(kWh)	**11,3%** (PTD/CID)

Table 24: Thermal Winter Discharging phase of the Mock-up

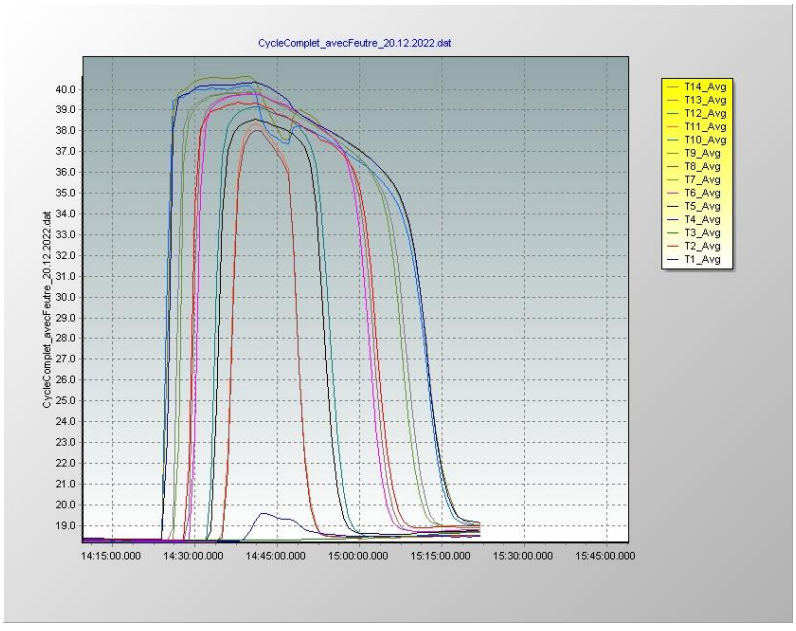

Figure 25: Temperature readings in the Mock-up during the complete cycle

9) Test on 21 December 2022 (morning): Complete cycle Mock-up with grid + felt

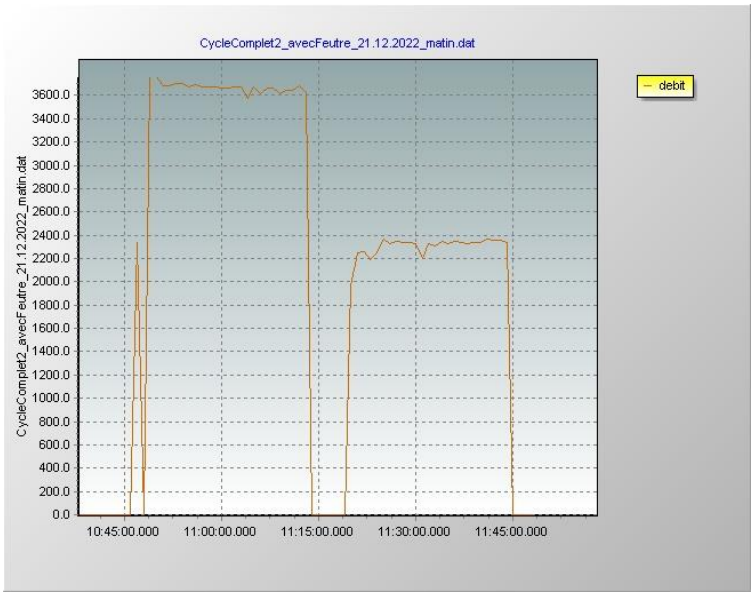

Graph 26: Thermal loading and unloading rate of the Mock-up (rate expressed in Hz; 1 kHz = 1.67 lit/min)

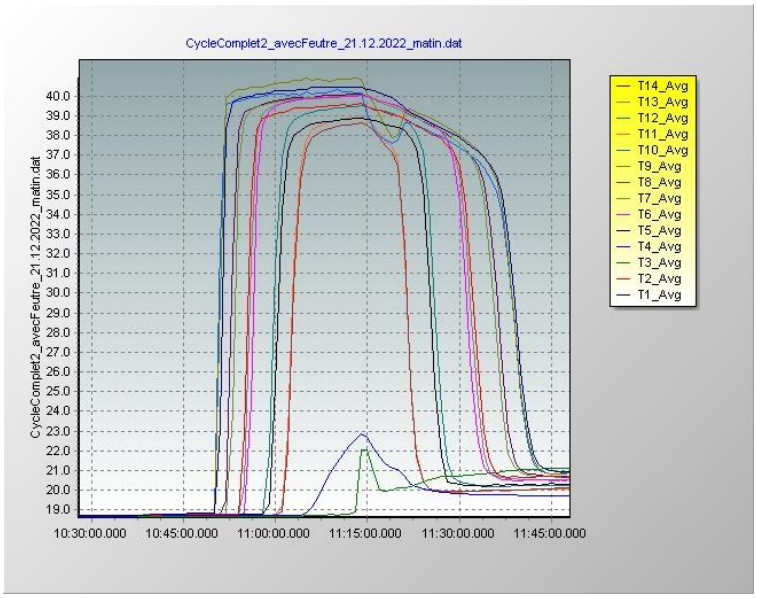

Figure 27: Temperature readings in the Mock-up during the complete thermal cycle

Note:

Prolonged loading of the Mock-up results in significant heating of the IBC tank. The temperature of the IBC tank (TC3) increases from 18.5 to 21˚C. As a result, the thermal potential of the Mock-up in relation to the IBC tank is reduced, but so is the heat loss from the Mock-up throughout the cycle. This is also observed for the afternoon test.

Increasing the flow rate and at the same time reducing the loading time should make it possible to limit the increase in the IBC tank temperature and therefore better reproduce the lake's thermal stability.

10) Test on 21 December 2022 (afternoon): Complete cycle of the Mock-up + felt

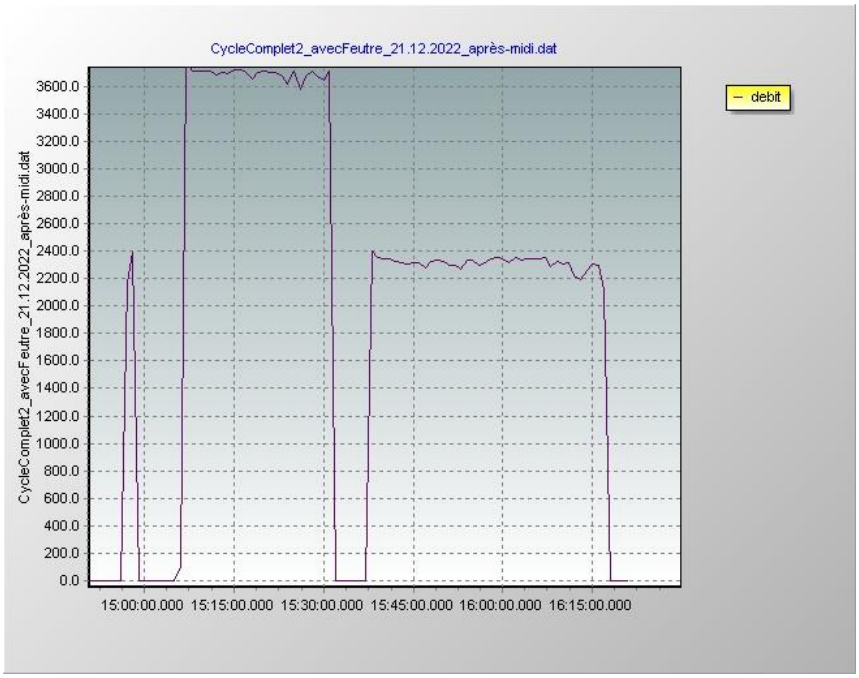

Graph 28: Thermal loading and unloading rate of the Mock-up (rate expressed in Hz; 1 kHz = 1.67 lit/min)

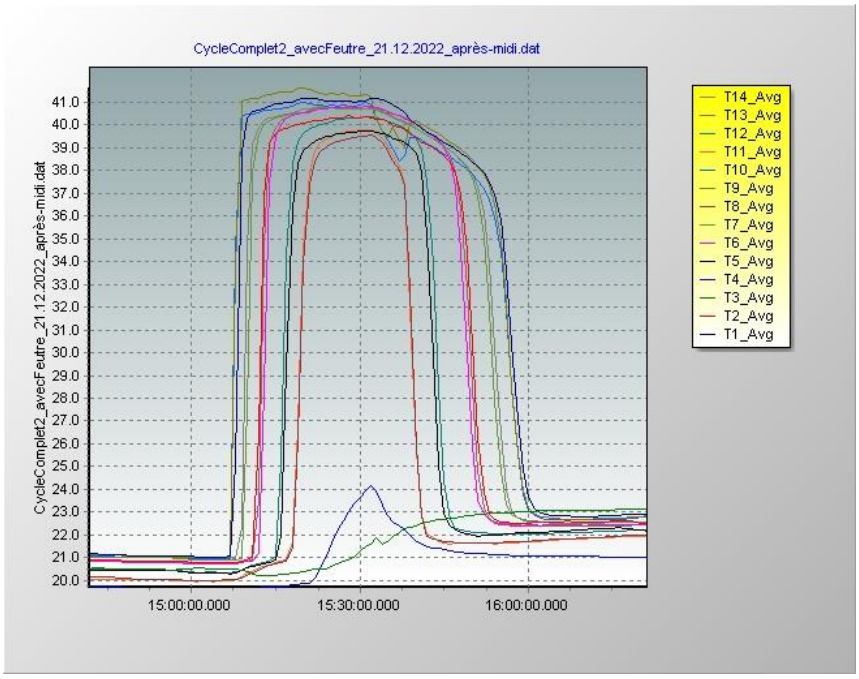

Figure 29: Temperature readings in the Mock-up during the complete thermal cycle on 21.12.2022

11) Test on 5 January 2023: Complete thermal cycle of the Mock-up with felt

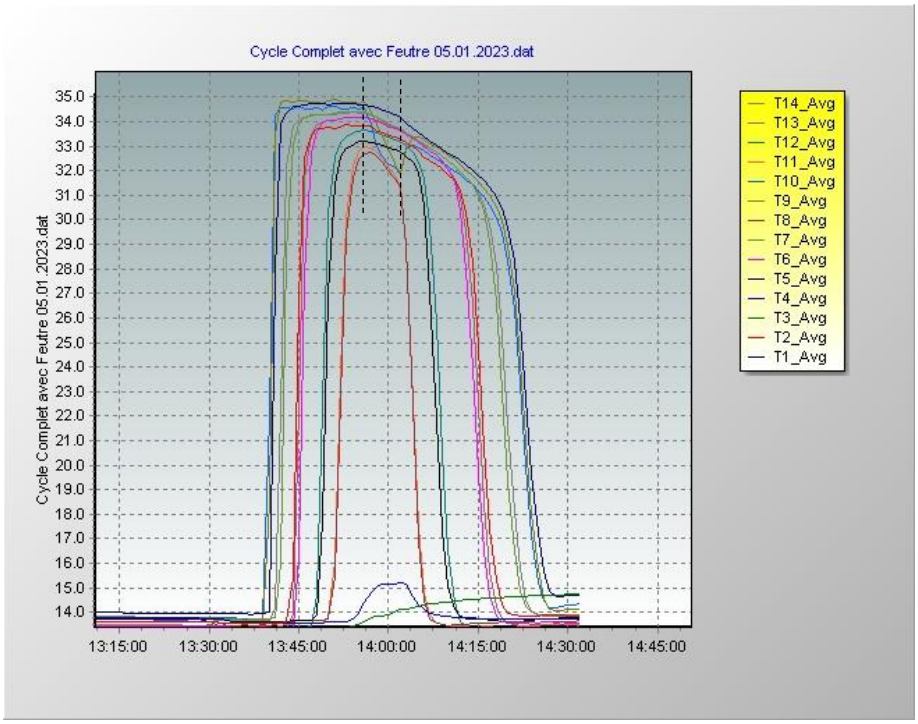

Figure 30: Temperature readings in the Mock-up during the complete thermal cycle on 5.1.2023

Annex 2: Measuring the hydrothermal conductance of the real Reservoir shell

In order to confirm the theoretical calculation of the thermal conductance of the envelope (§ 9) and to refine the parameters of the numerical simulation (COMSOL), an experimental device was set up. This will enable the physical measurement of the "hydrothermal" characteristics of the real Reservoir shell (hydraulic permeability and thermal conductivity).

As a reminder (§ 4, pg. 4), the envelope is insulated with cellular glass blocks (FOAMGLAS-F, density 165 kg/m^3, thickness 50 mm), which are sandwiched between three layers of type E glass fibre technical textiles. These insulating blocks, measuring 0.45 x 0.60 m, are spaced apart by a bead of needled felt, also made of glass fibre or basalt.

To carry out these measurements, a 50 mm thick FOAMGLAS slab is cut "crosswise" so as to reproduce an envelope surface corresponding to the junction of four isolation blocks. The beading at the joints between the slabs generates "thermal and hydraulic bridges" (heat and water leaks). They increase the overall thermal conductance (insulating blocks + thermal bridges) of the envelope, which must be quantified.

Figure 1: Chamber for measuring the thermal and hydraulic conductance of the ULISSE Reservoir shell

The four pieces of cellular glass blocks are arranged between the three layers of fibreglass and placed in a thermal box, compartmentalised into two watertight half-boxes filled with water. This set-up should make it possible to reproduce the pressure and temperature differential of the water through the representative sample of the Reservoir shell and thus to quantify the specific loss of water and heat through the shell of the ULISSE Reservoir.

An upper container (5 litres) of hot water supplies the compartment above the envelope to be tested, just as a lower container is connected to the compartment below the envelope. The difference in height (Δh), between the two compartments, generates a differential hydrostatic pressure on the envelope (Δp). It reproduces that due to the difference in density (Δρ) between the hot water in the Reservoir and the cold water in the surrounding lake.

This differential pressure is likely to generate Water Leakage (WL) through the relative hydraulic permeability (μ) of the envelope. By measuring the flow rate of water leakage (DWL) between the two vessels that passes through the jacket, we can determine the potential flow rate of water leakage (Fe) per unit of surface area and temperature of the ULISSE Reservoir (DWL/m^2 @ Tr).

However, initial tests have revealed problems with the tightness of the casing closure, which distorts the measurement of the DWL leakage rate through the casing. If accurate measurements are to be obtained, it will be essential to improve the tightness of the casing (as part of the ULISSE project).

Regardless of these measurement problems, the hydraulic tightness of the ULISSE Reservoir shell can be improved if necessary. This could be done, for example, with a waterproofing coating based on silicone or PTFE, applied to the textile in the middle of the shell (protected from direct contact with the lake). This waterproofing coating would be limited to the upper part of the Reservoir, where the hydrostatic pressure is greatest. However, the biocompatibility of this coating remains to be assessed.

$$\Delta p = \Delta h * \Delta \rho * g \qquad [m.w.c.] \qquad (1)$$

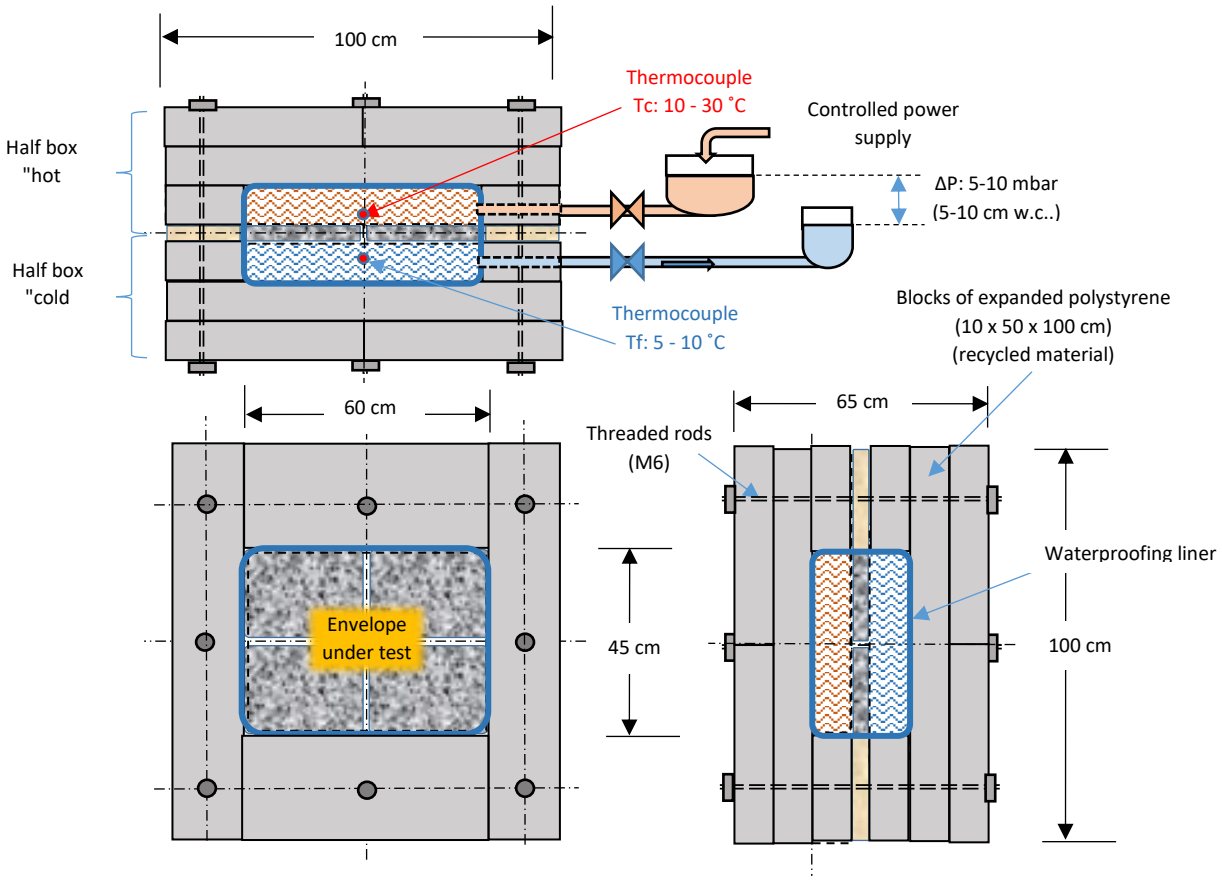

Figures 2: Casing for measuring the - thermal and - hydraulic conductance of the envelope

On the other hand, the theoretical calculation of the Thermal Conductivity of the Reservoir envelope, including the insulation blocks, the interlayer joints and the junctions of the envelope strips, has nevertheless been carried out.

Appendix 3: Analysis of a hydrothermal partitioning veil

The phenomena that lead to *Exergy* losses (second-law losses) could possibly be partially limited by "hydrothermal partitioning". This is achieved by interposing a mobile veil (Fig. 1) in the Reservoir, which separates the cold water at the base from the hot water above. As well as reducing the mixing of water masses of different temperatures, the thermal insulation of this veil would also reduce heat transfer by diffusion between the upper and lower compartments thus formed. It would consolidate and maintain the flat front of the thermocline inside the Reservoir.

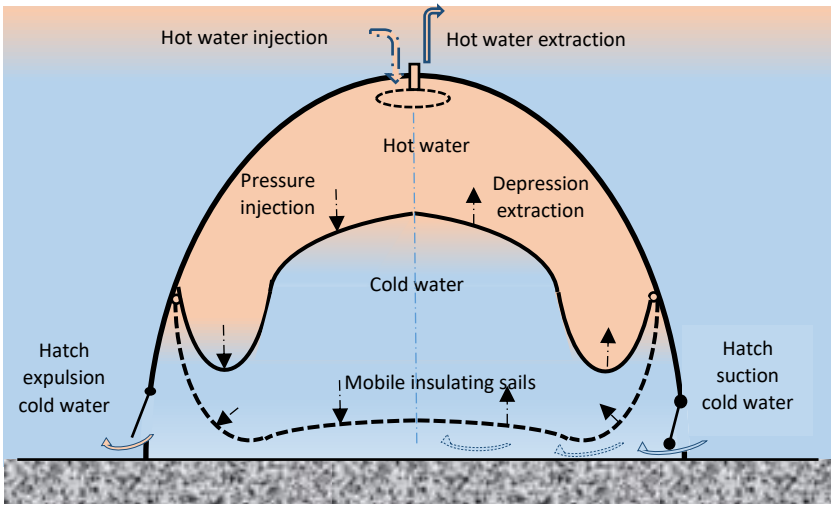

Figure 1: Example of the principle of a Reservoir thermal insulation veil with water circulation in thermal recharge phase (left half) and (right half) in thermal discharge phase.

Water movements should be limited to the currents induced by the "voluntary" introduction and extraction of water in the said compartments. This could be done, for example, by means of "hatches" located at the base of the Reservoir, or simply by the small free space between the lake bed and the skirt around the perimeter of the Reservoir envelope (≈ 1'300 m for an ULISSE Reservoir 500 m long and with a transverse radius of 50 m).

The material constitution of the veil could be similar to that of the outer hyperbolic envelope of the Reservoir. With the low density of the cellular glass insulation, the veil would also adopt a convex curvature between its own lateral anchoring points and would tend to rise spontaneously, making it necessary to hold it in place at the desired height by means of adequate anchoring.

If the veil were completely sealed hydraulically with the hyperbolic envelope, its vertical movement would be produced, by piston effect, by the pressure/depression difference exerted by the loading/unloading pump, like a diaphragm in a hydraulic expansion tank (Fig. 1).

On the other hand, if the veil were not completely watertight, this pressure differential would be smaller or non-existent due to the leakage flow between the veil and the Reservoir shell. The movement and height of the veil in the Reservoir would then have to be controlled by an **Active Positioning Device (APD)**; for example, by means of pulley cables, counterweights and guide rails against the Reservoir shell (Fig. 2 below). This APD system would target the maximum temperature difference at the veil interface and would be based on the volume of hot water (active volume) in the Reservoir.

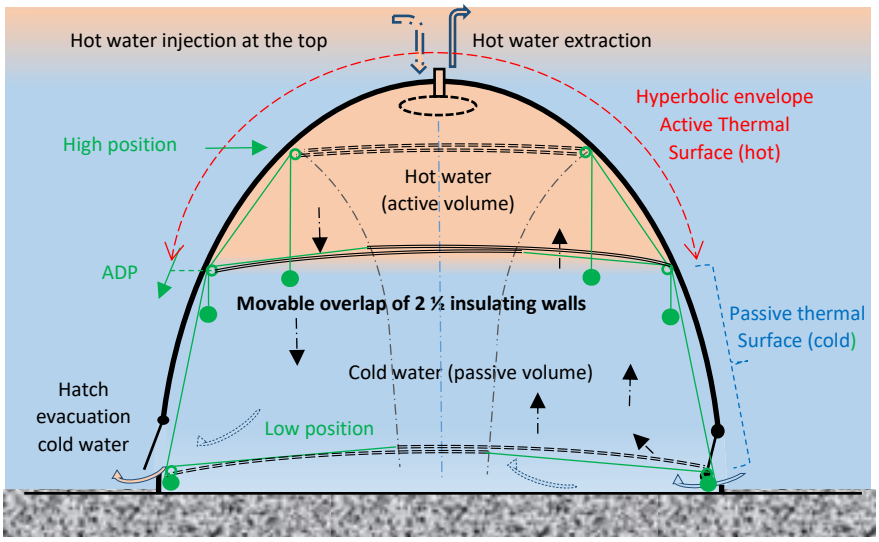

Figure 2: Example of thermal partitioning by mobile overlapping of two insulating half-sheets, controlled by an ***Active Positioning Device*** *(APD). Left half of figure = thermal loading of hot water (summer period), right = thermal unloading (winter period).*

In more detail in Figure 3 below and according to the example in Figure 2, each half-vail is guided vertically by a track against one inner side of the hyperbolic envelope and pulled horizontally towards the opposite side using a counterweight connected by a cable (made of stainless-steel). The guide roller attached to each half-vail is held vertically by a motorised winch. The winch positions the guide roller vertically along the track. Ultimately, the vails could be evenly weighted (e.g., with gravel) to reduce their buoyancy and the forces in the cables.

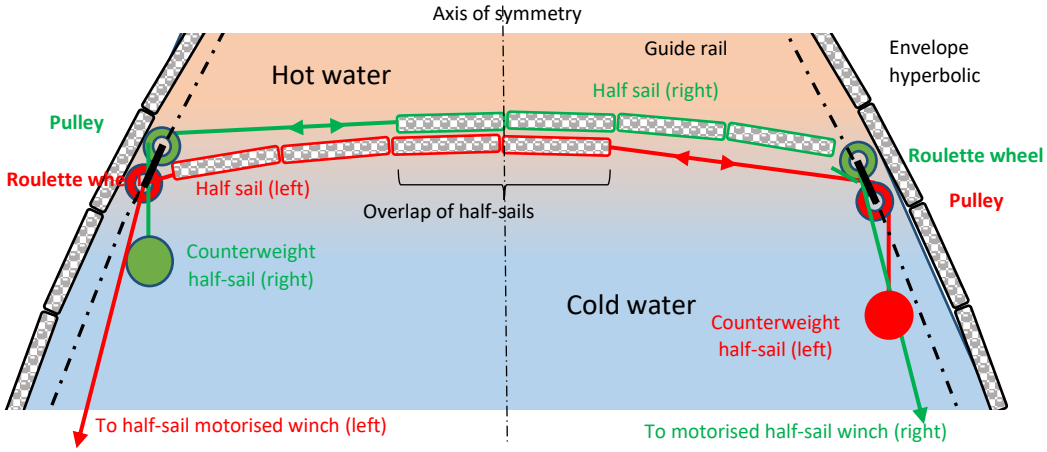

Figure 3: Operating details of an example of an Active Positioning Device (APD) half-sails for hydraulic partitioning and thermal stratification

Given the hyperbolic transverse curvature of the Reservoir and the flow rate (D) for loading and unloading the hot water, the speed (V) of the vertical movement of the veil would be different. Thus, despite a constant water extraction flow rate (D), the speed (V) of ascent of the mobile sail would increase until it reaches its top position, while conversely its speed would decrease during the injection or top loading of hot water.

If the two half-sails each have a width equal to half the transverse base of the hyperbolic envelope and remain stretched horizontally until they touch, in their upper position, the two transverse edges of the envelope (where they completely overlap), then, for an equal flow of water (D), the speed of their vertical displacement (Vd) would vary in the ratio of their *covering surface* (Sc), i.e., from simple (at the base) to double (at the top): Vd = D/Sc.

According to Figures 2 and 3, the overlapping of the two half-sails, depending on their height in the Reservoir, would modify their Surface (Sv) and, through the resulting average thickness, their thermal conductivity (W/m^2K). This would reduce the surface thermal conductivity of the entire "active" envelope, comprising the *Active*

Hyperbolic Surface (Sha) and the Surface of the Movable Veil (Sv), as the "active" volume of hot water decreases and its overall surface decreases.

Irrespective of the movement of the veil, its thermal conductivity, combined with that of "immobile" water (0.6 W/mK by molecular diffusion with no overall movement of matter), would produce a downward-flow heat transfer from hot water to cold water through the veil.

In this way, the hot water cools as it comes into contact with the sail. As it becomes denser, it will tend to flow downwards through the passages in the sail. Conversely, the cold water under the sail would heat up and tend to rise, slowed down by the counter-current of the warm water. The resulting displacements of the water masses would therefore be limited in intensity and localised to the sail's immediate environment. Temperate water of intermediate density would then form at the level of the sail, with the front of the internal thermocline gradually spreading out locally.

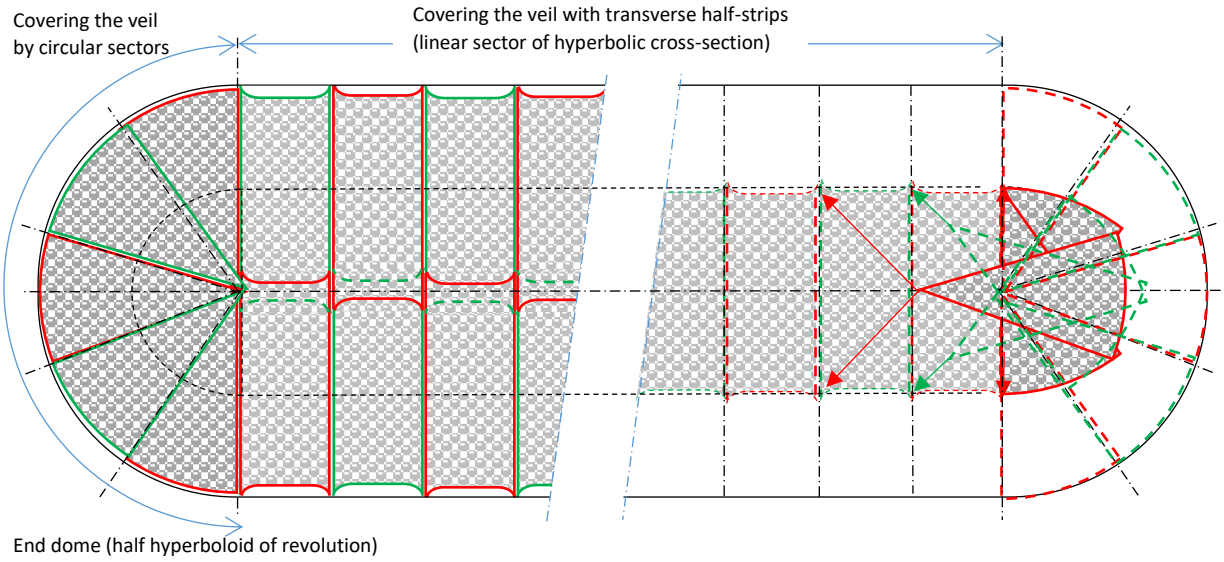

Figure 4: Top view of the hydrothermal blanket,
left half down and right half up

At the cost of the complexity of such a system, the main function of the veil would be to form a "hydrothermal partition" to reduce the convection and advection currents which tend to mix waters of different temperatures and reduce thermal stratification (reduction in the spread of the front of the thermocline inside the Reservoir).

However, initial tests on the experimental model and numerical simulation (COMSOL Multiphysics) seem to show a certain stability of thermal stratification or the maintenance of the front of the thermocline inside the Reservoir during the complete operating cycle.

At this stage of the exploratory study, the use of a hydrothermal partitioning veil for the ULISSE Reservoir does not appear to be required and is not developed further but, if necessary, is kept in mind.

Appendix 4: Preliminary analysis of the risks associated with lake currents threatening the structural integrity of ULISSE Reservoir

h e p i a
Haute école du paysage, d'ingénierie et d'architecture de Genève

Rue de la Prairie 4
CH-1202 Genève

Tél. +41 (0)22 546 24 00
Fax +41 (0)22 546 24 10

hepia@hesge.ch
www.hesge.ch/hepia

Analyse préliminaire des risques liés aux courants lacustres menaçant l'intégrité structurale d'ULISSE

1. Introduction

Le projet ULISSE, conduit par Monsieur William van Sprolant, s'inscrit dans le programme d'encouragements SWEET de l'Office fédéral de l'énergie (OFEN). Il vise à promouvoir l'emploi de l'énergie renouvelable, par une méthode innovante qui, au moyen d'un réservoir immergé dans un lac, emmagasine l'eau « chaude » en été et la rend exploitable en hiver pour une climatisation efficiente des bâtiments.

Si l'analyse de la faisabilité du projet ULISSE pour les aspects énergétiques notamment et d'implantation est bien avancée, celle des risques liés en particulier à l'hydrodynamique d'un lac doit encore être menée. Le spécialiste en hydraulique de HEPIA, le professeur Dr Zsolt Vecsernyés, met en garde sur la mise en danger de la structure immergée d'ULISSE par les courants puissants d'un lac et notamment si celui-ci est stratifié. En effet, la thèse de doctorat de Monsieur Vecsernyés (Vecsernyes, 1991) porte sur l'étude de l'hydrodynamique lacustre et des mécanismes de mélange entre les masses d'eau stratifiées du Léman.

Le présent document constitue un recueil des phénomènes physiques en jeu et une proposition des analyses à conduire au Laboratoire d'hydraulique appliquée (LHA) de HEPIA, pour identifier les contraintes sur la structure d'ULISSE afin de proposer des mesures de préservation de ses éléments structurels.

2. La genèse des courants lacustres

2.1. Les forçages

Les courants lacustres sont générés par ce qu'on appelle les « forçages » (Figure 1). Le plus important parmi eux est le **rayonnement solaire**. Il engendre les variations de pression et de température dans l'atmosphère, créant ainsi les **vents**. Sur les lacs, ils en résultent les **vagues** (ondes de propagation) provoquées par le frottement de l'air sur l'eau, et les **seiches** (ondes stationnaires) créées par un changement rapide et puissant de la pression atmosphérique. Les vagues créent des courants de surface dont l'effet ne s'étend que jusqu'à quelques mètres de profondeur. La seiche met en mouvement toute la masse d'eau d'un lac. Le rayonnement solaire modifie la structure des lacs, conduisant à leur **stratification thermique** qui évolue au fil des saisons. Les courants lacustres se comportent différemment suivant le degré de stratification d'un lac.

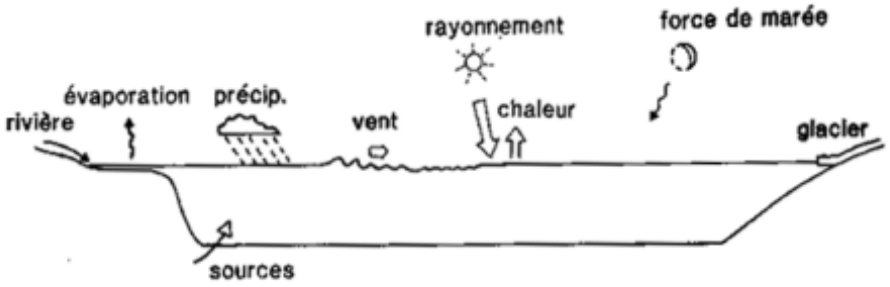

Figure 1 Forçages naturels, ayant un effet plus ou moins important sur la genèse des courants lacustres.

Le forçage lié à la **rotation de la Terre**, décrit par l'effet de Coriolis, dévie les courants lacustres suivant sur quel hémisphère se trouve le lac et à quelle latitude. Son influence est importante dans les grands lacs, comme le Léman.

L'arrivée d'eau des rivières et la sortie d'un débit du lac par son **émissaire** peuvent créer des courants lacustres locaux forts.

Les autres forçages ont un effet négligeable sur les courants lacustres, comme les marées, les précipitations, l'arrivée de faibles débits d'eau de surface ou souterraine et l'évaporation.

2.2. La stratification thermique

Au cours de chaque été, le rayonnement solaire réchauffe l'eau des lacs par la surface. Par son poids spécifique plus faible que celui des eaux fraiches des profondeurs, l'eau chaude reste en surface, qui au fil la saison conduit à la **stratification thermique** du lac par la formation de trois couches principales superposées, de densité et de température différentes (Figure 2). La couche supérieure d'eau chaude (20°C) d'une épaisseur de 20 à 30 m pour le Léman est **l'épilimnion,** la couche de transition de 5 à 30 m de mètres est **la thermocline** et la masse d'eau froide (7°C) qui s'étend jusqu'au fond est **l'hypolimnion**.

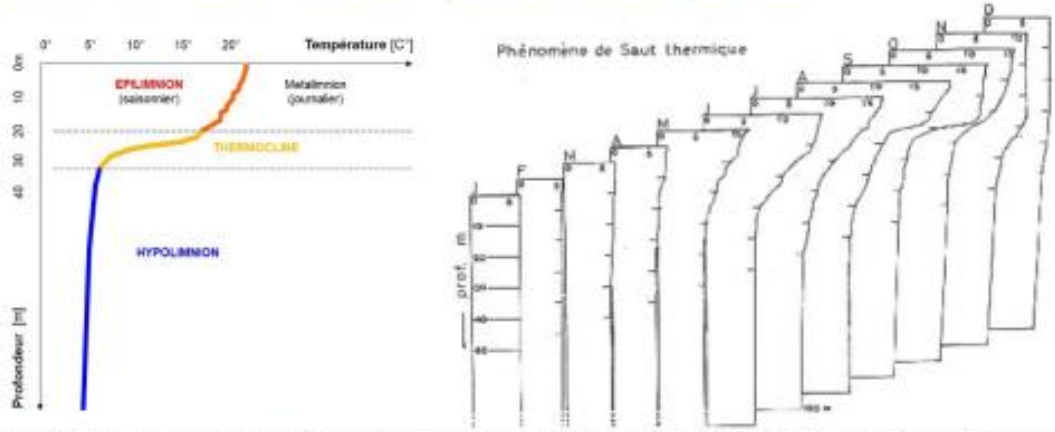

Figure 2 Gauche : Profil de température (°C) d'un lac profond, montrant sa stratification thermique estivale, avec l'épilimnion de surface, la thermocline de transition et l'hypolimnion des profondeurs. Droite : évolution de la stratification du Léman au fil des 12 mois de l'année (J : janvier ; D : décembre).

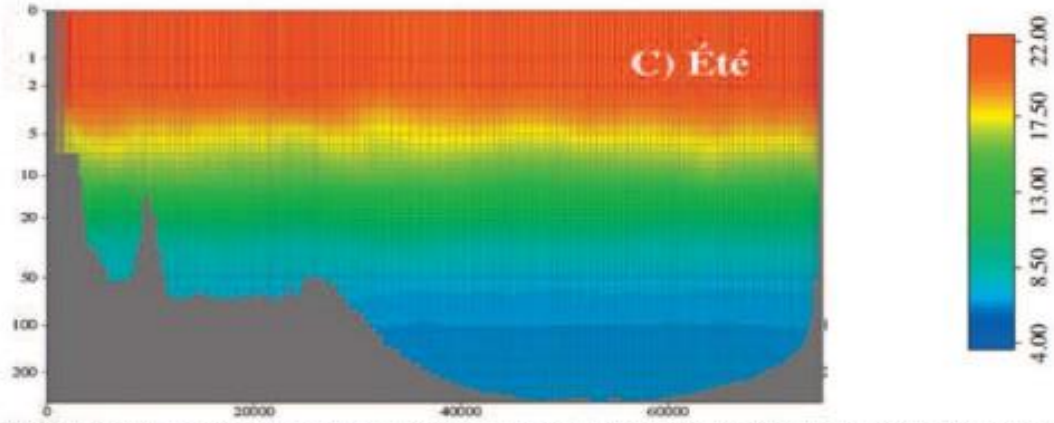

Figure 3 Profil de température (en °C) du Léman, de Genève (gauche) et à Villeneuve (droite), démontrant la stratification thermique estivale (Le Thi et al. 2012).

2.3. L'effet des vents dominants sur les courants lacustres

Les vents en général et plus encore les vents dominants, comme le Vent et de Bise pour le Léman (Figure 4), ont un rôle prépondérant sur le comportement des masses d'eau. Ils forment les vagues accompagnées d'un courant de surface (Figure 5), et les ondes stationnaires accompagnées de courant internes complexes (Figure 6). En agissant par la surface, les vents favorisent le mélange des masses par turbulence (Vecsernyés, 1991) et le transfert de l'oxygène, des nutriments et des panaches d'eau à température variable vers les profondeurs, en fonction de l'état thermique du lac.

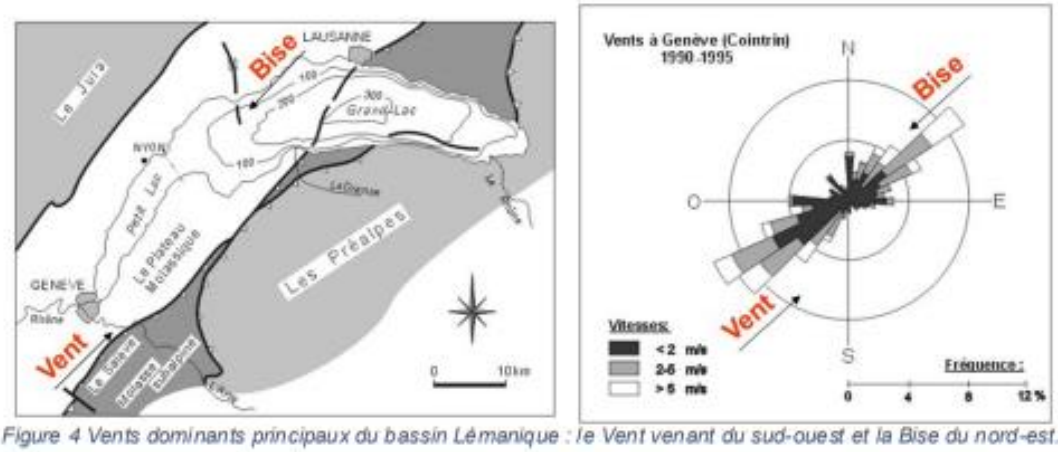

Figure 4 Vents dominants principaux du bassin Lémanique : le Vent venant du sud-ouest et la Bise du nord-est.

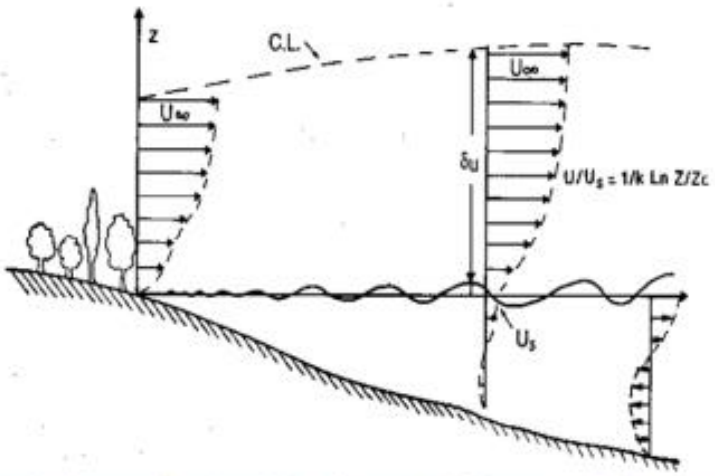

Figure 5 Les vagues et les courants de surface liés se forment par le frottement de l'air sur la surface du lac.

Les puissants vents dominants soufflant au-dessus d'un lac créés par un fort changement de pression provoquent l'oscillation de toute la masse d'eau, de nature similaire à la vibration d'une corde pincée d'une guitare. Ce phénomène d'onde stationnaire, étudié en détail la première fois par François-Alfonse FOREL à Morges (1895), est appelé la **seiche.**

La **seiche de surface** possède une amplitude de quelques décimètres, 20-30 cm pour le Léman. Un courant de surface est créé dans le sens du vent, accompagné d'un courant de retour plus faible passant par le fond lacustre (Figure 6).

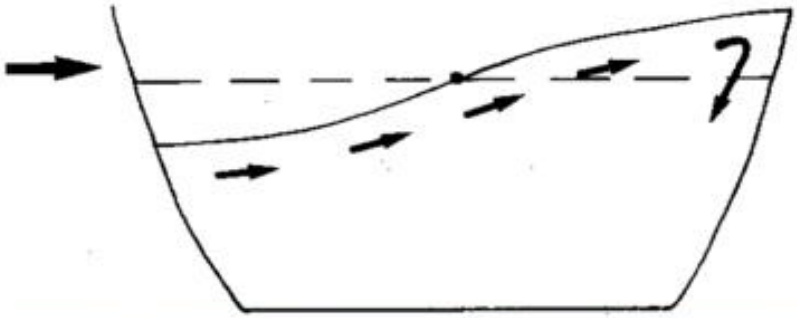

Figure 6 La seiche se forme sous l'effet d'un fort vent brusque dû à un changement de pression atmosphérique. L'oscillation observable à la surface (seiche) engendre un courant de surface dans le sens du vent et un courant de retour plus faible par le fond.

Avec la stratification thermique estivale, l'oscillation de l'épilimnion entraine, en opposition de phase, celle de la thermocline appelée **seiche interne**, et donc de l'hypolimnion sous-jacent. Dans l'épilimnion, le courant de surface s'écoule dans le sens du vent, celui de l'hypolimnion s'écoule en sens opposé (Figure 7).

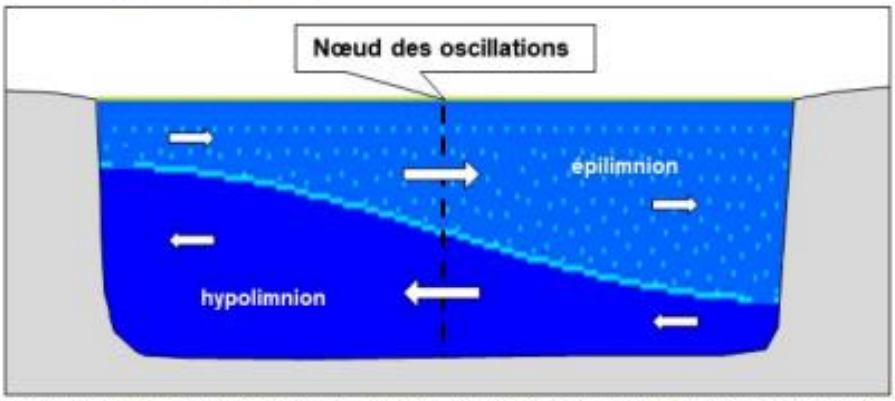

Figure 7 Due à la stratification thermique les courants engendrés par un épisode de seiche et seiche interne s'opposent entre l'épilimnion et l'hypolimnion. Les plus forts courant se créent sous le(s) nœud(s) d'oscillation.

L'oscillation de la thermocline peut atteindre une dizaine de mètres d'amplitude dans le Léman (Vecsernyés 1991), avec une périodicité de 10-12 h (Figure 8). Les courants s'inversent par la demi-fréquence des oscillations, toutes les 5-6 h.

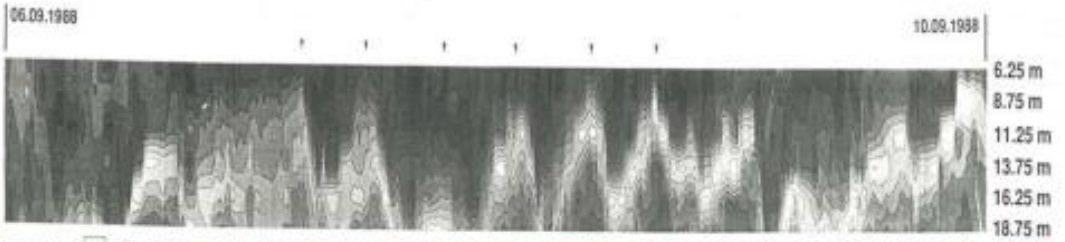

Figure 8 L'oscillation de la thermocline (seiche interne) possède une périodicité de 10-12 h dans le Léman. Ces ondes internes ont une amplitude d'une dizaine de mètres. Vecsernyes, 1991.

2.4. L'effet de Coriolis influençant les courants lacustres

La rotation de la Terre joue un rôle déterminant sur le positionnement des plus forts courants des lacs de grande taille. Le courant généré par une forte Bise (pour le Léman) persiste jusqu'à 72 h, suffisant pour que la Terre fasse plus d'une rotation autour de son axe. Sur l'hémisphère nord, **le courant** propulsé sur une trajectoire rectiligne par la seiche sous l'effet d'un vent puissant **est « dévié » sur la droite**, qu'ils s'agissent du Vent ou de la Bise (pour le Léman). C'est l'effet de Coriolis.

Ainsi, en se plaquant contre les côtes, les plus forts courants se créent dans le Grand-Lac de manière systématique le long de la côte nord suisse s'écoulant d'est en ouest et la côte sud française d'ouest en est (Vecsernyés 1991, Le Thi et al. 2012), (Figure 9, Figure 10).

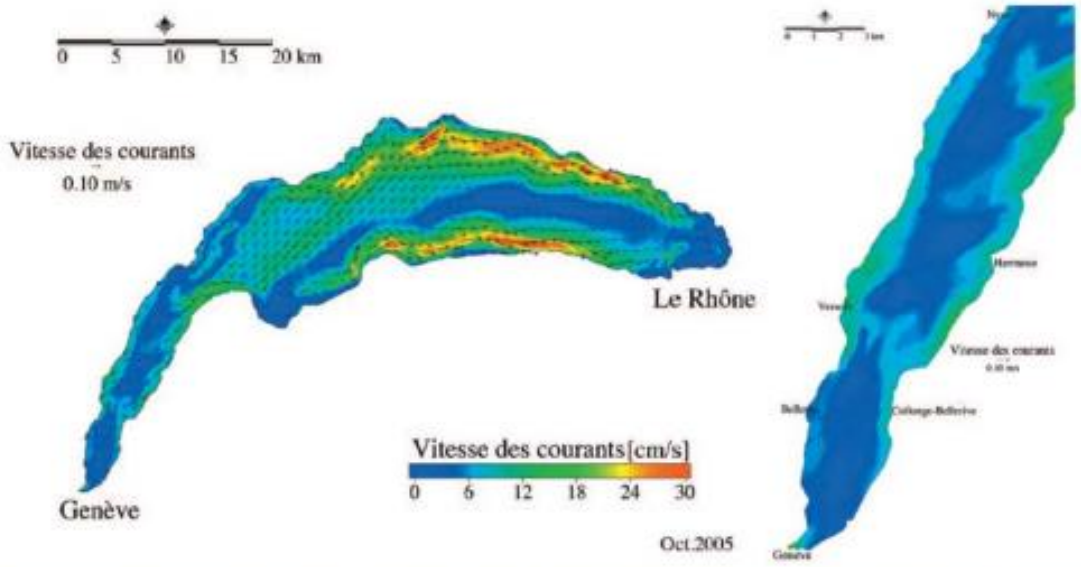

Figure 9 Les vents dominants créent, par les épisodes de seiche notamment, des courants systématiques. Ils sont déviés par l'effet de Coriolis sur la droite, et longent les côtes sud et nord du Grand-Lac dans le Léman. Le Thi et al. 2012.

L'étirement et l'aplatissement verticaux des masses d'eau créent des **courants** horizontaux **d'advection** (Figure 10), pouvant atteindre 30-40 cm/s le long des côtes.

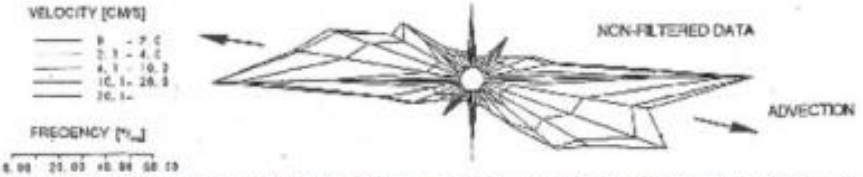

Figure 10 Courant d'advection mesuré à Ouchy (Suisse, côte nord du Léman), formé par la Bise et dévié par l'effet de Coriolis. Vecsernyes, 1991.

3. Risques sur le réservoir ULISSE liés aux courants lacustres

Le réservoir ULISSE se déploiera entre 10 m et 60 m de profondeur (Figure 11), avec sa voile et son système d'ancrage qui l'attache au fond lacustre.

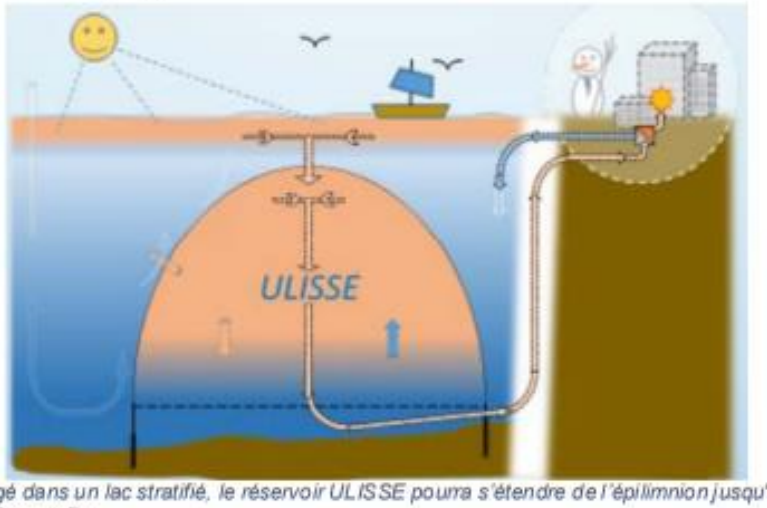

Figure 11 Immergé dans un lac stratifié, le réservoir ULISSE pourra s'étendre de l'épilimnion jusqu'à l'hypolimnion, en traversant la thermocline.

Les vagues sont des ondulations de faible amplitude diminuant depuis la surface avec la profondeur, jusqu'à ne plus avoir d'effet au-delà d'une dizaine de mètres dans les lacs. Le courant de surface lié se cantonne aux premiers mètres. Ces phénomènes ne constitueront donc pas de risque pour ULISSE, même lors d'une tempête.

Les **seiches de surface et internes** en revanche, provoquent le déplacement massif de l'eau. **En hiver**, par l'absence de la stratification thermique, les plus forts courants se manifestent dans la masse d'eau supérieure, mais un courant de retour plus faible se crée par le fond. **En été**, due à la stratification thermique, la seiche engendre le déplacement massif des eaux de l'épilimnion et dans le sens opposé celui de l'hypolimnion. Les plus forts **courants horizontaux** se trouvent dans la verticale du(des) nœud(s) des oscillations (Figure 7).

ULISSE subira les courants internes du lac au fil des saisons sans ou avec la stratification thermique de la colonne d'eau. En été, la partie supérieure de la voile pourra se trouver dans l'épilimnion, sa partie centrale traversera la thermocline et sa partie inférieure s'étendra dans l'hypolimnion. Lors des seiches internes, elle sera ainsi exposée à **l'effet de cisaillement** dû aux courants puissants opposés de l'épilimnion et de l'hypolimnion. De surcroît, le sens de ces courants change toutes les 5 - 6 heures, correspondant à la moitié de la période d'oscillation de la seiche. Ces courants engendreront des mouvements, des déformations et des efforts internes de l'enveloppe d'ULISSE ainsi que ses ancrages. Si l'enveloppe du réservoir est ouvert par le bas, sa **déformation cyclique** expulsera de précieux mètres cube d'eau chaude stockée, pour aspirer ensuite de l'eau froide.

En conclusion, provoquées par les vents dominants, les courants lacustres puissants et oscillants des seiches constituent un danger, auquel le réservoir ULISSE sera exposé au cours de son exploitation, ce qui présente un risque sur la stabilité structurale et de la pérennité de ULISSE. Afin de connaître le comportement de la voile et de ses ancrages et les efforts mécaniques qui y naîtront, il serait important d'étudier les phénomènes hydrodynamiques et de stabilité structurale d'ULISSE de manière appropriée par des spécialistes, dans un laboratoire d'hydraulique.

L'emplacement du réservoir ULISSE doit être défini avec attention. Sa taille projetée (50m de haut, 100m de large, 500m de long) pourrait avoir un impact sur les courants lacustres, d'autant plus si plusieurs unités sont implantées en parallèle. La réduction de la section mouillée du lac **accentue la vitesse de courant**, en tout cas dans la proximité d'ULISSE. Ces aspects également devront faire l'objet d'analyses hydrodynamiques par un spécialiste.

4. Etudes hydrauliques proposées

4.1. Modèle physique

A la lumière des éléments théoriques présentés sur les courants lacustres au chapitre 2 et des risques démontrés sur la stabilité structurale de la voile et les ancrages d'ULISSE au chapitre 3, le Laboratoire d'hydraulique appliquée (LHA) de HEPIA propose de concevoir un modèle physique hydraulique spécifique et de conduire une recherche appliquée dédiée. Les analyses porteront d'une part sur le comportement général d'ULISSE face aux phénomènes hydrauliques liées aux seiches de surface et internes, et sur les efforts structuraux provoqués dans ses ancrages.

Le modèle physique permettra de

- créer les conditions d'une masse d'eau stratifiée, et non stratifiée ;
- générer les seiches de surface et internes de la masse d'eau, par un dispositif mécanique conçu pour le modèle ;
- suivre et enregistrer la fréquence d'ondulation des seiches de surface et interne, au moyen de sondes UVP (Ultrasound velocity probe) ;
- enregistrer les vitesses de courant en différents points horizontaux et verticaux stratégiques de la masse d'eau, au moyen de sondes UVP ;
- mesurer les efforts dans les ancrages au moyen de jauges de contrainte installées.

La construction et l'instrumentation du modèle physique se fera par les collaborateurs du Laboratoire d'hydraulique appliquée et des étudiants en cours formation bachelor de HEPIA. **Le calibrage** du modèle aux conditions hydrodynamiques est prévue par les collaborateurs du LHA, avec les instruments de mesure appropriés. La **recherche** scientifique sera menée par les collaborateurs du LHA et des étudiants bachelor voire master de la HES-SO.

Au cours des analyses, des échanges de travail sont prévus entre spécialistes, des visites sont proposées pour les mandants et financeurs de l'étude ainsi que les administrations et le public scientifique. A la fin de la recherche un rapport technique sera rédigé en français.

La durée de ces opérations est estimée, du début de la construction jusqu'à la fin des études, environ 18 mois.

4.2. Simulation numérique

Les courants lacustres seront influencés par le(s) réservoir(s) ULISSE. L'impact d'ULISSE sur l'hydrodynamique lacustre devrait être étudié par simulation numérique hydrodynamique 2D ou 3D. Les configurations hydrodynamiques à analyser sont :

- La réduction de la section mouillée du lac par un ou plusieurs réservoirs, modifiant le champ de courant lacustre ;
- La déformation cyclique du réservoir par la seiche, créant des courants d'échange entre le volume d'eau stockée par ULISSE et celui se trouvant à proximité.

Le LHA est tout à fait à même à modéliser l'hydrodynamique lacustre liée à ULISSE en 2D et en 3D, avec les logiciels Mike 21 (DHI) et respectivement Flow 3D (Flow science). Le **montage des modèles**, leur **calibrage** et les premières **analyses** pourraient être réalisés par les spécialistes du LHA et un(e) étudiant(e) bachelor ou master de la HES-SO. Les analyses détaillées devraient être conduites par les spécialistes du LHA et un(e) étudiant(e) master.

Au cours des analyses, des échanges sont prévus entre spécialistes de l'hydraulique et de la thermique du projet ULISSE. A la fin de la recherche un rapport technique sera rédigé en français.

Afin d'harmoniser tous les projets conduits par les experts, une durée totale comparable à celle de la modélisation physique devra être pour les simulations hydrauliques numériques.

4.3. Valorisation de la recherche

Le Laboratoire d'hydraulique appliquée de HEPIA se réserve le droit de valoriser les résultats de la recherche dans des revues scientifiques et des congrès nationaux et internationaux.

Des présentations grand-public, dans des forums des associations professionnelles (ex. ARPEA, VSA, SIA), tout comme la parution des articles dans la presse écrite et télévisée, devront aussi être programmées.

Bibliographie

Forel, Fraçois-Alfonse, 1895, FOREL FA. 1895.Le Léman. Tome 2. F Bouge, Lausanne

Le Thi, A.D. ; De Pascalis, F. ; Umgiesser, G. ; Wildi, W., 2012, Structure thermique et courantologie du Léman, UNIGE

Lemmin, U. ; Mortimer, C.H. ; Bäuerle, E., 2005, Internal seiche dynamics in Lake Geneva, Limnology and Oceanography, 50(1), 2005, 207–216, American Society of Limnology and Oceanographyq 2005, by the American Society of Limnology and Oceanography, Inc.

Vecsernyes, Zsolt, 1991, Horizontal mixing dynamics in the upper layer of Lake Geneva, Thèse de doctorat n° 943 - EPFL, Suisse

Vecsernyes, Z. ; Lemmin, U. ; Graf, W.H., 1988 On the fine-scale mixing in the metalimnion and the seasonal thermocline of the Leman (Lake Geneva, Switzerland), Activities Report of the Hydraulics Research Laboratory 17 p (SEE N90-25281 19-34) - EPFL, Suisse

Vecsernyes, Z.; Lemmin, U.; Graf, W.H., 1990, Horizontal turbulent mixing dynamics on large-scale and fine-scale in Lake Geneva, Activities Report of the Laboratory for Hydraulic Research 18 p (SEE N91-20432 12-34) - EPFL, Suisse

Genève, le 18 juillet 2022

Prof. Dr Zsolt VECSERNYES
Dir. du LHA de HEPIA

Appendix 5: Simulation of an Under Lake Infrastructure for Capture and Storage of Solar Energy (ULISSE), COMSOL Conference Munich 2023 [66]

COMSOL CONFERENCE 2023 MUNICH

Simulation of an Under Lake Infrastructure for Capture and Storage of Solar Energy (ULISSE)

D. Bello-Mendes[1], R. Rozsnyo[1], W. van Sprolant[2]
[1]hepia, HES-SO, Geneva, Switzerland
[2]CvS Énergies sàrl, Geneva, Switzerland

Abstract

In this paper we present a Comsol Multiphysics simulation model of a reduced size ULISSE mock-up. The mock-up is immersed in a container, playing the role of the lake. Both are filled with water at the room temperature. Then starts a cycle imitating the change of seasons. Hot water at 33.5 °C is injected by a pump in the ULISSE mock-up chasing the initial water. After a period of rest, the water is pumped back. The recovered energy is calculated. Real-time measurements are made by temperature sensors and water flow sensors allowing comparisons with the simulation results.

Keywords: Renewable Energies, Lacustrine Thermal Energy, Energy Storage, Multiphysics Simulation

Introduction

The transition from fossil fuels to renewable energies requires finding new sources of energy. It turns out that the hydrothermal potential of the lakes would cover a significant part of these renewable energy needs [1]. The existing Thermal Lacustrine Networks (TLNs) are efficient in summer allowing the building air conditioning by « free-cooling » (without heat pumps) thanks to the cold water pumped from the bottom of the lakes. However, in winter, the heating of the buildings is 4 to 5 times less efficient due the use of heat pumps and because of the lower temperature differential of the water round-trip of the lakes. The ULISSE project, supported by the Swiss Federal Office of Energy, aims to build an underwater tank made of a semi-rigid envelope that could be filled with the warm water pumped from the surface of the lakes, heated by the sun during the hot season and to keep that water as warm as possible thanks to the thermal insulation properties of the envelope until the cold season [2]. In winter, that water would be pumped back from the tank. The higher temperature (versus normally at the lake bottom) of the pumped water would allow to reduce by 95% the pumping energy and thus provide an important heat source for the heat pumps (twice their efficiency) of the said TLNs (Fig. 1). This concept reproduced over the fifteen largest lakes in Switzerland would allow to economize 3 TWh of electricity consumption during the winter [3].

Experimental Set Up

The ULISSE tank immersed under a lake is a huge construction challenging many fields of engineering. Before trying to build such a tank, it made sense to prove the concept over a reduced size mock-up and to study the ability of the system to store the solar energy (Fig. 2). The experimental model makes it possible to reproduce the different operating phases of the ULISSE tank to analyze and establish the efficiency of its sub-lacustrine seasonal energy-heat

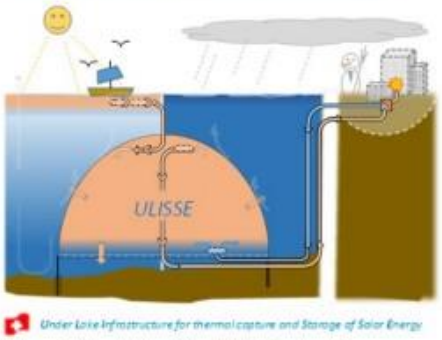

Figure 1. Illustration of the ULISSE principle.

Figure 2. The reduced size ULISSE mock-up.

storage capacity. The autumn stagnation phase is used to establish the stagnation heat loss and the cooling time constant characteristic. In addition, the experimental model also makes it possible to reproduce and measure the heat exchange flows, during the « dynamic » phases, of summer loading of temperate water and winter unloading. The test model (Fig. 2) has a reduced scale of 1/175th. At the two longitudinal ends, the envelope is « strongly insulated » (pseudo athermal walls) by a 4 cm thick extruded polystyrene plate. The hyperbolic envelope of the mock-up is reduced to a thin (2 mm) and transparent sheet of polycarbonate. This sheet (62 x 90 cm = 5'580 cm^2) is curved in its large dimension (90 cm) and is fixed at the base between two threaded stainless steel rods spaced 57 cm apart and a third located at the top. Two other threaded rods are still placed halfway up. These threaded rods are used to hold the enclosure between the two end insulating plates. The resulting curvature being close to the hyperbola with an average radius of 30 cm. The corresponding volume of the mock-up is 77 liters.

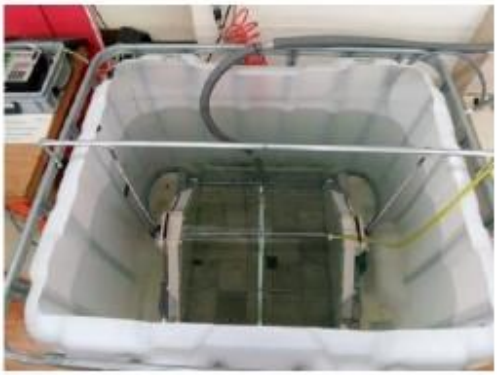

Figure 3. The reduced size ULISSE mock-up immersed in a container.

As a first approximation, this makes it possible to neglect the longitudinal heat loss of the experimental model and to highlight the predominance of the transverse heat loss of the envelope, including that by the lake bottom as well as the free convection which tends to reduce the stratification internal, leading to energetic losses.

The mock-up is placed in a plastic IBC container with a 1'000 liter frame (Fig. 3), fixed on a plastic pallet (120 x 100 cm). The ratio between the volume of water in the tank and the mock-up is a maximum of 12. For the introduction of the mock-up, a rectangular opening (100 x 80 cm) is made at the top of the tank. The mock-up is maintained on the bottom of the container (against the Archimedes thrust of the PSX end plates), by a ballast made of 4 stainless steel flats (10 kg gross recovery) and by the support of two adjustable retaining rods from the tank structure. The lower opening of the mock-up is placed on two layers of concrete pavers (total thickness 8 cm) reproducing the conductivity and the thermal capacity of the lake bottom.

The temperature of the water in a real ULISSE type reservoir is a priori around 20°C while that at the bottom of the lake is 5°C, i.e. a difference of 15°C. The experiments on the mock-up are made with a supply from the domestic hot water and cold water network. The temperature is regulated by a conventional shower mixer and an intermediate thermal stabilization tank (Fig. 4). For example, with a temperature difference of 15°C and considering the ratio between the volumes of water between the mock-up and the container, the temperature of the container can gradually increase by about 1°C if it is insulated and not cooled.

Figure 4. The water thermo-regulation system.

Measurements

The mock-up is equipped in its upper part with a ramp for injection and extraction of temperate water to reproduce the summer loading and the winter unloading of energy in the form of heat (Fig.5).

Figure 5. The injection-extraction ramp.

The temperature and water flow measurements at the level of the ramp make it possible to quantify the heat-energy introduced and extracted from the mock-up over a complete cycle (pseudo-annual). The measurements are mainly thermal in order to know the temperature and also to indirectly deduce the convective movements of water in the mock-up as well as those in the container representing the lake. The temperature probes (Fig. 6) are type K thermocouples and are placed in the mock-up on a transverse PVC support which can be moved longitudinally as well as on the upper water distribution/extraction ramp. Nine thermocouples

are placed, in pairs, at different heights on the transverse support; one on the central axis and the other on the side edge of the support as well as two laterally (in position or opposite end) on the summit ramp (Fig. 7, 11). As shown by Figure 2, the support is placed in the transverse symmetry plane of the mock-up. The thermocouples are connected to a micro logger measurement and data acquisition interface (CR3000 from Campbell Scientific). The latter also records the flow rate/volume of loading and unloading hot water from the mock-up, via the pulse flow meter located on the hydrothermal supply plate.

Figure 6. Type K thermocouples.

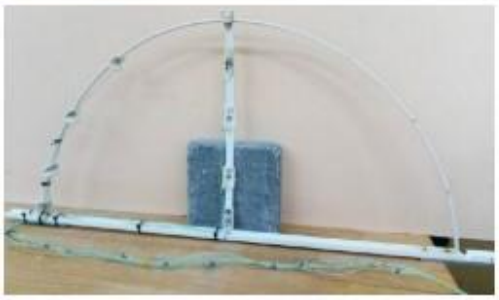

Figure 7. The cross support of thermocouples.

Governing Equations

Fluid flow modelling

We assume the water flow in the system laminar and incompressible. The flow is due to the natural convection and the injected water. Thus, the equations governing the flow are the Navier-Stokes equations without taking into account the viscosity of the water. The momentum conservation is given by Eq. 1:

$$\rho_w \frac{\partial \boldsymbol{u}}{\partial t} + \rho_w(\boldsymbol{u}\cdot\nabla)\boldsymbol{u} = -\nabla p + \rho_w \boldsymbol{g}, \qquad (1)$$

where, $\boldsymbol{u}$ is the velocity field, $\boldsymbol{g}$ the gravity field, ρ_w the water density and p the pressure scalar field. This equation must be completed by the equation of the mass conservation, Eq. 2:

$$\nabla\cdot\boldsymbol{u} = 0. \qquad (2)$$

However, to take into account the effects of the gravity field, we used the Boussinesq approximation on the density [4]:

$$\rho_w = \rho_{ref}\left(1-\alpha_p\right)\left(T-T_{ref}\right), \qquad (3)$$

where ρ_{ref} is the reference density of the water, i.e. at the reference temperature, $T_{ref} = 20\,°C$, and α_p is the dilatation coefficient at constant pressure at the reference temperature given by Eq. 4:

$$\alpha_p = -\frac{1}{\rho_w}\left(\frac{\partial \rho_w}{\partial T}\right)_p. \qquad (4)$$

Eq. 1 and Eq. 2 must be completed by the boundary and the initial conditions. The boundary conditions are on the walls (interior and exterior) $\boldsymbol{u} = \boldsymbol{0}$ and on the free surface $p = p_{ref}$ where p_{ref} is the atmospheric pressure. At the initial conditions, corresponding to $t = 0$, the water has a velocity field $\boldsymbol{u} = \boldsymbol{0}$ and a pressure field given by the relation $p = p_{ref} + \rho_w \boldsymbol{g}\cdot(\boldsymbol{r}-\boldsymbol{r_{ref}})$ where $\boldsymbol{g}\cdot(\boldsymbol{r}-\boldsymbol{r_{ref}})$ corresponds to the hydrostatic pressure.

Heat transfer in solids and fluids modelling

The heat transfer in all media is governed by Eq. 5:

$$\rho C_p \frac{\partial T}{\partial t} + \rho C_p \boldsymbol{u}\cdot\nabla T - \nabla\cdot(-k\nabla T) = 0, \qquad (5)$$

where, ρ is the density of a given medium, C_p its heat capacity at constant pressure and k its thermal conductivity. The bidirectional coupling between Eq. 1 and Eq. 5 is made through the convective term $\rho C_p \boldsymbol{u}\cdot\nabla T$ and the Boussinesq approximation. Eq. 5 must be completed by boundary and initial conditions. At $t = 0$, the system was in thermal equilibrium with the exterior. Thus, the initial temperature, T_0, is given by the exterior temperature, $T_0 = T_{ext} = 21.3°C$. The boundaries of the water injection holes are set to the temperature $T_i = 33.5°C$ during the phase of injection and to thermal insulation during the other phases. All the other boundaries are set to a convective heat flux boundary condition. The convection coefficient, h, was set to the value $h = 11\,W\cdot m^{-1}\cdot K^{-1}$.

In general, the process having three phases, the initial conditions for a given phase is the last state of the system in the previous one.

Modelling with Comsol Multiphysics

The geometry of the system has two plane symmetries. For the sake of simplicity, we didn't represent details such as screws, nuts, probe holders and the walls of the container. Thus, the simulation domain is the water with the immerged mock-up. A quarter of the system, shown by Figure 8, has been modelled. The height of the system is the initial water height in the container.
The Laminar Flow interface of the CFD Module and the Heat Transfer in Solids and Fluid interface of the Heat Transfer Module were used. The Nonisothermal Flow interface ensured the multiphysics coupling between the fluid flow and the heat transfer. The Boussinesq approximation was selected for that coupling.

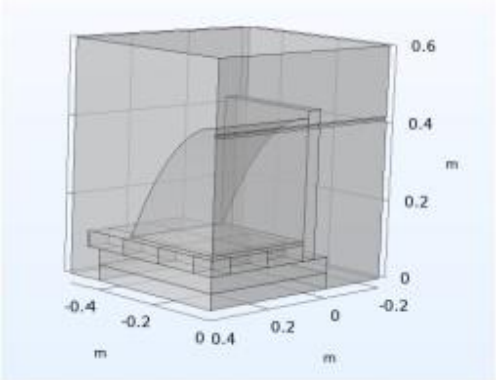

Figure 8. The geometrical representation in Comsol.

In order to complete the governing equations and the boundary conditions described in the previous section, two symmetry conditions were added at the symmetry planes locations as boundary conditions due to the geometrical representation.
The simulation was done with the default time dependent solver. The whole cycle consists in three studies corresponding to three phases summarized in Table 1.

Phase	Description	Time Range (min)
1	Water injection	[0;64]
2	Relaxation	[64;70]
3	Water extraction	[70;134]

Table 1: The three phases

During the phase 1, the water in the tank at ambient temperature is flushed by the injected water from the injection ramp. Then follows a period of relaxation, phase 2, where the water in the tank is cooled due to diffusion and convection. In the phase 3, the water is pumped out from the tank. The question to be answered is how much energy can be recovered from the amount that what was stored in the phase 1.

The volume of the water in the container is changing during the injection and pumping phases. The injected volume in the mock-up is about 140 liters, corresponding to an increase of the water height in the container about 12 cm. We assumed that this height change had a low impact on the temperature evolution inside the mock-up. Thus, in order to spare computation time, we didn't model the volume evolution of the container (by a deformed mesh or a diphasic air-water flow technique). We simply set an Outflow condition at the free surface boundary, activating the Back Flow Suppression during the phases 1 and 2 and disabling it during the phase 3. The Normal Flow option and the Compensation for Hydrostatic Pressure remained always activated at the open boundary. The mock-up hyperbolic boundary (Fig. 9), was defined as an Interior Wall. Its material properties were defined as a single layer material.

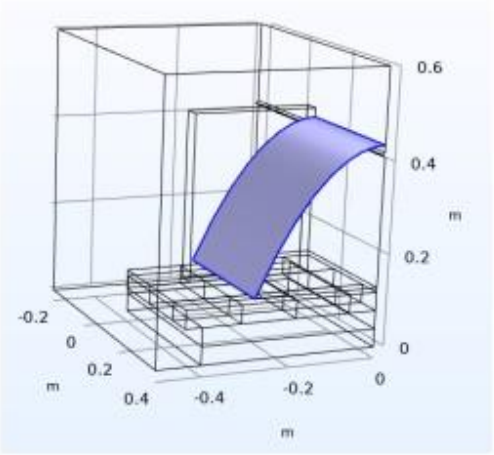

Figure 9. The mock-up hyperbolic boundary.

The boundaries of the injection ramp (Fig. 10) from where injection or pumping occurs were set the boundary conditions given by the Table 2 where the velocity of the injection is $v_0 = 0.3096\ m \cdot s^{-1}$. The area of the surface of injection of a hole being equal

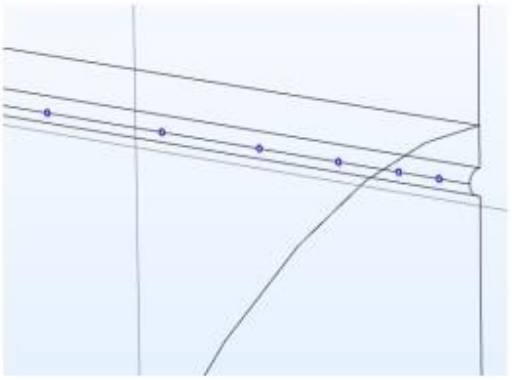

Figure 10. The water injection and pumping boundaries.

to $S = 4.9159 \cdot 10^{-6}\ m^2$, the corresponding water debt per hole is $0.0913\ l \cdot min^{-1}$ which is about $2.19\ l \cdot min^{-1}$ for the total injection debt. The injection velocity was ramped in order to get numerical stability.

Phase	Laminar Flow	Heat Transfer
1	v_0 (ramped)	T_0
2	No Slip	Thermal Insulation
3	$-v_0$ (ramped)	Thermal Insulation

Table 2: Boundary conditions for injection boundaries at the different phases.

Simulation Results, Comparison with Experimental Measurements.

We used for comparisons between simulation and experimental measurements the temperature evolution at the location of the probes shown by Figure 11 during a full cycle: injection, relaxation, extraction.

Figure 11. Probes position for comparisons between simulation results and measurements.

The experimental results are shown by Figure 12.

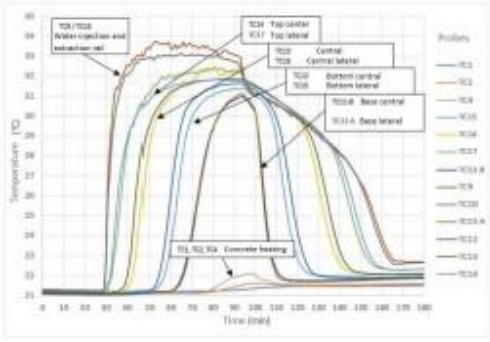

Figure 12. Temperature evolution measured by probes during a full cycle.

The probes were also placed in the Comsol model at the same locations. The temperature evolution obtained by simulation is shown by Figure 13.

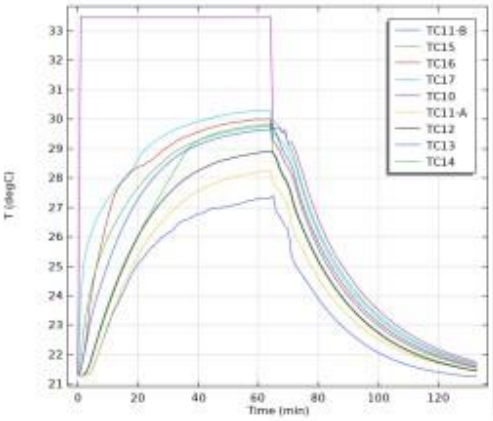

Figure 13. Temperature evolution obtained by simulation during a full cycle.

Figure 14 shows the temperature distribution at the end of water injection. We may notice that the tank is filled with warm water between approximatively 27 °C and 33.5 °C.

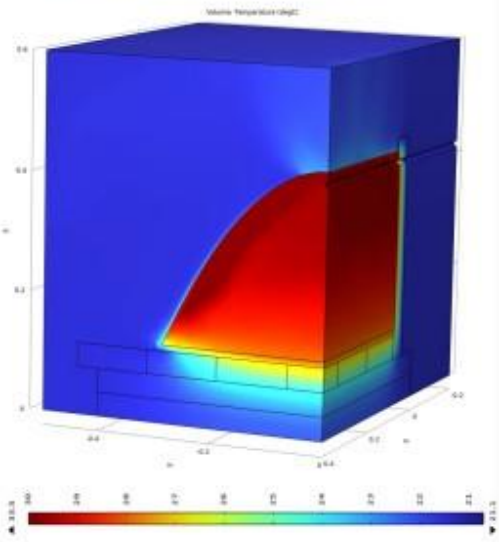

Figure 14. Temperature distribution at t = 64 min at the end of water injection. The range of temperature is from 21.1 °C (blue) to 33.5 °C (red).

Figure 15 shows the velocity distribution at the end of water injection. We may notice the existence of convection currents surrounding and on the top of the insulating shell.

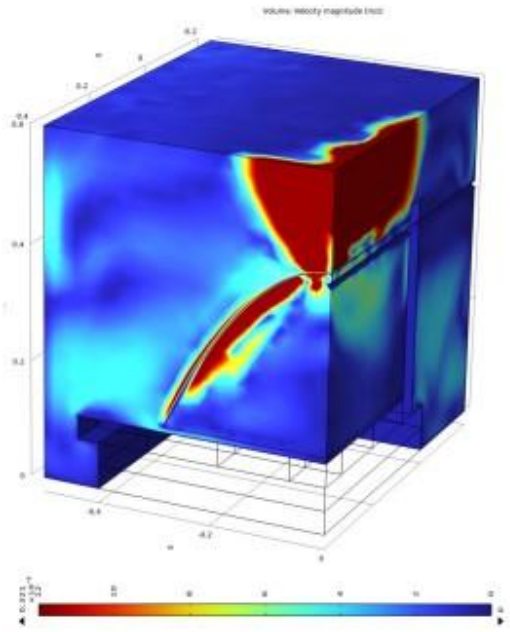

Figure 15. Velocity magnitude distribution at t = 64 min at the end of water injection showing the convection currents. The range of velocity magnitude is from 0 $m \cdot s^{-1}$ (blue) on the walls to 0.321 $m \cdot s^{-1}$(red), at injection inlet.

Figure 16 shows the temperature distribution while extracting water. We may notice the gradient of the temperature distribution and the energy dissipation from the mock-up to the bottom of the system.

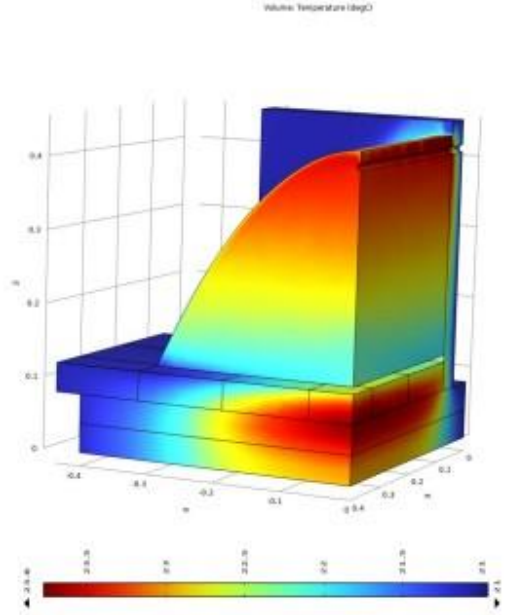

Figure 16. Temperature distribution at t = 89 min during water extraction. The range of temperature is from 21 °C (blue) to 23.8 °C (red).

Comparing the temperature response by simulation to the temperature response by experiments, we may notice the same global behavior and that the reached temperatures are coherent. The simulation curves look like the voltage curve response of a charge and discharge of an electric capacitor, except in the relaxation phase (6 min of duration) where the inflexion of the response curve is inverted. In the experimental curves this inverted inflexion lasts longer and we have a much more important response delay between the probes.

In order to explain the differences, we must bear in mind the simplification made in the geometry of our simulation model. For instance, the support of the probes has not been modeled. The probes are screwed on the support and probably there is a perturbation of the measures due to heat absorption by the support elements and the probes themselves. The probes also have an uncertainty of ± 1.5°C in the range of working temperatures according to the manufacturer's specifications. Their location, in the experiment versus in the simulation model, has also an uncertainty that was difficult to be quantified and that might be a sensitive factor. We may also notice that the injection temperature in the experiments is not homogeneous in the injection ramp, oscillating between 33°C and 33.8°C, whereas in the simulation model it's constant equal to 33.5°C. Thus, the evolution of temperatures shown by the simulation is close to the reality even if we don't have exactly the same curve shapes. However, that point has still to be investigated.

The qualitative behavior of the system is pretty well reproduced by the simulation which helps to understand how the convection currents move away the thermal energy stored in the mock-up from its bottom open boundary, evacuating heat along its exterior boundaries to the container open boundary above the top of the container (Fig. 15). An amount of the thermal energy is also absorbed by diffusion in the concrete ground of the system. While pumping out the warm water, we may observe the gradient of temperature distribution, the colder water replacing the warmer water from the bottom to the top, where occurs pumping out.

Our target being the quantification of the recovered energy after storage [5], we analyzed in the postprocessing the energy balance during the cycle. The theoretical amount of internal energy, U_0, stored in the tank of volume, V_{tank}, at $t = 0$ min is:

$$U_0 = \rho_w(T_0) V_{tank} C_p(T_0)\left(T_0 - T_{ref}\right). \quad (6)$$

The theoretical amount of internal energy, U_i, injected into the mock-up during 64 min is:

$$U_i = 24\rho_w(T_i) v_0 S \Delta t C_p(T_i)\left(T_i - T_{ref}\right), \quad (7)$$

where S is the area of the surface of injection of each of the 24 injection holes and Δt is the duration of the injection in seconds. The injected water is assumed

to have a constant temperature. The internal energy of the tank at any time may also be calculated directly by Comsol Multiphysics: the internal energy of a domain at a given temperature distribution is the energy necessary to increase the temperature of the system from the reference temperature, T_{ref}, to that temperature distribution. Formula (7) may also be implemented in Comsol. If U_{64} is the internal energy at the end of injection, we expect to have the relation $U_{64} < U_0 + U_i$ because, during the injection, a part of the energy in the mock-up is lost through convection and diffusion. Thus, the stored energy, E_S, is given by the difference $E_s = U_{64} - U_0$. If U_{70} is the internal energy of the mock-up at the end of the relaxation phase, corresponding to time t_{70}, the stored energy available for extraction, E_a, is given by $E_a = U_{70} - U_0$. The energy loss, E_L, during relaxation is $E_L = U_{64} - U_{70}$. The internal energy of the extracted water, U_x, was computed with Comsol Multiphysics by using a probe giving the average surface temperature at the time t, $\bar{T}_k$, on the extraction surface of each of the 6 holes of the simulation model and time integration over the phase 3 ending at time t_{134}:

$$U_x = 4v_0 S \sum_{k=1}^{6} U_k \qquad (8)$$

where,

$$U_k = \int_{t_{70}}^{t_{134}} \rho_w(\bar{T}_k) C_p(\bar{T}_k)(\bar{T}_k - T_{ref})dt \qquad (9)$$

and where the factor 4 takes into account the two symmetries of the simulation model. The results are summarized in Table 3 where the energies are given in Mega Joules. The energy recovered by extraction is $E = U_x - U_0 = 1.9757\ MJ$ which represents about 82% of the amount of energy stored. The real energy balance must consider the energy used for pumping and the losses in the extraction tubes. Thus, the effective amount of energy available for usage would be less. However, the result shows the huge potential of the system to store energy. We also must bear in mind that the energy of the injected water is coming from the sun and is free of charge.

U_0	U_i	U_{64}	U_{70}
0.3861	7.8920	2.7891	2.4608
E_S	E_a	E_L	U_x
2.403	2.0747	0.3283	2.3618

Table 3: Energy balance results (MJ)

Conclusions

This work shows the ability to use multiphysics simulation with Comsol Multiphysics to understand the behavior of the ULISSE system. Provided that the simulation model represents with enough accuracy the system, it would be possible to predict with a good approximation the energy balance. The model we did shows with a good agreement the evolution the system in the range of uncertainty and enhances the importance of the convection currents and diffusion in the energy loss. The consequence is the adaptation of the water extraction debt in order to minimize these losses.

The next steps of improvement of the multiphysics modelling would be to integrate in the model the fluid structure interaction. In a lake, the dynamics of water is more complex, producing underwater mechanical waves [6], [7]. The integration of that dynamics in the Comsol Multiphysics model should help to understand the resistance of the ULISSE structure to such waves. The project should be continued by the construction of a bigger mock-up in conditions closer to the real operation and allow to improve the numerical modelling.

References

[1] *Proposal for the CORSAIRE energy project as part of a sustainable development effort*, W. van Sprolant, EPS 10 Trends in Physics, 10th General Conference of the European Physical Society, September 9-13, 1996, Sevilla (Spain)

[2] Utilisation thermique des eaux superficielles, Potentiel des lacs et rivières suisses A. Gaudard; M. Schmid, Eawag; A. Wüest, Eawag et EPFL, AQUA & GAS N° 6. , 2018

[3] The cold store for a pumped thermal energy storage system, T.R.Davenne et al. Journal of Energy Storage 14 (2017) 295-310

[4] https://www.comsol.com/model/free-convection-in-a-water-glass-195

[5] Benkhelifa, A. & Bouhdjar, Amor. (1998). Influence des forces d'inertie sur les performances de stockage thermique dans une cuve durant les phases de charge et de décharge. Revue des Études Renouvelables. 1.

[6] Seasonality modulates wind-drive mixing pathways in a large lake, Beito Fernandez castro et al. Communications earth & environment (2012)2 :215

[7] Vecsernyés, Zsolt. (1991). Horizontal mixing dynamics in the upper layer of lake Geneva. 10.5075/epfl-thesis-943.

Acknowledgements

The authors wish to kindly thank the Swiss Federal Office of Energy (OFEN, CH-Bern) for having supported this project.